Acta Universitatis Szegediensis

Acta Biologica Szegediensis

Volume 63,
Number 2,
2019

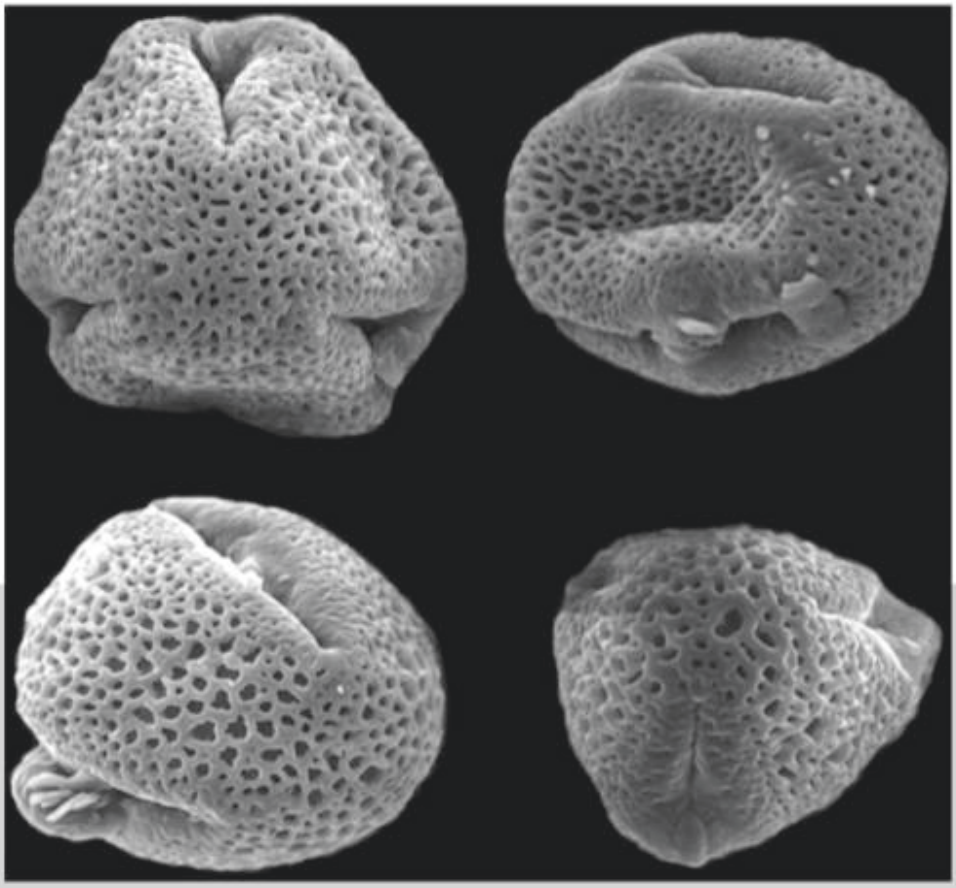

University of Szeged, Szeged, Hungary

http://abs.bibl.u-szeged.hu/index.php/abs

Acta Biologica Szegediensis

Volume 63(2):83-90, 2019
Acta Biologica Szegediensis
http://abs.bibl.u-szeged.hu/index.php/abs
DOI:10.14232/abs.2019.2.83-90

ARTICLE

Effect of subclinical mastitis on milk yield and milk composition parameters in dairy camels

Leyla Hadef[1,2]*, Brahim Hamad[1,2], Hebib Aggad[2]

[1]University of El Oued, Faculty of Life and Natural Sciences, Department of Agronomy, 39000 El Oued, Algeria
[2]University of Tiaret, Institute of Veterinary Sciences, Laboratory of Hygiene and Animal Pathology, 14000 Tiaret, Algeria

ABSTRACT This study investigated the effects of subclinical mastitis on milk yield and milk composition parameters in dairy camels. A total of 140 camel milk samples were collected from multiparous she-camels (7-10 years old) and were subjected to bacteriological culture studies; 76 samples displayed subclinical mastitis and 64 samples were healthy. Furthermore, the samples were analyzed via standard procedures to determine the yield and composition parameters of the milk such as pH, electrical conductivity, protein, fat, lactose, and ash content. The results showed that the milk yield was significantly low ($p < 0.05$) in infected animals compared to healthy animals (3.80 vs 4.32 L·day^{-1}). Moreover, compared to the values observed in healthy milk samples, milk from animals with subclinical mastitis showed significantly decreased ($p < 0.05$) protein (3.33 vs 3.40%) and fat (3.67 vs 3.74%) contents. However, no significant changes ($p > 0.05$) were observed in pH, electrical conductivity, lactose, or ash content. The results of the uninfected milk samples revealed that there was significant correlation between the protein and fat content ($r = 0.781$; $p < 0.01$) and between the lactose and ash content ($r = 0.701$; $p < 0.01$). Conversely, the infected ones showed that there was higher significant correlation between the protein and fat contents ($r = 0.807$; $p < 0.01$) and a medium correlation between the lactose and ash contents ($r = 0.603$; $p < 0.01$). In conclusion, the results suggest that subclinical mastitis is negatively associated with a reduced milk yield and lower protein and fat content. Thus, these parameters can be used to diagnose mastitis in dairy camels.
Acta Biol Szeged 63(2):83-90 (2019)

KEY WORDS
camels
composition
milk yield
subclinical mastitis

ARTICLE INFORMATION
Submitted
3 November 2019.
Accepted
12 December 2019.
***Corresponding author**
E-mail: leila.hadef@yahoo.fr
hadef-leyla@univ-eloued.dz

Introduction

Dromedary camels are considered the best livestock animals in arid, semiarid, and desert areas; camel milk is a valuable source of both nutrition and income in these areas (Saleh and Faye 2011; Ali et al. 2016; Legesse et al. 2017; Elbashir and Elhassan 2018). Camels can produce more milk for a longer period of time in arid zones and harsh environments than any other domestic livestock species (Seifu and Tafesse 2010; Eissa et al. 2011; Alluwaimi et al. 2017). Nevertheless, similar to other dairy animals, camels are affected by udder infections such as mastitis, which is a complex disease occurring worldwide among such animals. Heavy economic losses can occur as a result of clinical and subclinical mastitis (Toroitich et al. 2017; Gramay and Ftiwi 2018; Ali et al. 2019).

Mastitis, particularly the subclinical type, is one of the most persistent and widely spread disease condition that affect milk hygiene and quality among dairy camels (Husein et al. 2013; Hadef et al. 2016). The prevalence of subclinical mastitis in this species varies among different studies (15-67.4%; Bhatt et al. 2004; Abera et al. 2010; Seifu and Tafesse 2010; Alamin et al. 2013). Subclinical mastitis causes the animal to suffer, reduces the milk yield, alters milk properties, impairs preservation and processing, and represents a public health concern for consumers of camel milk (Saleh and Faye 2011). In the same context, according to Fazlani et al. (2011), mastitis is known to cause a loss of approximately 70% of the camel milk production. Moreover, Ali et al. (2016) reported that subclinical mastitis modifies the composition of camel milk by decreasing the protein, fat, and lactose content; increasing enzymatic activity; and creating a higher electrical conductivity.

Therefore, many studies have been performed to investigate the effects of subclinical mastitis on milk yield and composition in other animal species. However, there are no reports in the literature regarding this association in camels. Thus, this study aimed to determine the impact of subclinical mastitis on milk yield and milk composition parameters in dairy camels.

Materials and methods

Study area

This study was performed in a dairy farm located in Bir Naam, Southeast Algeria. This area is characterized by an arid climate with an average annual temperature of 21.8 °C and an average precipitation of 11.75 mm. The rainy period begins at the start of September and lasts until May with a maximum of 19 mm of precipitation in November. The remainder of the year, pastures in the region are considered arid with an average maximum temperature of 33.6 °C and a very low precipitation of 2 mm in July. The vegetation commonly consists of steppe plants such as *Stipa tenacissima* and *Ampelodesmos tenax.*

Animals

The present study evaluated 140 milk samples obtained from multiparous healthy dairy she-camels. The animals were between 7 and 10 years old, with an average weight of 300 to 350 kg and an average milk yield of 4.04 ± 0.10 L·day^{-1}. All animals were maintained under the same conditions (grazing and supplementary farming systems). The animals were submitted to the same diet, which was primarily based on pasture (grass pasture system). The animals were supplemented with some barley concentrate and dry hay straw, with a higher intake during the dry season. The animals were hydrated regularly and hand-milked twice daily at 12-hour intervals. Calving generally occurs during the winter season and starts as early as November.

Sample collection

At the beginning of the experiment, all the camels were subjected to clinical examinations. The camels' udders were examined visually and by palpitation for the presence of any lesions by assessing redness, pain, heat, and swelling. Moreover, milk samples from each animal were obtained and assessed for any change in color and consistency. In this study, the 140 milk samples were collected just before the morning milking during the late stages of lactation. The teats were washed thoroughly and dried with a single-use paper towel. The first three streams of milk from each teat were discarded. The teat end and orifice were sanitized with cotton swabs soaked in 70% alcohol. The samples were collected from each animal in a sterile bottle. Furthermore, the milk samples were labeled, stored in an ice box, and transported immediately within 2-4 hours after collection to the laboratory for the bacteriological and physicochemical analyses.

Milk analysis

Measurement of milk production

Upon arrival to the laboratory, the quantity of the collected milk from each animal was measured with a graduated cylinder. The daily milk yield of the animals was the sum of the morning and evening milking.

Bacteriological analysis

The microbiological cultures were established according to the standard procedures of the National Mastitis Council (NMC 1987). All milk samples were used for the detection of specific bacteria that cause subclinical mastitis. For this purpose, a loopful of each milk sample was cultured on defibrinated sheep blood agar (7%), nutrient agar, BCP (Bromcresol Purple Lactose) agar, and Chapman agar. Moreover, the plates were incubated at 37 °C for 24-48 hours. A sample was considered positive for subclinical mastitis when the growth of five or more identical colonies was detected on the streaks (Contreras et al. 1997; Pradieé et al. 2012). However, the growth of two or more different bacterial colonies (> 5 CFUs per type) was considered contamination, and the result was removed from the analysis (Gonzalo et al. 2002; Pradieé et al. 2012). The resulting growth was identified based on morphology, colony characteristics, Gram reaction, hemolytic characteristics, catalase test, and classic biochemical tests. Staphylococci and micrococci were identified based on their growth characteristics on triple sugar iron agar, mannitol salt agar, the nitrate reductase test, the urease test, the coagulase test, and the catalase test (Forbes et al. 2002; Quinn et al. 2011). Isolates that were tentatively identified as streptococci were evaluated according to their growth characteristics on the sheep blood agar, catalase production, and sugar fermentation tests. Gram-negative isolates were sub-cultured on BCP agar and were further tested using triple sugar iron agar, motility assessments, the IMViC test (Indole, Methyl red, Voges-Proskauer, and citrate utilization tests), and the urease test (Forbes et al. 2002; Quinn et al. 2011).

Physical analysis

The pH of the milk samples was determined using a pH-meter (Hanna HI 99161, Romania) equipped with a combined glass electrode after calibration in buffer solutions of pH 4 and 7. Furthermore, the electrical conductivity was estimated with an electrical conductivity meter (Hanna EC 215) after the device was calibrated using standard buffer solutions.

Chemical analysis

The protein content was determined through quantification of the nitrogen content by the Kjeldahl method

following the AOAC (2000). Nitrogen was then multiplied by a standard factor (6.38) so that the results were expressed as total protein content. The fat content was determined by the Gerber method according to the AOAC (2000). The lactose content was determined by Bertrand's method (AFNOR 1993). The ash content was determined by an AOAC (2000) technique using carbonization of the samples in a direct flame and subsequent calcination in a muffle at 550 °C for 4-6 hours.

Statistical analysis

The data were analyzed using the Statistical Analysis System Program SPSS v.16.0. The model applied included the fixed effect of subclinical mastitis. Data are displayed in the tables as the mean ± SEM. Differences in the mean values were tested using the independent-samples T test or the Mann-Whitney U test after evaluating the normal distribution by the Shapiro-Wilk and Kolmogorov-Smirnov tests. Pearson's correlation test was used to interpret the relationship between the various studied parameters. A probability level (p) of 0.05 was chosen as the limit for statistical significance in all tests.

Results

The effect of subclinical mastitis on milk yield and composition parameters is shown in Table 1. Among the 140 samples analyzed, 76 were positive and 64 were negative. In addition, our study indicated that subclinical mastitis had a significant ($p < 0.05$) effect on milk yield (3.80 vs 4.32 L·day^{-1}), protein content (3.33 vs 3.40%), and fat content (3.67 vs 3.74%), with these parameters being significantly lower in the positive samples than in the negative samples ($p < 0.05$). However, no significant ($p > 0.05$) effect of subclinical mastitis was found on pH, electrical conductivity, lactose, or ash contents.

Table 1. Effect of subclinical mastitis on milk yield and composition parameters (n =140).

Parameters	**Means ± SEM**		***p*-value**
	Healthy	Infected	
Number of samples	64	76	
Milk yield (L·day-1)	4.32 ± 0.14	3.80 ± 0.14	0.023
pH	6.56 ± 0.01	6.53 ± 0.01	0.220
EC (mS·cm-1)	6.84 ± 0.14	6.98 ± 0.13	0.459
Protein (%)	3.40 ± 0.02	3.33 ± 0.02	0.039
Fat (%)	3.74 ± 0.01	3.67 ± 0.01	0.006
Lactose (%)	4.20 ± 0.04	4.10 ± 0.03	0.066
Ash (%)	1.02 ± 0.02	0.94 ± 0.02	0.064

EC: Electrical conductivity; SEM: standard error of mean. Means in the same row are significantly different (p < 0.05).

The correlations between all of the studied parameters are reported in Table 2. In the healthy samples, the results showed that protein had a highly significant positive correlation with fat content ($r = 0.781$; $p< 0.01$) and moderate positive correlation with ash ($r = 0.264$; $p < 0.05$). In comparison with the uninfected samples, the protein was significantly correlated with fat content ($r = 0.807$; $p < 0.01$), lactose ($r = 0.343$; $p < 0.01$) and ash (r

Table 2. Relationship between the different studied parameters (n =140).

Healthy (64)						
	pH	EC	Protein	Fat	Lactose	Ash
Milk yield	- 0.200	- 0.173	- 0.108	- 0.075	- 0.139	- 0.205
pH		- 0.147	0.032	0.147	- 0.067	- 0.011
EC			- 0.084	- 0.176	0.275*	0.227
Protein				0.781**	0.196	0.264*
Fat					0.068	0.187
Lactose						0.701**
Infected (76)						
	pH	EC	Protein	Fat	Lactose	Ash
Milk yield	0.188	0.070	0.006	- 0.035	0.035	0.068
pH		- 0.049	- 0.077	- 0.061	0.044	0.005
EC			- 0.020	- 0.126	0.162	0.295**
Protein				0.807**	0.343**	0.390**
Fat					0.348**	0.299**
Lactose						0.603**

*: $p < 0.05$. **: $p < 0.01$. All Pearson correlation coefficients are significant at $P < 0.05$.

= 0.390; $p < 0.01$) in the infected samples. Moreover, a medium significant positive correlation was found in the samples with subclinical mastitis between fat and lactose ($r = 0.348$; $p < 0.01$) and between fat and ash ($r = 0.299$; $p < 0.01$). Likewise, lactose was positively correlated with ash in the healthy samples ($r = 0.701$; $p < 0.01$) and in the infected samples ($r = 0.603$; $p < 0.01$). Similarly, the electrical conductivity showed significant positive correlations with lactose ($r = 0.275$; $p < 0.05$) in the uninfected milk samples and with ash ($r = 0.295$; $p < 0.01$) in the infected ones. Furthermore, in the healthy samples the milk yield was negatively correlated with all studied parameters; however, these relationships were not significant ($p > 0.05$). Conversely, in the samples with subclinical mastitis the milk yield was negatively correlated with fat ($r = - 0.035$; $p > 0.05$) only.

Discussion

Unlike clinical mastitis, which is responsible for high economic losses but easier to eliminate, subclinical mastitis is quite problematic because of its chronicity and relative incurability in dairy herds. Moreover, microbial infections alter the milk composition and render milk less suitable for consumption and processing.

In the present investigation, subclinical mastitis had a significant negative effect on milk yield. Such findings concur with previous reports in dairy cows (Tesfaye et al. 2010; Gonçalves et al. 2018), dairy goats (Pleguezuelos et al. 2015; Gelasakis et al. 2016; Hanuš et al. 2017), and dairy sheep (Marti De Olives et al. 2013). In these studies, a significantly lower milk yield was reported in mastitic animals than in non-mastitic animals. Nevertheless, no reports are available about the changes in the milk yield of mastitic she-camels. The decrease in the milk yield is attributed to the fact that mastitis is associated with mammary tissue damage, which reduces the number and activity of epithelial cells and consequently contributes to the decreased milk production (Zhao and Lacasse 2008).

The milk pH in our study was not affected by subclinical mastitis; this result differs from that of Ali et al. (2016), who mentioned that the pH of infected milk significantly increases in relation to the severity of the CMT reaction. According to Hadef et al. (2016), determining the pH of camel milk is not a suitable method for detecting subclinical mastitis in camels. The pH of milk may depend on other factors such as milk yield, lactation stage, milk composition, and the nature of fodder. In addition, the insignificant change in pH might also be due to the increased levels of citrates and bicarbonates during subclinical mastitis (Ogola et al. 2007).

Similarly, the electrical conductivity of the milk samples did not differ significantly between healthy and infected milk in our study. This observation is in agreement with the findings of Eberlein (2007), who suggested that the electrical conductivity values in his study seem to be correlated in some camels with a positive CMT reaction but show no correlation to CMT and total bacterial counts or pathogenic bacteria in other camels or in the same camels on other days. Furthermore, several studies have demonstrated that electrical conductivity was not considered adequate as a method of diagnosing mastitis in camels (Younan et al. 2001; Bhatt et al. 2004; Eberlein 2007; Hadef et al. 2016). Contrary to the results of this study, Ali et al. (2016) found that the electrical conductivity of mastitic milk was significantly higher than that of milk obtained from healthy animals; they attributed their finding to the increased milk somatic cells. Moreover, the augmentation of electrical conductivity is due to the increased leakage of various ions and salts as a result of the increased permeability of vascular membranes following inflammatory reactions.

These contradictory results regarding the variation of electrical conductivity in relation to subclinical mastitis may be caused by breed differences, feeding, stage of lactation, parity number, and season. Furthermore, cell membrane permeability is altered during mastitis, which leads to the increased leakage of blood components into the udder and changes the milk composition (Sharif and Muhammad 2008).

In this study, the protein concentration decreased in the milk of she-camels affected with subclinical mastitis. Similarly, Eman Fathi et al. (2012) and Ali et al. (2016) reported that healthy she-camels produce milk with a higher protein percentage relative to mastitic camels (3.87 vs. 2.90%, respectively). The change in protein may be explained by epithelial cell damage (decrease in synthesis) and an increase in vascular permeability with the passage of immunoglobulins, serum protein, and enzymes from the blood, which may lead to increased proteolysis (Forsbäck et al. 2010). Moreover, subclinical mastitis was associated with a decrease in milk fat percentage. These results are in agreement with other studies (Eman Fathi et al. 2012; Ali et al. 2016). The decrease in fat percentage seems to be a result of a decrease in the synthesis and secretion activities of mammary glands (Le Maréchale al. 2011). It is also important to note that variations in the fat percentage can be affected by the stage of lactation (Abdalla et al. 2015; Hadef et al. 2018), genetics, management, season (Shuiep et al. 2008), and geographic location (Konuspayeva et al. 2009).

Data in the literature regarding the effect of subclinical mastitis on the total concentration of milk protein and fat in other animal species (cows, goats, and sheep) are very conflicting. Some authors sustain that there is a decrease

of these parameters in mastitis cases (Yarabbi et al. 2014; Barrón-Bravo et al. 2013; Bianchi et al. 2004), whereas others report an increase of these parameters (Guariglia et al. 2015; Pleguezuelos et al. 2015; Olechnowicz et al. 2010). By contrast, other studies have reported that subclinical mastitis has no significant influence on protein and fat contents in milk (Hachana et al. 2018; Ying et al. 2002; Summer et al. 2012).

The current study showed that there is an inverse but non-significant relationship between the values of lactose and subclinical mastitis ($p > 0.05$). Our result is consistent with previous reports on camel milk (Eman Fathi et al. 2012). Moreover, Ali et al. (2016) agree that there is a reduction in the concentration of lactose in milk obtained from animals with subclinical mastitis; however, their results were significant. According to Leitner et al. (2011), the lactose concentration in milk closely reflects both the reduction in milk yield and the deterioration of milk's ability to curdle. Furthermore, the decrease in lactose content can be explained by a decreased capacity for synthesis of the disaccharide by the mammary gland or an increase in the NaCl concentration in the milk, resulting in osmotic disruption in the gland and sugar deprivation by bacteria (Rysanek and Babak 2005).

In addition, according to the literature, factors other than mastitis can also influence the milk lactose content. In the same context, Aljumaah et al. (2012) found that the lactose percentage in camel milk is significantly influenced by the management system, breed parity, and stage of lactation. The present results indicate that the concentrations of ash obtained from infected and healthy she-camels were not significantly different ($p > 0.05$). This finding is in agreement with the results reported by Alemu et al. (2013) who indicated that there was no significant difference in the concentrations of ash in cattle. This finding can be attributed to the relationship between the ash content and the electrical conductivity, which are intimately linked. Consequently, these two parameters did not display significant variation in our study (Kaikci et al. 2012).

The significant positive correlation observed in the present study in the uninfected and infected milk samples between protein and fat contents agreed with the results of previous studies (Musaad et al. 2013; Elobied et al. 2015; Nagy et al. 2017). Similarly, Konuspayeva et al. (2010) sustain that the correlation between protein and fat is widely described in other dairy animals. Moreover, the significant relationship found in the two groups between the other parameters included in this study was in agreement with the results of Musaad et al. (2013) and Elobeid et al. (2015), except for the positive significant correlations observed between electrical conductivity and lactose in the uninfected samples and ash in the infected ones. In the same context, Musaad et al. (2013) reported a significant negative correlation of electrical conductivity with lactose and ash, whereas Elobeid et al. (2015) declared that there was no significant correlation between the previous parameters. According to Eberlein (2007), the relationship observed between electrical conductivity and ash in the samples with subclinical mastitis in this study can be explained by damage caused to the udder parenchyma cell membranes in mastitis cases. The increase of the permeability of the barrier between blood and milk occurred due to an increase in the contents of chloride (Cl^-) and sodium (Na^+), which leads to a higher electrical conductivity of milk. In addition, unlike our study, Nagy et al. (2017) found a negative correlation between fat and lactose concentrations.

Moreover, the current study revealed that the correlations between the all studied parameters and milk yield in the healthy samples were negative, which was in agreement with previous reports (Musaad et al. 2013; Elobied et al. 2015; Nagy et al. 2017). The observed negative correlation between milk production and other milk components can be attributed to the dilution effect due to the changing milk quantity that had been described earlier. In contrast, in the infected samples the milk yield was negatively correlated only with fat content. This finding can be explained by the significant decrease of the quantity of milk produced by the infected animals; thus, the dilution effect was attenuated in this case.

In conclusion, this study showed that the subclinical infection of mammary glands had a statistically significant negative effect on the milk yield, protein, and fat contents in dairy camels. Therefore, monitoring changes in these parameters is a suitable method for the diagnosis of subclinical mastitis in this species. However, no significant influence of subclinical mastitis was found on pH, electrical conductivity, lactose, and ash content. Therefore, this study indicates that subclinical mastitis is a significant cause of deterioration of important milk components, which has an economic impact on the productivity of this animal species.

Acknowledgments

The authors are very much thankful to the camel farm owners for agreement to participate in this study.

References

Abdalla EB, Ashmawy AEHA, Farouk MH, Salama OAR, Khalil FA, Seioudy AF (2015) Milk production potential in Maghrebi she-camels. Small Rum Res 123:129-135.

Abera M, Abdi O, Abunna F, Megersa B (2010) Udder health problems and major bacterial causes of camel mastitis in Jijiga, Eastern Ethiopia: implication for impacting food security. Trop Anim Health Prod 42:341-347.

AFNOR (1993) Association Française de Normalisation: Contrôle de la qualité des produits alimentaires, Lait et produits laitiers. AFNOR ed, Paris.

AOAC (2000) Association of Official Agricultural Chemists: Official Methods of Analysis, 17th ed. Washington, DC, AOAC International.

Alamin MA, Alqurashi AM, Elsheikh AS, Yasin TE (2013) Mastitis incidence and bacterial causative agents isolated from lactating she-camel (*Camelus dromedaries*). IOSR J Agric Vet Sci 2:7-10.

Alemu S, Tamiru F, Almaw G, Tsega A (2013) Study on bovine mastitis and its effect on chemical composition of milk in and around Gondar Town, Ethiopia. J Vet Med Anim Health 5:215-221.

Ali M, Avais M, Ijaz M, Chaudhary M, Hussain R, Aqib AI, Khan NU, Sohail ML, Khan M, Khan MA, Ahmad M, Hasni MS, Qaiser I, Rashid G, Haq I, Khan I (2019) Epidemiology of Subclinical Mastitis in Dromedary Camels (*Camelus dromedarius*) of Two Distinct Agro-Ecological Zones of Pakistan. Pak J Zool 51:527-532.

Ali F, Hussain R, Qayyum A, Gul ST, Iqbal Z, Hassan MF (2016) Milk somatic cell counts and some hematobiochemical changes in sub-clinical mastitic dromedary she-camels (*Camelus dromedarius*). Pak Vet J 36:405-408.

Aljumaah RS, Almutairi FF, Ismail E, Alshaikh MA, Sami A, Ayadi M (2012) Effects of production system, breed, parity, and stage of lactation on milk composition of dromedary camels in Saudi Arabia. J Anim Vet Adv 11:141-147.

Alluwaimi AM, Al Mohammad Salem KT, Al-Ashqar RA, Al-Shubaith IH (2017) The Camel's (*Camelus Dromedarius*) Mammary Gland Immune System in Health and Disease. J Adv Dairy Res 5:1-6.

Barrón-Bravo OG, Gutiérrez-Chávez AJ, Ángel-Sahagún CA, Montaldo HH, Shepard L, Valencia-Posadas M (2013) Losses in milk yield, fat and protein contents acccording to different levels of somatic cell count in dairy goats. Small Rum Res 113:421-431.

Bhatt L, Chahar A, Tuteja FC, Verma D (2004) Prevalence, etiology and antibiogram of subclinical mastitis isolates from camel. Vet Pract 5:61-65.

Bianchi L, Bolla A, Budelli E, Caroli A, Casoli C, Pauselli M, Duranti E (2004) Effect of udder health status and lactation phase on the characteristics of Sardinian ewe milk. J Dairy Sci 87:2401-2408.

Contreras A, Corrales JC, Sanchez A, Sierra D (1997) Persistence of subclinical intramammary pathogens in goats throughout lactation. J Dairy Sci 80:2815-2819.

Eberlein V (2007) Hygienic status of camel milk in Dubai (United Arab Emirates) under tow different milking management systems. Dissertation Thesis. University of München, Germany.

Eissa EA, Yagoub AEA, Babiker EE, Ahmed IAM (2011) Physicochemical, Microbiological and Sensory Characteristics of Yoghurt Produced from Camel Milk During Storage. Electron J Environ Agric Food Chem 10:2305-2313.

Elbashir MHM, Elhassan SF (2018) Seasonal Effect on Camel Milk Composition (*Camelus dromedaries*) Under Traditional and Intensive Management Systems in Butana Area-Sudan. Am Sci Res J Eng Tech Sci 39:197-205.

Elobied AA, Osman AM, Abu Kashwa SM, Ali AS, Ibrahim MT, Salih MM (2015) Effect of parity and breed on some physico-chemical components of Sudanese camel milk. Res Opin Anim Vet Sci 5:20-24.

Eman Fathi M, Raghib RW, Saudi AM, El-Essawy HA (2012) Chemical and microbiological assessment of raw camel's milk with special reference to subclinical mastitis monitoring in Egypt. Assiut Vet Med J 58:1-15.

Fazlani SA, Khan SA, Faraz S, Awan MS (2011) Antimicrobial susceptibility of bacterial species indentified from mastitic milk samples of camel. Afr J Biotechnol 10:2959-2964.

Forbes BA, Sahm DF, Weissfield AS (2002) Bailey and Scotts Diagnostic Microbiology. 11th ed. Mosby Inc, Missouri.

Forsbäck L, Lindmark-Mansson H, Andrén A, Svennersten-Sjaunja K (2010) Evaluation of quality changes in udder quarter milk from cows with low-to-moderate somatic cell count. Animal 4: 617-626.

Gelasakis AI, Angelidis AS, Giannakou R, Filioussis G, Kalamaki MS, Arsenos G (2016) Bacterial subclinical mastitis and its effect on milk yield in low-input dairy goat herds. J Dairy Sci 99:3698-3708.

Gonçalves JL, Kamphuis C, Martins CMMR, Barreiro JR, Tomazi T, Gameiro AH, Hogeveen H, Dos Santos MV (2018) Bovine subclinical mastitis reduces milk yield and economic return. Livest Sci 210:25-32.

Gonzalo C, Ariznabarreta A, Carriedo JA, San Primitivo F (2002) Mammary Pathogens and their relationship to somatic cell count and milk yield losses in dairy Ewes. J Dairy Sci 85:1460-1467.

Gramay S, Ftiwi M (2018) Camel Milk Production, Prevalence and Associated Risk Factors of Camel Mastitis Inaysaita Woreda Afar Regional State, North East Ethiopia. ARC J Anim Vet Sci 4:17-37.

Guariglia BAD, Dos Santos PA, De Souza Araújo L, Giovannini CI, Neves RBS, Nicolau ES, Da Silva MAP (2015) Effect of the somatic cell count on physicochemical components of milk from crossbred cows. Afr J Biotechnol 14:1519-1524.

Hachana Y, Znaidi A, M'Hamdi N (2018) Effect of somatic cell count on milk composition and mozzarella cheese

quality. Acta Aliment 47:88-96.
Hadef L, Aggad H, Hamad B, Mahmoud MS, Adaika A (2016) Subclinical mastitis in dairy camels in Algeria: Comparison of screening tests. Acta Agric Slov 108:85-92.
Hadef L, Aggad H, Hamad B, Saied M (2018) Study of yield and composition of camel milk in Algeria. Scientific Study & Research Chemistry & Chemical Engineering, Biotechnology, Food Industry 19:1-11.
Hanuš O, Roubal P, Kučera J, Klimešová M, Jedelská R, Kopecký J (2017) Somatic cell count and milk yield losses in goats. Acta Univ Agric Silvic Mendelianae Brun 65: 1149-1160.
Husein A, Haftu B, Hunde A, Tesfaye A (2013) Prevalence of camel (*Camelus dromedaries*) mastitis in Jijiga Town, Ethiopia. Afr J Agric Res 8:3113-3120.
Kaikci G, Cetin O, Bingol EB, Gunduz MC (2012) Relations between electrical conductivity, somatic cell count, California mastitis test and some quality parameters in the diagnosis of subclinical mastitis in dairy cows. Turk J Vet Anim Sci 36:49-55.
Konuspayeva G, Faye B, Loiseau G (2009) The composition of camel milk: a meta-analysis of the literature data. J Food Compos Anal 22:95-101.
Konuspayeva G, Faye B, Loiseau G, Narmuratova M, Ivashchenko A, Meldebekova A, Davletov S (2010) Physiological change in camel milk composition (*Camelus dromedarius*) 2. Physicochemical composition of colostrums. Trop Anim Health Prod 42:501-505.
Legesse A, Adamu F, Alamirew K, Feyera T (2017) A Comparative Study on the Physicochemical Parameters of Milk of Camel, Cow and Goat in Somali Regional State, Ethiopia. Chem Sci J 8:4.
Leitner G, Merin U, Silanikove N (2011) Effects of glandular bacterial infection and stage of lactation on milk clotting parameters: Comparison among cows, goats and sheep. Int Dairy J 21:279-285.
Le Maréchal C, Thiéry R, Vautor E, Le Loir Y (2011) Mastitis impact on technological properties of milk and quality of milk products-a review. Dairy Sci Technol 91:247-282.
Marti De Olives A, Díaz JR, Molina MP, Peris C (2013) Quantification of milk yield and composition changes as affected by subclinical mastitis during the current lactation in sheep. J Dairy Sci 96:7698-7708.
Musaad AM, Faye B, Al-Mutairi SE (2013) Seasonal and physiological variation of gross composition of camel milk in Saudi Arabia. Emir J Food Agric 25:618-624.
Nagy P, Fábri N, Varga L, Reiczigel J, Juhász J (2017) Effect of genetic and nongenetic factors on chemical composition of individual milk samples from dromedary camels (*Camelus dromedarius*) under intensive management. J Dairy Sci 100:8680-8693.
NMC (1987) Laboratory and Field Handbook on Bovine Mastitis. National Mastitis Council Inc., Madison.
Ogola H, Shitandi A, Nanua J (2007) Effect of mastitis on raw milk compositional quality. J Vet Sci 8: 237-242.
Olechnowicz J, Sobek Z, Jakowski JM, Antosik P, Bukowska D (2010) Connection of somatic cell count and milk yield as well as composition in dairy ewes. Arch Tierz 53:95-100.
Pleguezuelos FJ, De La Fuente LF, Gonzalo C (2015) Variation in Milk Yield, Contents and Incomes According to Somatic Cell Countin a Large Dairy Goat Population. J Adv Dairy Res 3: 145.
Pradieé J, Moraes CR, Gonçalves M, Vilanova MS, Corrêa GF, Lauz OG, Osorio MTM, Schmidt V (2012) Somatic cell count and California castitis cest as a diagnostic tool for subclinical mastitis in ewes. Acta Sci Vet 40: 1038.
Quinn PJ, Markey BK, Leonard FC, Hartigan P, Fanning S, FitzPatrick ES (2011) Veterinary Microbiology and Microbial Disease. 2nd ed. John Wiley and Sons Ltd, Chicester, UK.
Rysanek D, Babak V (2005) Bulk tank milk somatic cell count as an indicator of the hygiene status of primary milk production. J Dairy Res 72:400-405.
Saleh SK, Faye B (2011) Detection of subclinical mastitis in dromedary camels (*Camelus dromedarius*) using somatic cell counts, California mastitis test and udder pathogen. Emir J Food Agric 23:48-58.
Seifu E, Tafesse B (2010) Prevalence and etiology of mastitis in traditionally managed camels (*Camelus dromedarius*) in selected pastoral areas in eastern Ethiopia. Ethiop Vet J 14:103-113.
Sharif A, Muhammad G (2008) Somatic cell count as an indicator of udder health status under modern dairy production: A review. Pak Vet J 28:194-200.
Shuiep ES, El Zubeir IEM, El Owni OAO Musa HH (2008) Influence of season and management on composition of raw camel (*Camelus dromedarius*) milk in Khartoum State, Sudan. Trop Subtrop Agroecosyst 8:101-106.
Summer A, Malacarne M, Sandri S, Formaggioni P, Mariani P, Franceschi P (2012) Effects of somatic cell count on the gross composition, protein fractions and mineral content of individual ewe milk. Afr J Biotechnol 11:16377-16381.
Tesfaye GY, Regassa FG, Kelay B (2010) Milk yield and associated economic losses in quarters with subclinical mastitis due to *Staphylococcus aureus* in Ethiopian crossbred dairy cows. Trop Anim Health Prod 42:925-931.
Toroitich KC, Gitau GK, Kitala PM, Gitao GC (2017) The prevalence and causes of mastitis in lactating traditionally managed one-humped camels (*Camelus dromedarius*) in West Pokot County, Kenya. Livest Res Rural Dev 29: Article 62.
Yarabbi H, Mortazavi A, Mehraban M, Sepehri N (2014) Effect of somatic cells on the physic-chemical and microbioal properties of raw milk in different seasons. Int J Plant Anim Environ Sci 4:289-298.

Ying C, Wang HT, Hsu JT (2002) Relationship of somatic cell count, physical, chemical and enzymatic properties to the bacterial standard plate count in dairy goat milk. Liv Prod Sci 17:63-77.

Younan M, Ali Z, Bornstein S, Muller W (2001) Application of California mastitis test in intra mammary *Streptococcus agalactiae* and *Staphylococcus aureus* infection of camels (*Camelus dromedaries*) in Kenya. Prev Vet Med 51:307-316.

Zhao X, Lacasse P (2008) Mammary tissue damage during bovine mastitis: causes and control. J Anim Sci 86:57-65.

Acta Biologica Szegediensis

Volume 63(2):91-101, 2019
Acta Biologica Szegediensis
http://abs.bibl.u-szeged.hu/index.php/abs

DOI:10.14232/abs.2019.2.91-101

ARTICLE

Micromorphological, anatomical and molecular study of *Hedera* species (Araliaceae) in Iran

Elham Amini[1], Fatemeh Nasrollahi[2], Ali Sattarian[1*], Mahboobeh Haji Moradkhani[1], Sohrab Boozarpour[1], Meisam Habibi[1]

[1]Department of Biology, Faculty of Sciences, Gonbad Kavous University, Gonbad, Iran.
[2]Department of Biology, Faculty of Sciences, University of Qom, Qom, Iran.

ABSTRACT *Hedera*, with 12 extant species, is a genus of evergreen climbers native to Europe, north Africa, and south Asia. In this study, the micromorphological, anatomical structure and molecular evidences of 11 populations from two species of *Hedera* (*H. helix* and *H. pastuchovii*) have been considered to evaluate the relationships in *Hedera*. In total, seven quantitative and qualitative characters of pollen were selected and measured. Based on this study, the anticlinal wall and surface sculpturing of seed support for separation of two species of *Hedera*. Micromorphology of epidermis illustrated two types of epidermal cells: puzzle-shaped and polygonal cells. Using nuclear (nrDNA ITS) marker, we reconstructed phylogenetic relationships within two species of *Hedera*. This data set was analyzed by phylogenetic methods including Bayesian inference, maximum likelihood, and maximum parsimony. In phylogenetic analyses, all members of two species formed a well-supported clade (PP = 1; ML/BS = 100/100) and divided into two major clades (A and B). Neighbor Net diagram demonstrated separation of the studied populations. The results showed that these taxa differ in taxonomically important micromorphological, anatomical and molecular characteristics and these data provide reliable evidence for separation of these two species.
Acta Biol Szeged 63(2):91-101 (2019)

KEY WORDS
anatomical structure
Hedera
Neighbor Net
nrDNA ITS
pollen
seed

ARTICLE INFORMATION
Submitted
18 July 2019.
Accepted
26 November 2019.
***Corresponding author**
E-mail: sattarian.ali@gmail.com

Introduction

Hedera L. (Araliaceae), with 12 extant species, is a genus of evergreen climbers native to Europe, north Africa, and south Asia (Vargas et al. 1999; Grivet and Petit 2002; Ackerfield and Wen 2003; Valcárcel et al. 2003a; Valcárcel and Vargas 2010; Valcárcel et al. 2014) and occupies forest under stories and riparian vegetation in temperate latitudes throughout Europe, N Africa and Asia (Meusel et al. 1965; Mabberley 1997). *Hedera* is a considerable element in Asian and European woodlands, comprising a large component of the forest understory.

The taxonomical treatments of *Hedera* published through the second half of the 20th century recognized between three and 19 species (Seemann 1868; Tobler 1912; Lawrence and Schulze 1942; Pojarkova 1951). More recently authors have accepted the 12 entities proposed by McAllister and Rutherford (McAllister 1982, 1988; Rutherford 1984, 1989; McAllister and Rutherford 1990; Rutherford et al. 1993) with slight changes at the subspecies level (Ackerfield and Wen 2002; Valcárcel 2008; Valcárcel and Vargas 2010). Since McAllister and Rutherford's treatment, the identification and delimitation of *Hedera* species have mainly been based on a combination of trichome morphology (stellate-multiangulate, stellate-rotate, and scale like hairs; Seemann 1868; Lum and Maze 1989; McAllister and Rutherford 1990; Ackerfield and Wen 2002; Valcárcel and Vargas 2010), juvenile leaf morphology (from entire to 3–7 lobate; Rutherford et al. 1993; Ackerfield and Wen 2002; Valcárcel 2008; Valcárcel and Vargas 2010), and ploidy level (from 29 to 89; Vargas et al. 1999).

Micromorphological characters are good diagnostic value to recognize many taxa, fundamentally in the species level. The pollen morphological analysis is successfully used as an additional document for delimitation of the taxa (Amini et al. 2018; 2019). Van Helvoort and Punt (1984) in the Northwest European Pollen Flora mentioned that pollen class of *Hedera* is 3-zonocolporate, sub erect to semi-erect with reticulate ornamentation. In Scandinavian pollen flora, apocolpium diameter of pollen grains is about 10 p. Colpi is narrow; exine thickness is about 2.5 p and sometimes distinctly thicker at poles (Erdtman et al. 1961).

The anatomical structure of some *Hedera* species

show that anatomical features can be valuable in species delimitation especially about similar taxa. Taxonomic value of epidermis anatomical features is well documented in botanical literature (Dilcher 1974; Metcalf 1985). Savulescu and Luchian (2009) studied the diagnostic value of *Hedera* epidermis and illustrated that epidermis is made up of only one cells layer with polygonal cells with thin lateral walls and corrugated.

Molecular data can provide extra criteria for systematic classification of the species studied that have been only based on the morphological characters (Chase et al. 1993). Nuclear ribosomal DNA provides highly informative variation that has been used to infer phylogenetic relationships in angiosperms. Its value stems from the high rate of divergence at the specific, and sometimes, the populational level (Baldwin 1993; Vargas et al. 1998; Vargas et al. 1999). The internal transcribed spacer (ITS) is the region of the 18S-5.8S-26S nuclear ribosomal cistron (Baldwin et al. 1995) and have often been used for inferring phylogeny at the generic and infrageneric relationships of genera (e.g., Baldwin 1992; Baldwin et al. 1995; Amini et al. 2018; Nasrollahi et al. 2019). Previous molecular and cytogenetic studies identified two main centers of diversity for *Hedera*, the eastern and western parts of the Mediterranean region. Molecular phylogenetic reconstructions of 37 of the 41 Araliaceae genera clearly placed *Hedera* within the Asian Palmate group (Lowry et al. 2001; Wen et al. 2001; Valcárcel et al. 2003; Plunkett et al. 2004).

Vargas et al. (1999) applied variation in chromosome number and internal transcribed sequences (ITS) of nrDNA to infer phylogenetic relationships of a wide range of *Hedera* species. Polyploidy was found to be frequent in *Hedera*, with diploid, tetraploid, hexaploid and octoploid populations being detected. Valcárcel and Vargas (2012) studied the phylogenetic reconstruction of key traits in the evolution of ivies (*Hedera* L.) and the analyses of the nrDNA ITS and plastid *trn*T-L sequences revealed multiple connections between the Mediterranean region and Asia and suggest recurrent colonization between these two areas. Valcárcel et al. (2014) studied the origin of the early differentiation of ivies (*Hedera*) and the radiation of the Asian Palmate group (Araliaceae). Genome incongruence and hard nuclear and plastid basal polytomies are detected for the Asian Palmate group where the lineage of *Hedera* is placed.

Despite ecological impacts and economic significance of *Hedera* to the horticultural industry, the taxonomy of *Hedera* is controversial and historical relationships are poorly defined.

The specific goals of this study were as follows: (1) to examine pollen and seed micro-morphological characters that could be useful for the diagnosis of taxa; (2) to determine the patterns of variation in epidermal characteristics in two species; (3) to evaluate the affinities and relationships of taxa; (4) to investigate molecular properties of *Hedera* in Iran.

Materials and Methods

Morphological methods

In the present study, 11 populations of two *Hedera* species were collected from different locations in North Iran and preserved in the Gonbad Kavous University Herbarium (GKUH). Identification of populations was carried out based on Flora Iranica (Browicz 1973). The list of voucher populations and details of localities are given in Table 1.

Palynological studies on pollens of *H. helix* L. and *H. pastuchovii* Woron. Ex Grossh was made using a light microscope (LM) (Olympus, Vanox AHBS3) with a DP12 digital camera and a scanning electron microscope (SEM; Tescan, *Vega*-3 *LMU*). For SEM investigations, the pollen grains were transferred directly to double-sided tape affixed stubs and were sputter-coated with gold plates. The applied terminology based on Punt et al. (2007). For LM studies, the samples were acetolyzed following Erdtman's technique (Erdtman 1952). The pollen samples were obtained mostly from freshly collected herbarium populations. The measurements were based on at least 30 pollen grains per population. The characters of pollen grains of the studied *Hedera* species are summarized in Table 2.

In order to detect significant differences in the studied characters among the investigated species, an analysis of variance (ANOVA) was done. To determine the species relationships, we have used cluster analysis and principal component analysis (PCA; Ingrouille 1986). For multivariate analysis, the mean of the quantitative characters was calculated. Qualitative characters were coded as binary or multistate. Variables were standardized for multivariate statistical analysis. Average taxonomic distances and squared Euclidean distances were calculated as dissimilarity coefficient in the cluster analysis of pollen data. In order to determine the most variable characters among the studied species, factor analysis based on principal components analysis was performed. SPSS ver. 20 and PAST ver. 2.17c (2013) softwares were performed for statistical analysis.

Seeds of the two species of *Hedera* were taken from herbarium samples: before mounted directly on aluminum stubs using double-sided adhesive, they were examined under a stereomicroscope to ensure the normal size and development. After having been coated with a thin layer (ca. 25 nm) of gold they were analyzed using a SEM (Tescan, *Vega*-3 *LMU)* at an accelerating voltage of 15-22 kV at

Table 1. List of species used in the study along with localities and vouchers.

Taxa	Collection data	GenBank accession no./ITS
H. helix L.	Tehran: Research Institute of Forests and Rangelands, Haji Moradkhani, 803298, GKUH	LC508655
H. helix	Golestan: Gonbad Kavous, Haji Moradkhani, 803297, GKUH	LC508656
H. helix	Fars: Kamfiruz, Tang-e Bostan, Haji Moradkhani, 803299, GKUH	LC508657
H. pastuchovii Woron. Ex Grossh.	Golestan: Gorgan, Naharkhoran forest, Haji Moradkhani, 803270, GKUH	LC508658
H. pastuchovii	Golestan: Gorgan, Ziarat village, Haji Moradkhani, 803273, GKUH	LC508659
H. pastuchovii	Gilan: Gisum forest, Haji Moradkhani, 803289, GKUH	LC508660
H. pastuchovii	Gilan: Fuman forest, Mirmahaleh, Haji Moradkhani, 803292, GKUH	LC508661
H. pastuchovii	Gilan: Somee Sara, Haji Moradkhani, 803290, GKUH	LC508662
H. pastuchovii	Mazandaran: Nur forest, Haji Moradkhani, 803279, GKUH	LC508663
H. pastuchovii	Mazandaran: Najardeh, Haji Moradkhani, 803278, GKUH	LC508663
H. pastuchovii	Mazandaran: Sari, Haji Moradkhani, 803295, GKUH	LC508665
Trevesia palmata Vis.	GenBank	KF591487
Brassaiopsis mitis Clarke	GenBank	AY304801

GKUH: Gonbad Kavous University Herbarium

Research Institute of Razi (Tehran, Iran). For recording gross morphology and size parameters, at least 10 seeds were measured.

Anatomical methods

All materials were boiled for 15 min, and then fixed in Carnoy solution (alcohols to acetic acid in proportion 3:1). The epidermis was separated with H_2O_2 and acetic acid (1:1), in order to prepare the leaves. Materials were kept warm in a tube with previous lotions (the above-mentioned solutions) for 4 hours, then the leaves were cleaned. After cleaning, the materials were washed in distilled water. Epidermis separation followed. Epidermal samples were stained with 2% aceto-carmine and were mounted on microscopic glass slides. Slide sections were studied and photographed with the help of an Olympus light microscope by using a Olympus DP12 Digital Camera. Some characters (stomata length/weight, number of stomata, number of epidermal cells) were measured with Image Tools ver. 3.0 and Axio Vision 4.8. (Table 5).

Molecular methods

Taxon sampling

Sampling includes plants from 3 populations of *H. helix* and 8 populations *H. pastuchovii* were chosen as ingroup for nrDNA ITS. *Trevesia palmata* Vis. and *Brassaiopsis mitis* Clarke were chosen as outgroup following previous molecular phylogenetic studies (Wen et al. 2001). A list of all the taxa used in this study and the sources,

Table 2. Pollen morphological characters for the examined taxa of *Hedera*.

Taxon	Length of polar axis (µm ± SD)	Length of equatorial axis (µm ± SD)	P/E	Shape	Colpus length (µm ± SD)	Colpus width (µm ± SD)	Ornamentation
H. helix	21.55 ± 1.48	18.77 ± 0.43	1.14	Subprolate	18.60 ± 0.12	1.23 ± 0.05	Microperforate
H. helix	21.05 ± 1.17	19.65 ± 0.27	1.07	Subprolate	18.80 ± 0.09	1.14 ± 0.01	Microperforate
H. helix	22.05 ± 1.17	18.65 ± 0.27	1.07	Subprolate	17.80 ± 0.09	1.25 ± 0.01	Microperforate
H. pastuchovii	38.75 ± 2.03	27.37 ± 0.32	1.41	Prolate	24.70 ± 0.15	2.05 ± 0.09	Reticulate
H. pastuchovii	33.65 ± 1.19	24.43 ± 0.35	1.37	Prolate	25.16 ± 0.16	2.74 ± 0.04	Reticulate
H. pastuchovii	36.79 ± 1.18	25.67 ± 0.29	1.43	Prolate	23.96 ± 0.07	2.63 ± 0.01	Reticulate
H. pastuchovii	38.73 ± 1.31	27.35 ± 0.34	1.41	Prolate	24.36 ± 0.21	2.85 ± 0.03	Reticulate
H. pastuchovii	34.65 ± 1.36	22.43 ± 0.31	1.54	Prolate	25.10 ± 0.16	2.70 ± 0.01	Reticulate
H. pastuchovii	36.75 ± 0.41	24.47 ± 0.44	1.50	Prolate	23.98 ± 0.12	2.34 ± 0.07	Reticulate
H. pastuchovii	37.64 ± 0.34	25.35 ± 0.17	1.48	Prolate	25.49 ± 0.28	2.45 ± 0.04	Reticulate
H. pastuchovii	35.44 ± 0.38	23.65 ± 0.28	1.49	Prolate	25.70 ± 0.19	2.78 ± 0.06	Reticulate

voucher information and GenBank accession numbers are given in Table 1.

DNA extraction, PCR and sequencing

Total genomic DNA was extracted from dried leaf materials deposited in Gonbad Kavous University Herbarium (GKUH), using Kit method. The nrDNA ITS (Nuclear ribosomal DNA Internal Transcribed Spacer) region was amplified using the primers ITS5m of Sang et al. (1995) and ITS4 of White et al. (1990). PCR amplification of the DNA regions followed procedures described in detail by Naderi Safar et al. (2014). The quality of PCR products was checked by electrophoresis in 1% agarose gels in 1 × TAE (pH 8) buffer and were photographed with an UV gel documentation system (UVItec, Cambridge, UK). PCR products along with the same primers were sent for Sanger sequencing at Macrogen (Seoul, South Korea) through Pishgam (Tehran-Iran).

Sequence alignment

Single dataset was aligned using the web-based version of MUSCLE (Edgar 2004, at http://www.ebi.ac.uk/Tools/msa/muscle/) under default parameters followed by manual adjustment. The alignment of dataset required the introduction of numerous single and multiple-base indels (insertions/deletions). Positions of indels were treated as missing data for the ITS dataset.

Phylogenetic inferences

Parsimony method

Maximum parsimony (MP) analyses were conducted using PAUP* version 4.0a157 (Swofford 2002). The heuristic search option was employed for nuclear dataset using tree bisection-reconnection (TBR) branch swapping, with 1000 replications of random addition sequence and an automatic increase in the maximum number of trees. Uninformative characters were excluded from the analyses. Branch support values (MPBS) were estimated using a full heuristic search with 1000 bootstrap replicates (Felsenstein 1985) each with simple addition sequence.

Likelihood method

Maximum likelihood (ML) analyses were carried out using the RAxML-HPC2 on XSEDE (8.2.8) at the CIPRES Science Gateway. Bootstrap values (LBS) were calculated in RAxML-HPC2 based on 1000 replicates with one search replicate per bootstrap replicate.

Bayesian inference

For Bayesian inference (BI) analyses, models of sequence evolution were selected using the program MrModeltest version 2.3 (Nylander 2004) based on the Akaike information criterion (AIC) (Posada and Buckley 2004). This program indicated a GTR+G model for nrDNA ITS. BI analyses were performed using MrBayes version 3.2 (Ronquist et al. 2012) on the CIPRES Science Gateway (Cyber infrastructure for Phylogenetic Research cluster) (Miller et al. 2010, https://www.phylo.org) for the dataset. Bayesian analyses were performed, with default priors (uniform priors) and the best-fit model of sequence evolution for dataset, with two runs of ten million generations and four simultaneous chains (one cold and three heated with a heating parameter of 0.2), by saving trees every 100 generations. The trees sampled after discarding 25% as "burn-in" were collected to build a 50% majority rule consensus phylogram were used to calculate posterior probability values (PP). Tree visualization was carried out using Tree View version 1.6.6 (Page 2001).

Phylogenetic networks

NeighborNet (NN) a distance-based network construction method (Bryant and Moulton 2004) was implemented in SplitsTree4, version 4.14.4 (Huson and Bryant 2006) based on the uncorrected *p*-distance between populations that was calculated from the ITS sequence data. The ITS matrice was modified prior to analysis by excluding the outgroup.

Results

Pollen morphology

The pollen grains of the studied species revealed some variations and separated two species of *Hedera*. All palynological structures and measurements for the examined species concerning pollen type from polar view, polar (P) and equatorial (E) measurements, P/E ratio, colpus length and width, pollen shape and exine ornamentation were shown in Table 2. Selected SEM micrographs of the pollens and their surfaces are shown in Fig. 1. Generally, type of pollen grain aperture is observed tricolporate among studied species (Fig. 1). Length of polar and equatorial axis were found useful in separating two species. Polar axis (P) length of pollen grains ranging from the smallest size for *H. helix* (21.05 μm) to the largest size for *H. pastuchovii* (38.75 μm). Equatorial axis (E) length of pollen grains ranged from the smallest size in *H. helix* (18.65 μm) to the largest size in *H. pastuchovii* (27.37 μm). The shape classes are based on the ratio between the length of polar axis (P) and equatorial diameter (E) (Erdtman 1952). The P/E ratio ranged from 1.07 to 1.54, therefore the pollen shape is subprolate in *H. helix* but prolate in *H. pastuchovii*. The ornamentation of tectum is microperforate in *H. helix* (Fig. 1B) and is reticulate in *H. pastuchovii* (Fig. 1C).

In order to define the diagnostic value of pollen grains

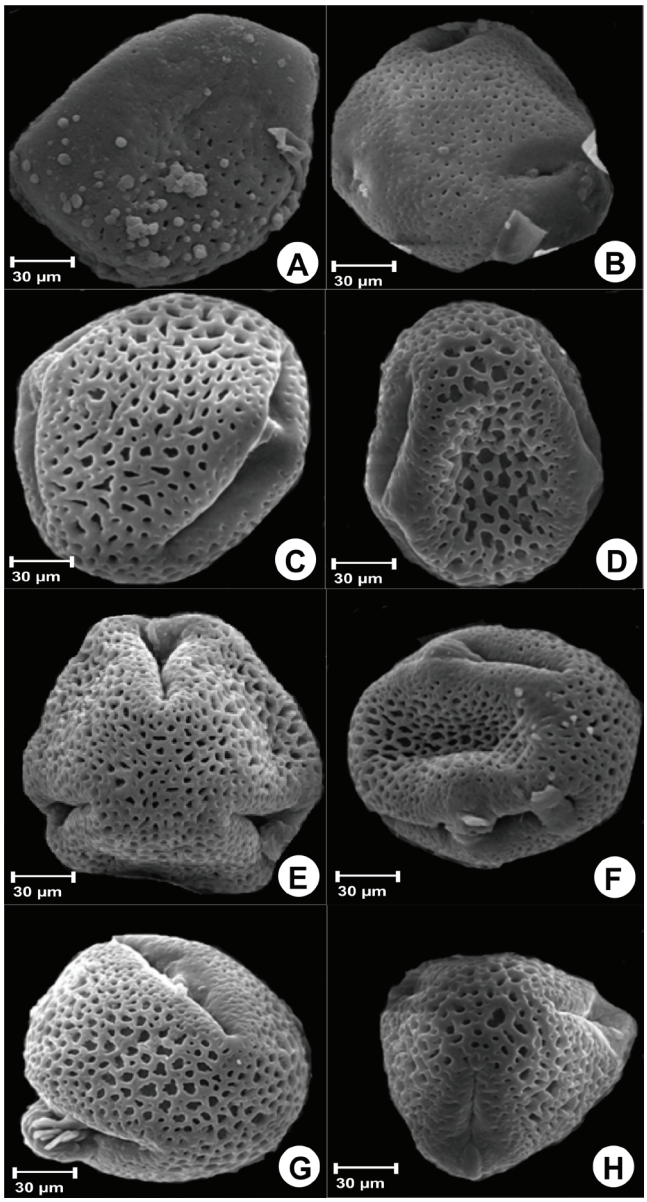

Figure 1. Scanning electron micrographs (SEM) of pollen surface in *H. helix* and *H. pastuchovii*. (A, B) *H. helix*, (C, D) *H. pastuchovii*, (E, F) *H. pastuchovii*, and (G, H) *H. pastuchovii*.

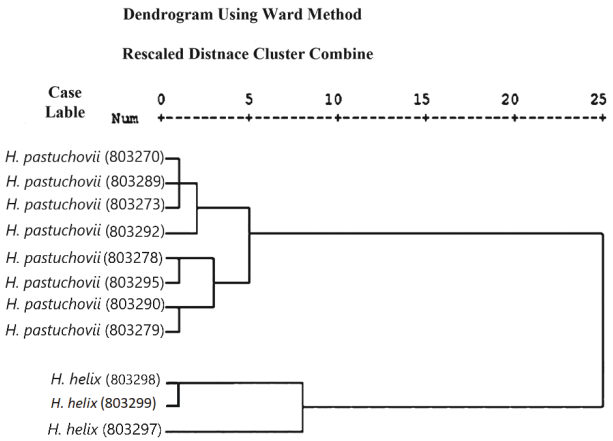

Figure 2. Cluster analysis (Ward's method) based on pollen features of *Hedera*.

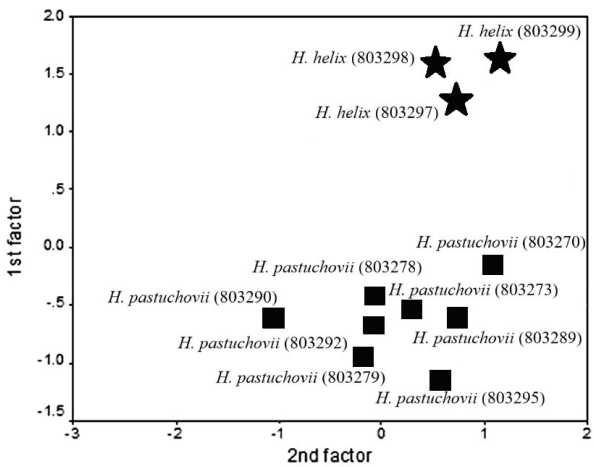

Figure 3. PCA plot of *Hedera* species based on observed pollen data.

in species delimitations in studied *Hedera* species, cluster analysis by Ward's method was performed on the base of seven qualitative and quantitative features (Fig. 2). Ward's dendrogram showed two main clusters (Fig. 2). First cluster composed of populations of *H. helix*. Second cluster composed of two subclusters and contained populations of *H. pastuchovii*. Principal component analysis revealed that there were two components providing more than 76% of total observed variation in studied pollen grains. Studying the component loading was evident that shape and ornamentation of tectum are most important features in the first factor and P/E ratio and length of polar axis are most significant in the second factor. PCA confirmed the results of cluster analysis by Ward's method based on qualitative and quantitative features of pollen grains (Fig. 3).

Seed shape and size

Taxonomic importance of selected seed features in the examined taxa are summarized in Table 3. Selected SEM micrographs of the seeds and their surfaces are shown in Fig. 4. Seed size differs significantly between two species of *Hedera*. Generally, seeds of *H. helix* are slightly smaller than those of *H. pastuchovii*. The length of the seeds ranged from 3.18 mm in *H. helix* to 5.45 mm in *H. pastuchovii* (column 2 in Table 3), and their width varied from 2.08 mm in *H. helix* to 4.87 mm in *H. pastuchovii* (column 3 in Table 3). In general, the seeds shapes have been observed

Table 3. Some diagnostic seed micromorphological features in species of *Hedera*.

Taxon	Length (mm)	Width (mm)	Length/Width	Shape	Anticlinal wall	Sculpturing
H. helix	3.40 ± 0.01	2.08 ± 0.04	1.63	Almond to Circular	Shallowly undulate	Smooth
H. helix	3.38 ± 0.04	2.18 ± 0.05	1.55	Almond to Circular	Shallowly undulate	Smooth
H. helix	3.18 ± 0.02	2.28 ± 0.04	1.39	Almond to Circular	Shallowly undulate	Smooth
H. pastuchovii	5.15 ± 0.06	4.28 ± 0.04	1.20	Almond to Circular	Deeply undulate	Polygonal
H. pastuchovii	5.25 ± 0.02	4.47 ± 0.06	1.17	Almond to Circular	Deeply undulate	Polygonal
H. pastuchovii	5.15 ± 0.03	4.87 ± 0.05	1.05	Almond to Circular	Deeply undulate	Polygonal
H. pastuchovii	5.30 ± 0.02	4.37 ± 0.06	1.21	Almond to Circular	Deeply undulate	Polygonal
H. pastuchovii	5.05 ± 0.01	3.67 ± 0.07	1.37	Almond to Circular	Deeply undulate	Polygonal
H. pastuchovii	5.18 ± 0.04	4.27 ± 0.06	1.21	Almond to Circular	Deeply undulate	Polygonal
H. pastuchovii	5.20 ± 0.01	4.17 ± 0.06	1.24	Almond to Circular	Deeply undulate	Polygonal
H. pastuchovii	5.45 ± 0.07	4.16 ± 0.02	1.31	Almond to Circular	Deeply undulate	Polygonal

almond to circular in two species (Figs. 4A and 4G).

Seed Sculpturing

In terms of exomorphology, the surface of the seed in *H. helix* is smooth and the anticlinal walls are shallowly undulate (Figs. 4B, 4D and 4F). In *H. pastuchovii*, the seeds have a polygonal surface and the anticlinal walls are observed deeply undulate (Figs. 4H, 4J and 4L).

Epidermal cell description

Epidermal and stomata characters of the leaves, such as cell shape, anticlinal wall patterns, stomata index, density, size, and types were examined (Table 4). There were two types of epidermal cells: puzzle-shaped and polygonal cells could be seen, and anticlinal walls have been observed the wavy and sinuous shapes. There are polygonal cells with wavy anticlinal walls on the adaxial leaf side of *H. helix* (Figs. 5A). Puzzle-shaped cells with sinuous cell walls were seen in *H. pastuchovii* (Figs 5C, 5E and 5G). Abaxial leaf epidermal cells were irregular, with wavy anticlinal walls in *H. helix* (Fig. 5B). No stomata were seen on the adaxial surface of the examined species (Figs. 5A and 5C). All studied species had stomata on the abaxial leaf surface. All treated populations were of the anemocytic stomata type (Figs. 5B and 5D). The largest in size stomata were observed in *H. pastuchovii* (Figs. 5F and 5H) and the smallest were observed in *H. helix* (Fig. 5B). The maximum stomatal index and density were registered in *H. helix* (Table 4).

Table 4. Leaf epidermal anatomical features of *Hedera*.

Adaxial epidermis				Abaxial epidermis				
Taxon	Cell shape	Anticlinal walls	Stomatal apparatus cell	Anticlinal walls	Stomata index (mm^2)	Stomata density (mm^2)	Stomata size (µm)	Stomata type
H. helix	Pol	Wa	-	Irr	7 ± 0.01	191.70 ± 2.3	49.62 × 42.24	Anemocytic
H. helix	Pol	Wa	-	Irr	9 ± 0.04	198.50 ± 4.3	46.31 × 40.43	Anemocytic
H. helix	Pol	Wa	-	Irr	7 ± 0.02	189.32 ± 3.3	52.41 × 46.34	Anemocytic
H. pastuchovii	Puz	Sin	-	Sin	11 ± 0.09	120.25 ± 2.1	71.32 × 66.24	Anemocytic
H. pastuchovii	Puz	Sin	-	Sin	13 ± 0.02	107.18 ± 1.4	62.45 × 53.14	Anemocytic
H. pastuchovii	Puz	Sin	-	Sin	12 ± 0.03	132.23 ± 1.2	61.41 × 54.32	Anemocytic
H. pastuchovii	Puz	Sin	-	Sin	10 ± 0.04	121.16 ± 3.2	72.43 × 65.30	Anemocytic
H. pastuchovii	Puz	Sin	-	Sin	12 ± 0.01	95.19 ± 2.5	65.25 × 51.20	Anemocytic
H. pastuchovii	Puz	Sin	-	Sin	10 ± 0.04	108.14 ± 4.2	60.42 × 52.33	Anemocytic
H. pastuchovii	Puz	Sin	-	Sin	13 ± 0.07	135.28 ± 1.7	73.40 × 62.30	Anemocytic
H. pastuchovii	Puz	Sin	-	Sin	12 ± 0.09	140.19 ± 3.5	65.41 × 55.34	Anemocytic
H. pastuchovii	Puz	Sin	-	Sin	14 ± 0.04	153.14 ± 4.2	72.35 × 66.30	Anemocytic
H. pastuchovii	Puz	Sin	-	Sin	13 ± 0.03	109.24 ± 6.5	66.40 × 58.34	Anemocytic

Irr: Irregular; **Pol**: Polygonal; **Puz**: Puzzle-shaped; **Sin**: Sinuous; **Wa**: Wavy.

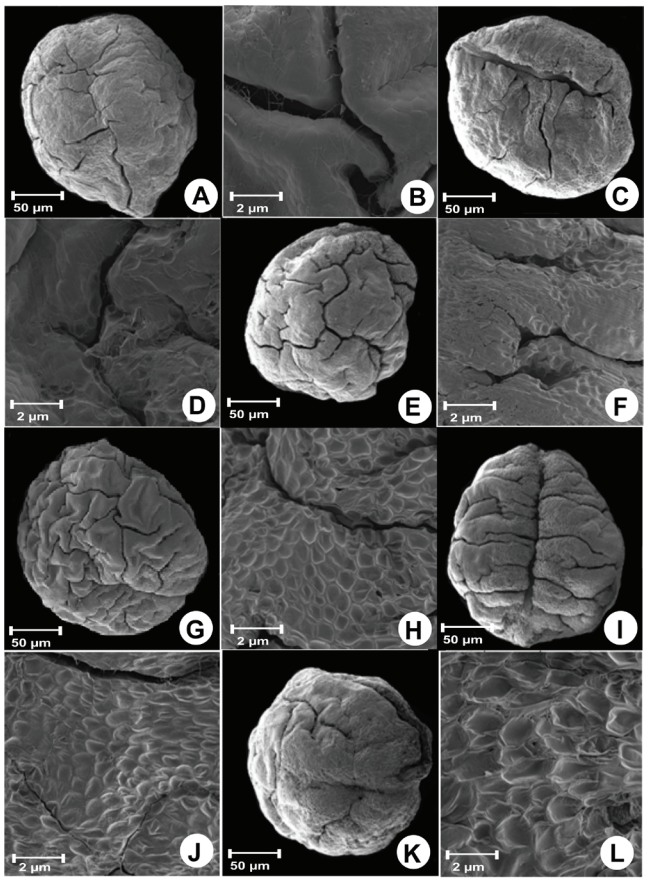

Figure 4. Scanning electron micrographs (SEM) of seed surface in *H. helix* and *H. pastuchovii*. For each taxon, the first micrograph shows the outline of the seed indicating its general shape, and the second micrograph is a close view of the seed surface.(A, B) *H. helix*, (C, D) *H. helix*, (E, F) *H. helix*, (G, H) *H. pastuchovii*, (I, J) *H. pastuchovii*, and (K, L) *H. pastuchovii*.

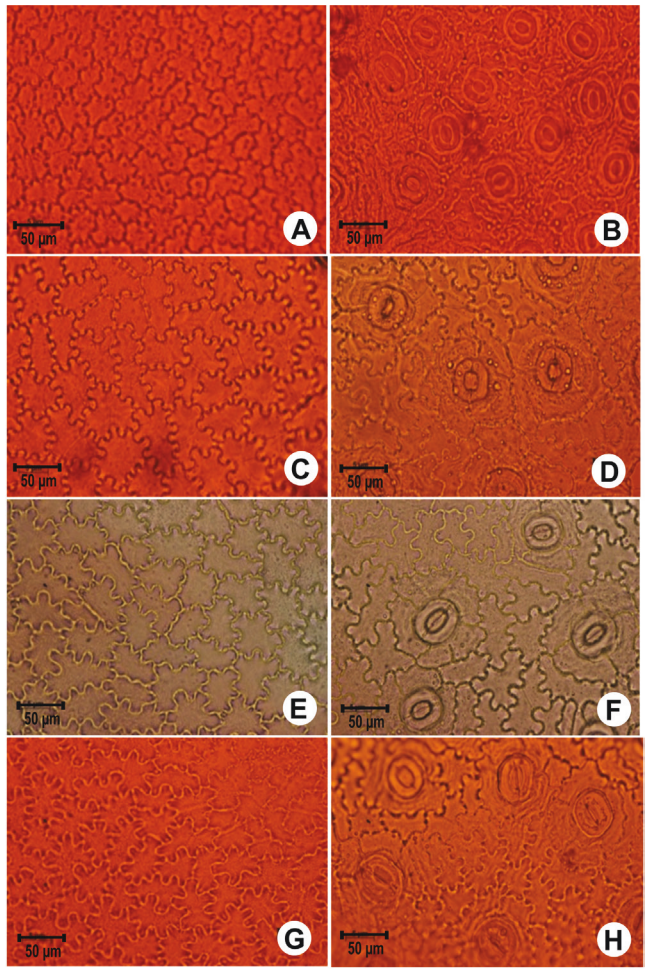

Figure 5. Epidermal cells on the adaxial and abaxial side of the specimens' leaves: shape, size, anticlinal wall and stomata under light microscopy.(A, B) *H. helix*, (C, D) *H. pastuchovii*, (E, F) *H. pastuchovii*, and (G, H) *H. pastuchovii*.

Phylogenetic analysis

Detailed information about alignment characteristics, selected model of nucleotide substitution, as well as tree statistics from the single analysis of the nrDNA ITS region, are summarized in Table 5. The aligned nrDNA ITS matrix comprises 602 characters. The maximum parsimony, maximum likelihood and Bayesian analyses of the nrDNA ITS produced congruent trees and gave similar results. All members of this genus form a well-supported clade (PP = 1, ML/BS = 100/100) (Fig. 6). The *Hedera* clade is composed of two clades. Clade A includes the populations of *H. helix* (PP = 0.96, ML/BS = 98/100) and the clade B (PP = 0.95, ML/BS = 100/100) comprises the rest of the species of *Hedera* (*H. pastuchovii*) (Fig. 6).

Phylogenetic networks

The NeighborNet diagram (Fig. 7) revealed almost complete separation of the studied populations within the network, supporting the phylogenetic results that the *Hedera* is composed of two clades. Populations of *H. helix* (1, 2 and 3) are distinct and stand separately from the other

Table 5. Dataset and tree statistics from single analysis of the nuclear region.

Total sample	nrDNA ITS
Number of sequences	13
Number of ingroup sequences	11
Alignment length [bp]	602
Number of parsimony- informative characters	56
Number of MPTs	16
Length of MPTs	74
Consistency index (CI)	0.98
Retention index (RI)	0.87
Evolutionary model selected (under AIC)	GTR+G

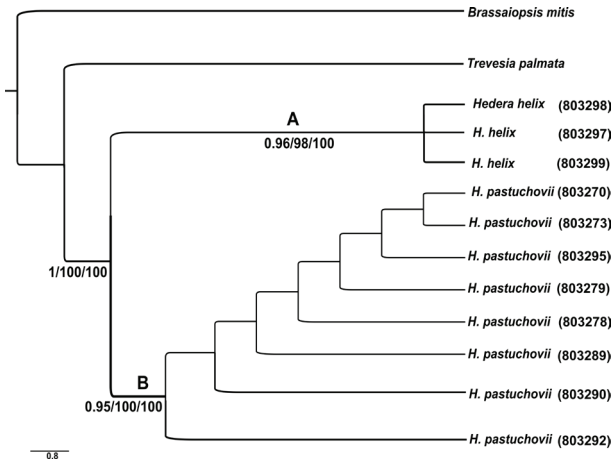

Figure 6. Consensus tree (50% majority rule) resulting from the Bayesian phylogenetic analysis of the nrDNA ITS dataset. Numbers of the branches are posterior probability (PP) from the BI and bootstrap support (BS) values from a MP and ML analysis, respectively (values <50% were not shown).

populations at a major distance. The groups formed in the splits graph are readily correlated to the clades recovered in the phylogenies. We use the term "lineage" to refer to groups of populations in the NN diagram (Fig. 7), and "clade" to refer to groups in the phylogenies (Fig. 6). The ITS splits graph revealed two main groups (Fig. 7). One of these, lineage "I" correlates to clade "A" in Fig. 6 and is composed of populations of *H. helix*. The later, lineage "II" that is includes the populations of *H. pastuchovii*, corresponding to clade "B" in Fig. 6. Populations of *H. pastuchovii* (4-11) show a more near genetic affinity and are placed close to each other (Fig. 7).

Discussion

Hedera has gained little attention in previous micromorphological and phylogenetic studies, hence, this study presents the first comprehensive investigation of this genus in Iran. Our achievement provides statistical support for the recognition of two species as well as the two major groups traditionally recognized in *Hedera* based on trichomes: the stellate group (*H. helix*) and the scale-like group (*H. pastuchovii*) in agreement with Valcárcel and Vargas (2010). Natural distribution of *H. helix* is Europe and ploidy level and somatic chromosome number of it is 2n = 2x = 48. Whereas *H. pastuchovii* distributed mainly in Caucasus, Iran and Afghanistan with 2n = 6x = 144 somatic chromosome number. In general, it can be concluded that, reproductive traits such as pollen and seed traits have achieved the end of their evolution and are valuable in systematic studies. Pollen grains of *H. helix* are smaller rather than *H. pastuchovii*. This is consistent with their different ploidy level that *H. helix* is diploid (2n = 2x = 48), whereas *H. pastuchovii* is hexaploid (2n = 6x = 144) (Valcárcel and Vargas 2010).

In consistence with finding of Savulescu and Luchian (2009), our results show that epidermis is made up of only one cells layer with polygonal cells with thin lateral walls and corrugated. Stomata are present on the lower (abaxial) surfaces of leaves only. Locality and habitats of the species also significantly affect the stomata density. *Hedera helix* occupies forest and open woodlands with high humidity. In woodland habitats, it frequently forms a dense ground cover occupying large areas and made up of many individuals (Metcalfe 1958). So high stomata density was observed in *H. helix* and low density in *H. pastuchovii*. Two species demonstrated an anemocytic type of stomata. Stomata have a significant role as valuable differentiating characters at different levels of plant ecology, taxonomy and physiology. Furthermore, the stomata type, density and structure may affect plant physiology, water efficiency and biomass (Luo and Zhou 2001). Humidity in the forest areas can affect the stomata density because the plants do not suffer from drought in such areas. Generally, plants have different strategies to cope with ecological factors. The findings in the current study are in accord with those in other studies relating to the stomata and structure (Miller 1983).

Plant molecular studies chiefly advanced in the recent years and molecular phylogenetic investigation has dramatically alternated our views of organismal relationships (Soltis and Soltis 2000). Nuclear molecular technique has been successfully used for research of infraspecific variations in different genera (Sheidai et al. 2013, 2014). Therefore, we decided to use the molecular approach for research of infra-specific variations between *Hedera* species. The results of molecular studies based on nuclear DNA sequence data are congruent with taxonomy.

Phylogenetic analyses indicated the monophyly of *Hedera* with strongly support (PP = 1.00, ML/BS = 100/100) and divided into two major clades. Our result is also in concordance with Vargas et al. (1999) and that

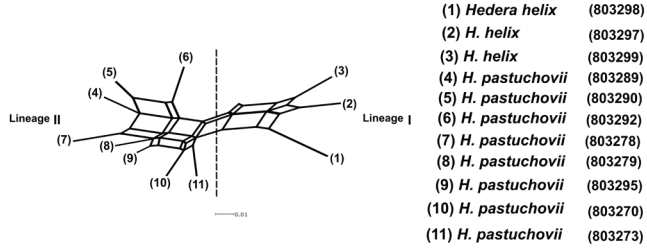

Figure 7. NeighborNet for ITS sequences of *Hedera*. Two major groups were recovered (i.e., lineage I and lineage II).

in their analysis *H. helix* is belonging to diploid clade and *H. pastuchovii* is nested in polyploid clade. Molecular study (nrDNA ITS and *trn*T-L sequences) conducted by Valcárcel and Vargas (2012), did not confirm any close relationship between *H. helix* and *H. pastuchovii*. Thus, it is maybe due to variable levels of polyploidy and low gene flow between these two species. Even though, we confirm the monophyly of the genus *Hedera* relationships among populations of each species in clades A and B, were poorly resolved and form a polytomy. NeighborNet analysis of data set displayed a clear correlation between genetic clusters and geographical groups as natural distribution of *H. helix* is Europe, Whereas *H. pastuchovii* distributed mainly in Asia. Geographical distribution of genetic diversity is also consistent with this cytotaxonomic diversity pattern as the highest genetic diversity is found in the Mediterranean basin while other areas have lower levels of genetic diversity (Vargas et al. 1999; Grivet and Petit 2002; Ackerfield and Wen 2003; Valcárcel et al. 2003; Valcárcel 2008; Green et al. 2011).

In conclusion, present study was carried out to provide additional evidence for taxonomists. These taxa differ in taxonomically important micromorphological and molecular characteristics. Generally, statistical and bioinformatics tests revealed the great difference between two species. In fact, sequence divergence among populations of each species was generally low, resulting in a lack of phylogenetic resolution, so it is necessary to use chloroplast markers and some other molecular techniques useful at the population level for example AFLP, ISSR, microsatellites to better resolve the relationships between the populations of one species. A number of fast evolving genes will be necessary for resurrecting subspecies or verities in these two species.

Acknowledgements

The authors would like to thank Razi Institute (Tehran, Iran) staff for their assistance in scanning electron microscope, and all of persons who helped us in this research work. The present study was financially supported by Gonbad Kavous University.

References

Ackerfield J, Wen J (2002) A morphometric analysis of *Hedera* L. (the ivy genus, Araliaceae) and its taxonomic implications. Adansonia 324:197-212.

Ackerfield J, Wen J (2003) Evolution of *Hedera* (the ivy genus, Araliaceae): insights from chloroplast DNA data. Int J Pl Sci 164:593-602.

Amini E, Nasrollahi F, Sattarian A, Khormali A, Habibi M (2019) Micro-morphological and molecular study of four species of *Lonicera* (Caprifoliaceae) in Iran. Phytol Balc 25(2):181-190.

Amini E, Kazempour-Osaloo Sh, Maassoumi AA, Zare-Maivan H (2018) Phylogeny, biogeography and divergence times of *Astragalus* section *Incani* DC. (Fabaceae) inferred from nrDNA ITS and plastid *rpl*32-*trn*$L_{(UAG)}$ sequences. Nord J Bot 37. DOI: 10.1111/njb.02059.

Amini E, Nasrollahi F, Sattarian A, Kor S, Boozarpour S (2018) Molecular and micro-morphological evidences of the genus *Cuscuta* in Iran. Rostaniha 19:113-129.

Baldwin BG, Sanderson MJ, Porter JM, Wojciechowski MF, Campbell CS, Donoghue MJ (1995) The ITS region of nuclear ribosomal DNA: a valuable source of evidence on angiosperm phylogeny. Ann Missouri Bot Gard 82:247-277.

Baldwin BG (1992) Phylogenetic utility of the internal transcribed spacers of nuclear ribosomal DNA in plants: An example from the Compositae. Mol Phyl Evol 1:3-16.

Browicz K (1973) *Hedera*. In Rechinger KH, ed., Flora Iranica. Akademische Druck-U. Verlagsanstalt, Graz, Austria. 1-4.

Bryant D, MoultonV (2004) NeighborNet: An agglomerative method for the construction of phylogenetic networks. Mol Biol Evol 21:255-265.

Chase MW, Soltis DE, Olmstead RG, Morgan D, Les DH, Mishler BD, Duvall MR, Price RA, Hills HG, Qiu Y-L, Kron KA, Rettig JH, Conti E, Palmer JD, Manhart JR, Sytsma KJ, Michaels HJ, Kress WJ, Karol KG, Clark WD, Hedren M, Gaut BS, Jansen RK, Kim KJ, Wimpee CF, Smith JF, Furnier GR, Strauss SH, Xiang Q-Y, Plunkett GM, Soltis PS, Swensen SM, Williams SE, Gadek PA, Quinn CJ, Eguiarte LE, Golenberg E, Learn GH, Jr, Graham SW, Barrett SCH, Dayanandan S, Albert VA (1993) Phylogenetics of seed plants: an analysis of nucleotide sequences from the plastid gene rbcL. Ann Missouri Bot Gard 80:528-580.

Edgar RC (2004) Muscle: Multiple sequence alignment with high accuracy and high throughput. Nucl Acids Res 32:1792-1797.

Erdtman G (1952) Pollen Morphology and Plant Taxonomy. Angiosperms. Chronica Botanica Co., Waltham, Massachusettes. Copenhagen.

Erdtman G, Praglowski J, Nilsson S (1963) An Introduction to a Scandinavian Pollen Flora II. Almqvist and Wiksell, Uppsala, 89 pp.

Felsenstein J (1985) Confidence limits on phylogenies: An approach using the bootstrap. Evolution 39:783-791.

Green AF, Ramsey TS, Ramsey J (2011) Phylogeny and biogeography of Ivies (*Hedera* spp., Araliaceae), a polyploid complex of woody vines. Syst Bot 36:1114-1127.

Grivet D, Petit RJ (2002) Phylogeography of the common ivy

(*Hedera* sp.) in Europe: genetic differentiation through space and time. Mol Ecol 11:1351-1362.
Hammer O, Harper DAT, Ryan PD (2001) PAST: Paleontological statistics software package for education and data analysis. Palaeontol Electron 4:1-9.
Huson DH, Bryant D (2006) Application of phylogenetic networks in evolutionary studies. Mol Biol Evol 23:254-267.
Ingrouille MJ (1986) The construction of cluster webs in numerical taxonomic investigation. Taxon 35:541-545.
Lawrence GHM, Schulze AE (1942) The cultivated Hederas. Gentes Herbarum 6:107-173.
Lowry PP II, Plunkett GM, Wen J (2001) Generic relationships in Araliaceae: looking into de crystal ball. S African J Bot 70:382-392.
Lum C, Maze J (1989) A multivariate analysis of the trichomes of *Hedera* L. Watsonia 17:409-418.
Luo Y, Zhou ZK (2001) Cuticle of *Quercus* sugen. *Cyclobalanopsis* (Oerst.) Chneid. (Fagaceae). Acta Phytophysiol Sin 39:489-501.
Mabberley DJ (1997) The Plant-book. A portable dictionary of the vascular plants. Cambridge University Press, Cambridge.
McAllister HA (1982) New work on ivies. Int Dendrol Soc 1981:106-109.
McAllister HA (1988) Canary and Algerian ivies. The Plantsman 10:27-29.
McAllister HA, Rutherford A (1990) *Hedera helix* L. and *H. Hibernica* (Kirchner) bean (Araliaceae) in the British Isles. Watsonia 18:7-15.
Metcalfe DJ (1958) *Hedera helix* L. Biological Flora of The British Isles. List Br Vasc Pl, No. 268.
Metcalfe CR, Chalk L (1985) Anatomy of Dicotyledons. Vols I and III. Oxford University Press.
Meusel H, Jäger E, Weinert E (1965) Vergleichende Chorologie der Zentraleuropäischen Flora. Veb Gustav Fischer Verlag, Jena.
Miller EC (1983) Plant Physiology. McGrow Hill Book Company, New York, USA.
Miller MA, Pfeiffer W, Schwartz T (2010) Creating the CIPRES Science Gateway for Inference of Large Phylogenetic Trees. Proceedings of the Gateway Computing Environments Workshop (GCE), New Orleans, Louisiana. Piscataway: IEEE. 45-52.
Naderi Safar K, Kazempour-Osaloo Sh, Maassoumi AA, Zrre Sh (2014) Molecular phylogeny of *Astragalus* section *Anthylloidei* (Fabaceae) inferred from nrDNA ITS and plastid *rpl*32-*trn*$L_{(UAG)}$ sequence data. Turkish J Bot 38:637-652.
Nasrollahi F, Kazempour-Osaloo Sh, Saadati N, Mozaffarian V, Zare-Maivan H (2019) Molecular phylogeny and divergence times of *Onosma* (Boraginaceaes.s.) based on nrDNA ITS and plastid *rpl*32-*trn*$L_{(UAG)}$ and *trn*H–*psb*A sequences. Nordic J Bot, DOI: 10.1111/njb.02060.
Nylander JAA (2004) MrModeltest v2. Program distributed by the author. Evolutionary Biology Centre. Uppsala University, Uppsala.
Page DM (2001) Tree View (Win32) version 1.6.6. Available: http://taxonomy.zoology.gla.ac.uk/rod/treeview.html.
Plunkett GM, Wen J, Lowry PP II (2004) Infrafamilial classifications and characters in Araliaceae: insights from the phylogenetic analysis of nuclear (ITS) and plastid (*trn*L-*trn*F) sequence data. Plant Syst Evol 245:1-39.
Pojarkova AI (1951) The Chinese species of ivy and their taxonomic and geographic connections. Nat Syst ex Herb Bot nom V.L. Komarovii Acad Sci URSS XIV, 224-264.
Posada D, Buckley TR (2004) Model selection and model averaging in phylogenetics: Advantages of akaike information criterion and Bayesian approaches over likelihood ratio tests. Syst Biol 53:793-808.
Punt W, Reitsma TJ, Reuvers AAML (1976) The Northwest European pollen flora, 2. Caprifoliaceae. Rev Palaeobot Palynol 17:5-29.
Punt W, Hoen PP, Blackmore S, Nilsson S, Thomas AL (2007) Glossary of pollen and spore terminology. Rev Palaeobot Palynol 143:1-81.
Ronquist F, Teslenko M, van der Mark P, Ayres DL, Darling A, Höhna S, Larget B, Liu L, Suchard MA, Huelsenbeck JP (2012) MrBayes 3.2: efficient Bayesian phylogenetic inference and model choice across a large model space. Syst Biol 61:539-542.
Rutherford A (1984) The history of the Canary Islands ivy and its relatives. Ivy J 10:13-18.
Rutherford A (1989) The ivies of Andalusia (Southern Spain). Ivy J 15:7-17.
Rutherford A, McAllister HA, Mill RR (1993) New ivies from the Mediterranean area and Macaronesia. The Plantsman 15:115-128.
Sang T, Crawford DJ, Stuessy T (1995) Documentation of reticulate evolution in peonies (*Paeonia*) using internal transcribed spacer sequences of nuclear ribosomal DNA: Implication for biogeography and concerted evolution. Proc Natl Acad Sci USA. 92:6813-6817.
Savulescu E, Luchian V (2009) Comparative anatomy of the vegetative organs of the *Hedera helix*. (Araliaceae). Sci Papers, USAMV Bucharest, Ser A, Vol LII.
Seemann B (1868) Revision of the Natural Order Hederaceae. L Reeve and Co., London.
Sheidai M, Zanganeh S, Haji-ramezanali R, Nouroozi M, Noormohammadi Z, Ghsemzadeh-baraki S (2013) Genetic diversity and population structure in four *Cirsium* (Asteraceae) species. Biologia 68:384-397.
Sheidai M, Ziaee S, Farahani F, Talebi SY, Noormohammadi Z, Hasheminejad-Ahangarani-Farahani Y (2014) Infraspecific genetic and morphological diversity in *Linum album* (Linaceae). Biologia 69:32-39.
Soltis DE, Soltis PS (2000) Contributions of plant molecular

systematics to studies of molecular evolution. Plant Mol Biol 42:45-75.

Swofford DL (2002) PAUP*: Phylogenetic Analysis Using Parsimony (*and Other Methods), Version 4.0b10. Sunderland: Sinauer Associates.

Tobler F (1912) Die Gattung *Hedera*. Gustav Fischer, Jena.

Valcárcel V (2008) Taxonomy, systematics and evolution of *Hedera* L. (Araliaceae). Ph.D. dissertation, Universidad Pablo de Olavide, Sevilla, Spain (English/Spanish).

Valcárcel V, Vargas P (2012) Phylogenetic reconstruction of key traits in the evolution of ivies (*Hedera* L.). Plant Syst Evol, DOI: 10.1007/s00606-012-0734.

Valcárcel V, Fiz O, Vargas P (2003) Chloroplast and nuclear evidence for multiple origins of polyploids and diploids of *Hedera* (Araliaceae) in the Mediterranean basin. Mol Phylogenet Evol 27:1–20.

Valcárcel V, Vargas P (2010) Quantitative morphology and species delimitation under the general lineage concept: optimization for *Hedera* (Araliaceae). Amer J Bot 97:1555-1573.

Valcárcel V, Fiz-Palacios O, Wenc J (2014) The origin of the early differentiation of Ivies (*Hedera* L.) and the radiation of the Asian Palmate group (Araliaceae). Mol Phylogenet Evol 70:492-503.

Van Helvoort HAM, Punt W (1984) The Northwest European Pollen Flora, 29. Araliaceae. Rev Palaeobot Palynol 42:1-5.

Vargas P, McAllister HA, Morton C, Jury SL, Wilkinson MJ (1999) Polyploid speciation in *Hedera* (Araliaceae): phylogenetic and biogeographic insights based on chromosome counts and ITS sequences. Pl Syst Evol 219:165-179.

Wen J, Plunkett GM, Mitchell AD, Wagstaff SJ (2001) The evolution of Araliaceae: a phylogenetic analysis based on ITS sequences of nuclear ribosomal DNA. Syst Bot 26:144-167.

White TJ, Bruns T, Lee S, Taylor J (1990) Amplification and direct sequencing of fungal ribosomal RNA genes for phylogenetics. In Innis MA, Gelfand DH, Sninsky JJ, White TJ, eds, PCR Protocols: A Guide to Methods and Applications. Academic Press, San Diego. 315-322.

Acta Biologica Szegediensis

Volume 63(2):103-111, 2019
Acta Biologica Szegediensis
http://abs.bibl.u-szeged.hu/index.php/abs
DOI:10.14232/abs.2019.2.103-111

ARTICLE

Physiological and morphological responses of sugar beet (*Beta vulgaris* L.) subjected to nano-boron oxide at different growth stages

Alireza Pirzad*, Mahmood Mazlomi Mamyandi, Razieh Khalilzadeh

[1] Department of Plant Production and Genetics, Faculty of Agriculture and Natural Resources, Urmia University, Urmia, Iran

ABSTRACT The deficiency and toxicity of boron may lead to noticeable yield reduction and quality loss of sugar beet. To evaluate the effects of nano-boron on the root yield and quality of sugar beet, factorial experiment was conducted based on a randomized complete block design with three replications at Urmia University. Treatments were spraying of nano-boron oxide (0, 2, 3 and 4 g L^{-1}) at different growth stages (20, 40, 60, 80 and 100% of ground cover). Increasing levels of boron up to 3 g L^{-1} resulted in the highest SPAD (Soil Plant Analysis Development) value, leaf number and relative water content. With optimal leaf area (86.47 cm^2), the highest yields of root, sugar, white sugar, and technological sugar (144.53, 28.23, 26.19 and 25.32 t ha^{-1}) were determined in the treatment of 4 g L^{-1} boron at 40% of ground covered. Increasing nano-boron level under different growth stages increased sugar and white sugar contents, on contrary impurities (Na, K and α-amino-N) loss and molasses sugar percentage were decreased. More than 3 g L^{-1} nano-boron exhibited the highest values of purity. Application of 3 g L^{-1} boron at 40% of ground cover increased sugar and white sugar contents by 12.45 and 18.72%, respectively. **Acta Biol Szeged 63(2):103-111 (2019)**

KEY WORDS
growth stage
impurity
sugar beet
molasses sugar
nano-boron

ARTICLE INFORMATION
Submitted
18 December 2019.
Accepted
03 February 2020.
***Corresponding author**
E-mail: a.pirzad@urmia.ac.ir

Introduction

Sugar beet (*Beta vulgaris* L., Amaranthaceae) is one of the important sugar crops with high yield, high adaptability and high biological activity. It is also rich in minerals and organic nutrients (Grzegorzewski et al. 2017). Although sugar beet is well adapted to a wide range of growing conditions and soils, nutritional disorders caused by boron deficiency are quite common (Dordas 2007). Sustainable production requires the efficient use of inputs including adequate and balanced fertilization of both macro- and micro-nutrients (Singh et al. 2017). Deficiency of soil nutrients such as nitrogen (N), phosphorus (P), potassium (K), zinc (Zn) and boron (B) should be added to the rhizosphere according to plant needs and has been known as the major limitations in beet crop production (Abidow 2012). Boron is unique among the essential mineral micronutrients because of normal presence in soil solution as a non-ionized molecule over the vast pH range (Hirparan et al. 2018). It is also essential for plant in development and growth (Abido 2012) through the cell wall structure, membrane integrity and function (Nyomora et al. 2019), sugar translocation from source to sink (Rawashdeh and Sala 2013) physiological functions such as carbohydrates metabolism, indole acetic acid metabolism, formation amino acid (Singh et al. 2017), nitrogen fixation (Rawashdeh and Sala 2013) and photosynthetic pigments (Abd El-hady 2017).

Deficiency of boron causes reduction in photosynthesis due to disturbs the activities of proton pumping ATPase and electron transport chain (Nadeem et al. 2019; Rehman et al. 2018), inhibition of leaf expansion, inhibitions root elongation through limiting mitosis and cell enlargement and division (Gemici et al. 2003), early enlargement due to clear limitation of its phloem mobility and reduced growth of new shoots and leaf (Ullah et al. 2013; Ali et al. 2015). Without an adequate supply and consumption of boron in large quantities, it may lead to marked yield reduction and quality loss of sugar production in soil application (Abbas et al. 2014; Tlili et al. 2017; Armin and Asgharipour 2012). Because boron has been considered to have only limited phloem mobility and cannot readily be redistributed within the plant (Brown et al. 1999), the amount of yield losses directly depends upon the duration of deficiency and the plant growth stage at which it occurs (Ali et al. 2015). Deficiencies of boron result in many anatomical, biochemical and physiological changes

in plants (Ali et al. 2015). Therefore, the management of boron in soil has become a worldwide agricultural problem in the recent years (Tlili et al. 2017).

Foliar fertilization has the advantage of low application rates, treated rapidly, uniform distribution and quick plant responses to applied nutrients (Asad et al. 2003; Saadati et al. 2013). Moreover, a number of previous studies have increased the significance of the role of foliar boron application in the productivity of crop plants (Perica et al. 2001; Dordas 2006; Abido 2012; Kristek et al. 2006). Also, to get the desired results, nanomaterial can be utilized by foliar application with much-decreased concentration (Prasad et al. 2012). After entering the cells the nanoparticles transport from one cell to another through plasmodesmata. The chemical and biological activities of most substances increase at the nanoscale (Dewdar et al. 2018). Root yield, sugar percentage significantly increased by increasing boron doses (Abbas et al. 2014). Dordas et al. (2006) reported that spraying of boron lead to a higher quality of sugar and root yield compared to the time using boric acid mixed with soil. El-Geddawy and Makhlouf (2015) found that there was a significant positive increase in root diameter and root length of sugar beet due to the gradual increase in the spraying concentration of boron from 105 to 210 ppm. Armin and Asgharipour (2012) reported that the maximum root yield and sugar percentage was achieved by foliar application of 12% boric acid. Abd El-hady (2017) reported that root and sugar yields were increased by 19.4% and 39.5% compared with control treatment.

A better understanding of the physiological basis of the response of sugar beet may help in programs aiming to evaluate yield. Therefore, this work aimed to evaluate the effects of different amounts and time of nano-boron oxide spraying on the quantitative and qualitative aspects of sugar beet.

Materials and Methods

Site and experimentation

All experiments were conducted during 2011-2012 cropping seasons in North-Western Iran Iran, i.e. Naghadeh (27°45' N latitude and 22°37' E longitude; Alt 1300 m) and were situated in the wet zone with moderate winter and hot summer. The experimental design was randomized factorial experiment based on a randomized complete block design with three replications. The soil type was silty loam and possessed around 7.95 pH, EC about 2.3 dS m^{-1}, total organic C = 1.20% and Zn = 32 mg kg^{-1}. The experimental soil was fertilized with 250 kg N ha^{-1} in the form of urea (was applied as ½ at sowing, ½ at 6-8 leaf), 250 kg P ha^{-1} in the form of triple superphosphate, and 100 kg K ha^{-1} in the potassium nitrate at planting time. Experiment factors were the amount of nano-boron (Nano-B) oxide concentration (0, 2, 3 and 4 g L^{-1} of nano chelate powder, with 99.5% of purity and 80 nm particle size, obtained from Khazra Company containing 9% chelated boron, absorbable at pH 3-11, and completely soluble in water) and spraying time included (20, 40, 60, 80 and 100 of ground cover by plant canopy). Each plot was consisted of 5 rows with 5 m long. The inter row and intra-row spacing was 10 and 15 cm, respectively. The sugar beet cultivar (Montarosa cv. a commonly grown cultivar of sugar beet in Naghdeh area) was sown at the depth of 20 cm on May 10.

Measurements of quantity and quality parameters of sugar beet

Harvesting was done manually 180 days after sowing (DAS). In order to measure the root length (cm), root diameter (cm) and leaf number traits, 10 plants in each plot were randomly harvested. Root yield (t ha^{-1}) was obtained from plants harvested of 5 m^2 in each experimental unit and juice quality characteristics were analyzed. The percentage of sucrose was determined according to Le-Docte (1927). Sodium and potassium (%) were determined by using a flame photometer (Model 410 Classic), nitrogen was determined according to the semi-micro Kjeldahl method (Model NA 1500) (Edwards 2014). Total soluble solids (TSS%) was measured in fresh roots using hand refractometer (model REF-113ATC). Juice purity% was also determined as a ratio between sucrose% and TSS% according to Carruthers and Oldfield (1961).

Sugar yield and root quality were calculated via the following equations:

$$SY\ (t\ ha^{-1}) = RY\ (t\ ha^{-1}) \times SC(\%)$$

Where, SY: sugar yield; RY: root yield; SC: sugar content.

$$MS = 0.12\ (K + Na) + 0.24(\alpha\text{-amino-N}) + 0.48$$

Where, MS: molasses sugar (%); K: potassium (mmol/100 g root), Na: sodium (mmol/100 g root); α-amino-N: alpha-amino-nitrogen (mmol/100 g root) (Buchholz et al. 1995).

$$AC: (K + Na)/\ N.$$

Where, AC: alkalinity coefficient.

$$WSC(\%) = SC\% - MS\%$$

Where, WSC: white sugar content.

$$WSY\ (t\ ha^{-1}) = RY \times WSC\ \%$$

Where, WSY: white sugar yield.

$$TSY\ (t\ ha^{-1}) = RY\ (t\ ha^{-1}) \times [SC\ (\%) - \text{loss of sugar productivity}\ (\%)]$$

Where, TSY: technological sugar yield (Buchholz et al. 1995).

$$LSP\ (\%) = MS\ (\%) + 0.6$$

Where, LSP: loss of sugar productivity (Carruthers et al.1961).

$$\text{Sugar productivity (SP)} = \frac{\text{SC - loss of sugar productivity}}{\text{SC}}$$

Where, SP: sugar productivity.

The leaf length was measured as the distance between the beginning of leaf formation on the leaf stem and the top of the leaf. The leaf width was measured at its widest point with a ruler. Based on measured leaf width (W, mm) and leaf length (L, mm) the area of each leaf (A, mm²) is calculated using the following relationship (Mirschel 2018):

$$A = W \times L \times 0.675$$

The chlorophyll content of leaves was estimated with a SPAD-502 (Konica Minolta Sensing, Osaka, Japan) (Jifon et al. 2019). Relative water content was estimated according to the method of Tambussi et al. (2005).

Analysis of variance (ANOVA) and means comparison on data was performed using the SAS Statistical Package Program. Least Significant Difference (LSD) method was used to test the differences between means comparison of main effects and interactions.

Results

Analysis of variance showed that the significant interaction effect between Nano-B concentration and spraying stage on the relative water content (RWC), leaf area, root length, root and sugar yield, white and technological sugar yield, sugar content, white sugar content, sugar productivity, loss of sugar productivity, sodium, potassium, α-amino-N and molasses sugar. There was a significant effect of Nano-B foliar application on the alkalinity coefficient (Table 1). SPAD, leaf number, root diameter, purity% and TSS% were affected by the Nano-B concentration and spraying stage (Table 1).

Chlorophyll index, relative water content, leaf area and leaf number

The maximum of SPAD (73.50) and leaf number (52.26) was obtained in B_3 and B_4, respectively (Table 1). Chlorophyll index was increased about by 34.71% in 3 g L^{-1} Nano-B (Table 1). The highest content of SPAD and leaf number markedly increased from spraying of Nano-B at 80 of ground cover as G_4 (Table 1). However, the difference in mention traits was not statistically significant in a comparison between G_2, G_3 and G_4. The increasing of Nano-B at all growing stages up to 3 g L^{-1} resulted in the highest RWC. The highest and lowest RWC was respectively achieved in B_3G_2 and B_1G_5 (Table 2). A gradual increase in leaf area as growth stages improved up to G_4 was recorded regardless of boron levels. The application of B_3G_4 caused an increase in leaf area of 60% in comparison with B_1G_4.

Root length and diameter

It could be noticed that increasing boron rates significantly increased root diameter. The plant sprayed with 3 g L^{-1} of nano- boric acid revealed the highest root diameter (12.70 cm). Data also cleared that the late application of boron (G_4) recorded the highest value of root diameter (12.79 cm). Results showed that, the crops were fertilized early or late at different rates of boron, had any considerable differences on root length. Application of 2 g L^{-1} at 100% of ground covered (B_2G_5), produced the highest root length (38.16 cm), while the lowest value (25.50 cm) was recorded in the B_1G_1 (Table 2).

Sugar beet yields

Application of 4 g boron L^{-1} at the early stage of plant (40% ground cover), can significantly increase root yield (144.53 t ha^{-1}), sugar yield (28.23 t ha^{-1}), white sugar yield (26.19 t ha^{-1}), and technological sugar yield (25.32 t ha^{-1}) to the highest amounts. Spraying nano-boric acid at the levels of B_2, B_3 and B_4 increased root yield by about 29%, 48% and 79% at early growth stage (G_2), as compared to control treatment (B_1), respectively. However, Abd El-hady (2017) reported that B element (1.0 kg B/ha) was increased root and sugar yields by 19.4% and 39.5% compared with control treatment.

Quality of sugar beet

The highest sugar and white sugar content were found to be in the B_3G_2 treatment with average of 19.86% and 18.39%, respectively. However, their effects were also similar to B_4G_2. Also, the lowest of SC and WSC are related to B_1G_1 treatment with an average of 15.80% and 14.14%, respectively (Table 3). Compared to the control, spraying 3 g L^{-1} Nano-B at 40% of ground covered improved SC and WSC by 12.45% and 15.37%, respectively. Data in Table 1

Table 1. Effects of nano-boron oxide concentration and spraying time (growth stage) on growth and yield of sugar beet.

Nano-B (B)	SPAD	RWC (%)	Leaf number	Leaf area (mm^2)	Root length (cm)	Root diameter (cm)	Root yield	Sugar yield	WSY	TSY
							($t\ ha^{-1}$)			
B_1 = no nano-B as control	54.56b	73.98b	33.73c	49.52c	26.70c	10.73b	88.77d	14.93d	13.39d	12.86d
B_2 = 2 g L^{-1}	59.55b	82.07a	41.46b	67.63b	30.53b	11.23b	108.25c	18.92c	17.26c	16.61c
B_3 = 3 g L^{-1}	73.50a	84.82a	52.26a	74.55ab	31.00b	11.36b	117.09b	21.73b	20.05b	19.35b
B_4 = 4 g L^{-1}	68.35a	83.27a	49.33a	82.85a	34.68a	12.70a	127.65a	24.15a	22.42a	21.65a
LSD (p<0.05)	5.20	4.08	4.96	10.47	2.49	1.24	8.05	1.70	1.60	1.55
Growth stage (G)										
G_1= 20% of ground cover	58.89b	81.74ab	41.58b	55.65c	28.87cd	10.25c	98.94b	17.28b	15.82b	15.23b
G_2 = 40% of ground cover	64.38a	83.48a	44.16ab	69.57abc	27.91d	11.04bc	114.39a	21.36a	19.65a	18.96a
G_3 = 60% of ground cover	65.70a	81.59ab	46.16ab	73.80ab	30.26bc	11.26bc	113.007ab	20.69a	19.09a	18.41a
G_4 = 80% of ground cover	66.92a	81.68ab	48.08a	80.15a	31.20b	12.79a	115.52a	20.40ab	18.66ab	17.96ab
G_5 = 100% of ground cover	64.07ab	76.69b	41b	64.03bc	35.37a	12.18ab	110.35ab	19.94ab	18.19ab	17.53ab
LSD (p<0.05)	5.36	5.53	5.30	14.18	2.10	1.33	14.49	3.33	3.24	3.16
B × G	ns	**	ns	*	**	ns	**	*	**	*
C.V.	10.14	5.18	14.51	14.96	8.28	11.89	7.12	8.31	8.55	8.65

ns: show no significant differences.
* and **: show significant differences at 0.05 and 0.01 probability level, respectively.
RWC: relative water content; WSY: white sugar yield; TSY: technological sugar yield.

Table 1 (Continued). Effects of nano-boron oxide concentration and spraying time (growth stage) on growth and yield of sugar beet.

Nano-B (B)	SC (%)	WSC (%)	Purity %	SP	LSP	Na	K	α-amino-N	AC	MS	TSS %
						(mmol/100 g root)					
B_1 = no nano-B as control	16.84b	15.11c	75.92c	0.861d	2.33a	1.20a	6.84a	1.18a	6.99c	1.73a	22.20a
B_2 = 2 g L^{-1}	17.50b	15.96b	82.83b	0.877c	2.13b	0.79b	6.27b	0.85b	8.46b	1.53b	21.15b
B_3 = 3 g L^{-1}	18.54a	17.11a	92.12a	0.890b	2.03c	0.68b	5.77c	0.74b	8.97b	1.43c	20.18bc
B_4 = 4 g L^{-1}	18.90a	17.54a	95.72a	0.896a	1.96d	0.52c	5.61c	0.60c	10.44a	1.36d	19.91c
LSD (p<0.05)	0.69	0.67	4.90	0.005	0.07	0.117	0.45	0.118	1.12	0.07	0.96
Growth stage (G)											
G_1= 20% of ground cover	17.40b	15.92b	88.42a	0.879b	2.08ab	0.69b	7.07abc	0.77a	9.00a	1.47ab	19.95c
G_2 = 40% of ground cover	18.53a	17.009a	88.30a	0.884a	2.12ab	0.70b	6.30ab	0.84a	8.71a	1.52ab	21.09abc
G_3 = 60% of ground cover	18.21ab	16.77ab	85.26ab	0.886a	2.044b	0.82a	5.61c	0.80a	8.73a	1.44b	21.43ab
G_4 = 80% of ground cover	17.58ab	16.06ab	81.89b	0.878b	2.11ab	0.90a	6.00bc	0.87a	8.44a	1.51ab	21.54a
G_5 = 100% of ground cover	18.01	16.41ab	89.38a	0.877b	2.20a	0.87a	6.63a	0.93a	8.70a	1.60a	20.30bc
LSD (p<0.05)	0.99	1.072	4.68	0.0043	0.137	0.094	0.59	0.22	1.65	0.137	1.22
B × G	**	*	ns	*	**	**	**	*	ns	**	ns
C.V.	4.06	4.42	6.54	0.58	2.63	14.23	6.56	16.43	17.11	3.66	5.20

ns: show no significant differences.
* and **: show significant differences at 0.05 and 0.01 probability level, respectively.
SC: sugar content; WSC: white sugar content; K: potassium; Na: sodium; α-amino-N: alpha-amino-nitrogen; AC: alkalinity coefficient; TSS: total soluble solids; SP: sugar productivity; LSP: loss of sugar productivity MS: molasses sugar.

noticeably showed that B_4 and B_3 treatments recorded the highest values of purity percentage by 95.72% and 92.12%, respectively. It is worth mentioning that, considerable differences in purity% were not significant (Table 1). The later application at G_5 insignificantly surpassed the earlier application at G_5 in effecting purity%. Increasing the doses of B application from 0 to 4 g L^{-1} provided the lowest LSP and MS 1.79 and 1.19 % with a decrease of 20.44% and 27.87%, respectively at the 60% of ground covered.

Root impurities (K, Na and α-amino-N) and AC

The values of impurities differed greatly due to the different treatments of time and boron rates (Table 3). There was a negative relationship between impurities and boron

Table 2. Means comparison the effects of Nano-B concentration and spraying time (growth stage) on RWC, leaf area, root length, root yield, sugar yield, WSY and TSY of sugar beet.

Treatment		RWC (%)	Leaf area (mm^2)	Root length (cm)	Root yield	Sugar yield	WSY	TSY
Nano-B	Growth stage				($t\ ha^{-1}$)			
B_1	G_1	77.34±3.65	52.10±6.53	25.50±2.50	82.87±7.17	13.08±1.055	11.17±0.89	11.21±0.85
	G_2	79.18±2.06	50.66±2.51	26.66±1.52	80.93±1.88	14.28±0.42	12.90±0.39	12.41±0.39
	G_3	75.65±2.64	58.61±6.88	25.33±1.52	90.56±9.19	15.06±1.72	13.55±1.54	13.01±1.49
	G_4	79.16±3.50	57.57±2.97	27.50±2.17	100.88±8.64	16.39±1.17	14.68±1.09	14.08±1.04
	G_5	58.57±5.09	28.69±1.69	36.16±1.89	88.61±8.10	15.84±1.66	14.13±1.47	13.60±1.42
B_2	G_1	81.64±3.22	51.49±6.04	31.33±1.25	98.36±6.93	17.43±1.02	15.99±0.96	15.40±0.92
	G_2	82.22±3.87	66.32±10.35	27.50±2.00	112.21±5.77	19.13±0.73	17.46±0.67	16.79±0.65
	G_3	82.33±1.86	74.23±15	34.56±3.84	106.85±10.80	19.51±1.46	17.91±1.36	17.26±1.30
	G_4	81.25±1.16	84.36±5.99	34.83±2.84	115.25±10.36	19.68±2.05	17.87±1.99	17.18±1.93
	G_5	82.93±2.44	61.78±17.16	38.16±2.25	108.61±7.77	18.87±2.30	17.09±2.10	16.44±2.05
B_3	G_1	85.23±4.76	53.45±4.49	29.16±1.52	111.17±3.47	19.11±0.85	17.58±0.78	16.92±0.78
	G_2	88.86±9.10	74.83±9.15	25.66±2.36	119.89±10.14	23.81±2.23	22.05±2.10	21.34±2.05
	G_3	85.41±1.38	76.06±12.47	33.00±4.35	119.06±13.26	22.97±2.30	21.28±2.19	20.57±2.13
	G_4	83.56±10.56	92.13±18.71	32.16±2.75	118.42±5.98	21.37±0.59	19.59±0.46	18.88±0.43
	G_5	83.51±2.20	79.30±15.30	30.83±2.84	116.90±6.79	21.38±1.89	19.74±1.77	19.04±1.73
B_4	G_1	82.78±2.47	65.57±9.14	29.50±1.32	103.38±7.20	19.49±1.16	18.02±1.10	17.40±1.07
	G_2	83.66±0.31	86.47±10.87	31.83±1.75	144.53±6.95	28.23±2.026	26.19±2.01	25.32±1.98
	G_3	82.99±0.46	86.29±8.96	28.16±1.15	135.54±6.011	25.24±2.89	23.62±2.85	22.80±2.82
	G_4	82.74±1.99	89.36±8.50	30.33±2.75	127.54±2.52	24.14±0.60	22.49±0.56	21.72±0.54
	G_5	81.74±2.03	86.56±14.19	36.33±4.01	127.28±7.60	23.67±1.56	21.81±1.44	21.04±1.40
$LSD_{0.05}$		6.94	16.97	4.21	13.01	2.73	2.58	2.52

B_1 indicates no application; B_2, B_3 and B_4 indicate application of 2, 3 and 4 g L^{-1} of Nano-B, respectively.
G_1, G_2, G_3, G_4 and G_5 indicate foliar application Nano-B at 20, 40, 60, 80 and 100% of ground cover, respectively.

foliar application. Data in Table 3 exposed that, increasing the boron concentrations from 0 to 4 g L^{-1} contributed the last potassium and α-amino-N content of 4.58 and 0.45 mmol/100 g root at 60% growth stage. On the other hand, without the application of boron (B_1) resulted in the maximum mean values of K (7.69) and α-amino-N (1.47) content at B_1G_5. The significant lowest sodium content 0.50 and 0.49 mmol/100 g root related to a reduction in impurity 60.37% and 66.66%, at the application of B_4G_3 and B_4G_4, respectively.

Discussion

Foliar application of Nano-B at 3 g L^{-1} resulted in a consistent improvement in vegetative growth of sugar beet, but on increasing Nano-B concentration up to B_4, vegetative growth decreased compared with B_3. In addition, the increases of yield-related responses like chlorophylls and leaf area (Table 2) of sugar beet at high Nano-B concentration (B_3 and B_4) could be reflected upon the increase of sugars percentage and reduction of impurities (Table 3), so, the optimal leaf area value for root and sugar yields was 86.47 cm^2 at B_4G_2. Leaf number and low chlorophyll content at high boron concentration are associated with toxicity of this element (Armin and Asgharipour 2012). Adequate boron supply through foliar application improved the chlorophyll content, leaf number and leaf area enabling them to capture more light and produce more assimilate for loading to root. Ullah et al. (2013) reported that B deficiency causes to reduced growth of new leaf and shoot due to clear limitation of boric acid phloem mobility. Such enhancement effect of B could be related to the favorable influence of them on photosynthetic pigments (Wanas 2002; Abd El-hady et al. 2017), metabolism, enzyme activity (El-Sherbeny et al. 2007), photosynthesis efficiency (Abou El-Yazied and Mady 2012) which in turn encourage vegetative growth and increasing dry matter production. Also, this enhancement could be an indicator of expectable high sugar beet yield. Also, Abd El-hady et al. (2017) informed that these results might be attributed to that B is an essential element for photosynthetic pigments, where it increases CO_2 fixation, rates of photosynthetic O_2 evolution and decreases respiration and the activities of oxidative pentose phosphate enzymes.

It seems that the increase in root diameter at 3 g L^{-1} of

Table 3. Means comparison the effects of Nano-B concentration and spraying time (growth stage) on sugar content, WSC, SP, loss of sugar productivity, Na, K, N and MS of sugar beet.

Treatment		SC (%)	WSC (%)	SP	LSP	Na	K	N	MS
Nano-B	Growth stage					(mmol/100g root)			
B_1	G_1	15.80±0.20	14.14±0.27	0.857±0.006	2.25±0.085	0.94±0.16	6.93±0.71	0.96±0.11	1.65±0.081
	G_2	17.66±0.83	15.94±0.74	0.868±0.0025	2.32±0.094	0.96±0.27	7.03±0.87	1.17±0.24	1.72±0.096
	G_3	16.63±0.73	14.97±0.75	0.863±0.0077	2.25±0.058	1.26±0.22	6.33±0.59	1.11±0.19	1.65±0.060
	G_4	16.26±0.41	14.56±0.37	0.859±0.003	2.29±0.070	1.47±0.101	6.23±0.24	1.22±0.14	1.69±0.067
	G_5	17.86±0.64	15.94±0.58	0.859±0.002	2.52±0.070	1.37±0.061	7.69±0.79	1.47±0.14	1.92±0.068
B_2	G_1	17.73±0.30	16.26±0.23	0.883±0.002	2.07±0.072	0.66±0.047	5.84±0.28	0.85±0.21	1.46±0.071
	G_2	17.06±0.64	15.58±0.65	0.877±0.0049	2.08±0.011	0.76±0.035	5.93±0.13	0.84±0.03	1.48±0.011
	G_3	18.30±0.79	16.79±0.77	0.885±0.0045	2.10±0.043	0.83±0.100	5.96±0.19	0.86±0.19	1.50±0.045
	G_4	17.06±0.50	15.49±0.54	0.872±0.0073	2.17±0.081	0.81±0.081	9.56±0.32	0.86±0.14	1.57±0.081
	G_5	17.33±0.90	15.69±0.83	0.871±0.0034	2.23±0.075	0.91±0.085	7.05±0.52	0.83±0.05	1.63±0.072
B_3	G_1	17.20±0.80	15.82±0.78	0.885±0.0049	1.97±0.055	0.63±0.062	5.59±0.30	0.60±0.09	1.37±0.057
	G_2	19.86±0.80	18.39±0.79	0.896±0.0040	2.06±0.025	0.57±0.028	6.30±0.24	0.67±0.07	1.46±0.021
	G_3	19.33±0.98	17.90±0.98	0.894±0.0061	2.02±0.050	0.69±0.060	5.56±0.27	0.80±0.20	1.42±0.052
	G_4	18.06±0.50	16.56±0.50	0.883±0.0040	2.10±0.052	0.83±015	5.99±0.36	0.84±0.09	1.50±0.052
	G_5	18.26±0.57	16.86±0.55	0.890±0.0023	2.00±0.20	0.67±0.105	5.41±0.21	0.78±0.12	1.39±0.019
B_4	G_1	18.86±0.64	17.44±0.66	0.893±0.0050	2.02±0.034	0.53±0.041	5.92±0.11	0.69±0.10	1.42±0.035
	G_2	19.53±0.90	18.11±0.91	0.896±0.0050	2.02±0.052	0.52±0.058	5.94±0.48	0.68±0.03	1.41±0.054
	G_3	18.60±1.56	17.40±1.58	0.903±0.0091	1.79±0.046	0.50±0.073	4.58±0.33	0.45±0.08	1.19±0.047
	G_4	18.93±0.23	17.63±0.25	0.899±0.0030	1.90±0.043	0.49±0.072	5.23±0.20	0.55±0.18	1.30±0.043
	G_5	18.60±0.52	17.13±0.55	0.888±0.0047	2.06±0.041	0.54±0.032	6.37±0.03	0.64±0.15	1.46±0.039
$LSD_{0.05}$		1.207	1.20	0.0085	0.092	0.188	0.66	0.22	0.091

B_1 indicates no application; B_2, B_3 and B_4 indicate application of 2, 3 and 4 g L^{-1} of Nano-B, respectively.
G_1, G_2, G_3, G_4 and G_5 indicate foliar application Nano-B at 20, 40, 60, 80 and 100% of ground cover, respectively.

Nano-B by means of high leaf number and chlorophyll content and efficient assimilates portioning towards sink parts. These results could be explained by the role of boron in plant metabolism, development and growth (Rawashdeh and Sala 2013; Abido 2012), cell wall formation and meristematic tissue extension and cell elongation the root (Nalini et al. 2013). Cell enlargement and increase in a number of cells contribute to the increase of yield can be due to the role of boron in the biosynthesis of auxin in the meristematic activity and increase in the IAA-oxidase activity. Similar observations were recorded by Abdelaal et al. (2015) and Dugger (1973) in sugar beet.

Armin and Asgharipour (2012) stated that the maximum root yield and sugar percentage was achieved by foliar application of 12% boric acid. Considering this, Nano-B spraying may be used to enhance root and sugar yield, resulting in reduce boron fertilizer. Foliar Nano-B application predominantly affects at vegetative growth compared with reproductive growth in sugar beet. Results in Table 2 exhibited that sugar yield and white sugar yield was significantly improved by increasing of B from B_1 to B_4. These results were true in the five growth stages. While that sugar content was decreased by B_4 when compared with B_3 treated plants (Table 2), the increase in sugar yield accompanying high boron level might have been due to the increase in root yield as well as sucrose content. These results are in agreement by those of Gezgin et al. (2001).

It seems that, better translocation of photosynthates from high leaf area (Table 2) and higher dry matter accumulation with high root length led to increasing in root yield (Table 2). The increase in tops and roots fresh and dry weights, caused by boron application, could be attributed to the stimulating effect of boron on the photosynthesis process in the plants such as translocation of sugar and carbohydrates of assimilates from the top to root, which leads to increase in root and sugar yield. On the other hand, when photosynthetic activity is high, any factor that increases the leaf area may have a positive effect on WSY. The enhancement of dry matter in sugar beet roots may be attributed to the improvement of leaf area, leaf number, RWC and chlorophyll content which results in improvement of growth-related traits such as root length and root diameter, and consequently root yield sugar yield (Table 2). Similar results were also observed by Abdel-Motagally (2015) and Mohammadian et al. (2014) who reported that early beginning of photosynthetic

transmission from leaf to root and consequently, it would increase WSY at the harvest time.

The rise of WSC may be due to the increase in sugar percentage and the reduction of impurities in terms of sodium, potassium and α-amino-N content (Table 3). Further, if optimum B is available at the early growth stage, the plant continues to partition it in the sink part as have been observed in this study. This finding suggested that sugar content is the key factor conferring B phloem mobility due to the bonding of sugar and boric acid (Liakopoulos et al. 2005). The Nano-boron facilitates the transport of sugars in the plants because it had a crucial role in the biosynthesis of auxin (Dugger 1973; Ullah et al. 2013). The high amount of juice purity would be desirable to provide sugar content. The important role of the boron element on the percentage of purity comes through its beneficial effect on the values of sucrose content (Table 3). Boron dominates in the early-stage, building up the highest TSS for the sugar beets (Table 1).

The result showed that, at low concentration of boron, a lower percentage of sugar had been achieved. Therefore, sugar in the form of molasses in these plants is higher in amount than that which has received enough boron (Table 3). Reduction of impurities like sodium, potassium and α-amino-N content in beet roots cause to decrease of sucrose molasses under application of a higher rate of boron application. These results are an agreement with the finging of Abbas et al. (2014) who reported that increasing the concentration of B cause to the reduction of sugar molasses. Hellal et al. (2009) showed that juice purity, sugar and root yield of sugar beet improved by increasing of B spraying which could be related to the reduction of sodium and potassium uptake in root juice.

The reasons for the improvement in sugar beet quality could be due to the fact that B plays a role in cell division, enhanced enzymatic activity, the membrane integrity, calcium uptake and carbohydrate metabolism (Nalini et al. 2013; Rawashdeh and Sala 2013). An increased boron supply decreases the nitrate levels via inhibiting transcript level in the roots and altering the nitrate transporter activity, leading to reduced plasma membrane enzymes activities (Camacho-Cristobal and Gonzalez-Fontes 2007). Evidence proposes that sugar alcohols synthesis and the later transport of the B-sugar alcohol compound in the phloem to sink tissues is the main factor that confers phloem B mobility to a plant species (Brown et al. 1999). The least accumulation of sodium at the later application (G_3 and G_4) could be due to the increased of leaf area at this time and facilitate the improvement of B absorption. Similar results were obtained by Abbas et al. (2014) who reported that spraying dates lead to significantly different in sodium content. Also, Armin and Asgharipour (2012) and Abbas et al. (2014) showed that boron application improved juice quality by declining K and Na content.

Conclusion

Application of Nano-B rates showed a significant increase in quantitative and qualitative sugar beet traits under study. The highest SPAD and RWC, leaf area and leaf number were observed in 3 g L^{-1} of Nano-B resulted in a consistent improvement in vegetative growth of sugar beet but with increasing concentration of Nano-B mentioned parameters were decreased. The increasing of boron fertilizer at all growing stages resulting in the highest root yield, sugar content and white sugar content thus led to increasing sugar yield, white and technological sugar yield. The decrease in sucrose molasses in a high level of boron accompanying due to the reduction in impurities in terms of sodium, potassium and α-amino-N content in sugar beet roots. Therefore, B_4G_2 treatment (4 g L^{-1} boron at 40% of ground covered) with the highest root and sugar yield may be recommended for the cultivation of sugar beet in terms of time and fertilizer saving.

Acknowledgements

We thank "Iran's National Elites Foundation" for their help during the course of experimentation.

References

Abbas MS, Dewdar MDH, Gaber EI, Abd El-Aleem HA (2014) Impact of boron foliar application on quantity and quality traits of sugar beet (*Beta vulgaris* L.) in Egypt. Res J Pharm Biol Chem Sci 5(5):142-151.

Abdelaal KAA, Shimaa AB, Shahrzd MMN (2015) Effect of foliar application of microelements and potassium levels on growth, physiological and quality characters of sugar beet (*Beta vulgaris* L.) under newly reclaimed soils. Mansoura J Plant Prod 6:123-133.

Abdel-Motagally FMF (2015) Effect concentration and spraying time of boron on yield and quality traits of sugar beet grown in newly reclaimed soil conditions. ASSIUT J Agric Sci 46(6):15-26.

Abido WAE (2012) Sugar beet productivity as affected by foliar spraying with methanol and boron. Int J Agr Sci 4(7):287-292.

Abou El-Yazied A, Mady MA (2012) Effect of boron and yeast extract foliar application on growth, pod setting and both green pod and seed yield of broad bean (*Vicia faba* L). J Appl Sci Res 8(2):1240-1251.

Ali F, Ali A, Gul H, Sharif M, Sadiq A, Ahmed A, Ullah A,

Mahar A, Kalhoro SA (2015) Effect of boron soil application on nutrients efficiency in tobacco lLeaf. Am J Plant Sci 6:1391-1400.

Amin GA, Badr EA, Afifi MHM (2013) Root yield and quality of sugar beet (*Beta vulgaris* L.) in response to bio fertilizer and foliar application with micro-nutrients. World Appl Sci J 27(11):1385-1389.

Armin M, Asgharipour M (2012) Effect of time and concentration of boron foliar application on yield and quality of sugar beet. Am Eurasian J Agric Environ Sci 12(4):444-448.

Asad A, Blamey FPC, Edwards DG (2003) Effects of boron foliar applications on vegetative and reproductive growth of sunflower. Ann Bot 92(4):565-570.

Brown PH, Bellaloui N, Hu H, Dandekar A (1999) Transgenically enhanced sorbitol synthesis facilitates phloem boron transport and increases tolerance of tobacco to boron deficiency. Plant Physiol 119(1):17-20.

Buchholz K, Märländer B, Puke H, Glattkowski H, Thielecke K (1995) Neubewertung des technischen Wertes von Zuckerrüben. Zuckerindustry 120:113-121.

Carruthers N, Oldfield JFT (1961) Methods for assessment of beet quality. Int Sugar J 63:137-139.

Dewdar DHM, Abbas MS, El Hassanin AS, Abd El-Aleem HA (2018) Effect of nano micronutrients and nitrogen foliar applications on sugar beet (*Beta vulgaris* L.) of quantity and quality traits in marginal soils in Egypt. Int J Curr Microbiol Appl Sci 7(8):4490-4498.

Dewdar MDH, Abbas MS, Gaber EI, Abd El-Aleem HA (2015) Influence of time addition and rates of boron foliar application on growth, quality and yield traits of sugar beet. Int J Curr Microbiol Appl Sci 4(2):231-238.

Dordas C, Apostolides GE, Goundra O (2007) Boron application affects seed yield and seed quality of sugar beets. J Agric Sci 145:377-384.

Dordas C (2006) Foliar boron application affects lint and seed yield and improves seed quality of cotton grown on calcareous soils. Nutr Cycl Agroecosys 76:19-28.

Dugger WM (1973) Functional aspects of boron in plants. Adv Chem Ser 123:112-129.

Edwards AH (2014) The semi-micro Kjeldahl method for the determination of nitrogen in coal. J Appl Chem 4(6):330-340.

El-Geddawy Dalia IH, Makhlouf BSI (2015) Effect of hill spacing and nitrogen and boron fertilization levels on yield and quality attributes in sugar beet. Minufiya J Agric Res 4(1):959-980.

El-Geddawy IH, Abd-Elhakim AM, Saif LM (2000) Multivariate analysis of yield and relative contribution of variables to its variation under some cultural practices in sugar beet. Egypt J Basic Appl Sci 78:449-469.

Abd El-hady M (2017) Response of sugar beet growth, productivity and quality to foliar application of different forms of boron microelement and number of sprays under new reclaimed soil conditions. Egypt J Basic Appl Sci 39(3):401-410.

El-Sherbeny SE, Khalil M, Hussepn MS (2007) Growth and productivity of rue (*Ruts graveolens*) under different foliar fertilizers application. J Appl Sci Res 3(5):399-407.

Gemici M, Aktas LY, Turkyilmaz B, Guven A (2003) The effects of the boron application on indole-3-acetic acid levels in *Triticum durum* Desf. cv. Gediz seedlings. CÜ Fen-Edebiyat Fakültesi 23(2):17-24.

Gezgin S, Hamurcu M, Apaydin M (2001). Effect of boron application on the yield and quality of sugar beet. Turk J Agric For 25:89-95.

Grzegorzewski K, Ciećko Z, Szostek R (2017) Influence of mineral fertilization on the yield and macroelement content in sugar beet. Acta Agrophys 24(2):221-237.

Hellal FA, Taalab AS, Safaa AM (2009) Influence of nitrogen and boron nutrition on nutrient balance and sugar beet yield grown in calcareous soil. Ozean J Appl Sci 2(1):1-10.

Hirparan DV, Sakarvadia HL, Savaliya CM, Ranpariya VS, Modhavadiya VL (2018) Effect of different levels of boron and molybdenum on growth and yield of summer groundnut (*Arachis hypogaea* L.) under medium black calcareous soils of south Saurashtra region of Gujarat. Int J Chem Stud 5(5):1290-1293.

Iqbal S, Farooq M, Cheema SA, Afzal I (2017) Boron seed priming improves the seedling emergence, growth, grain yield and grain biofortification of bread wheat. Int J Agric Biol 19:177-182.

Jifon JL, Syvertsen JP, Whaley E (2019) Growth environment and leaf anatomy affect nondestructive estimates of chlorophyll and nitrogen in citrus sp. leaves. J Am Soc Hortic Sci 130(2):152-158.

Kristek A, Stojic B, Kristek S (2006) Effect of the foliar boron fertilization on sugar beet root yield and quality. Poljopriverda 12(1):22-26.

Le-Docte AM (1927) Commercial determination of sugar in the beet root using the sacksle-docte process. Int Sugar J 29:488-492.

Makhlouf BSI, Abd El-All AEA (2017) Effect of deficit irrigation, nitrogen and potassium fertilization on sugar beet productivity in sandy soils. Menoufia J Plant Prod 2:325-346.

Mirschel W (2018) Manual Leaf Area Measurement on Individual Sugar Beet Plants Taking Plant Density and Irrigation into Account. Leibniz Centre for Agricultural Landscape Research (ZALF), Müncheberg, Germany.

Mohammadian R, Ghasemi H, Bazrafshan M, Moharramzadah M (2014) Identification of morpho-physiological traits affecting white sugar yield in sugar beet. J Plant Physiol Breed 4(2):23-34.

Nadeem F, Farooq M, Nawaz A, Ahmad R (2019) Boron improves productivity and profit ability of bread wheat

under zero and plough tillage on alkaline calcareous soil. Field Crops Res 239:1-9.

Nalini P, Gupta B (2013) The impact of foliar boron sprays on reproductive biology and seed quality of black gram. J Trace Elem Med Biol 27:58-64.

Nyomora AMS, Brown PH, Pinney K, Polito VS (2019) Foliar application of boron to almond trees affects pollen quality. J Am Soc Hortic Sci 125(2):265-270.

Perica S, Brown PH, Connell JH, Nyomora AMS, Dordas C, Hu H, Stangoulis J (2001) Foliar boron application improves flower fertility and fruit set of olive. Sci Hortic 36(4):714-716.

Prasad TNVKV, Sudhakar P, Sreenivasulu Y, Latha P, Munaswamy V, Reddy, KR, Sreeprasad TS, Sajanlal PR, Pradeep T (2012) Effect of nanoscale zinc oxide particles on the germination, growth and yield of peanut. J Plant Nutr 35(6):905-927.

Rawashdeh H, Sala F (2013) Effect of different levels of boron and iron foliar application on growth parameters of wheat seedlings. Afric Crop Sci Conf Proceed 11:861-864.

Rehman A, Farooq M, Rashid A, Nadeem F, Stuerz S, Asch F, Bell RW, Siddique KHM (2018) Boron nutrition of rice in different production systems. A review. Agron Sustain Dev 38:25.

Saadati S, Moallemi N, Mortazavi SMH, Seyyednejad SM (2013) Effects of zinc and boron foliar application on soluble carbohydrate and oil contents of three olive cultivars during fruit ripening. Sci Hortic 164:30-34.

Singh Z, Ghosh G, Debbarma V (2017) Effect of different levels of nitrogen, sulphur and foliar application of boron in sunflower (*Helianthus annuus* L.). Int J Curr Microbiol Appl Sci 6(10):1336-1342.

Tambussi EA, Nogués S, Araus JL (2005) Ear of durum wheat under water stress: water relations and photosynthetic metabolism. Planta 221(3):446-458.

Tlili A, Dridi I, Fatnassi S, Hamrouni H, Gueddari M (2019) Boron characterization, distribution in particle-size fractions, and its adsorption-desorption process in a semiarid Tunisian soil. J Chem Article ID 2508489, 1-8.

Ullah S, Khan AS, Malik AU, Afzal I, Shahid M, Razzaq K (2013) Foliar application of boron influences the leaf mineral status, vegetative and reproductive growth, yield and fruit quality of 'Kinnow' mandarin. J Plant Nutr 36(10):1479-1495.

Wanas HA (2002) Petrography, geochemistry and primary origin of spheroidal dolomite from the upper Cretaceous/Lower Tertiary Maghra El-Bahari Formation at Gabal Ataqa, Northwest Gulf of Suez, Egypt. Sediment Geol 151(3-4):211-224.

Acta Biologica Szegediensis

Volume 63(2):113-118, 2019
Acta Biologica Szegediensis
http://abs.bibl.u-szeged.hu/index.php/abs
DOI:10.14232/abs.2019.2.113-118

ARTICLE

Characterization of barley germplasm for leaf stripe (*Pyrenophora graminea*) resistance based on incidence and severity parameters

Arabi M.I.E.*, Jawhar M. and Al-Shehadah E.

Department of Molecular Biology and Biotechnology, AECS, Damascus, Syria.

ABSTRACT Barley leaf stripe (BLS) caused by *Pyrenophora graminea* is an important seed-borne disease of barley causing significant yield and quality losses worldwide. The development of resistant cultivars has proven difficult, therefore, in this work, BLS-resistant barley germplasm was developed by crossing six barley cultivars currently used in Europe and West Asia. Out of 270 doubled haploid lines derived from these crosses, 40 lines were evaluated under field artificial infection conditions using incidence (*I*; proportion of diseased plants) and severity (*S*; proportion of infected leaf area per plant). Disease resistance parameters showed a broad range of variation in mean *I* and *S* values with a continuum of resistance levels ranging from highly susceptible to highly resistant with values being consistently higher in the susceptible ones. However, eight promising resistant lines with high yield per plant were identified. Moreover, BLS severity increased linearly as incidence increased (r = 0.76, P < 0.001). This work suggests that BLS resistance sources identified in this study can be used for further genetic analysis and introgression for varietal improvement, and that the positive correlation between *I* and *S* parameters may be beneficial for many types of studies on this disease.
Acta Biol Szeged 63(2):113-118 (2019)

KEY WORDS
barley
Hordeum vulgare L.
incidence
leaf stripe
severity

ARTICLE INFORMATION
Submitted
03 December 2019.
Accepted
02 February 2020.
***Corresponding author**
E-mail: ascientific@aec.org.sy

Introduction

Leaf stripe caused by *Pyrenophora graminea* Ito & Kuribayashi [anamorph *Drechslera graminea* (Rabenh. ex. Schlech. Shoem)] is a seed-borne disease of barley (*Hordeum vulgare* L.) found worldwide (Mathre 1997). The fungus can infect barley plants during seed germination, and hyphae accelerate its intercellular growth within the coleorhizae, the embryo, the roots and scutellar node, in order to establish a full-scale infection in the seedling (Platenkamp 1976; Arabi and Jawhar 2005). In susceptible plants, the disease causes severe stunting, premature death, and complete loss of grain (Çelik et al. 2016).

The development of resistant cultivars is the most economic, reliable and environmentally safe way to control leaf stripe (Nielsen 2012; Benkorteby-Lyazidi et al. 2019), especially in developing countries where most farmers are small to marginal and unable to afford costly fungicides and other technologies. In Syria, sources of complete resistance to BLS have not been identified, and current barley cultivars are only moderately resistant toward this disease (Arabi et al. 2004). However, both incidence (proportion of diseased plants) and severity (proportion of plant surface showing symptoms) are the commonly used measures to estimate BLS disease. However, incidence is a measure of diseased or not diseased, this makes it easier and reproducible to measure than severity. In addition, severity is considered to be more important and useful measure than incidence for setting the effectiveness of disease management planning (Campbell and Madden 1990). Consequently, a quantitative relationship between incidence and severity would greatly facilitate the evaluation of disease intensity when accurate assessments of severity are not available or possible (Arabi and Jawhar 2010; Carisse et al. 2013).

As part of a large breeding program from Syriato develop barley varieties with resistance to BLS, hundreds of accessions including landraces, advanced breeding lines, and elite barley varieties were screened. Here we report five crosses of barley cultivars presently grown in Europe and West Asia to screen barley breeding lines for resistance to BLS disease through incidence and severity parameters under Syrian field conditions which is typical of Mediterranean environments.

Table 1. Parental cross and progeny susceptibility to BLS (*Pyrenophora graminea*)*

Cross	Progeny				
	Highly resistant	Resistant	Moderately resistant	Susceptible	Highly susceptible
Arabi Abiad X IC-9	1	1	7	3	3
PK30-136 X IC-9	0	3	3	8	1
Arrivate X PK30-136	0	0	1	1	1
CI5791 X Igri	0	2	0	2	0
Arabi Abiad X Arrivate	0	1	0	2	0
Total	1	7	11	16	5

*Based on a scale described by Delogu et al (1989).

Materials and Methods

Plant material

A total of 40 out of 270 barley double haploid linesproduced according to Kasha and Kao (1970) were screened under preliminary field experiments based on desirable agronomic characteristics and evaluated inthis study (Table 1). These lines were produced through five resistant-by-susceptible barley crosses made between six parents possessing different BLS reactions. Arabi Abiad is a Syrian local cultivar, PK130-36 is a Pakistan cultivar, Arrivate was received from USA, IC-9 is a new cultivar developed at ICARDA (International Center for Agricultural Research in Dry Areas), CI5791 is an Ethiopian cultivar, and Igri is a German cultivar. Briefly, spikes were manually emasculated and pollinated with fresh pollen. Pollinated spikes were treated with 2,4-dichlorophenoxyacetic acid (2,4-D). Tillers were collected from donor plants when most microspores were at mid- to late-uninucleate stage of development. Then they were placed in Hoagland's salt solution and stored at 4 °C in the dark for 21 days. Anthers were excised and transferred to FW culture medium (Arabi et al. 2005). Haploid plants were vernalized for 8 weeks. Subsequently, haploids were treated with colchicine solution for chromosome doubling (Subrahmanyam and Kasha 1975).

Inoculum preparation

The most Syrian virulent isolate Sy3 (Arabi et al. 2004) was used in this study. The fungus was grown on potato dextrose agar (PDA, DIFCO, Detroit, MI, USA) and incubated for 7 days at 20 ± 1 °C in the darkness. Inoculation was carried out using the modified technique of Hammouda (1986). Seeds were surface-sterilized in 2% sodium hypochlorite for 5 min, dried for 3-4 h, then placed on 8-day-old mycelial culture growing on PDA medium in Petri dishes and incubated at 6 °C for 14 days in the dark. As a control, seeds were incubated on PDA medium alone.

Field trials

Inoculated and un-inoculated seeds of the DH lines and parents were planted under field conditions in Syria, at a site of 970 m altitude (550 mm rainfall average) in a randomized complete block design, with three replicates. The location of the experiment was chosen to be favorable for the development of BLS disease, since *P. graminea* infects barley in this location annually. Plot area was 1 x 1 m with a 1 m buffer. Each plot consisted of 5 rows 25 cm apart with 50 seeds sown per row. Experimental design, cultural practices and mist irrigation were as previously described (Arabi et al. 2004).

BLS assessments

Incidence and severity were estimated visually at several systematically selected sampling sites. Incidence (*I*) was recorded as the proportion of diseased plants (number of plants with non-zero severity divided by the total number of plants sampled). Severity (*S*) was recorded as infected leaf area per plant expressed as a proportion of the total area using a scale described by Delogu et al. (1989) where; highly resistant (*HR*) (0-5% of infected plants), resistant (*R*) (6-11%), moderately resistant (*MR*) (12-26%), susceptible (*S*) (27-78%) and highly susceptible (*HS*) (79-100% of infected plants).

Yield estimation

Three central rows of each replicate plot were harvested at maturity stage to measure grain yield (g/plant).

Statistical analyses

Data was subjected to analysis of variance using the STAT-ITCF statistical programme (2nd version). Differences between means were evaluated for significance by using Newman-Keuls test at 5% probability level (Anonymous 1988). For all the experiments data, each pair of *I* and *S* values from each sampling site was considered an observation for data analysis. The data were edited to remove observations with no diseased plants (i.e., $I = 0$ and $S = 0$), since the *I*-*S* relationship is only defined when

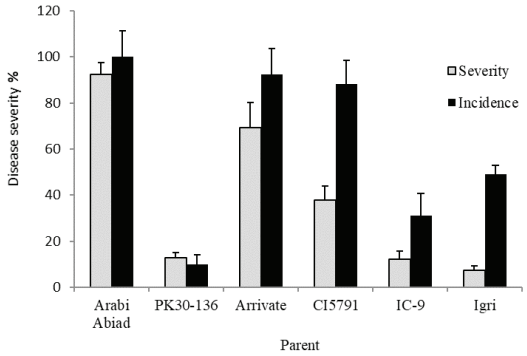

Figure 1. Frequency of LBS reactions incited on the barley parents (Arabi Abiad, Arrivate, CI5791, PK36-130, IC-9 and Igri) under field artificial conditions. Error bars are representative of the standard error (Mean ± SD; *n* = 3).

disease is present. The assumption of coincidence of the regression lines was tested using the ANCOVA procedure implemented in the software package Statistica 6.1.

Results and Discussion

In this present investigation, six barley parents with different resistance levels to BLS infections were used. As shown in Figure 1, the highest mean incidence and severity were recorded in parents cvs. Arrivate and Arabi Abiad, whereas, the lowest was found in the resistant parents cvs. PK30-136 and IC-9.

Data demonstrated that the distribution of BLS resistance type of the progenies can be observed in transgressive segregation toward greater resistance and susceptibility occurred in each of the crosses (Fig. 2; Table 1). However, according to a scale described by Delogu et al. (1989), the reactions of the 40 progeny lines to BLS under field tests were classified into five groups; 1 line as highly resistant, 7 resistant, 11 moderate, 16 susceptible and 5 highly susceptible (Table 1). However, significant differences ($P < 0.05$) in mean severity values were detected among different lines, and a continuum of genotypic reactions to the virulent strain SY3 from highly resistant to highly susceptible was observed (Table 2). On the other hand, significant differences ($P < 0.05$) in mean yield values were found among lines, with values being consistently higher in the susceptible ones (Table 2).

The data showed that B08-AS-5 line was highly resistant, and lines (B08-AS-12, 19, 20, 29, 35, 37 and 39) were resistant, whereas lines B08-AS 1 and 3 were the most susceptible lines (Table 2). The other lines had BLS ratings that ranged between moderately resistant and susceptible. On the other hand, Figure 3 shows that BLS severity increased linearly as incidence increased (r = 0.76, $P < 0.001$).

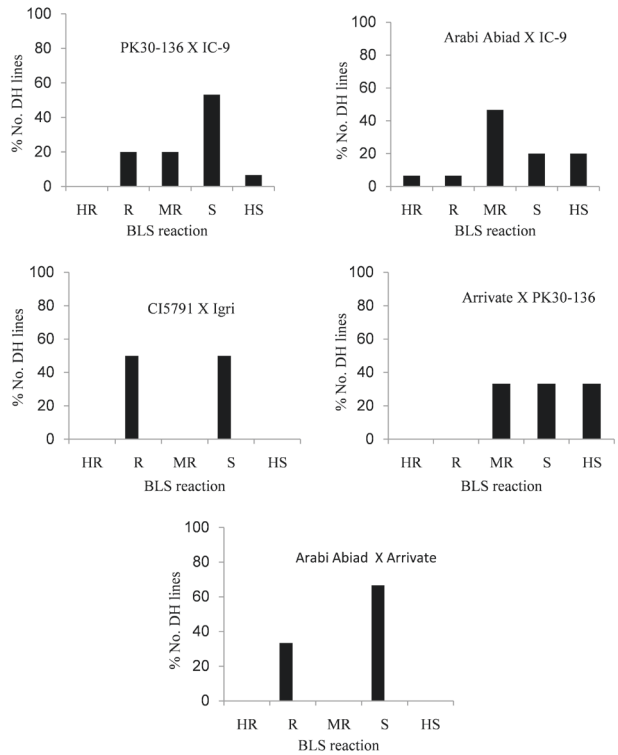

Figure 2. Distribution of BLS reactions which were highly resistant (HR), resistant (R), moderately resistant (MR), susceptible (S), and highly susceptible (HS) from the double haploid (DH) lines in the field experiments. Data were obtained from five crosses of barley parent.

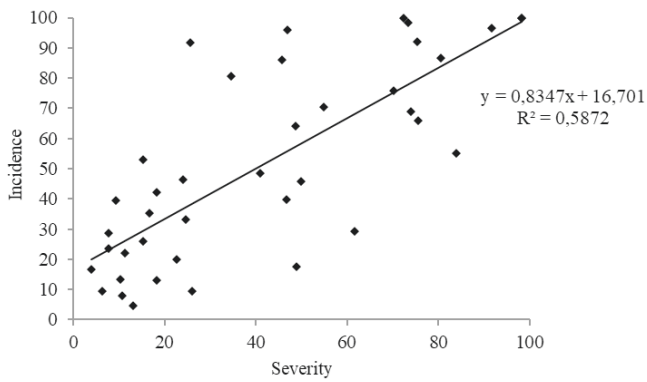

Figure 3. Incidence (I; proportion of diseased plants) and severity (S; proportion of plants showing disease symptoms) of barley leaf stripe under field artificial conditions. Data points shown represent many hidden observations.

In this work, barley lines varied greatly in resistance to BLS. However, the resistant cultivars to BLS may in fact have various resistance response to the spread of the fungus within the infected plants hence, for any given

Table 2. Mean leaf stripe disease incidence (I) and severity (S) and yield of the barley lines under field conditions.

Cross	No.	Lines	S	I	Yield (g/plant)
Arabi Abiad X IC-9	1	B08-AS-1	98.33a	100.00a	6.11 e
	2	B08-AS-2	13.00h	4.50h	15.58a
	3	B08-AS-3	98.33a	100.00a	7.65cd
	4	B08-AS-4	15.33g	25.96f	10.13bcd
	5	B08-AS-5	4.00h	16.56g	12.98bcd
	6	B08-AS-6	16.66g	35.26e	12.09bcd
	7	B08-AS-7	26.00f	9.43g	11.9bcd
	8	B08-AS-8	61.66d	29.26f	7.40d
	9	B08-AS-9	48.66e	64.03c	10.57bcd
	10	B08-AS-10	24.00g	46.53d	10.48bcd
	11	B08-AS-11	84.50b	55.16d	7.27d
	12	B08-AS-12	7.66h	28.66f	10.12bcd
	13	B08-AS-13	15.33g	52.90d	10.9bcd
	14	B08-AS-14	24.66g	33.30e	10.02bcd
	15	B08-AS-15	74.00c	68.83c	9.5bcd
PK30-136 X IC-9	16	B08-AS-16	49.00e	17.63g	9.97bcd
	17	B08-AS-17	18.33g	13.20g	10.20bcd
	18	B08-AS-18	75.66b	65.90c	9.68bcd
	19	B08-AS-19	9.33h	39.46e	10.02bcd
	20	B08-AS-20	6.33h	9.50g	16.10a
	21	B08-AS-21	41.00e	48.50d	8.93bcd
	22	B08-AS-22	55.00d	70.33c	7.50cd
	23	B08-AS-23	34.66f	80.73b	8.83bcd
	24	B08-AS-24	25.66f	91.83a	8.27bcd
	25	B08-AS-25	45.66e	86.03b	8.03bcd
	26	B08-AS-26	80.50b	86.66b	8.31bcd
	27	B08-AS-27	75.33b	92.13a	8.30bcd
	28	B08-AS-28	47.00e	96.00a	7.53cd
	29	B08-AS-29	7.66h	23.66f	13.72bcd
	30	B08-AS-30	18.33g	42.10e	13.77bcd
Arrivate X PK30-136	31	B08-AS-31	22.66g	20.10f	10.12 bcd
	32	B08-AS-32	46.66e	39.83e	10.9bcd
	33	B08-AS-33	91.83a	96.60a	6.53 ef
CI7591 X Igri	34	B08-AS-34	50.00e	45.93d	9.17bcd
	35	B08-AS-35	10.66h	7.86g	15.78a
	36	B08-AS-36	70.20c	75.76b	7.51cd
	37	B08-AS-37	10.33h	13.40g	15.12 a
Arabi Abiad X Arrivate	38	B08-AS-38	72.33c	100.00a	6.60 ef
	39	B08-AS-39	11.33h	22.00f	14.89 a
	40	B08-AS-40	73.33c	98.33a	6.10 e

*Values within a column followed by different letters are significantly different

incidence value, a wide range of severity values may be observed across cultivars. Our findings agree with the results of Paul et al. (2005) for fusarium head blight on winter wheat. McRoberts et al. (2003) reported that the *I–S* relationship might be used to draw conclusions about the relative rate of disease increase among cultivars with different levels of resistance. On the other hand, data showed that the average response to BLS disease differed with the differences in the susceptibility level of DH lines (Table 2). These results in a good agreement with those obtained by Delogu et al (1989). However, Table 2 demonstrated in general that when I and S values were high the mean yield per plant was low (lines B08-AS-1, 3, 26, 33, 36, 38 and 40). Moreover, DH lines with low

disease levels were associated with high yield although some of them not the highest yielding. Gaunt and Wright (1992) reported that the effect of BLS on grain yield may be attributed to reduced area of photosynthetically active tissue enhances respiration and transpiration or to disturbance in translocation of assimilates to the spike.

One of the major objectives of the Syrian barley breeding program is to develop high-yielding cultivars with resistance to BLS disease through the transfer of genes from resistant sources. The population of crosses CI5791/ Igri and PK30-136 /IC-9 will be used for mapping genes associated with BLS resistance. Some lines from this cross were recovered with a high degree of resistance to this disease. These will be tested in further work under multilocation trials to test their stability and adaptability.

Additionally, the data demonstrated that barley lines have enough variability for infection response to BLS pathogen. Therefore, inclusion of this diverse germplasm in the barley breeding program might increase the dominance effect and epistatic variations controlling quantitative traits such as BLS resistance (Çetin et al. 1995; Bayraktar and Akan 2012). These would also lead to extend segregation for various traits and in obtaining useful recombinants/transgressive segregants in the further generations. However, crossbreeding with a wide range of modern varieties accompanied with selection under field conditions will lead to an accumulation of partial resistances again. As partial resistances have a complex biological background, one should concentrate on the context in which the disease occurs. Barley plants will not be infected, if they survive cold temperatures in the juvenile stage (Prasad et al. 1976). The surprising high rates of resistances in DH lines derived from Ethiopia and Pakistan parents were recorded. This may be since in Ethiopia and Pakistan, barley often is cultivated at higher elevation, i.e. at cooler temperatures.

This study showed that the barley breeding lines had diversity for infection response to BLS pathogen. Eight promising sources of resistance with high yield per plant were identified that could be considered as possible donors in further barley breeding programs. In addition, a positive relationship between proportion of diseased plants and the proportion of infected leaf area was detected, however, characterizing the functional relationship between *I* and *S* is still highly important, since through this relationship scientists can identify cultivars with large or small severities for a given incidence (McRoberts et al. 2003), or through covariance analysis (when there are several pairs of *I-S* points for each cultivar), identify cultivars with an unusual *I-S* relationship compared with others.

Acknowledgements

The authors wish to thank the Director General of AECS and the Head of the Molecular Biology and Biotechnology Department for their continuous support throughout this work.

References

Anonymous (1988) STAT-ITCF, Programme, MICROSTA, realized by ECOSOFT, 2nd Version, Institut Technique des Cereals et des Fourrages Paris, pp.55.

Arabi MIE, Jawhar M, Al-Safadi B, MirAli N (2004) Yield responses of barley to leaf stripe (*Pyrenophora graminea*) under experimental conditions in southern Syria. J Phytopathol 152:519-523.

Arabi MIE, Al-Safadi B, Jawhar M. Mir-Ali N (2005) Enhancement of embryogenesis and plant regeneration from barley anther culture by low doses of gamma irradiation. In Vitro Cell Dev Biol 41:762-764.

Arabi MIE, Jawhar M (2005) Barley reaction to *Pyrenophora graminea* based on the fungus movement. Plant Pathol 34:405-407.

Arabi MIE, Jawhar M (2010) Interrelationship between incidence and severity of leaf stripe on barley. J Plant Pathol 92:503-505.

Bayraktar H, Akan K (2012) Genetic characterization of *Pyrenophora graminea* isolates and the reaction of some barley cultivars to leaf stripe disease under greenhouse conditions. Tur J Agri Forest 36:329-339.

Benkorteby-Lyazidi H, Zeghar I., Hanifi-Mekliche L, Bouznad Z (2019) Barley leaf stripe disease in Algeria: evaluation of virulent *Pyrenophora graminea* isolates and identification of resistant Algerian barley genotypes. Tarım Bilimleri Dergisi – J Agri Sci 25:367-372.

Delogu G, Porta-Puglia AC, Vannacci G (1989) Resistance of winter barley varieties subjected to natural inoculums of *Pyrenophora graminea*. J Genet Breed 43:61-65.

Campbell CL, Madden LV (1990) Introduction to Plant Disease Epidemiology. John Wiley & Sons, New York.

Carisse O, Lefebvre A, Van der Heyden H, Roberge L, Brodeur L (2013) Analysis of incidence–severity relationships for strawberry powdery mildew as influenced by cultivar, cultivar type, and production systems. Plant Dis 97:354-362.

Çelik Y, Karakaya A, Çelik Oğuz A, Mert Z, Akan K, Ergün N, Sayim İ (2016) Determination of the reactions of some barley landraces and cultivars to *Drechslera graminea*. Med Agri Sci 29:43-47.

Çetin L, Albustan S, Düsünceli F, Tosun H, Akar T (1995) Determination of resistance of barley breeding materi-

als developed for Central Anatolia to barley leaf stripe (*Pyrenophora graminea*). In: VII. Türkiye Fitopatoloji Kongresi, Adana, p. 126.

Delogu G, Porta-Puglia A C., Vannacci G (1989) Resistance of winter barley varieties subjected to natural inoculums of *Pyrenophora graminea*. J Genet Breed 43:61-65.

Gaunt RF, Wright AC (1992) Disease yield relationship in barley II. Contribution of stored stem reserves to grain filling. Plant Pathol 41:688-701.

Hammouda AM (1986) Modified technique for inoculation in leaf stripe of barley. Acta Phytopathol Entomol Hung 21:255-259.

Kasha KJ, Kao KN (1970) High frequency haploid production in barley (*Hordeum vulgare* L.). Nature 225:874-876.

McRoberts N, Hughes G, Madden LV (2003) The theoretical basis and practical application of relationships between different disease intensity measures in plants. Ann Appl Biol 142:191-211.

Mathre DE (1997) Compendium of barley diseases. 2nd ed. APS Press, St Paul.

Nielsen BJ (2012) Screening for resistance to leaf stripe (*Pyrenophora graminea*) in barley. In Yahyaoui AH, Brader L, Tekauz A, Wallwork H, Steffenson B, Eds, Proceedings of the 2nd International Workshop on Barley Leaf Blights, 7-11 April 2012, ICARDA, Aleppo, Syria. ICARDA, Aleppo, 277-280.

Prasad MN, Leonard KJ, Murphy CF (1976) Effects of temperatures and soil water potential on expression of leaf stripe incited by *Helminthosporium gramineum.* Phytopathology 66:631-634.

Paul PA, El-Allaf SM, Lipps PE, Madden LV (2005) Relationships between incidence and severity of fusarium head blight on winter wheat in Ohio. Phytopathology 95:1049-1060.

Platenkamp R (1976) Investigation on the infection pathway of *Drechslera graminea* in germinating barley. K Vet Landbohoejsk Arsskr 1976:49-64.

Subrahmanyam NC, Kasha KJ (1975) Chomosome doubling of barley haploids by nitrous oxide and colchicines treatments. Can J Genet Cytol 17:573-583.

Acta Biologica Szegediensis

Volume 63(2):119-124, 2019
Acta Biologica Szegediensis
http://abs.bibl.u-szeged.hu/index.php/abs
DOI:10.14232/abs.2019.2.119-124

ARTICLE

Phytochemical analysis, cytotoxicity and antioxidant activity of cuckoo pint (*Arum maculatum*) leaf extract

Hanady SA Al-Shmgani[1], Zahraa Hussein M Kadri[1], Mohammad MF Al-Halbosiy[2], Yaser Hassan Dewir[3,4*]

[1]Biology Department, College of Education for Pure Science/Ibn al-Haitham, University of Baghdad, Baghdad, Iraq
[2]Biotechnology Research Center, Al-Nahrain University, Baghdad, Iraq
[3]Plant Production Department, College of Food and Agriculture Sciences, King Saud University, Riyadh 11451, Saudi Arabia
[4]Department of Horticulture, Faculty of Agriculture, Kafrelsheikh University, Kafr El-Sheikh 33516, Egypt

ABSTRACT *Arum maculatum* is traditionally used for the control of many diseases and illnesses such as kidney pain, liver injury, hemorrhoids. However, the detailed biomedical knowledge about this species is still lacking. This study reports on the bioactive components and the possible mechanisms underlying the antioxidant, anti-inflammatory and cytotoxic activity of *A. maculatum* leaf extract. Gas chromatography-mass spectrometry (GC-MS) was used for phytochemical analysis. Assay of 3-(4,5-dimethylthiazol-2-yl)-2,5-diphenyltetrazolium bromide) (MTT) was used to determine the cytotoxicity in the murine cell line L20B upon exposure to different extract concentrations for 24 h. Enzyme-linked immunosorbent assay (ELISA) was used to detect pro-inflammatory cytokines and tumor necrosis factor-α (TNF-α). GC-MS analysis identified the presence of important phytochemical components, *e.g.*, 9-octadecenoic acid, methyl ester, (E), hexadecanoic acid, methyl ester, followed by benzenepropanoic acid, 3,5-bis(1,1-dimethylethyl)-4-hydroxy-, methyl ester (17.74%), heptadecanoic acid, 16-methyl-, methyl ester and dibutyl phthalate. The results indicated a significant dose-dependent decrease in L20B cell growth at a dose of 400 µg/ml (IC_{50}) that is associated with a significant 2,2-diphenyl-1-picrylhydrazyl (DPPH) scavenging activity. The results suggested that the aqueous extract of *A. maculatum* leaves have potent antioxidant activity and cytotoxicity against L20B cell line with potential pro-inflammatory activity. **Acta Biol Szeged 63(2):119-124 (2019)**

KEY WORDS
Arum maculatum
DPPH
GC-MS analysis
L20B cell line
MTT

ARTICLE INFORMATION
Submitted
20. September 2019.
Accepted
13. October 2019
***Corresponding author**
E-mail: ydewir@ksu.edu.sa
ydewir@hotmail.com

Introduction

A very large number of individuals around the world still rely on traditional medicine for the treatment of various acute and chronic diseases. Even in countries where the modern medicine is very advanced, these herbal extracts, syrups, essential oils and other formulations are sold in pharmacies and supermarkets. Botanical supplements are believed to be safe as there are no or minimal side-effects. Moreover, using herbal medicines is advantageous due to the occurrence of several biologically active compounds which in certain cases may act synergistically to deliver an effective curing power that cannot be attained by any one component in the natural mixture. On the other hand, they could also be harmful because of the possible presence of toxic components (Ekor 2014).

The genus *Arum*, belonging to the Araceae family, has a long history of traditional medicinal uses in the Middle East, southern Europe and northern Africa. In folk medicine, *Arum* species such as *A. dioscorides* (Afifi-Yazar et al. 2011) and *A. palaestinum* (Afifi-Yazar et al. 2011; Zaid et al. 2012; Naseef et al. 2017) have been used for the treatment of cancer. Cuckoo pint (*A. maculatum*) is a woodland plant that grows in the northern region of Iraq where it is commonly known as '*kardi*'. Cuckoo pint leaves are the edible parts consumed by the local population after removing the toxic constituents by cooking. Toxicity of *A. maculatum* is attributable to the presence of toxic volatiles, especially amines, oxalates, cyano compounds as well as contents such as alkaloids and saponins (Azab 2017).

The raw plant is not edible due to its toxic and allergenic properties. It has been reported to cause irritation to skin, mouth, tongue, and throat, resulting in throat swelling, difficulty in breathing, burning pain, and stomach ache (Robertson 2009). However, its therapeutic importance for many diseases, including kidney

and liver injuries, hemorrhoids and as a pain reliever has been reported (Abbasi et al. 2014; Kochmarov et al. 2015). Mice orally treated with *A. maculatum* methanolic extract showed different histological and antioxidant activity effects in the liver (Kadri et al. 2016). Other studies have shown antimicrobial and antifungal activities of this plant extract against a wide range of Gram-positive, Gram-negative bacteria and fungi (Safari et al. 2014; Çolak et al. 2009). The pro-inflammatory activity of monocot lectin isolated from *A. maculatum* has been reported to increase neutrophil migration (Alencar et al. 2005). The antitumor activity of *A. palaestinum* on different human cancer cells has been investigated by Farid et al. (2015), where significant anti-proliferative activity was reported. TNF-α initiate inflammation, either local or systemic, via stimulation of cytokines such as interleukin-1β (IL-1β) and IL-6. Other roles are the signal suppression of T-cell and the inhibition of antigen production by dendritic cells (O'Shea et al. 2002). IL-1β induces both local and systemic signs of inflammation. It also promotes the production of various enzymes, for example, cyclooxygenase type 2, adhesion molecules and importantly other cytokines and chemokines of pathogenic importance in some diseases (Dinarello et al. 2009). The present study aimed to investigate the active compounds in the aqueous extracts of *A. maculatum* leaves as well as their antioxidant, anti-inflammatory and cytotoxic effects.

Materials and Methods

Chemicals and reagents

Cell culture reagents were purchased from Lonza (Slough, Berkshire, UK). Culture plates were obtained from Becton Dickinson. Roswell Park Memorial Institute (RPMI) 1640 medium was purchased from Gibco (Paisley, UK). All other reagents and chemicals [(4-(2-hydroxyethyl)-1-piperazineethanesulfonic acid (HEPES), Fetal bovine serum (FBS) trypsin, DPPH and MTT] were of analytical grade and purchased from Sigma-Aldrich (St. Louis, MO, USA). Mouse IL-1β and TNF-α were obtained from Pierce Endogen (Rockford, IL, USA).

Plant collection and extract preparation

A. maculatum leaves were obtained from a local market in the Kurdistan region located north of Iraq and was identified by an eminent plant taxonomist at Baghdad University. Voucher specimens were deposited at the Herbarium of Bakrajo Agricultural Technical Institute (Sulaimani Polytechnic University, Kurdistan, Iraq). Leaves were air dried at room temperature, and then grounded into powder. The aqueous extraction method was selected to prepare *A. maculatum* extract because it is a commonly used method in folk medicine. The extract was prepared as follows (Taskeen et al. 2009): 50 g of powdered dried leaf powder was suspended in 500 ml of distilled water in conical flasks and stirred for 6 h using a magnetic stirrer. The extracts were filtrated using filter paper (Whatman No. 1) and centrifuged at 3000 rpm for 10 min. The supernatants were then transferred and dried under reduced pressure using a rotary evaporator and were kept at 4 °C for further analysis and experiments.

GC-MS analysis and identification of phytochemical components

The GC-MS analysis of aqueous cuckoo pint (*A. maculatum; 'kardi'*) extract was performed using a Clarus 500/580 Perkin Elmer GC (Connecticut, USA), including a AOC-20i auto-sampler, and equipped with a fused silica capillary column Elite-1 (100% methyl polysiloxane; 30 m × 0.25 mm, 0.25 μm). Helium (99.99%) was used as a carrier gas at a constant flow rate of 1 ml/min. 0.5 μl samples were injected at a split ratio (1:10). Injector temperature was 280 °C. Oven temperature was programmed to automatically increase at a rate of 10 °C/min from 110 °C up to 200 °C, then at 5 °C/min further up to 280 °C (10 min). Mass scans were taken at electron energy 70 eV (0.5 sec scan interval) and in the range of 40-450 Da; with a total run time of 36 min. Analysis of mass spectrum of GC-MS was done using the database of the National Institute Standard and Technology (NIST). The mass spectrum of the unknown components was compared with the spectrum of the components stored in the NIST library (Nezhadali et al. 2010; Sathyaprabha et al. 2011).

Antioxidant activity measurement

The antioxidant activity was determined using 2,2-diphenyl-1-picrylhydrazyl (DPPH) according to Mimica-Dukic et al. (2003). The DPPH assay has been widely used to detect the scavenging activities of plant extracts. The principle of the assay is based on reduction of DPPH via hydrogen donation from antioxidant by which the color change can be spectrophotometrically recorded. Briefly, 1 ml of the samples was mixed with an equal volume of the DPPH solution (60 μM). After 30 min incubation at 37 °C in darkness, the absorbance was recorded at 517 nm spectrophotometrically (Perkin-Elmer Lambda 25, Germany). L-ascorbic acid was used as a positive control and measurements were carried out in triplicate. Inhibition of free radicals by DPPH was calculated by the following equation:

$$\text{DPPH scavenging activity (\%)} = \text{Ac-As/Ac} \times 100$$

Where, Ac = control absorbance and As = sample absorbance

Cell culture

The murine cell line L20B was provided by the Center of Biotechnology at Al-Nahrain University (Baghdad, Iraq). L20B cell line is derived from mouse cells (fibroblasts) and has been found to express the human poliovirus receptor (Pipkin et al. 1993). RPMI-1640 medium containing 10% fetal bovine serum (FBS), 1% antibiotic (containing 10 000 U/ml penicillin G, 10 mg/ml streptomycin and 25 μg/ml amphotericin B) was used for cell culture and maintenance. Cells were incubated at 37 °C in humidified 5% CO_2 and cultured to 2.5×10^5 cells/ml concentration.

Measurement of cell viability

The colorimetric cell viability MTT assay was carried out as described before (Nouri et al. 2015). Cells were seeded in 96-well plates at a concentration of 1×10^5 cell/ml. After 48 h of incubation, 100 μl of plant extracts at concentrations of 0.4, 4, 40 and 400 μg/ml were added to each well followed by an incubation period of 24 h. After the incubation, 10 μl of MTT solution (5 mg/ml) was added to each well and the plates were further incubated at 37 °C for 4 h. Finally, 50 μl of dimethyl sulfoxide (DMSO) was added to each well and incubated for 10 min. L20B cells cultured in medium without *A. maculatum* extract served as the control. The absorbance was measured at 620 nm using a microplate reader (VersaMax, Molecular Devices, Sunnyvale, CA). Percent of inhibition ratio was calculated according to the following formula:

$$GI\% = \frac{(\text{OD of control wells - OD of test wells})}{\text{OD of control wells}} \times 100$$

Where GI = growth index and OD = optical density.

Detection of pro-inflammatory cytokines by enzyme-linked immunosorbent assay (ELISA)

Protein levels of TNF-α and IL-1β in the serum were measured using an ELISA kit (Pierce Endogen, Rockford, IL, USA) according to the manufacturer instructions. Briefly, 50 μl/well of samples (treated mice with 50 and 100 μg/ml and control mice which received normal saline solution of 0.9% NaCl) was added to the anti-mouse TNF-α and IL-1β-pre-coated 96-well plates. After washing with phosphate buffered saline (PBS, containing 0.05% Triton X-100), the detection antibodies (0.5 μg/ml) were dissolved in 2% bovine serum albumin (BSA) in PBS and then added to the plates before incubation for 4 h at room temperature. After washing, 50 μl of conjugate streptavidin-horseradish peroxidase (HRP) dissolved in 2% BSA (in PBS) (1:250) was added to each well. After washing with the buffer, 100 μl of chromogenic substrate tetramethylbenzidine (TMB) was added to each well before incubation for 15 min at room temperature to allow color development. To stop the reaction, the HRP was denatured by adding 1 M sulfuric acid (50 μl/well) resulting in a color change to yellow. Absorbance was read at 450 nm using a plate reader (VersaMax, Molecular Devices, Sunnyvale, CA, USA) equipped with SoftMax Pro software version 5.4. The cytokine concentrations were determined by comparison with the values for standard recombinant human cytokines (0-5 ng/ml) and all samples were analyzed in triplicate.

Statistical analysis

Statistical analysis was performed using SPSS software version 16.0. All results are presented as means ± standard error. Significance was calculated using analysis of variance (ANOVA) and Fisher Least Significant Difference (LSD) test.

Results and Discussion

GC-MS analysis

GC-MS analysis of the leaf extracts showed the presence of major components (peak area > 1%). The major compounds identified are: 9-octadecenoic acid, methyl ester, (E) (24.76%), hexadecanoic acid, methyl ester (22.45%), followed by benzenepropanoic acid, 3,5-bis(1,1-dimethylethyl)-4-hydroxy-, methyl ester (17.74%). These constituents have been investigated for their biological and therapeutic properties, including the anti-inflammatory (Othman et al. 2015), antioxidant (Pinto et al. 2017), antibacterial and antifungal activities (Agoramoorthy et al. 2007). Previous investigation has shown that palmitic acid induces apoptosis in the human leukemic cell line and demonstrated *in vivo* antitumor activity in mice (Harada et al. 2002). Our results are supported by those of a previous report (Kianinia and Farjam 2018) of the essential oil of Iranian *A. maculatum* extracts, mainly consisting of palmitic acid, phytol, methyl 9,12,15-octadecatrienoate and methyl linolenate.

Antioxidant activity

The aqueous extract was tested for its antioxidant activity at concentrations of 100, 150, 200, and 250 μg/ml using DPPH. Results showed that the extracts showed a significantly higher and concentration-dependent radical scavenging activity up to 200 μg/ml, as compared with the positive control (L-ascorbic acid). Higher activity ($P \leq 0.01$) was observed at 250 μg/ml while the lowest activity was observed at 100 μg/ml ($P \leq 0.05$) compared with the ascorbic acid control (Fig. 1).

The antioxidant activity of phenols and flavonoids has been attributed to their redox activities, allowing them to act as reducing agents and free radical scaven-

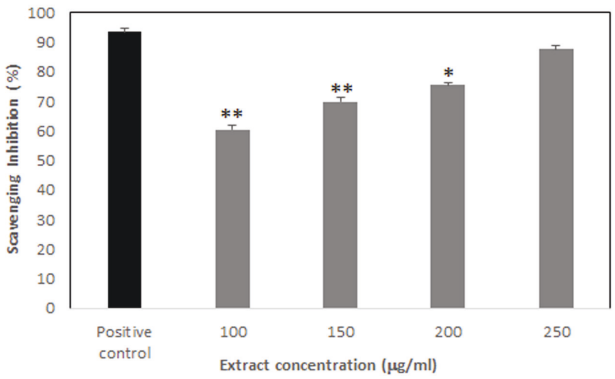

Figure 1. DPPH free radical scavenging activity of *A. maculatum* leaf extract measured at 517 nm. Values presented are means ± SE (n = 3). Stars mean significant difference at $P \leq 0.05$ (*) and $P \leq 0.01$(**), respectively, as compared to positive control (L-ascorbic acid).

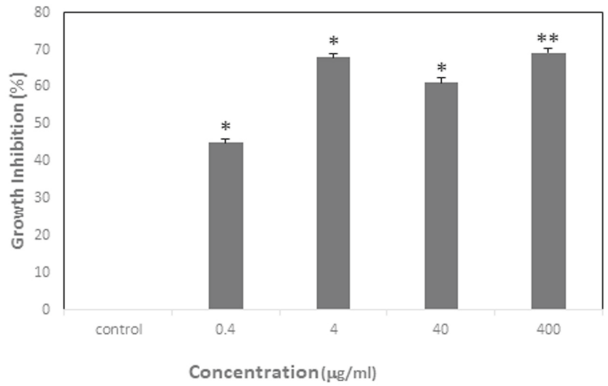

Figure 2. Growth inhibition of L20B cell lines treated with different concentrations of *A. maculatum* leaf extract using MTT assay after 24 h of treatment. Values presented are means ± SE (n = 3). Stars mean significant difference at $P \leq 0.05$ (*) and $P \leq 0.01$(**), respectively, as compared to control.

gers. The observed DPPH scavenging activities indicate an antioxidant protective role against oxidative stress, which is implicated in several diseases. The DPPH assay has been widely used to detect the radical scavenging activity of extracts of several medicinal plant species, including *Panax ginseng* (Ali et al. 2006), *Echinacea purpurea* (Paek et al. 2009), *Withania somnifera* (Dewir et al. 2010) and *Albizia odoratissima* (Banothu et al. 2017). The results reported herein suggest that *A. maculatum* leaf extracts contain hydrogen donating compounds that can eliminate free radicals and therefore could explain their therapeutic application for different pathological injuries caused by oxidation.

Cell viability

Our results showed that treatment with *A. maculatum* extract significantly ($P \leq 0.01$) inhibited cell growth as compared to control cultures (Fig. 2). The highest inhibition (69% ± 0.024) was recorded at 400 µg/ml and it decreased when extract concentration was reduced, reaching only 45% ± 0.020 cell growth inhibition at 0.4 µg/ml. Therefore, the suppression of LB20 cell proliferation was concentration dependent. These results might be due to the presence of flavonoids, glycosides, polyphenols and saponins which act as active agents against cell death. It has been previously reported that fatty acids may play a role in triggering apoptosis associated with trauma in the central nervous system (CNS) and peripheral nervous system (PNS) (Ulloth et al. 2003). Our results indicated that the major compounds present in *A. maculatum* extract are fatty acids, including hexadecanoic acid, palmitic acid (a saturated fatty acid), and 9-octadecenoic acid, methyl ester, (E) (elaidic acid), an unsaturated fatty acid.

Generally, fatty acids and their methyl ester derivatives are biologically active compounds with antioxidant, anticancer and antihistaminic properties (Melariri et al. 2012). Palmitic acid has been reported earlier as a potential anticancer drug (Harada et al. 2002) as significant loss of viability of nerve growth factor (NGF)-differentiated PC12 cells was observed after 24 h treatment with stearic and

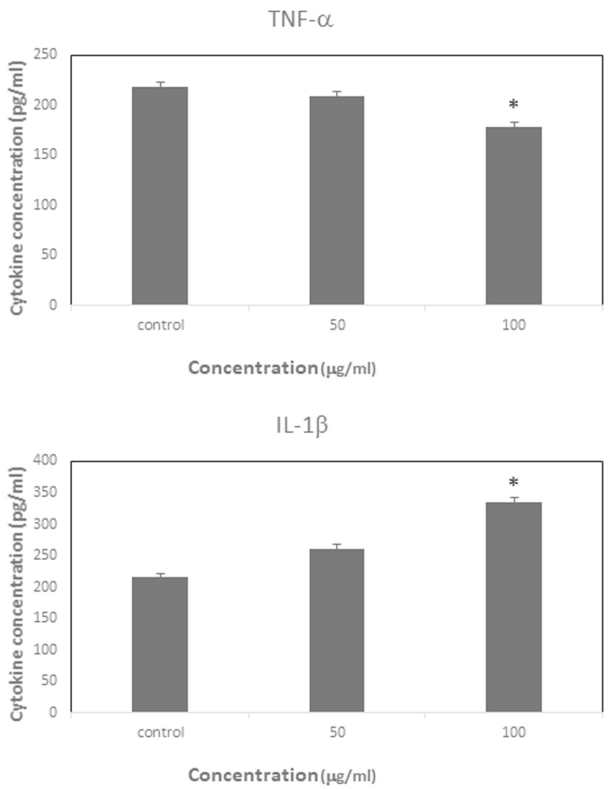

Figure 3. Concentrations of pro-inflammatory cytokines TNF-α and IL-1β determined by ELISA from mice serum in response to treatment with different concentrations of *A. maculatum* leaf extract. Values presented are means ± SE (n = 3). Stars means significantly different at $P \leq 0.01$ (*) as compared to control.

palmitic acids. Additionally, a fortified aqueous extract of *Arum palaestinum* contained high levels of isovanillin, linolenic acid and β-sitosterol which significantly reduced the number of live prostate cancer cells line in a dose-dependent manner, shifting the percentage of dead cells from 30% to 55% at the highest dose (doses of 0.015 to 6.25 mg/ml) (Cole et al. 2015).

Determination of pro-inflammatory cytokines

ELISA showed that the mean concentrations of the two cytokines (IL-1β and TNF-α) were dose-dependent (Fig. 3). Mice treated with *A. maculatum* extract at 100 ng/ml showed significantly ($P \leq 0.05$) decreased TNF-α cytokine levels, whereas 50 ng/ml caused no significant reduction. However, treatment with 50 and 100 ng/ml increased IL-1β level in the blood and significantly higher cytokine levels ($P \leq 0.05$) were observed with 100 ng/ml, as compared to controls.

A. maculatum agglutinin reportedly shows both dose-dependent and independent pro-inflammatory activity, inducing neutrophil migration by the resident cells and in the presence of macrophages, respectively (Alencar et al. 2005). It has been reported that the underlying mechanism of the anti-inflammatory and anti-microbial activities of flavones are due to their ability to regulate the Toll receptor/ NFκB axis which is responsible for the expression of mediator inflammation such as TNF-α, IL-1β and cyclooxygenase-2 (Jiang et al. 2016). Gupta et al. (2010) proposed that the small molecules that suppress NF-κB activation might have a prospective therapeutic potential by phosphorylation of the NFκB p65 subunit. Inhibition of p65 phosphorylation reduces the expression of inflammatory cytokines, limiting characteristic cell damage of acute inflammation.

Conclusion

Determination of pro-inflammatory cytokines, MTT assay and DPPH tests revealed that *A. maculatum* leaf extracts possess anti-inflammatory, cytotoxic and antioxidant activities. Therefore, our findings substantiate *A. maculatum* as a potentially useful herb in alternative medicine against some serious human health problems. Further research on cytotoxicology is required to guarantee herbal drug safety.

Acknowledgments

The authors are thankful to the Researchers Support & Services Unit (RSSU) at King Saud University for their technical support.

References

Abbasi N, Karkondi VR, Asadollahi K, Tahmasebi M, Ghobad A, Taherikalani M, Parisa A (2014) Analgesic effects of *Arum maculatum* plant extract in rats compared to other routine analgesics. J Med Plants Res 8:1025-1030.

Afifi-Yazar FU, Kasabri V, Abu-Dahab R (2011) Medicinal plants from Jordan in the treatment of cancer: Traditional uses vs. *in vitro* and *in vivo* evaluations - Part 1. Planta Med 77:1203-1209.

Agoramoorthy G, Chandrasekaran M, Venkatesalu V, Hsu MJ (2007) Antibacterial and antifungal activities of fatty acid methyl esters of the blind-your-eye mangrove from India. Braz J Microbiol 38:739-742.

Alencar VB, Alencar MNN, Assreuy AMS, Mota, ML, Brito GAC, Aragão KS, Bittencourt FS, Pinto VPT, Debray H, Ribeiro RA, Cavada BS (2005) Pro-inflammatory effect of *Arum maculatum* lectin and role of resident cells. Int J Biochem Cell Biol 37:1805-1814.

Ali MB, Singh N, Shohael AM, Hahn EJ, Paek KY (2006) Phenolics metabolism and lignin synthesis in root suspension cultures of *Panax ginseng* in response to copper stress. Plant Sci 171:147-154.

Azab A (2017) *Arum*: a plant genus with great medicinal potential. Eur Chem Bull 6:59-68.

Banothu V, Neelagiri C, Adepally U, Lingam J, Bommareddy K (2017) Phytochemical screening and evaluation of *in vitro* antioxidant and antimicrobial activities of the indigenous medicinal plant *Albizia odoratissima*. Pharm Biol 55:1155-1161.

ÇolaK F, Savaro IF, Ihan S (2009) Antibacterial and antifungal activities of *Arum maculatum* L. leaves extracts. J Appl Biol Sci 3:13-16.

Cole C, Burgoyne T, Lee A, Stehno-Bittel L, Zaid G (2015) Erratum to: *Arum palaestinum* with isovanillin, linolenic acid and β-sitosterol inhibits prostate cancer spheroids and reduces the growth rate of prostate tumors in mice. BMC Complement Altern Med 15:322.

Dewir YH, Chakrabarty D, Lee SH, Hahn EJ, Paek KY (2010) Indirect regeneration of *Withania somnifera* and comparative analysis of withanolides in *in vitro* and greenhouse grown plants. Biol Plant 54:357-360.

Dinarello CA (2009) Immunological and inflammatory functions of the interleukin-1 family. Annu Rev Immunol 27:519-550.

Ekor M (2014) The growing use of herbal medicines: Issues relating to adverse reactions and challenges in monitoring safety. Front Pharmacol 4:1-10.

Farid MM, Hussein SR, Ibrahim LF, Desouky MAE, Elsayed AM, Oqlah AAE, Saker MM (2015) Cytotoxic activity and phytochemical analysis of *Arum palaestinum* Boiss. Asian Pac J Trop Biomed 11:944-947.

Gupta SC, Sundaram C, Reuter S, Aggarwal BB (2010)

Inhibiting NF-κB activation by small molecules as a therapeutic strategy. Biochim Biophys Acta 1799:775-787.

Harada H, Yamashita U, Kurihara H, Fukushi E, Kawabata J, Kamei Y (2002) Antitumor activity of palmitic acid found as a selective cytotoxic substance in a marine red alga. Anticancer Res 22:2587-2590.

Jiang N, Doseff AI, Grotewold E (2016) Flavones: From biosynthesis to health benefits. Plants (Basel) 5(2):27.

Kadri ZHM, Ibrahim NA, Al-Shmgani HS (2016) Hepatotoxicity evaluation of methanol leaves extract of *Arum maculatum.* IIOABJ 7:435-440.

Kianinia S, Farjam MH (2018) Chemical and biological evolution of essential oil of *Arum maculatum*. Iran J Sci Technol Trans Sci 42:395-399.

Kochmarov V, Kozuharova E, Naychov Z Momekov, G Mincheva I (2015) Ethnobotany and ethno-pharmacology of *Arum maculatum* L. (Araceae) in Bulgaria with an emphasis on its effect against hemorrhoids. Int J Pharm Chem Biol Sci 5:394-402.

Melariri P, Campbell W, Etusim P, Smith P (2012) In vitro and in vivo antimalarial activity of linolenic and linoleic acids and their methyl esters. Adv Stud Biol 4:333-349.

Mimica-Dukic N, Bozin B, Sokovic M, Mihajlovic B, Matavulj M (2003) Antimicrobial and antioxidant activities of three *Mentha* species essential oils. Planta Med 69:413-419.

Naseef H, Qadadha H, Abu Asfour Y, Israr Sabri I, Al-Rimawi F, Abu-Qatouseh L, Farraj M (2017) Anticancer, antibacterial, and antifungal activities of *Arum palaestinum* plant extracts. World J Pharm Res 6:31-43.

Nezhadali A, Nabavi M, Akbarpour M (2010) Chemical composition of ethanol/n-hexane extract of the leaf from *Tanacetum polycephalum* subsp. *duderanum* as a herbal plant in Iran. Der Pharmacia Sinica 1:147-150.

Nouri MA, Al-Halbosiy MMF, Dheeb BI, Hashim AJ (2015) Cytotoxicity and genotoxicity of gliotoxin on human lymphocytes *in vitro.* J King Saud Univ-Sci 27:193-197.

O'Shea JJ, Ma A, Lipsky P (2002) Cytokines and autoimmunity. Nat Rev Immunol 2:37-45.

Othman AR, Abdullah N, Ahmad S, Ismail IS, Zakaria MP (2015) Elucidation of *in-vitro* anti-inflammatory bioactive compounds isolated from *Jatropha curcas* L. plant root. BMC Complement Altern Med 15:11.

Paek KY, Murthy H, Hahn EJ (2009) Establishment of adventitious root cultures of *Echinacea purpurea* for the production of caffeic acid derivatives. In Jain SM, Saxena PK, (eds), Protocols for *In Vitro* Cultures and Secondary Metabolite Analysis of Aromatic and Medicinal Plants. Methods in Molecular Biology (Methods and Protocols), Vol 547, Humana Press, Totowa, NJ.

Pinto MEA, Araújo SG, Morais MI, Sá NP, Lima CM, Rosa CA, Siqueira EP, Johann S, Lima LARS (2017) Antifungal and antioxidant activity of fatty acid methyl esters from vegetable oils. An Acad Bras Cienc 89:1671-1681.

Pipkin PA, Wood DJ, Racaniello VR, Minor PD (1993) Characterization of L cells expressing the human poliovirus receptor for the specific detection of polioviruses *in vitro.* J Virol Methods 41:333-340.

Robertson J (2009) Arum maculatum, cuckoopint, lords and ladies. The Poison Garden. http://www.thepoisongarden.co.uk/atoz/arum_maculatum.htm

Safari E, Amiri M, Bahador A, Amiri M, Esmaeili D (2014) The study of antibacterial effects of alcoholic extracts of *Arum maculatum*, *Allium hirtifolium* and *Teucrium polium* against nosocomial resistance bacteria. Int J Curr Microbiol App Sci 3:601-605.

Sathyaprabha G, Kumaravel S, Panneerselvam A (2011) Bioactive compounds identification of *Pleurotus platypus* and *Pleurotus eous* by GC-MS. Adv Appl Sci Res 2:51.

Taskeen A, Naeem I, Mubeen H, Mehmood T (2009) Reverse phase high performance liquid chromatographic analysis of flavonoids in two *Ficus* species. N Y Sci J 2:32-35.

Ulloth JE, Casiano CA, De Leon M (2003) Palmitic and stearic fatty acids induce caspase-dependent and -independent cell death in nerve growth factor differentiated PC12 cells. J Neurochem 84:655-668.

Zaid H, Silbermann M, Ben-Arye E, Saad B (2012) Greco-Arab and Islamic herbal-derived anticancer modalities: From tradition to molecular mechanisms. Evid-Based Complement Alternat Med, Article ID 349040.

Acta Biologica Szegediensis

Volume 63(2):125-133, 2019
Acta Biologica Szegediensis
http://abs.bibl.u-szeged.hu/index.php/abs
DOI:10.14232/abs.2019.2.125-133

ARTICLE

Impact of exogenous alpha tocopherol on peanut seedlings (*Arachis hypogaea* L.) treated by norflurazon

Imene Manaa*, Reda Djebbar, Ouzna Abrous-Belbachir

* Laboratory of Biology and Physiology of Organisms (LBPO), Faculty of Biological Sciences, University of Sciences and Technology Houari Boumediene, El Alia, Bab Ezzouar, Algeria

ABSTRACT Norflurazon 100 µM alone or in combination with α-tocopherol (0.25 mM) was applied in pre-emergence of peanut seedlings (*Arachis hypogaea* L.). Norflurazon treatment allowed to partially or totally photobleach plants which were noticeably smaller than the control. Norflurazon impaired the photosynthetic activity by decreasing photosynthetic pigments (carotenoids and chlorophylls) and by reducing quantities of soluble sugar. The determination of malondialdehyde (MDA) showed that its content was higher in treated plants in relation with enhancement of reactive oxygen species by the herbicide and decreased the endogenous α-tocopherol. The addition of exogenous α-tocopherol reduced the damage done by the herbicide at the membrane level because of the MDA content was less important than in norflurazon treated seedlings. Furthermore, the norflurazon decreased the glutathione S-transferase (GST) activity in the leaves and the roots of peanut seedlings, while it increased the level of reduced glutathione. This activity decreased even more with the application of exogenous α-tocopherol in combination with the herbicide. The herbicide alone or in association with the antioxidant α-tocopherol increased ascorbic acid content. The supplementation of α-tocopherol did not decrease the phytotoxicity of norflurazon although we observed a decrease in MDA content.
Acta Biol Szeged 63(2):125-133 (2019)

KEY WORDS
Arachis hypogaea
carotenoids
lipid peroxidation
norflurazon
α-tocopherol

ARTICLE INFORMATION
Submitted
13 August 2019.
Accepted
19 October 2019.
***Corresponding author**
E-mail: oabrous@yahoo.fr

Introduction

Environmental stresses like biotic and abiotic factors, adversely affect the productivity and quality of agriculturally important crops. To improve the yield of peanuts, pesticides are usually used to protect crops from weeds, diseases and pests. Unfortunately, the agricultural products can be contaminated with pesticides by the improper and abusive use of them as well as due to the plants' uptake of them from contaminated water and soil. Unlike hydrocarbons, pesticides are deliberately abused by humans in order to increase agricultural yields.

Abiotic stresses are known to cause damage to plants, either directly or indirectly through Reactive Oxygen Species (ROS) formation (Jung et al. 2000). Oxidative stress, characterized by excess accumulation of ROS, could result from various environmental stresses such as herbicides (Doulis 1994). The ROS are toxic and may result in a series of damages to plant metabolism. It damages photosynthetic components, inactivates proteins, destroys cell membrane structures and lower membrane permeability by causing lipid peroxidation (Mittler et al. 2004). ROS are also sensed by the plant cells and can act as a signal molecule that can induce ROS-detoxifying responses (Karuppanapandian et al. 2011). Norflurazon is a systemic herbicide which penetrates the plant through the roots. It is able to remotely reach the sensitive cell sites by means of the conducting vessels (Scalla 1991).

Norflurazon is a bleaching herbicide used in many research laboratories; the target of norflurazon is the phytoene desaturase, a key enzyme of carotenoid biosynthetic pathway (Breitenbach et al. 2001). Carotenoid deficiency causes oxidative stress due to significant increase of ROS content (Jung et al. 2000). So, carotenoids are not only accessory pigments in the photosynthetic apparatus, they also act as photoprotective agents by absorbing excess energy of triplet excited states of chlorophyll (^{3}Chl) and detoxifying of singlet oxygen $^1O_2$ (Vencill 2002). Norflurazon also inhibits the unsaturation of chloroplast lipids (Abrous-Belbachir et al. 2009).

Plants possess various antioxidants systems to cope with the oxidative stress conditions. These include non enzymatic antioxidants such as carotenoids, tocopherols, ascorbic acid, glutathione, phenolic compounds and antioxidants enzymes such as superoxide dismutases (SOD), catalases, and the ascorbate-glutathione cycle enzymes (Apel and Hirt 2004). In plants, herbicides can be me-

tabolized by a sequential action of several enzymes as cytochrome P450 (CYP450) and glutathione S-transferases (GSTs). Glutathione S-transferases catalyze the conjugation of reduced glutathione (GSH) with some xenobiotic compounds (Higgins and Hayes 2011).

Under the herbicide treatment, plants initiate some defensive and protective mechanisms. One of them is associated with changes in concentrations of vitamins including α-tocopherol and ascorbic acid. Exogenous vitamins have been studied in relation to damage generated by the herbicides and other forms of environmental stresses. Tocopherols are known as tocochromanols, a group of lipophilic antioxidants that are exclusively synthesized by higher plants. Of the two classes of tocochromanols, tocopherols occur more widely in plants and the alpha form is typically abundant in the leaves (Szymańska and Kruk 2008). α-tocopherol, which is located within chloroplast membranes, has gotten the highest antioxidant activity against lipid oxidation (Mène-Saffrané and DellaPenna 2010); it can quench oxygen radicals, stabilize cell membranes and protect chlorophyll (Hess 1993). Tocopherol termination of lipid peroxidation chain is where α-tocopherol donates hydrogen to lipid radicals and turns it to a hydroperoxide molecule, which is then either reduced to an alcohol or further oxidized to other compounds (*e.g.,* n-hexanal, jasmonic acid, and traumatic acid) depending on the size and nature of the lipid chain.

The α-tocopherol radical formed after this process is either recycled back to α-tocopherol by ascorbate or forms other oxidized products (Munné-Bosch 2005). The presence of α-tocopherol can affect intracellular signaling by directly interacting with components of the signaling cascade or indirectly by controlling concentrations of secondary oxidation products (Sattler et al. 2004). Numerous reports are available about attempts that have been made to reduce oxidative stress in plants by exogenous application of tocopherols (Oertli 1987). Awad et al. (2005) reported that, exogenous application of α-tocopherol enhanced date palm plantlets' tolerance to environmental stresses. Peanut (*Arachis hypogaea* L.) is a dicotyledonous plant and an oil seed crop widely cultivated in many areas across the world. It is grown under different agro-climatic zones of tropical and subtropical regions of Asia, Africa, North and South America (Bhatnagar-Mathur et al. 2007). Peanut is an important source of edible oil, dietary minerals, vitamins and proteins. In Algeria, this annual legume is grown in different regions, especially in the south.

Materials and Methods

Used chemicals

Norflurazon (4-chloro-5-methylamino-2a,a,a-trifluoromethylphenyl-3-(2H) pyridazinone; San 9789) was used as a pre-emergence herbicide. It is commercially named Zorial and the recommended use is 2000 g/ha. The concentration here (100 μM) is similar, to the recommended doses. Vitamin E (α-tocopherol or 5,7,8-trimethyl-tocol) was used as exogenous antioxidant. It was purchased from (Fluka). The concentration used was 0.25 mM.

Plant growth conditions and treatments

Peanut (*A. hypogaea* L.) seeds were surface sterilized with diluted sodium hypochlorite 12% for 10 min and then rinsed thoroughly with water. Seed germination was induced by incubation on water-soaked paper at 27 °C for 3 days. Once germinated, seedlings were transplanted into plastic containers containing 160 g of soil. The treatment was carried out by watering the seeds sown in pots with solutions of norflurazon (100 μM) or in combination with α-tocopherol (0.25 mM). Plants were watered once with 20 ml of norflurazon alone or with norflurazon supplemented with α-tocopherol. Controls were irrigated with 20 ml of water. From the second day, plants (control and treated), were grown in a greenhouse and were regularly watered with an appropriate volume of water.

Estimation of growth and dry matter mass

The length of aerial parts was measured from the base of the stems (crown) to the apical bud for 30 days. Dry matter mass was obtained after total desiccation of aerial parts at 60 °C.

Measurement of the leaf surface

The leaf surface is calculated as follows: 1 cm^2 of a paper layer is taken and then weighed using a precision balance (0.1 mg). The shape of the leaf is drawn on the same type of paper, cut and then weighted. The leaf surface (X) is deducted by the following formula:

$$X = \frac{mf}{mp}$$

Mf: mass of paper cut; Mp: mass of 1 cm^2 of the paper

Photosynthetic pigments content

Total pigments from fresh leaves were extracted in 80% (v/v) acetone. Pigments content were determined by absorbance spectrophotometry as recommended by Lichtenthaler (1987).

Soluble sugars content

Soluble carbohydrates content was determined according to the method described by McCready et al. (1950). Measurements were performed at 630 nm. Soluble carbohydrate concentration was determined using a glucose

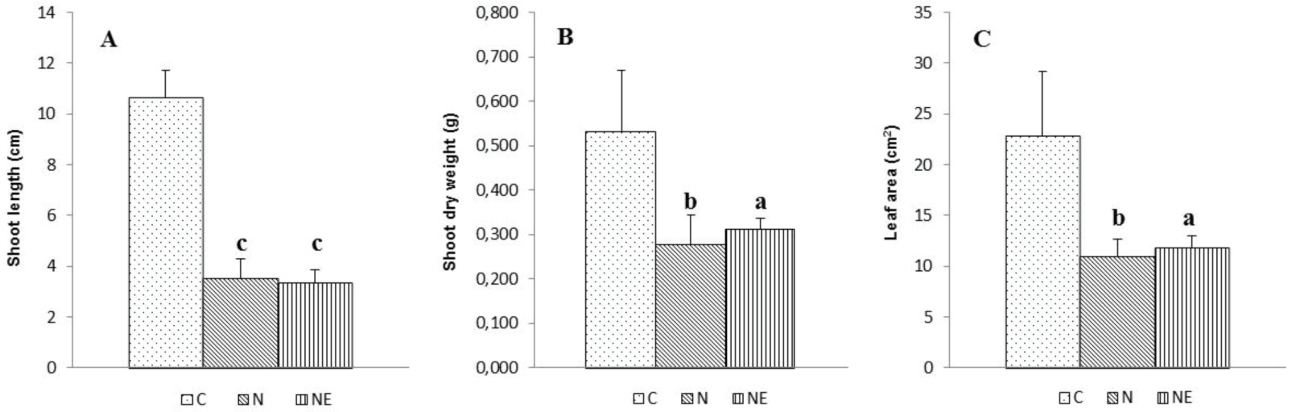

Figure 1. Effects of norflurazon on peanut growth. **C**: control; **N**: 100 µM norflurazon; **NE**: 100 µM norflurazon + 0.25 mM α-tocopherol. Letters indicate the significant differences between the treatments and the control. a: significant ($P < 0.05$); b: very significant ($P < 0.01$); c: highly significant ($P < 0.001$).

standard curve.

Lipid peroxidation analysis

Lipid peroxidation was determined by measuring the content of MDA using a TBARS (Thiobarbituric Acid Reactive Substances) assay as described by Sinnhuber and Yu (1958). The absorbance of the supernatant (TBA-MDA complex) was measured at 532 nm. The concentration of TBARS was calculated by using tetramethoxy-propane as a standard.

Determination of lipid-soluble antioxidant α-tocopherol

α-tocopherol was determined by HPLC, as described by Szymańska and Kruk (2008). The chromatographic conditions of analysis were as follows: the mobile phase was acetonitrile:dichloromethane:methanol (70:20:10, v/v/v), flow rate of 1 ml min^{-1}, UV detection at 292 nm, C_{18} reverse-phase column (220 x 4.6 mm). The levels of α-tocopherol were calculated using α-tocopherol as a standard.

Soluble antioxidants content ascorbate and glutathione

Ascorbate content was determined as described by Hodges et al. (1996) by the measure of absorbance at 525 nm. The ascorbate concentration was calculated from the standard curve using ascorbic acid. The GSH assay was based on the colorimetric method of Ellman (1959). Absorbance at 412 nm was determined by spectrophotometry. The concentrations were deducted from a standard curve established with reduced glutathione.

Glutathione S-transferase activity

GST activity was performed according to Habig et al. (1974), based on the reaction of conjugation between GSH and 1-chloro-2,4-dinitrobenzene (CDNB) in the presence of GST. This activity was measured at 340 nm using the molar extinction coefficient $\varepsilon = 9.6\ M^{-1}cm^{-1}$. Protein content was determined by the method of Bradford (1976) using bovine serum albumin (BSA) as a protein standard.

Statistical analysis

The results are obtained from three independent experiments. The statistical analysis was carried out by ANOVA analysis and Student's t-test.

Results

Morphological analysis

Plants growing in norflurazon-polluted soil were depigmented. Bleaching symptoms had begun at the base of the leaf in treated plantlets and then they spread to the rest of the leaf. Soaking peanut with norflurazon associated with α-tocopherol did not minimize the bleaching symptoms.

Peanut plant growth on soil soaked with norflurazon or norflurazon in combination with α-tocopherol

We measured plant growth over 30 days and compared control plants with plants growing in norflurazon-polluted soil (Fig. 1A). Control plants reached an average 10.65 (± 1.05) cm.

Norflurazon at the concentration of 100 µM had a severe effect on plant growth; it induced a decrease in size (67%) and dry weight (49%) (Fig. 1A, B) which can be due to a probable perturbation in the energetic metabolism. Leaf area in control seedlings was of 22.85 ± 6.36 cm^2, while in norflurazon treated seedlings it decreased

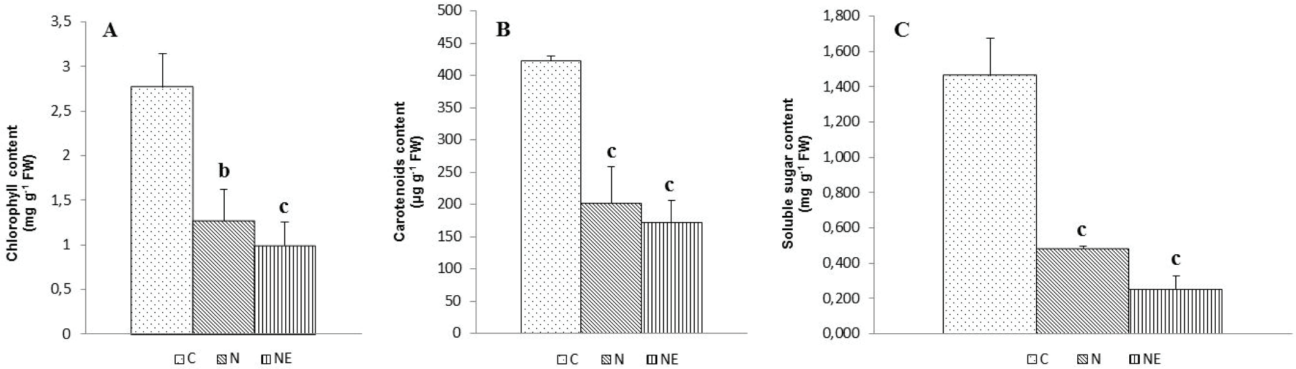

Figure 2. Effects of norflurazon on the content of total chlorophyll (A), carotenoids (B) and soluble sugar (C) in peanut plants. **C:** control; **N:** 100 µM norflurazon; **NE:** 100 µM norflurazon + 0.25 mM α-tocopherol. Letters indicate the significant differences between the treatments and the control. a: significant ($P < 0.05$); b: very significant ($P < 0.01$); c: highly significant ($P < 0.001$).

very significantly (52%) compared to the control (Fig. 1C). Furthermore, the association of norflurazon with α-tocopherol, did not ameliorate the growth of peanut seedlings.

Content of chlorophyll, carotenoids and soluble sugars in plants exposed to norflurazon or norflurazon combined with α-tocopherol

Thirty days after treatment, we quantified photosynthetic pigments. From 2.77 mg g^{-1} FW of chlorophyll in control plants, chlorophyll content was 54 and 64% less in plants grown on norflurazon alone or in combination with α-tocopherol, respectively (Fig. 2A). Concurrently, we found that plants grown in presence of norflurazon alone or combined with α-tocopherol accumulated less of carotenoids 50% to that of control plants (202.03 and 172.37 µg g^{-1} FW compared to 423.57 µg g^{-1} FW in control plants) (Fig. 2B). Figure 2C showed that the soluble sugar content in the leaves of control plants was 1.46 ± 0.21 mg g^{-1} FW. In the presence of norflurazon, this amount significantly reduced to 0.48 ± 0.01 mg g^{-1} FW. The application of α-tocopherol associated with norflurazon decreased the level of soluble sugars to 0.25 ± 0.07 mg g^{-1} FW corresponding to relatively 82% of reduction to control plants.

Norflurazon induced oxidative damage in lipids

The basal level of MDA which was 0.09 nmol g^{-1} in control seedlings, increased to 55% with 100 µM norflurazon treatment; the presence of α-tocopherol lowered the magnitude of increasing MDA to 22% (Fig. 3).

Norflurazon modified non enzymatic antioxidant levels

α-tocopherol content in the control plants was 0.34 ± 0.00 mg g^{-1} FW, this content decreased in the presence of norflurazon treated plants to 0.18 ± 0.08 mg g^{-1} FW corresponding to 47% of reduction; exogenous application of α-tocopherol did not change the level of endogenous α-tocopherol in the norflurazon treated plants which was 0.20 ± 0.08 mg g^{-1} FW (Fig. 4A).

Analysis of ascorbic acid content in leaves of control seedlings, revealed an amount of 1.90 µmol g^{-1} FW of this soluble antioxidant, while, norflurazon treatment resulted in no significant accumulation of ascorbic acid contents compared to controls (Fig. 4B). The presence of α-tocopherol associated with norflurazon greatly elevated the level of ascorbic acid to >2-fold more (3.81 µmol g^{-1} FW) (Fig. 4B). GSH content in leaves (Fig. 4C) increased for norflurazon (93%) or norflurazon in association with α-tocopherol treatment (18%) comparatively to control

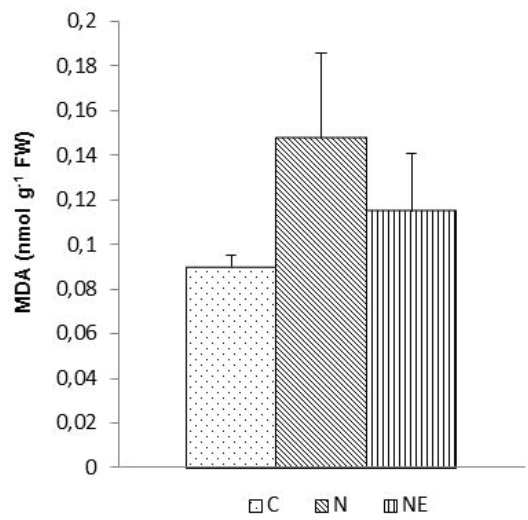

Figure 3. Effects of norflurazon on the content of MDA in peanut plants. **C**: control; **N**: 100 µM norflurazon; **NE**: 100 µM norflurazon + 0.25 mM α-tocopherol.

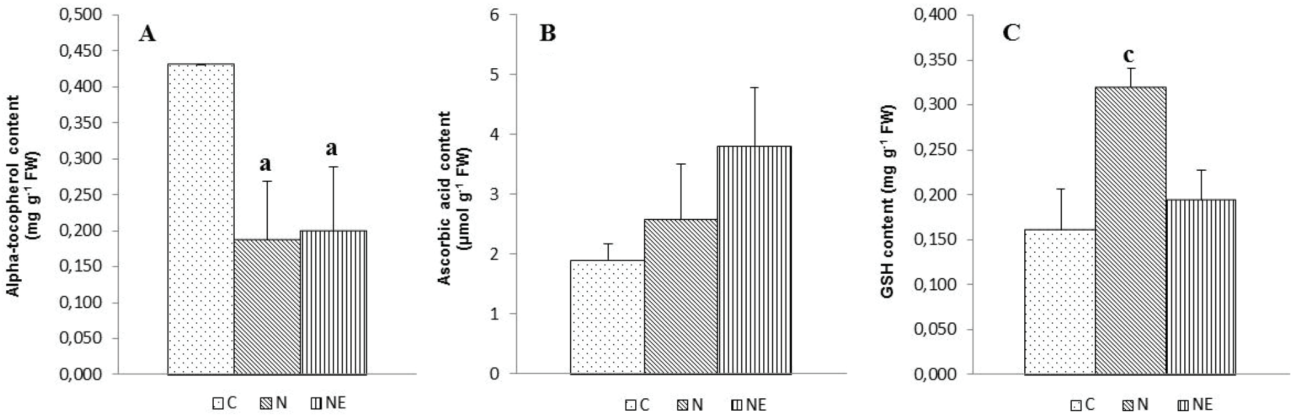

Figure 4. Effects of norflurazon on the content of α-tocopherol (A), ascorbic acid (B) and reduced glutathione (GSH) (C) in peanut plants. **C:** control; **N**: 100 µM norflurazon; **NE**: 100 µM norflurazon + 0.25 mM α-tocopherol. Letters indicate the significant differences between the treatments and the control. a: significant ($P < 0.05$); b: very significant ($P < 0.01$); c: highly significant ($P < 0.001$).

seedlings.

Norflurazon Induced changes in glutathione S-transferase (GST) activity

GST activity was >4-fold higher in leaves compared to roots (0.38 and 0.095 mmol mn^{-1} mg^{-1} respectively) (Fig. 5). In leaves, the herbicide application resulted in decreasing of GST activity which was lowered to 50%. In the presence of norflurazon associated with α-tocopherol, the GST activity was also reduced by about 57% compared to the control (Fig. 5A). In roots, variation of GST activity followed no significant decrease for the application of norflurazon alone. GST activity, however, decreased for the application of norflurazon in association with α-tocopherol with a 55% lower level than in the control (Fig. 5B).

Discussion

Norflurazon is a phytoene desaturase inhibitor which catalyzes a rate-limiting step in carotenoid biosynthesis. In the present study, symptoms of norflurazon toxicity (bleaching of foliage) were apparent after a 100 µM treatment. These symptoms also occurred at 0.25 mM of α-tocopherol associated with norflurazon. Depigmentation or photobleaching was the main morphological symptom observed after treatment with some herbicides such as *e.g.*, norflurazon, amitrole, and acifluorfen (Scalla 1991).

Our results showed that 100 µM of norflurazon had an overall negative effect on peanuts growth. Other plant species, such as maize growing in the presence of norflurazon, also displayed a growth reduction (DallaVecchia et al. 2001). Furthermore, other herbicides such as R-40244 (St John 1985), amitrole (DallaVecchia et al. 2001), chlortoluron (Song et al. 2007), isoproturon (Nemat Alla and Hassan 2014), bentazone (Khan et al. 2004), pendimethalin (Wágner and Nádasy 2006), chlorimuron-ethyl (Scarponi et al. 1998) showed also a growth-reducing effects on their studied plants. At the concentration of 100 µM, norflurazon reduced the content of photosynthetic pigments in peanut seedlings. This was in accordance with previous findings using substituted pyridazinones (Lichtenthaller and Klendgen 1977).

The decrease in carotenoids that we observed was due to the inhibition of desaturation of phytoene to phytofluene, which has resulted in phytoene accumulation (Linden et al. 1990). Because of carotenoids' conjugated double bonds, they are the most abundant quenchers of $^1O_2$ in the pigment bed of the photosynthetic apparatus (Young 1991), so their absence lead to the formation of active oxygen molecules (Jung et al. 2000). Decrease in chlorophylls content observed in depigmented leaves of

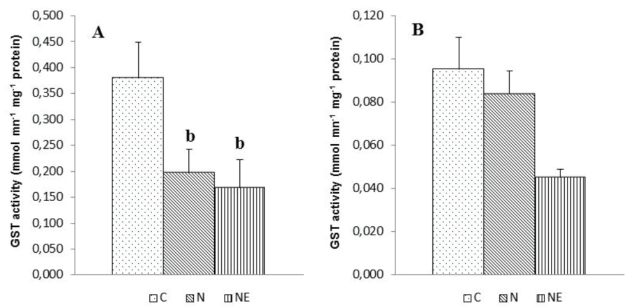

Figure 5. Effects of norflurazon on the activity of GST in leaves (A) and roots (B) on peanut plants. **C**: control; **N**: 100 µM norflurazon; **NE**: 100 µM norflurazon + 0.25 mM α-tocopherol. Letters indicate the significant differences between the treatments and the control. a: significant ($P < 0.05$); b: very significant ($P < 0.01$); c: highly significant ($P < 0.001$).

peanut seedlings was due to photooxidation linked to the depletion of carotenoids (Dankov et al. 2009). The decrease in chlorophylls was also due to a deficiency in their biosynthesis. Oelmuller and Mohr (1986) showed that the last step of chlorophyll biosynthesis does not take place following the destruction of chloroplastic structures by the norflurazon. Interestingly, herbicides which primarily inhibit pigment biosynthesis also have a growth-reducing effect (DallaVecchia et al. 2001).

In our study, there is a positive correlation between decrease of photosynthetic pigments and level of sugar content. We can deduce that peanut plants growing in norflurazon-contaminated soil are impaired in their photosynthesis and display a reduction in growth. Similar results were obtained in maize treated with atrazine, linuron, prometryn, and pyrazon (Osman et al. 1988), wheat treated with isoproturon (Bandana, 2002) and in *Vitis vinifera* L. (bine) stressed with flumioxazin.

MDA, a decomposition product of polyunsaturated fatty acids hydroperoxides, has been utilized very often as a suitable biomarker for lipid peroxidation. The data presented here, show that norflurazon lead to MDA accumulation. Other herbicides as fluazifop-*p*-butyl lead to MDA increase in bristly starbur (Luo et al. 2004). Lipid peroxidation can be initiated by ROS. Norflurazon is known to induce oxidative stress in treated plants by generation of ROS that severely affects cell membranes functionality and integrity and can produce irreversible damages to the cell function (Yoshimura et al. 2004). On the other hand, Abrous-Belbachir et al. (2009) reported that norflurazon affects fatty acids (FA) composition of soybean seedlings and fatty acid desaturases resulting in a decrease in polyunsaturated fatty acids (PUFAs).

The variability in individual responses to herbicide treatment likely results from differences in either the absorption/transport of the herbicide or in metabolizing/detoxification mechanisms, such as those involving CYP450 and GST. GST activities from leaves and roots decreased in peanut seedlings after a 100 μM norflurazon treatment, suggesting an overload of ROS damage. The decrease in the activity of GST in seedlings treated with norflurazon indicated that a part of this herbicide is not conjugated in roots and leaves of the treated plants. Coşkun and Zihnioğlu (2002) suggested that the GST may not be the only enzyme induced by pesticides. Several pesticides can induce in plants differentiation in the other enzyme levels, which are effective in the protective and tolerant system such as the other glutathione related enzymes, and mixed-function oxidases. The conjugation of glutathione with 1-chloro-2,4-dinitrobenzene is widely used for detecting GST activity, but it may not detect all GST isozymes (Timmerman 1989). Ascorbate and glutathione are the two soluble antioxidants that constitute the ascorbate-glutathione cycle and are involved in tocopherol regeneration from α-tocopheroxyl radicals.

In the present study, we found that the soluble glutathione and ascorbate levels were increased in norflurazon treatment alone or combined with α-tocopherol compared to the control plants. Ascorbic acid and reduced glutathione are accumulated in many plant species in response to abiotic stress such as herbicides and water stress (Heber et al. 1996).

Accumulation of glutathione was also observed in unchallenged *Arabidopsis vte1* mutants (slightly but significantly) (Kanwischer et al. 2005) and outdoor grown *Arabidopsis vte1* and *vte4* mutants (Semchuk et al. 2009). The increased glutathione level in the norflurazon treated peanut plants could be interpreted in such a way that it may have triggered alterations in the ROS signaling networks, allowing these plants to achieve a new homeostasis to cope with the abiotic stress. Glutathione was previously proposed as a candidate transmitter of intracellular ROS signals (Foyer and Noctor 2011). The increase in ascorbate and reduced glutathione in treated peanut seedlings by the norflurazon suggests that peanut seedlings have not used these antioxidants to attenuate the deleterious effects of the herbicide. Ågren (1985) mentioned the effect of exogenous application of antioxidant compounds on the primary metabolites of various crops. Exogenous application of some antioxidants and other substances enhanced date palm plantlet tolerance to environmental stress (Awad et al. 2005).

The content of α-tocopherol decreased in peanut seedlings subjected to norflurazon only or the combination of norflurazon and α-tocopherol. The functions of tocopherols, especially α-tocopherol, are recognized as lipid antioxidants with the ability to scavenge and quench various ROS and protect PUFAs from lipid peroxidation (Munné-Bosch, 2005). Tocopherol-deficient mutant showed an increase in non-enzymatic lipid peroxidation products and a range of developmental defects in early seedling growth (Sattler et al. 2006).

Differences in tocopherol content may be due to growing conditions and environmental factors, especially stress conditions (Müller 1998). An *Arabidopsis* double mutant lacking both vitamin E and the carotenoid zeaxanthin was found to be sensitive to photooxidative stress (Havaux et al. 2005), indicating that vitamin E and carotenoids have overlapping functions and that the phototolerance of tocopherol-deficient single mutants was actually due to an increased activity of carotenoids compensating for the loss of tocopherols. Carotenoids, tocopherols, ascorbate and glutathione are interdependent in the control of ROS levels in plants under stress conditions and thus play a role in limiting damage due to induced oxidative stress.

The chemical scavenging of $^1O_2$ by α-tocopherol can

lead to a net tocopherol loss, since α-tocopherol quinone and other oxidation formed products cannot be recycled back to α-tocopherol (Munné-Bosch and Alegre 2002). Irreversible degradation of α-tocopherol may also occur when a-tocopheroxyl radicals, which result from the scavenging of lipid peroxyl radical by α-tocopherol, are not recycled back by ascorbate. This may occur, for example, when ascorbate availability in chloroplasts is limited (Munné-Bosch 2005). The changes in α-tocopherol level during plant responses to environmental stresses are characterized by two phases. In the first phase α-tocopherol levels will tend to increase and contribute to protection by reducing ROS levels and inhibiting lipid peroxidation. When the stress is too severe, tocopherol degradation exceeds its synthesis and levels decrease (phase II) (Munné-Bosch 2005). Peanut seedlings subjected to the norflurazon treatment might be in a severe phase of stress.

Conclusion

In conclusion, our results demonstrate in our culture conditions, that norflurazon at 100 μM induced a lethal physiological state. Both growth and biochemical parameters are profoundly affected, leading to an adverse effect on mechanisms of detoxification. The main effect was membrane destruction linked to a lack of carotenoids and MDA accumulation. The sharp reduction in carotenoids caused by norflurazon gives rise to a damage to morphological and biochemical level sometimes not reversed by the exogenous application of α-tocopherol.

The addition of the exogenous antioxidant α-tocopherol did not alleviate the phytotoxicity of norflurazon although we observed a decrease in MDA content. This result indicates that though α-tocopherol may afford a certain degree of protection against stress conditions, this protection is limited by the amount of other antioxidants present in membranes and/or by the ROS. As in the cases of the other antioxidants, the level of tocopherol is the result of synthesis, recycling and degradation (consumption).

In our conditions, it can be concluded that exogenous tocopherol has assumed its role as protectant of lipid peroxidation. But it seems that both carotenoids and tocopherols are required to overcome the stress which explains that the sharp decline in carotenoids by the norflurazon has significantly affected the growth and physiology of seedlings of peanut despite the presence of exogenous α-tocopherol.

References

Abrous-Belbachir O, De Paepe R, Tremolières A, Mathieu C, Aïd F, Benhassaine-Kesri G (2009) Evidence that norflurazon affects chloroplast lipid unsaturation in Soybean leaves (*Glycine max* L.). J Agric Food Chem 57:11434-11440.

Ågren GI (1985) Limits to plant production. J Theor Biol 113:92-98.

Apel K, Hirt H (2004) Reactive oxygen species: metabolism, oxidative stress, and signal transduction. Annu Rev Plant Biol 55:373-399.

Awad AM, Soaud AA, El-Konaissi MS, Zaid A, Eshkandi OH, Badawi MA (2005) Effect of elemental sulfur, some antioxidants and growth regulators on tolerance ability of *in vitro* produced plantlets and nutrient uptake, yield and fruit quality of mature date palm trees Part I. Tolerance ability of *in vitro* produced plantlets. The sixth Annual Research Conference at UAE University, 24-26 April, 2005.

Bandana SN (2002) Chlorophyll and sugar content in wheat leaves as influenced by isoproturon application and its relationship with grain sugar content. Indian J Plant Physiol 7:401-403.

Bhatnagar-Mathur P, Devi MJ, Reddy DS, Lavanya M, Vadez V, Serraj R, Yamaguchi-Shinozaki K, Sharma KK (2007) Stress inducible expression of At DREB1A in transgenic peanut (*Arachis hypogaea* L.) increases transpiration efficiency under water-limiting conditions. Plant Cell Rep 26:2071-2082.

Bradford MM (1976) A rapid and sensitive method for the quantitation of microgram quantities of protein utilizing the principle of protein-dye binding. Anal Biochem 72:248-259.

Breitenbach J, Zhu C, Sandmann G (2001) Bleaching herbicide norflurazon inhibits phytoene desaturase by competition with the cofactors. J Agric Food Chem 49:5270-5272.

Coşkun G, Zihnioğlu F (2002) Effect of some biocides on glutathione-s-transferase in barley, wheat, lentil and chickpea plants. Turk J Biol 26:89-94.

Dalla Vecchia F, Barbato R, La Rocca N, Moro I, Rascio N (2001) Responses to bleaching herbicides by leaf chloroplasts of maize plants grown at different temperatures. Journal of Experimental Botany 52:811-820.

Dankov K, Busheva M, Stefanov D, Apostolova EL (2009) Relationship between the degree of carotenoid depletion and function of the photosynthetic apparatus. J Photochem Photobiol B: Biology 96:49-56.

Doulis AG (1994) Antioxidant responses of pea (*Pisum sativum* L.) Protoplasts. PhD. PPWS, Virginia Tech.

Ellman GL (1959) Tissue sulfhydryl groups. Arch Biochem Biophys 82:70-77.

Foyer CH, Noctor G (2011) Ascorbate and glutathione: the heart of the redox hub. Plant Physiol 155:2-18.

Habig WH, Pabst MJ, Jakoby WB (1974) Glutathione S-transferases. The first step in mercapturic acid formation. J Biol Chem 249:7120-7130.

Havaux M, Eymery F, Porfirova S, Rey P, Dörmann P (2005) Vitamin E protects against photoinhibition and photooxidative stress in *Arabidopsis thaliana*. Plant Cell 17:3451-3469.

Heber U, Miyake C, Mano J, Ohno C, Asada K (1996) Monodehydroascorbate radical detected by electron paramagnetic resonance spectrometry is a sensitive probe of oxidative stress in intact leaves. Plant Cell Physiol 37:1066-1072.

Hess JL (1993) Vitamin E, α-tocopherol. In:R.G. Alscher and J.L. Hess (eds.) Antioxidants in higher plants. CRC press, Inc. Boca Rarton, Florida, 111-134.

Higgins LG, Hayes JD (2011) Mechanisms of induction of cytosolic and microsomal glutathione transferase (GST) genes by xenobiotics and pro-inflammatory agents. Drug Metab Rev 43:92-137.

Hodges M, Andrews D, Johson J, Hamilton I (1996) Antioxidant compound responses to chilling stress in differentially sensitive inbred maize lines. Phys Plant 98:685-692.

Jung SY, Kim JS, Cho KY, Tae GS, Kang BG (2000) Antioxidant responses of cucumber (*Cucumis sativus*) to photoinhibition and oxidative stress induced by norflurazon under high and low PPFDs. Plant Sci 153:145-154.

Kanwischer M, Porfirova S, Bergmüller E, Dörmann P (2005) Alterations in tocopherol cyclase activity in transgenic and mutant plants of *Arabidopsis* affect tocopherol content, tocopherol composition, and oxidative stress. Plant Physiol 137:713-723.

Karuppanapandian T, Moon JC, Kim C, Manoharan K, Kim W (2011) Reactive oxygen species in plants: their generation, signal transduction, and scavenging mechanisms. Aust J Crop Sci 5:709-725.

Khan MS, Zaidi A, Aamil M (2004) Influence of herbicides on chickpea-*Mesorhizobium* symbiosis. Agronomie 24:123-127.

Lichtenthaller HK, Klendgen HK (1977) Effect of the herbicide San 6706 on biosynthesis of photosynthetic pigments and prenyl quinones in *hordeum* seedlings. Z Naturforsch 32:236-240.

Lichtenthaler HK (1987) Chlorophylls and carotenoids: Pigments of Photosynthetic Biomembranes. Method Enzymol 148:350-382.

Linden H, Sandmann G, Chamouitz D, Hirschber GJ, Boger P (1990) Biochemical characterisation of synechoccus mutants selected against the bleaching herbicide norflurazon. Pestic Biochem Physiol 36:46-51.

Luo XY, Sunohara Y, Matsumoto H (2004) Fluazifop-butyl causes membrane peroxidation in the herbicide-susceptible broad leaf weed bristly starbur (*Acanthospermum hispidum*). Pestic Biochem Physiol 78:93-102.

McCready RM, Guggolz JJ, Silviera V, Owens HS (1950) Determination of starch and amylose in vegetables. Anal Chem 22:1156-1160.

Mène-Saffrané L, DellaPenna D (2010) Biosynthesis, regulation and functions of tocochromanols in plants. Plant Physiol Biochem 48:301-309.

Mittler R, Vanderauwera S, Gollery M, Van Breusegem F (2004) Reactive oxygen gene network of plants. Trends Plant Sci 9:490-498.

Müller H (1998) Drought-induce photooxidative stress and the role of antioxidative defence systems in drought tolerance of wheat genotypes. Universität Hohenheim.

Munné-Bosch S (2005) The role of α-tocopherol in plant stress tolerance. J Plant Physiol 162:743-748.

Munné-Bosch S, Alegre L (2002) Interplay between ascorbic acid and lipophilic antioxidant defences in chloroplasts of water-stressed *Arabidopsis* plants. FEBS Lett 524:145-148.

Nemat Alla MM, Hassan NM (2014) Alleviation of isoproturon toxicity to wheat by exogenous application of glutathione. Pestic Biochem Physiol 112:56-62.

Oelmuller R, Mohr H (1986) Photooxidative destruction of chloroplasts and its consequences for expression of nuclear genes. Planta 167:106-113.

Oertli JJ (1987) Exogenous application of vitamins as regulators for growth and development of plants: a review. Z Pflanzenernähr Bodenk 150:375-391.

Osman RO, Ahmed FA, Khalil FA, Ali MS (1988) Effect of some herbicides as plant growth regulators on the chemical composition of *Zea mays* grains. Food Chem 28:167-176.

Sattler SE, Gilliland LU, Magallanes-Lundback M, Pollard M, DellaPenna D (2004) Vitamin E is essential for seed longevity and for preventing lipid peroxidation during germination. Plant Cell 16:1419-1432.

Sattler SE, Mène-Saffrané L, Farmer EE, Krischke M, Mueller MJ, DellaPenna D (2006) Non-enzymatic lipid peroxidation reprograms gene expression and activates defense markers in *Arabidopsis* tocopherol-deficient mutants. Plant Cell 18:3706-3720.

Scalla R (1991) Les herbicides: mode d'action et principes d'utilisation. INRA, Paris.

Scarponi L, Younis ME, Standardi A, Martinetti L, Hassan NM (1998) Changes in carbohydrate formation and starch symptoms in *Vicia faba* L. treated with propachlor, chlorimuron-ethyl and imazethapyr. Agric Med 128:118-125.

Semchuk NM, Lushchak OV, Falk J, Krupinska K, Lushchak VI (2009) Inactivation of genes, encoding tocopherol biosynthetic pathway enzymes, results in oxidative stress in outdoor grown *Arabidopsis thaliana*. Plant Physiol

Biochem 47:384-390.
Sinnhuber RO, Yu TC (1958) Characterization of the red pigment formed in 2-thiobarbituric acid determination of oxidative rancidity. J Food Sci 23:626-633.
Song NH, Yin XL, Chen GF, Yang H (2007) Biological responses of wheat (*Triticum aestivum*) plants to the herbicide chlorotoluron in soils. Chemosphere 68:1779-1787.
St John JB (1985) Action of R-40244 on chloroplast pigments and polar lipid. Pestic Biochem Physiol 23:13-18.
Szymańska R, Kruk J (2008) Tocopherol content and isomers' composition in selected plant species. Plant Physiol Biochem 46:29-33.
Timmerman KP (1989) Molecular characterization of corn glutathione-s-transferase isozymes involved in herbicide detoxication. Physiol Plant 77:465-471.
Vencill WK (2002) Herbicide handbook. Weed Science Society of America, Lawrence.
Wágner G, Nádasy E (2006) Effect of pre-emergence herbicides on growth parameters of green pea. Commun Agric Appl Biol Sci 71:809-813.
Yoshimura K, Miyao K, Gaber A, Takeda T, Kanaboshi H, Miyasaka H, Shigeoka S (2004) Enhancement of stress tolerance in transgenic tobacco plants overexpressing *Chlamydomonas* glutathione peroxidase in chloroplasts or cytosol. Plant J 37:21-33.
Young AJ (1991) The photoprotective role of carotenoids in higher plants. Physiol Plant 83:702-708.

Acta Biologica Szegediensis

Volume 63(2):135-141, 2019
Acta Biologica Szegediensis
http://abs.bibl.u-szeged.hu/index.php/abs
DOI:10.14232/abs.2019.2.135-141

ARTICLE

Genetic diversity of *Salvia tomentosa* Miller (Lamiaceae) species using Touch-down Directed Amplification of Minisatellite DNA (Td-DAMD) molecular markers

Basel Saleh*

Department of Molecular Biology and Biotechnology, Atomic Energy Commission of Syria, Damascus, Syria.

ABSTRACT *Salvia tomentosa* Miller (Lamiaceae) a Mediterranean species has an important role in various pharmacological applications. To reveal genetic relationships among *S. tomentosa* natural populations, 35 samples were collected from different regions of Syria. Touch-down Directed Amplification of Minisatellite DNA (Td-DAMD) markers have been investigated for this goal. Td-DAMD assay produced 158 total bands of which 131 (82.911%) were polymorphic with a mean polymorphic information content (PIC) value of 0.264 and a mean marker index (MI) value of 2.269. Clustering profile based on Td-DAMD data showed that samples were grouped into two main clusters; the first cluster included Lattakia samples which split into two subclusters regardless their altitudes over the sea level. Whereas, the second cluster included Tartous and Hama samples. Td-DAMD assay successfully discriminate among the tested 35 samples belonged to the *S. tomentosa* natural population. **Acta Biol Szeged 63(2):135-141 (2019)**

KEY WORDS
genetic diversity
molecular marker
Salvia tomentosa
Td-DAMD

ARTICLE INFORMATION
Submitted
20 November 2019.
Accepted
20 January 2020.
***Corresponding author**
E-mail: ascientific3@aec.org.sy

Introduction

Salvia tomentosa Miller [(*S. grandiflora* Etling) (incl. *S. nusairiensis* Post)] is a perennial flowering plant belonging to the Lamiaceae family. This species with a common name of balsamic sage known as tomentose sage is endemic in Lebanon, Syria and Palestine or wholly or partially restricted species to East Mediterranean area (Mouterde 1983; Ramadan-Jaradi and Matar 2012). Its native range is South-Eastern Europe to Transcaucasia, including Albania, Bulgaria, East Aegean Islands, Greece, Crimea, Lebanon-Syria, Transcaucasia, Turkey and former Yugoslavia (Govaerts 2003).

It worth to mention that plant population genetic structure reflects various interaction processes involving various phenomena [long-term evolutionary history of the species (shift in distribution, habitat fragmentation, and population isolation), mutations, genetic drifts, mating system, gene flow, and selection]. Genetic diversity background of wild resources is considered as backgrounds for establishing plant breeding programs: these result improvement and sustainable production that accumulate various desirable traits together (Liber et al. 2014). Phylogeographic survey of *S. tomentosa* as an endemic plant in East Mediterranean area is important for its conservation implications.

Various *Salvia* species have been described as sources of extracts and metabolites with wide range of biological (e.g., antibacterial, antiviral, antifungal, antioxidant, and cytotoxic) activities (Georgiev et al. 2011; Yilar et al. 2018). Of which, *S. tomentosa* is displayed antibacterial and antioxidant (Hanlidou et al. 2014; Bayan and Genc 2017) and antifungal (Bayan and Genc 2017; Yilar et al. 2018) effects. Furthermore, it is used as condiment and tea around the world (Georgiev et al. 2011).

Molecular characterization of a given species could consider as a potent tool in its conservation and also in breeding programs. Previous studies investigated the phylogenetic relationships of some *Salvia* species within populations of a given genus. Such examples are when, e.g., in *S. hispanica* L. Random Amplified Polymorphic DNA (RAPD) markers (Cahill 2004), in *S. lachnostachys* Inter Simple Sequence Repeat (ISSR) markers (Erbano et al. 2015), in *S. lutescens* var. *intermedia* nuclear ribosomal DNA and plastid DNA sequences (Takano 2017), in *S. divinorum* Chloroplast Simple Sequence Repeats (cpSSR's) (Casselman 2016), in *S. japonica* chloroplast and nuclear ribosomal DNA sequences and allozyme polymorphisms (Sudarmono and Okada 2008) and in *Salvia* sp. Directed Amplification of Minisatellite Region DNA (DAMD) markers (Karaca et al. 2008) have been investigated. Several such studies targeted *S. miltiorrhiza* Bge, e.g., RAPD (Guo et al. 2002), Amplified Fragment Length Polymorphism (AFLP) (Wen et al. 2007), Sequence-related Amplified Polymorphism (SRAP) and ISSR (Song et al.

2010), nrDNA Internal Transcribed Spacer (nrDNA ITS) sequences (Zhang et al. 2012) and ISSR (Zhang et al. 2013) markers have been investigated. Recently, Fabriki-Ourang and Yousefi-Azarkhanian (2018) applied Target Region Amplification Polymorphism (TRAP) and Conserved Region Amplification Polymorphism (CoRAP) markers in *Salvia* sp.

Previously, the Touch-down Directed Amplification of Minisatellite DNA Polymerase Chain Reaction (Td-DAMD-PCR) approach has been successfully employed in phylogenetic studies in *Salvia* species (Ince and Karaca 2012), in common bean landraces (Ince and Karaca 2011), in *Allium* sp. (Deniz et al. 2013), in carnation cultivars (Ince and Karaca 2015) as well as in commercial cotton (Gocer and Karaca 2016).

Despite of the importance of *S. tomentosa* species in various pharmaceutical and industrial applications, until now limited attention has been paid to its genetic variation. Thereby, this study has been focused on its genetic variability among different samples belonged to the *S. tomentosa* natural population.

Materials and methods

Plant materials

Leaf samples of *S. tomentosa* natural population included 35 samples (29 samples from Lattakia, 4 samples from Tartous and 2 samples from Hama); these represented different geographical regions in Syria which varied in term of altitude and annual rainfall (Table 1). Sample collection has been carried out during blooming stage. Wild *Stachys nivea* L. (Lamiaceae; collected from Damascus) was included as a outside reference.

Table 1. Original sites in term of their altitude (m) and annual rainfall (mm) in which the *S. tomentosa* natural population was collected.

Collection site	Code	Altitude (m)	Annual rainfall (mm)
Lattakia	L1	157	800
	L2	250	1000
	L3	346	1000
	L4	400	1100
	L5	420	1100
	L6	400	1100
	L7	500	1100
	L8	520	1100
	L9	482	1100
	L10	680	1250
	L11	134	800
	L12	153	800
	L13	198	800
	L14	123	800
	L15	150	800
	L16	114	800
	L17	347	800
	L18	194	850
	L19	350	1400
	L20	594	1000
	L21	540	1100
	L22	395	1000
	L23	465	850
	L24	212	1400
	L25	195	1400
	L26	200	1400
	L27	854	1500
	L28	830	1350
Tartous	L29	1100	1300
	T30	377	1500
	T31	240	1350
	T32	511	1500
	T33	346	1400
Hama	H34	300	1400
	H35	400	1500
Damascus	SN	970	240

DNA extraction

Total genomic DNA of was extracted according to CTAB (cetyltrimethylammonium bromide) protocol as previously reported by Doyle and Doyle (1987). DNA concentration was determined by DNA fluorimeter. Extracted DNA was kept at -80 °C until further use.

Td-DAMD-PCR test and data analysis

Sixteen DAMD primers (Table 2) were tested to investigate DNA genetic relationships among the studied samples. Td-DAMD amplification was performed according to Ince and Karaca (2012) in a total volume of 25 µl. PCR amplification was carried out in a T-gradient Thermal Cycler (Bio-Rad, USA) programmed as following: 1 cycle for 4 min at 94 °C, followed by ten cycles of pre-PCR involving of 30 s at 94 °C for denaturation, 45 s at 60 °C for annealing, and 3 min at 72 °C for extension. Annealing temperature was reduced 0.5 °C/cycle for the first 10 cycles. Then 30 cycles at a constant 55 °C as annealing temperature; followed by final extension at 72 °C for 10 min. Final PCR products were separated on a 2% ethidium bromide-stained agarose gel (Bio-Rad) in 0.5× Tris-borate-EDTA (TBE) buffer. Electrophoresis was carried out at 85 V for 2.5 h and visualized with a UV transilluminator. A VC 100bp Plus DNA Ladder (Vivantis) standard was used to estimate molecular weight of Td-DAMD-PCR amplification products.

The presence or absence of each band size was manually scored as 1 or 0, respectively. The Unweighted Pair

Table 2. Selected DAMD primers used in the current study.

Primer Nr.	Primer name	Primer sequence 5'-3'
1	URP1F	ATCCAAGGTCCGAGACAACC
2	URP2R	CCCAGCAACTGATCGCACAC
3	URP4R	AGGACTCGATAACAGGCTCC
4	URP9F	ATGTGTGCGATCAGTTGCTG
5	URP38F	AAGAGGCATTCTACCACCAC
6	HBV3	GGTGAAGCACAGGTG
7	14C2	GGCAGGATTGAAGC
8	6.2H(+)	AGGAGGAGGGGAAGG
9	M13	GAGGGTGGCGGCTCT
10	HBVb	GGTGTAGAGAGAGGGGT
11	URP2F	GTGTGCGATCAGTTGCTGGG
12	URP6R	GGCAAGCTGGTGGGAGGTAC
13	URP17R	AATGTGGGCAAGCTGGTGGT
14	M13	GAGGGTGGCGGTTCCT
15	HVA	AGGATGGAAAGGAGGC
16	HVV	GGTGTAGAGAGGGGT

Group Mean Arithmetic average (UPGMA) was constructed based on percent disagreement values (PDV) using Statistica program (Statistica 2003). Whereas, polymorphic information content (PIC) was determined according to the following formula:

$$PIC = 1 - \Sigma(Pij)^2$$

where Pij is the frequency of the i-th pattern revealed by the j-th primer summed across all patterns revealed by the primers (Botestein et al. 1980).

Moreover, marker index (MI) was determined as reported by Powell et al. (1996) according to the following formula:

$$MI = PIC \times \eta\beta$$

where PIC is the mean PIC value, η the number of bands, and β is the proportion of polymorphic bands.

Results

Td-DAMD amplification using sixteen DAMD primers produced 158 total bands of which 131 bands (82.911%) were polymorphic (Table 3). PCR products sizes yielded by Td-DAMD assay ranged between 150-3000 bp. Td-DAMD polymorphism profiles yielded by HBVb (a), URP17R (b) and HVA (c) DAMD primers for natural *S. tomentosa* population are presented in Fig. 1. Total band numbers ranged between 5 (URP2F) and 15 (M13 & HVA) bands with an average of 9.875 bands/primer (Table 3).

Table 3. Td-DAMD amplified fragments scored in term of Total Bands (TB), Polymorphic Bands (PB), Polymorphic % (P%), Polymorphic Information Content (PIC) and Marker Index (MI).

Primer name	TB	PB	P%	PIC	MI
URP1F	13	10	76.923	0.189	1.890
URP2R	11	10	90.909	0.386	3.860
URP4R	6	6	100.000	0.408	2.448
URP9F	7	6	85.714	0.296	1.776
URP38F	10	10	100.000	0.365	3.650
HBV3	7	6	85.714	0.216	1.296
14C2	10	8	80.000	0.197	1.576
6.2H(+)	14	9	64.286	0.225	2.025
M13	9	7	77.778	0.280	1.960
HBVb	10	9	90.000	0.390	3.510
URP2F	5	5	100.000	0.244	1.220
URP6R	8	4	50.000	0.093	0.372
URP17R	10	6	60.000	0.119	0.714
M13	15	15	100.000	0.319	4.785
HVA	15	13	86.667	0.290	3.770
HVV	8	7	87.500	0.207	1.449
Sum	158	131			
Average	9.875	8.188	83.468	0.264	2.269

The number of polymorphic bands ranged between 4 (URP6R) and 15 (M13) with an average of 8.188 polymorphic bands/primer (Table 3).

PIC value ranged between 0.093 (URP6R) and 0.408(URP4R) with a mean average of 0.264. The MI value ranged between 0.372 (URP6R) and 4.785 (M13) with a mean average of 2.269 (Table 3).

The relatedness degree among natural populations of *S. tomentosa* (Fig. 2) was calculated based on the Unweighted Pair Group Mean Arithmetic average (UPGMA) using Statistica program and Percent Disagreement Values (PDV). For the 35 *S. tomentosa* samples tested, two main clusters were revealed: one cluster involved the 29 *S. tomentosa* samples collected from Lattakia which divided further two subclusters. The first subcluster included 6 samples (L20, L21, L22, L27, L28 and L29); of which L27 and L28 were close with a PDV value of 0.10. The second subcluster was composed of the remaining 23 samples. Within Lattakia samples, the highest PDV values (0.37) were recorded between L2 and L29, L5 and L29, as well as between L6 and L29. The lowest PDV values (0.08) were recorded between L4 and L5 and between L6 and L7 samples.

The second main cluster was also separated into two subclusters, the first of which included Tartous samples T30 and T31, while the second one included T32 and T33, as well as the samples collected from Hama (H34 and H35).

Overall, the lowest PDV was 0.03 between H34 and

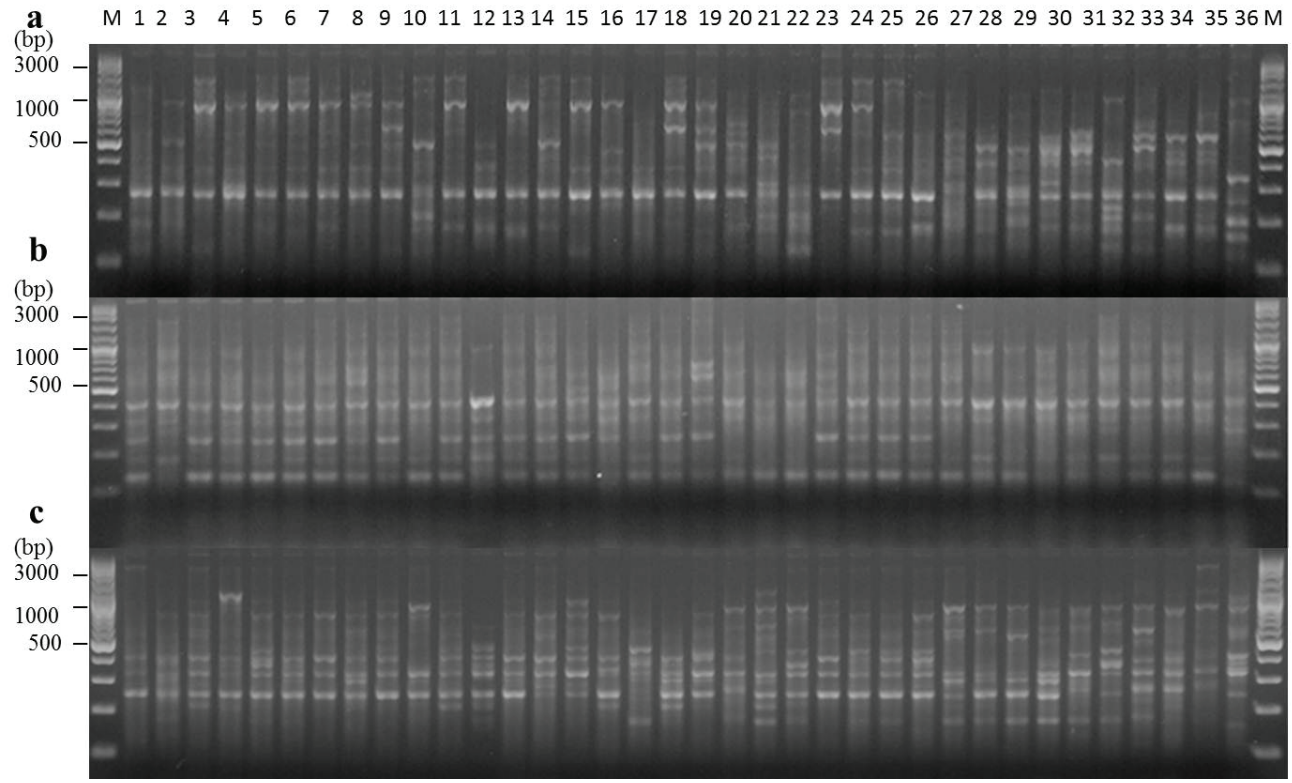

Figure 1. Td- DAMD polymorphism profile yielded by HBVb (a), URP17R (b) and HVA (c) DAMD primers for natural *S. tomentosa* population; 1-29: samples collected from Lattakia, 30-33: samples collected from Tartous and 34-35: samples collected from Hama; 36: *S. nivea* as an outside reference. M: A VC 100bp Plus DNA Ladder (Vivantis).

H35, whereas, the highest one was 0.44 between L15 and T32 followed by 0.43 between L4 and T30, L2 and T32 and between L15 and T30. These values were comparable with the mean PDV average of 0.25 observed for all tested samples. Based on the mean PDV average of 0.25, the current study could suggest that the 29 *S. tomentosa* samples collected from Lattakia were genetically distinct from the samples collected from Tartous and Hama.

Discussion

Genetic relationship investigation for 35 *S. tomentosa* samples collected from different regions in Syria has been performed using Td-DAMD markers. Td-DAMD assay produced 158 total bands (markers) of which 131 (82.911%) were polymorphic. This was in agreement with the results of Guo et al. (2002) who reported P% of 80.44% in *S. miltiorrhiza* Bge using RAPD analysis with 11 primers.

Cahill (2004) reported that DNA genetic diversity in *S. hispanica* L. samples (collected from Mexico) revealed by RAPD analysis, was higher among natural samples compared to cultivated (domesticated) once. However, Song et al. (2010) reported low genetic diversity in *S. miltiorrhiza* using SRAP and ISSR markers. Moreover, Zhang et al. (2012) applied nrDNA ITS sequences to investigate phylogenetic relationships within *S. lachnostachys* population in relation to other *Salvia* taxa. They reported that *S. miltiorrhiza* f. alba, *S. bowleyana*, *S. cavaleriei* var. *simplicifolia*, and *S. yunnanensis* were the most closely related taxa to *S. miltiorrhiza* species; they could be considered as new gene germplasm candidates for *S. miltiorrhiza*. Ince and Karaca (2012) reported a total of 17, 13, 9, 11 and 20 species-specific Td-DAMD-PCR markers for *S. sclarea, S. fruticosa, S. tomentosa, S. dichroantha* and *S. virgate,* respectively, using 22 DAMD primers.

Zhang et al. (2013) reported the high importance of DNA genetic diversity of *S. miltiorrhiza* (studied by ISSR markers) in plant breeding programs. Erbano et al. (2015) reported genetic variation in *S. lachnostachys* populations collected from Brazil using ISSR-based markers. ISSR marker yielded 159 bands of which 152 (95.6%) were polymorphic; reflecting high genetic diversity level for *S. lachnostachys.* Takano (2017) reported deference among *Salvia lutescens* var. *intermedia* and its allies based on morphological traits and molecular analyses of nuclear

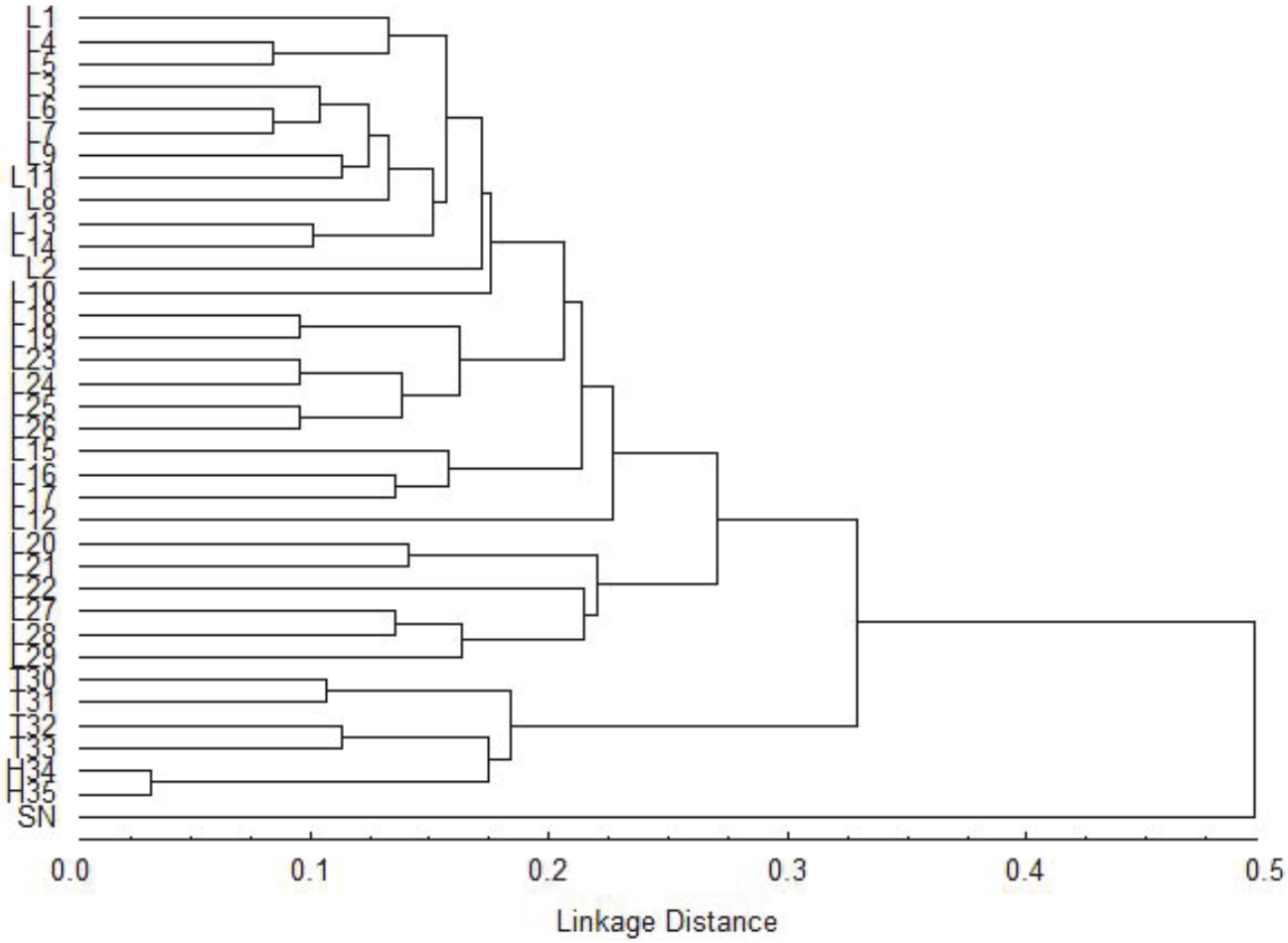

Figure 2. UPGMA cluster analysis-based on the percent disagreement value (PDV) for Td-DAMD fingerprints showing genetic relationship for natural *S. tomentosa* population.

ribosomal DNA and plastid DNA sequences.

Td-DAMD marker has been successfully employed for fingerprinting of other plant species, e.g., Deniz et al. (2013) used 10 DAMD primers and reported 454 total bands of which 245 (53.96%) were polymorphic between *Allium elmaliense* and *Allium cyrilli*. They found that *A. elmaliense* Deniz & Sumbul is a distinct species and not a synonym of *A. cyrilli* Ten. Ince and Karaca (2015) reported a total of 858 bands of which 570 (66.43%) were polymorphic and PIC ranged from 0.120 to 0.341, with an average of 0.249/primer when genetic variation of 16 carnation cultivars were studied using 12 DAMD primers. Gocer and Karaca (2016) reported 120 total bands, 42 (35%) of which were polymorphic among 26 cotton samples using 10 DAMD primers.

Recently, Fabriki-Ourang and Yousefi-Azarkhanian (2018) applied TRAP and CoRAP markers to evaluate genetic diversity among 25 *Salvia* ecotypes/species in Iran. They reported that the 6 primer combinations of TRAP gave a mean average total bands of 181 of which 15 were polymorphic with a mean PIC and MI values of 0.42 and 3.05, respectively. Whereas, CoRAP with 6 primer combinations gave a mean average total bands of 153 bands of which 15 were polymorphic with a mean PIC and MI values of 0.377 and 2.49, respectively.

It has been demonstrated that genetic structure in plant populations is influenced by various factors like, e.g., reproductive biology, gene flow, seed dispersal and natural selection (Erbano et al. 2015), of which reproductive biology plays a fundamental role (Zhao et al. 2007). On the other hand, the higher observed diversity previously observed for *Salvia* within populations was related to the outcrossing strategy (Bijlsma et al. 1994). This is particularly probable with high population densities where outcrossing rates are higher. Recently, Radosavljević et al. (2019) reported that interspecies hybridization affects genetic and epigenetic alterations through DNA methylation patterns modification. Consequently, ap-

pearance of new phenotypic variants in hybrid progeny was more originated from epigenetic compared to genetic recombination.

It worth to mention that moderate genetic variation observed within natural population of *S. tomentosa* in this study could be attributed to one or more following factors: i) big size of this population; ii) occurrence a huge number of individuals in this population; iii) outcrossing process as similarly reported for *S. officinalis* (Stojanović et al. 2015) or to spontaneous hybrids occurred in the wild or in cultivated *Salvia* (Tychonievich and Warner 2011); or to be interspecific hybrid as similarly reported in *S. divinorum* (Casselman 2016) or to reproductive biology, gene flow, seed dispersal and nature selection (Erbano et al. 2015) encouraged efficient gene flow. This observation could support by the phylogenetic study done by Walker et al. (2004) suggested that the *Salvia* was polyphyletic involved 2-3 distinct lineages. This phenomenon could lead to inbreeding expansion and higher heterozygosity, leading consequently to increase their adaptive potential. This could explain their distribution wide spare in the selected sites at different altitudes and rain full.

Acknowledgements

I thank Dr. I. Othman (Director General of AECS) and Dr. N. Mirali (Head of Molecular Biology and Biotechnology Department in AECS) for their support, and also the Plant Biotechnology group for technical assistance.

References

Bayan Y, Genc N (2017) Determination of antifungal and antioxidant activities of *Salvia tomentosa* Mill. Iğdır Univ J Inst Sci Tech 7(4):17-21.

Bijlsma R, Ouborg NJ, Treuren R (1994) On genetic erosion and population extinction in plants: A case study in *Scabiosa columbaria* and *Salvia pratensis*. Cons Genet 68:255-271.

Botstein D, White RL, Skolnick M, Davis RW (1980) Construction of a genetic linkage map in man using restriction fragment length polymorphisms. Am J Hum Genet 32(3):314-331.

Cahill JP (2004) Genetic diversity among varieties of Chia (*Salvia hispanica* L.). Genet Res Crop Evol 51(7):773-781.

Casselman I (2016) Genetics and Phytochemistry of *Salvia divinorum*. PhD Thesis, Southern Cross University, Lismore, NSW, Australia.

Deniz IG, Genc I, Ince AG, Aykurt C, Elmasulu S, Sumbul H, Sonmez S, Cıtak S (2013) Taxonomic data supporting differences between *Allium elmaliense* and *Allium cyrilli*. Biologia 68(3):373-383.

Doyle JJ, Doyle JL (1987) A rapid DNA isolation procedure for small quantities of fresh leaf tissue. Phytochem Bull 19(1):11-15.

Erbano M, Schühli SG, dos Santos ÉP (2015) Genetic variability and population structure of *Salvia lachnostachys*: Implications for breeding and conservation programs. Inter J Mol Sci 16:7839-7850.

Fabriki-Ourang S, Yousefi-Azarkhanian M (2018) Genetic variability and relationships among *Salvia* ecotypes/species revealed by TRAP-CoRAP markers. Biotech Biotech Equip 32(6):1485-1495.

Georgiev V, Marchev A, Haas C, Weber J, Nikolova M, Bley T, Pavlov A (2011) Production of oleanolic and ursolic acids by callus cultures of *Salvia tomentosa* Mill. Biotech Biotech Equip 25(4-Suppl):34-38.

Gocer EU, Karaca M (2016) Genetic characterization of some commercial cotton varieties using Td-DAMD-PCR markers. J Sci Eng Res 3(4):487-494.

Govaerts R (2003) World Checklist of Selected Plant Families Database in ACCESS: 1-216203. The Board of Trustees of the Royal Botanic Gardens, Kew.

Guo B, Lin S, Feng Y, Zhao Y (2002) Primary research on genetic relationship among main populations of *Salvia miltiorrhiza* and genuineness of herb. Chin Tradit Herb Drugs 33:1113-1116.

Hanlidou E, Karousou R, Lazari D (2014) Essential-oil diversity of *Salvia tomentosa* Mill. in Greece. Chem Biodivers 11(8):1205-1215.

Ince AG, Karaca M (2011) Genetic variation in common bean landraces efficiently revealed by Td-DAMD-PCR markers. Plant Omic 4(4):220-227.

Ince AG, Karaca M (2012) Species-specific touch-down DAMD-PCR markers for *Salvia* species. J Med Plant Res 6(9):1590-1595.

Ince AG, Karaca M (2015) Td-DAMD-PCR assays for fingerprinting of commercial carnations. Turk J Biol 39:290-298.

Karaca M, Ince AG, Ay ST, Turgu K, Onus AN (2008) PCR-RFLP and DAMD-PCR genotyping for *Salvia* species. J Sci Food Agr 88(14):2508-2516.

Liber Z, Židovec V, Bogdanović S, Radosavljević I, Pruša M, Filipović M, Han Dovedan I, Jug-Dujaković M, Šatović Z (2014) Genetic diversity of Dalmatian Sage (*Salvia officinalis* L.) as assessed by RAPD markers. Agric Conspec Sci 79(2):77-84.

Mouterde PSJ (1983) Nouvelle Flore du Liban et de la Syria. 3. pp.159-170.

Powell W, Morgante M, Andre C, Hanafey M, Vogel J, Tingey S, Rafalsky A (1996) The comparison of RFLP, RAPD, AFLP and SSR (microsatellite) markers for germplasm analysis. Mol Breed 2(3):225-238.

Radosavljević I, Bogdanović S, Celep F, Filipović M, Satovic

Z, Surina B, Liber Z (2019) Morphological, genetic and epigenetic aspects of homoploid hybridization between *Salvia officinalis* L. and *Salvia fruticosa* Mill. Sci Rep 9:3276-3282.

Ramadan-Jaradi G, Matar D (2012) Final report. Biodiversity assessment and monitoring in the jabal Moussa biosphere reserve. UNESCO MAB Gobierno De Espana and APJM.

Song Z, Li X, Wang H, Wang J (2010) Genetic diversity and population structure of *Salvia miltiorrhiza* Bge in China revealed by ISSR and SRAP. Genetica 138:241-249.

Statsoft (2003) Statistica (Data Analysis Software System), Version 6. Statsoft Inc., 2003, www.statsoft.com.

Stojanović D, Aleksić JM, Jančić I, Jančić R (2015) A Mediterranean medicinal plant in the continental Balkans: a plastid DNA-based phylogeographic survey of *Salvia officinalis* (Lamiaceae) and its conservation implications. Willdenowia 45:103-118.

Sudarmono, Okada H (2008) Genetic differentiations among the populations of *Salvia japonica* (Lamiaceae) and its related species. HAYATI J Biosci 15(1):18-26.

Takano A (2017) Taxonomic study on Japanese *Salvia* (Lamiaceae): phylogenetic position of *S. akiensis*, and polyphyletic nature of *S. lutescens* var. *intermedia*. PhytoKeys 80:87-104.

Tychonievich J, Warner RM (2011) Interspecific crossability of selected *Salvia* species and potential use for crop improvement. J Am Soc Hort Sci 136(1):41-47.

Walker JB, Sytsma KJ, Treutlein J, Wink M (2004) *Salvia* (Lamiaceae) is not monophyletic: implications for the systematic, radiation, and ecological specializations of *Salvia* and tribe Mentheae. Am J Bot 91(7):1115-1125.

Wen C, Wu Z, Tian W, Liu M, Zhou Q, Xie X (2007) AFLP analysis of genetic diversity of *Salvia miltiorrhiza* Bge. Acta Agric Bor Sin22(S2): 122-125.

Yilar M, Kadioglu I, Telci I (2018) Chemical composition and antifungal activity of *Salvia officinalis* (L.), *S. cryptantha* (Montbret et Aucher Ex Benth), *S. tomentosa* (Mill) plant essential oils and extracts. Fresen Environ Bull 27(3): 1695-1706.

Zhang L, Zhao H, Fan X, Wang M, Ding C, yang R, Yin Z, Xie X, Zhou Y, Wan D. (2012) Genetic diversity among *Salvia miltiorrhiza* Bunge and related species inferred from nrDNA ITS sequences. Turk J Biol 36: 319-326.

Zhang Y, Li X, Wang Z (2013) Diversity evaluation of *Salvia miltiorrhiza* using ISSR markers. Biochem Genet 51(9-10): 707–721.

Zhao Y, Chen XY, Wang XR, Pian RQ (2007) ISSR analysis of genetic diversity among *Lespedeza bicolor* populations. J Plant Genet Resour 8:195-199.

Acta Biologica Szegediensis

Volume 63(2):143-155, 2019
Acta Biologica Szegediensis
http://abs.bibl.u-szeged.hu/index.php/abs
DOI:10.14232/abs.2019.2.143-155

ARTICLE

Systematic significance of micromorphological and palynological characteristics in *Lagochilus* Bunge ex Benth. (Lamiaceae) in Iran

Fatemeh Azimishad[1]*, Masoud Sheidai[1], Maryam Keshavarzi[2], Seyed Mehdi Talebi[3], Zahra Noormohammadi[4]

[1]Faculty of Life Sciences and Biotechnology, Shahid Beheshti University, Tehran, Iran
[2]Department of Plant Sciences, Faculty of Biological Science, Alzahra University, Tehran, Iran
[3]Department of Biology, Faculty of Sciences, Arak University, Arak 38156-8-8349, Iran
[4]Biology Department, Islamic Azad University, Sciences and Research Branch, Tehran, Iran

ABSTRACT *Lagochilus* is a genus with ten taxa (species, subspecies and variety) in Iran, which nine of them are endemic. This is the first micromorphological investigation of this genus. Micromorphological features of trichomes on the stems, leaves and calyces, and also pollen morphology of 19 populations were investigated by scanning electron microscopy. Two types of trichome (glandular and non-glandular) including 14 forms were described. Here, among the non-glandular trichomes, cell number and size of trichomes are considered as valuable characteristics, while the glandular trichomes are observed as stalked, sessile and peltate. *Lagochilus* pollen grains are tricolpate and small to medium sized. The basic shape of the pollen grains in most taxa is prolate, however prolate-subprolate pollen grains was recorded for *L. aucheri* ssp. *aucheri* var. *aucheri* 2. Four types of exine sculpture patterns were distinguished: bireticulate, reticulate, microreticulate and incomplete reticulate. Quantitative and qualitative characteristics were examined by multivariate analysis. The results indicated that the studied taxa were separated from each other; however varieties of *L. aucheri* did not grouped together. The results support the existence of known varieties in *L. aucheri*. In general, our investigations reveal the usefulness of micromorphological characteristics in taxon delimitation at the specific and infraspecific levels.
Acta Biol Szeged 63(2):143-155 (2019)

KEY WORDS
Lagochilus
Lamiaceae
SEM
trichome micromorphology
palynology

ARTICLE INFORMATION
Submitted
29 December 2019.
Accepted
03 March 2020.
***Corresponding author**
E-mail: ailarazimishad3@gmail.com

Introduction

The genus *Lagochilus* Bunge ex Benth. (1834), belong to family Lamiaceae, subfamily Lamioideae (Bendiksby et al. 2011), comprises about 44 species, from which six species occur in Iran (Jamzad 1988; Zhang et al. 2017). *Lagochilus* species are mostly distributed in dry slopes, valleys and deserts from Iran to Mongolia, Russia (south Siberia), northwest China and north Pakistan, but have wide distribution in Central Asia (Harley et al. 2004; Zhang et al. 2017).

The chemical components of several *Lagochilus* species were surveyed due to their medicinal uses. Lagochilin is a diterpene which was found in various species of the genus, and is thought to be responsible for the sedative, hypotensive and hemostatic effects of these species (Chizhov et al. 1970; Jiao et al. 2014). Taban et al. (2009) have reported the antibacterial activity of flowers and leaves of *L. kotschyanus* Boiss. (1848) oils against four Gram-positive and two Gram-negative bacteria.

These plants are subshrubs or perennial herbs with woody root and green-white, rigid stem with spiny bracteoles. Leaf blade is rhombic, palmatipartite or pinnatipartite with campanulate-tubular calyx and villous-pillose corolla. Nutlets flattened-obconical, oblong-obovoid or oblongovid (Jamzad 1988).

Ikramov (1976) investigated the classification, distribution, and community ecology of *Lagochilus* species in Central Asia of former USSR. Recently, Zhang et al. (2017) have studied *Lagochilus* species using chloroplast sequence data to reveal the species relationships as well as the date of divergence. However only three species sampled from Iran was included in their investigation and they were considered as a complex and very much different clade within the genus *Lagochilus* (Zhang et al. 2017).

Boissier (1879) mentioned 6 species, Parsa (1949) listed 6 species and two varieties and Rechinger (1982) recognized 5 species from Iran. Jamzad (1988) identified 6 species through revision of the genus *Lagochilus* in Iran, these

are *L. alutaceus* Bunge (1873), *L. aucheri* Boiss. (1844), *L. lasiocalyx* (Stapf) Jamzad (1988), *L. macranthus* Fisch. & C.A. Mey. (1841), *L. quadridentatus* Jamzad (1988) and *L. cabulicus* Benth. (1848). The first five species are endemic to Iran and are considered as the endangered species (Jalili and Jamzad 1999).

Jamzad (1988) described *L. quadridentatus* and 3 infraspecific taxa as *L. aucheri* ssp. *heterophyllus, L. aucheri* ssp. *aucheri* var. *elegans* and *L. aucheri* ssp. *aucheri* var. *tomentosus*. She found a complexity in naming of *L. aucheri* group. Morphological characteristics as calyx teeth number, calyx width, shape of leaves and indumentum type of different parts of calyx, nutlet and stem traits were used in identification key for specific and infraspecific level. However, according to the Plant List, there are five species in Iran and known subspecies and varieties by Jamzad are synonym names (Govaerts et al. 2013).

The taxonomic value of trichomes density and types and also pollen morphology in identification, delimitation and phylogenetic reconstruction of some members of the family Lamiaceae have been elucidated by many authors (Erdtman 1945; Wunderlich 1967; Abu-Asab and Cantino 1989; 1992; 1993a,b; 1994; Cantino 1990; Doaigey1991; Bini Maleci and Servettaz, 1991; Harley et al. 1992; Wagstaff 1992; Navarro and El Qualidi, 2000; Moon and Hong 2003; C¸elenk et al. 2008 a,b; Moon et al. 2008a,b,c; Salmaki et al. 2008; Hassan et al. 2009; Gairola et al. 2009; Salmaki et al. 2009; Özler et al. 2011; 2013; Firdous et al. 2015 ; Atalay et al. 2016a,b; Talebi et al. 2018a,b). Besides of systematic significance, trichomes have several roles in plants. For example, there are assumed to attraction of pollinators (Wagner 1991), protection from herbivores and pathogens (Xiao et al. 2017) and decrease the leaf temperature and transpiration (Peter and Shanower 1998).

Pollen morphology is generally supported segregation of some genera of Lamiaceae (Abu-Asab and Cantino 1994). Palynological study of the genus *Lagochilus* have been poorly investigated and is still lacking (Abu-Asab and Cantino 1994; Talebi and Rezakhanlou 2012; Badamtsetseg et al. 2012), so their work comprises only a few *Lagochilus* species.

Whereas phylogenetic and molecular studies of most *Lagochilus* species have not been investigated yet and also there is no comprehensive micromorphological and palynological study covering all species of *Lagochilus* in Iran and Asia, therefore, the main objectives of the present study are to provide a detailed investigation and description of trichomes and pollen micromorphology of the genus *Lagochilus*, mainly by scanning electron microscopy (SEM), to determine whether these data can be of value in the taxonomy of the genus and delimitation of the species. Furthermore, trichomes and pollen morphology of most species was described for the first time.

Table 1. Voucher specimens of the genus *Lagochilus* examined in the present study. Ns: number of plant samples.

Taxon	Ns	Locality	Latitude	Longitude	Altitude (m)	Voucher code
L. aucheri ssp. *aucheri* var. *aucheri* 2	5	Zanjan, Dash kasan Mt.	36° 43′ 58″	48° 79′ 20″	1700	HSBU2018650
L. aucheri ssp. *aucheri* var. *aucheri* 2	5	Zanjan, 90 km of Zanjan-Bijar road	35° 75′ 79″	48° 48′ 22″	1500	HSBU2018651
L. aucheri ssp. *aucheri* var. *aucheri* 2	5	Zanjan, Bulamaji village	36° 56 ′ 31 ″	48° 48 ′ 79 ″	1500	HSBU2019100
L. aucheri ssp. *aucheri* var. *aucheri* 1	5	Qazvin, Abegarm	35° 80′ 03″	49° 31′ 19″	1500	HSBU2018652
L. aucheri ssp. *aucheri* var. *aucheri* 3	5	Alborz, Karaj, Dizin	35° 82′ 00″	50° 97′ 00″	2500	HSBU2018653
L. aucheri ssp. *aucheri* var. *tomentosus*	5	Tehran, Firuzkuh, Sarbandan	35° 75′ 50″	52° 77′ 24″	2000	HSBU2018654
L. aucheri ssp. *aucheri* var. *tomentosus*	5	Tehran, Damavand, Voleyran	35° 68′ 84″	52° 06′ 38″	2000	HSBU2019101
L. aucheri ssp. *aucheri* var. *tomentosus*	3	Tehran, Damavand, Tar lake	35° 73′ 17″	52° 21′ 00″	1950	HSBU2019102
L. aucheri ssp. *aucheri* var. *kotschyanus*	4	Markazi, Delijan	34°06′ 38.7″	50° 32′ 23″	1511	HSBU2018658
L. aucheri ssp. *aucheri* var. *kotschyanus*	4	Markazi, Mahallat	34°00′ 43.2″	50° 32′ 14.2″	1910	HSBU2019103
L. aucheri ssp. *aucheri* var. *elegans*	5	Qazvin, Takestan	36° 07′ 21″	49° 70′ 13″	1450	HSBU2018660
L. alutaceus	5	Razavi Khorasan, Chenaran	36°30′ 52.3″	59°02′ 42 ″	1450	HSBU2018655
L. cabulicus	5	North Khorasan, Esfarayen	36°56′ 0.23″	57° 44′ 3″	1535	HSBU2018656
L. cabulicus	5	Razavi Khorasan, Chenaran	36°30′ 52.3″	59°02′ 42 ″	1450	HSBU2018661
L. macracanthus	5	Alborz, Eshtehard, Jafar abad village	35° 72′ 44″	50° 36′ 62″	1300	HSBU2018657
L. macracanthus	5	Alborz, Eshtehard, Nekujar village	35° 67′ 84″	50° 39′ 29″	1450	HSBU2019104
L. macracanthus	5	Tehran, Vardavard Mt.	35° 73′ 60″	51° 10′ 30″	1500	HSBU2019105
L. macracanthus	4	20-kilometer after Saveh, Samavak village.	35° 03′ 85″	50° 08′ 42″	1500	HSBU2019106
L. lasiocalyx	4	Isfahan, Bagherabad	33°51′ 12.4″	50° 33′ 9″	1638	HSBU2018659

Materials and Methods

Plant samples

Totally 19 accessions of 10 taxa (species, subspecies and variety) were examined. In each populations, three to five plants were sampled for the scanning electron microscopy (SEM). Vouchers were collected from nature (2016-2018) and identified based on the descriptions provided in Flora Iranica (Rechinger 1982) and Flora of Iran (Jamzad 2012). Accessions studied and voucher details are listed in Table 1. All vouchers of the current study were deposited in Herbarium of Shahid Beheshti University (HSBU).

Micromorphological characters

Micromorphological features of leaves, stems and calyces were assessed using SEM. One to five mature leaves, stems and calyces were selected from fresh plant materials from each population. Middle parts of the samples were mounted directly on aluminum stubs using double-sided adhesive tape. The samples were coated with gold by a magnetron, sputtering device for about 10 nanometer thickness and observed with a SU 3500 SEM (Hitachi).

The terminology used is based on Cantino (1990) and Navarro and El Qualidi (2000) for trichomes. Size measurements on SEM images were made using UTHSCSA Image Tool Ver.3.0. Trichomes density was calculated by dividing the hair number per mm^2 by the samples area (Gonzales et al. 2008). The distribution and types of trichomes were determined (Table 2).

Pollen grains

Fully matured anthers were obtained from the specimens and were prepared for study by SEM. Pollen grains were placed directly to aluminum stubs with double-sided cellophane tape and coated with gold by a magnetron sputtering device for about 10 nm thickness, then observed in a Hitachi SU 3500 SEM (in the Central Laboratory of Shahid Beheshti University) at 15 kV and photographed at magnifications ranging from×600 to ×10,000 to determine the exine ornamentation. Fully developed pollen grains (15-30 pieces) were selected and the following pollen measurements were taken: polar axis (P), equatorial axis (E), colpus length (Clg), mesocolpium thickness, apocolpium diameter and P/E ratio (Table 3). All of the measurements were performed using UTHSCSA Image Tool Ver. 3.0. The pollen terminology follows that of used by Faegri and Iversen (1975), Abu-Asab and Cantino (1994) and Hesse et al. (2009).

Statistical analysis

For multivariate analysis, the mean of quantitative characteristics was used, while qualitative characters were coded as binary/multistate features. Standardized variables (mean = 0, variance = 1) were used in the statistical analysis. For grouping the studied taxa, cluster analysis using UPGMA (Unweighted Paired Group with Arithmetic Average) methods was performed using Euclidean and taxonomic distance among the species. Principal Coordinate Ordination (PCO) and Principal Coordinate Analysis (PCA) were performed (Podani 2000). Moreover, the one-way analysis of variance (ANOVA) was used to compare the trichomes numbers among the studied species. PAST (Paleontological statistics software package) version 2.17 was used for statistical analysis (Podani 2000).

Results

Different trichome features as trichome type, size and density on the stems, leaves and calyces of the studied taxa along their palynological data are summarized in Tables 2 and 3, respectively. Selected SEM micrographs of different trichome types and pollen grains studied were presented in Figs. 1-3 and Figs. 4-6, respectively.

Micromorphological characters

In general, two main types of trichomes were observed in the studied taxa: non-glandular (NG) and glandular (G). Both non-glandular and glandular trichomes occur on the same organ, particularly in the leaves and calyces.

Non-glandular trichomes

Non-glandular type trichomes were simple and unbranched in the examined specimens. However, this type varied in density, size, cell number, thickness of cell wall and presence of papillae on the trichome surface, therefore they were classified into 4 types (A-D, Table 2):

Unicellular trichomes (A).

A1: prickles-hairs. These were the unicellular epidermal appendages. In terms of size, this form was shorter than 50 μm on the leaves of *L. cabulicus*, *L. macracanthus* and *L. aucheri* ssp. *aucheri* var. *elegans* (Fig. 1A-B) to 200 μm in the leaves and calyces of most specimens (except *L. aucheri* ssp. *aucheri* var. *aucheri* 3), which have papillate surface (Fig. 1C). The highest number of this kind of trichomes was seen on the leaves of *L. aucheri* ssp. *aucheri* var. *tomentosus* and its lowest amount was found on the leaves of *L. macracanthus* and *L. aucheri* ssp. *aucheri* var. *aucheri* 1 (Table 2).

A2: thin-walled trichomes. This form was triangular and very thin-walled hairs with ridges. In the term of size, thin-walled non-glandular trichomes can be subdivided into two types; short (i): shorter than 50 μm, which was found on the stems and calyces of *L. macracanthus* and *L. cabulicus* (Fig 1D) to hairs ranged from 50-300 μm on

Table 2. Indumentum characteristics of the *Lagochilus* taxa examined. Numbers refer to mean ± standard deviation of trichomes number. NG: non-glandular. A1: prickles-hairs. A2-i: short thin-walled trichomes. A2-ii: long thin-walled trichomes. B1: short bicelled trichomes densely covered by micropapillae. B2: short bicelled trichomes, the basal cell is without micropapillae. B3: long bicelled trichomes. C: long tricelled trichomes. D: long four-celled trichomes. G: glandular. G1: sessile capitate. G2: short-stalked capitate. G3: peltate.

Species	Leaf				Stem									
	NG		G		NG							G		
	A1	A2-i	G1	G3	A1	A2-i	A2-ii	B1	B2	B3	C	G1	G2	G3
L. aucheri ssp. *aucheri* var. *aucheri* 1	55.33 ± 4.5	0.00 ± 0.00	0.00 ± 0.00	10.5 ±1	0.00 ± 0.00	350 ± 90.7	0.00 ± 0.00	0.00 ± 0.00	0.00 ± 0.00	0.00 ± 0.00	0.00 ± 0.00	0.00 ± 0.00	0.00 ± 0.00	0.00 ± 0.00
L. aucheri ssp. *aucheri* var. *elegans*	117.3 ± 4.48	0.00 ± 0.00	35 ± 8.65	10 ± 0.00	0.00 ± 0.00	326.66 ± 43.15	0.00 ± 0.00	0.00 ± 0.00	0.00 ± 0.00	0.00 ± 0.00	3 ± 0.8	10 ± 4.00	8 ± 2.5	0.00 ± 0.00
L. aucheri ssp. *aucheri* var. *kotschyanus*	195 ± 72.23	0.00 ± 0.00	2.25 ± 0.55	10 ± 0.00	0.00 ± 0.00	183.35 ± 21.24	3 ± 0.00	142.66 ± 8.35	0.00 ± 0.00	0.00 ± 0.00	0.00 ± 0.00	0.00 ± 0.00	5.8 ± 1.2	2 ± 0.5
L.aucheri ssp. *aucheri* var. *tomentosus*	223.33 ± 23.5	0.00 ± 0.00	9.8 ± 0.57	10 ± 0.2	120 ± 2.8	138.66 ± 15.6	0.00 ± 0.00	0.00 ± 0.00	0.00 ± 0.00	0.00 ± 0.00	0.00 ± 0.00	18.75 ± 4.32	1.9 ± 1	0.00 ± 0.00
L. aucheri ssp. *aucheri* var. *aucheri* 2	140.67 ± 25.1	0.00 ± 0.00	0.00 ± 0.00	10 ± 0.00	0.00 ± 0.00	367.66 ± 52.33	0.00 ± 0.00	25.24 ± 6.33	0.00 ± 0.00	0.00 ± 0.00	0.00 ± 0.00	15.5 ± 6.33	0.00 ± 0.00	0.00 ± 0.00
L. aucheri ssp. *aucheri* var. *aucheri* 3	0.00 ± 0.00	282.33 ± 113.8	1.5 ± 0.3	30 ± 6.67	0.00 ± 0.00	250 ± 10.65	0.00 ± 0.00	0.00 ± 0.00	0.00 ± 0.00	0.00 ± 0.00	0.00 ± 0.00	5.5 ± 2.2	0.00 ± 0.00	4.5 ± 1.8
L. alutaceus	110 ± 35.61	0.00 ± 0.00	5.2 ± 1.20	28.33 ± 3.2	0.00 ± 0.00	20 ± 7.67	0.00 ± 0.00	0.00 ± 0.00	290.1 ± 48.88	0.00 ± 0.00	18.67 ± 3.5	7.5 ± 3.67	0.00 ± 0.00	0.00 ± 0.00
L. cabulicus	60 ± 2.65	0.00 ± 0.00	0.00 ± 0.00	26.33 ± 4.5	0.00 ± 0.00	293.33 ± 57.67	0.00 ± 0.00	0.00 ± 0.00	0.00 ± 0.00	0.00 ± 0.00	1.9 ± 0.5	1.2 ± 0.3	0.00 ± 0.00	2.66 ± 0.5
L. lasiocalyx	70.66 ± 3.55	0.00 ± 0.00	0.00 ± 0.00	5.3 ± 1.5	0.00 ± 0.00	201.66 ± 53.2	0.00 ± 0.00	0.00 ± 0.00	0.00 ± 0.00	2 ± 0.00	3 ± 0.00	8.5 ± 2.33	0.00 ± 0.00	0.00 ± 0.00
L. macracanthus	55.33 ± 5.66	0.00 ± 0.00	15.8 ± 4.5	10 ± 1.5	185 ± 55.33	276.67 ± 65.5	0.00 ± 0.00	0.00 ± 0.00	0.00 ± 0.00	0.00 ± 0.00	0.00 ± 0.00	5.8 ± 3.42	0.00 ± 0.00	0.00 ± 0.00

Table 2. Continued.

Species	Calyx							
	NG						G	
	A1	A2-i	B1	B3	C	D	G1	G3
L. aucheri ssp. *aucheri* var. *aucheri* 1	310 ± 77.33	0.00 ± 0.00	0.00 ± 0.00	0.00 ± 0.00	0.00 ± 0.00	0.00 ± 0.00	9 ± 3.7	22.51 ± 7.8
L. aucheri ssp. *aucheri* var. *elegans*	202.66 ± 13.56	0.00 ± 0.00	75.2 ± 20	0.00 ± 0.00	0.00 ± 0.00	24.5 ± 4	7 ± 2	23.84 ± 5.66
L. aucheri ssp. *aucheri* var. *kotschyanus*	633.33 ± 158.55	0.00 ± 0.00	0.00 ± 0.00	0.00 ± 0.00	17.67 ± 3.66	0.00 ± 0.00	17.6 ± 3.33	45 ± 10.15
L.aucheri ssp. *aucheri* var. *tomentosus*	236.77 ± 27.6	0.00 ± 0.00	30.67 ± 12.33	0.00 ± 0.00	0.00 ± 0.00	0.00 ± 0.00	12.54 ± 4.47	35 ± 3.6
L. aucheri ssp. *aucheri* var. *aucheri* 2	136 ± 14.53	0.00 ± 0.00	0.00 ± 0.00	0.00 ± 0.00	0.00 ± 0.00	0.00 ± 0.00	6.2 ± 3.33	7.9 ± 2.1
L. aucheri ssp. *aucheri* var. *aucheri* 3	0.00 ± 0.00	200 ± 35.7	0.00 ± 0.00	0.00 ± 0.00	0.00 ± 0.00	0.00 ± 0.00	8.8 ± 2.2	23.33 ± 5.3
L. alutaceus	122.3 ± 15.66	0.00 ± 0.00	0.00 ± 0.00	223.33 ± 102.2	0.00 ± 0.00	0.00 ± 0.00	5.5 ± 0.44	25 ± 6.8
L. cabulicus	110.2 ± 21.33	185.57 ± 28.63	0.00 ± 0.00	0.00 ± 0.00	0.00 ± 0.00	0.00 ± 0.00	1 ± 0.3	8.35 ± 4.45
L. lasiocalyx	125 ± 18.88	0.00 ± 0.00	0.00 ± 0.00	3 ± 1.5	5 ± 2.33	3 ± 0.9	9 ± 3.25	21.67 ± 5.00
L. macracanthus	210.15 ± 11.66	200 ± 52.5	0.00 ± 0.00	0.00 ± 0.00	0.00 ± 0.00	0.00 ± 0.00	22.2 ± 6.47	33.33 ± 6.74

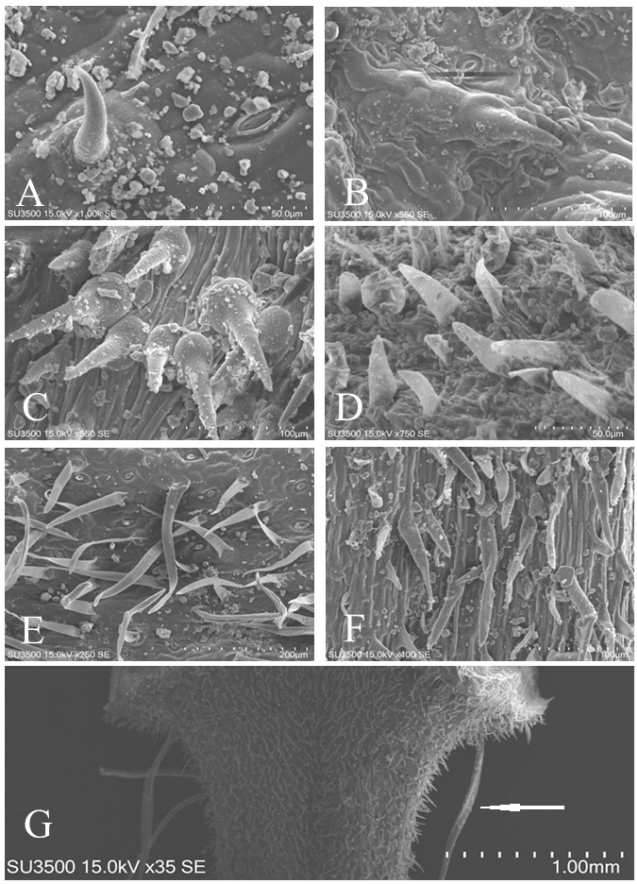

Figure 1. SEM micrographs of non-glandular unicellular trichomes in selected *Lagochilus* taxa. Prickles trichomes on the leaf (A-C). A: *L. aucheri* ssp. *aucheri* var. *elegans*. B: *L. cabulicus*. C: *L. aucheri* ssp. *aucheri* var. *aucheri* 2. Short thin-walled trichomes (D-F). D: on the stem of *L. macracanthus*. E: on the calyx of *L. aucheri* ssp. *aucheri* var. *aucheri* 3. F: on the stem of *L. aucheri* ssp. *aucheri* var. *aucheri* 1. Long thin-walled trichomes on the stem of *L. aucheri* ssp. *aucheri* var. *kotschyanus* (G).

the stems, leaves and calyces of *L. aucheri* ssp. *aucheri* var. *aucheri* 3 (Fig. 1E), and also on the stems of most specimens (e.g., *L. lasiocalyx*, *L. aucheri* ssp. *aucheri* var. *aucheri* 1 and *L. aucheri* ssp. *aucheri* var. *aucheri* 2, Fig. 1F). The stems of *L. aucheri* ssp. *aucheri* var. *aucheri* 2 and *L. alutaceus* had highest and lowest amounts of these types of trichomes, respectively (Table 2). Long thin-walled trichomes (ii): as long as 1000- 2000 μm only on the stems of *L. aucheri* ssp. *aucheri* var. *kotschyanus* (Fig. 1G).

Bicelled trichomes (B).

B1: short (50-200 μm in size), bicelled trichomes, densely covered by micropapillae; the apical cell is triangular and acute. This form was observed on the stems of *L. aucheri* ssp. *aucheri* var. *kotschyanus* and *L. aucheri* ssp. *aucheri* var. *aucheri* 2 (Fig. 2A) and on the calyces of *L. aucheri* ssp. *aucheri* var. *elegans* and *L. aucheri* ssp. *aucheri* var. *tomentosus* (Fig. 2B).

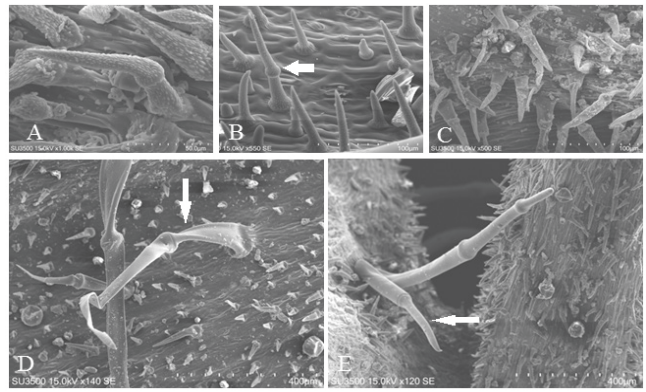

Figure 2. SEM micrographs of non-glandular trichomes in selected *Lagochilus* taxa. Bicelled trichomes type B1 on the stem of *L. aucheri* ssp. *aucheri* var. *aucheri* 2 (A) and on the calyx of *L. aucheri* ssp. *aucheri* var. *elegans* (B). Bicelled trichomes type B2 on the stem of *L. alutaceus* (C). Thin-walled bicelled trichomes type B3 on the calyx of *L. alutaceus* (D). Thick-walled bicelled trichomes type B3 on the stem of *L. lasiocalyx* (E).

B2: short (50-200 μm in size), bi- celled trichomes, the basal cell is without micropapillae. This form can distinguishable on the stem of *L. alutaceus* (Fig. 2C).

B3. Long (1000-1500 μm in size), bicelled trichomes with rare micropapillae, this form was thin – walled on the *L. alutaceus* calyx (Fig. 2D) and thick-walled on *L. lasiocalyx* stem (Fig. 2E).

Long, tricelled trichomes (1000-2000 μm)(C).

Elongated and thin-walled trichomes with rare micropapillae, can be observed on the stems of *L. aucheri* ssp. *aucheri* var. *elegans*, *L. cabulicus* and *L. alutaceus* (Fig. 3A-B), and thick-walled on the stems and calyces of *L. lasiocalyx* and *L. aucheri* ssp. *aucheri* var. *kotschyanus*, respectively (Fig. 2E and Fig. 3C).

Long, four-celled trichomes (D).

This type is found on the calyces of *L. lasiocalyx* and *L. aucheri* ssp. *aucheri* var. *elegans* (Fig. 3D-E).

Glandular trichomes

Three types of glandular trichomes were revealed by SEM micrographs, which all types were found in all studied specimens. The first type (G1) represented the sessile capitate glandular trichomes, (e.g., *L. aucheri* ssp. *aucheri* var. *aucheri* 1 and *L. macracanthus*; Fig. 3F). The second type (G2) represented the short-stalked capitate glandular trichomes (length of the stalk up to 10 μm) which were only registered on the stems of *L. aucheri* ssp. *aucheri* var. *elegans, L. aucheri* ssp. *aucheri* var. *kotschyanus* and *L.aucheri* ssp. *aucheri* var. *tomentosus* (Fig. 3G). The dominant glandular hairs, peltate glandular trichomes (G3), consist of a

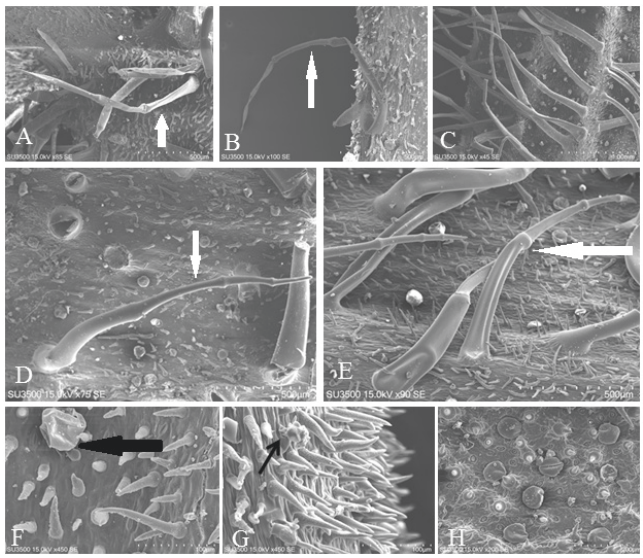

Figure 3. SEM micrographs of non-glandular and glandular trichomes in selected *Lagochilus* taxa. Long tricelled thin- or thick-walled trichomes of type C (A-C). Thin-walled trichomes on the stems *L. alutaceu*s (A) and *L. cabulicus* (B). Thick-walled trichomes on the calyx of *L. aucheri* ssp. *aucheri* var. *kotschyanus* (C). Long, four-celled trichomes on the calyx of *L. lasiocalyx* (D) and *L. aucheri* ssp. *aucheri* var. *elegans* (E). Sessile capitate glandular trichomes on the calyx of *L. aucheri* ssp. *aucheri* var. *aucheri* 1. (F). Short stalked capitate glandular trichomes on the stem of *L. aucheri* ssp. *aucheri* var. *tomentosus* (G). Peltate glandular trichomes on the leaf of *L. alutaceus* (H).

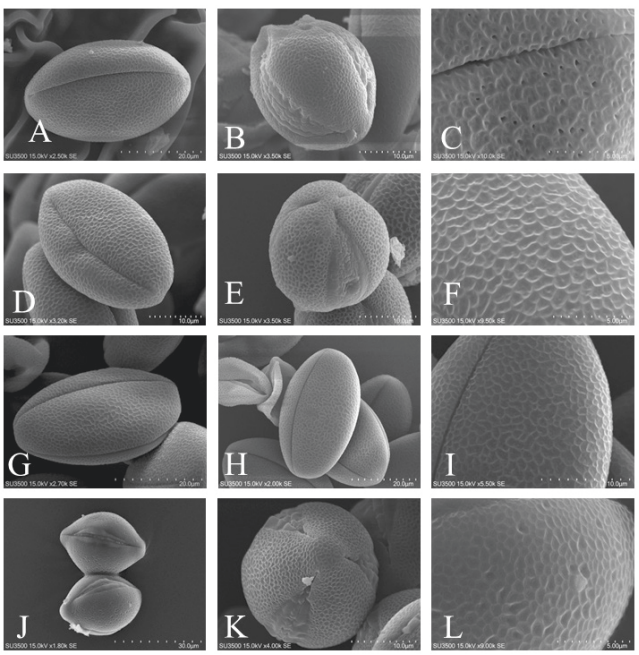

Figure 5. SEM micrographs of pollen grains in the *Lagochilus* taxa examined. A-C: *L. macracanthus*. D-F: *L. aucheri* ssp. *aucheri* var. *kotschyanus.* G-I: *L. aucheri* ssp. *aucheri* var. *aucheri* 1. J-L: *L. aucheri* ssp. *aucheri* var. *aucheri* 2.

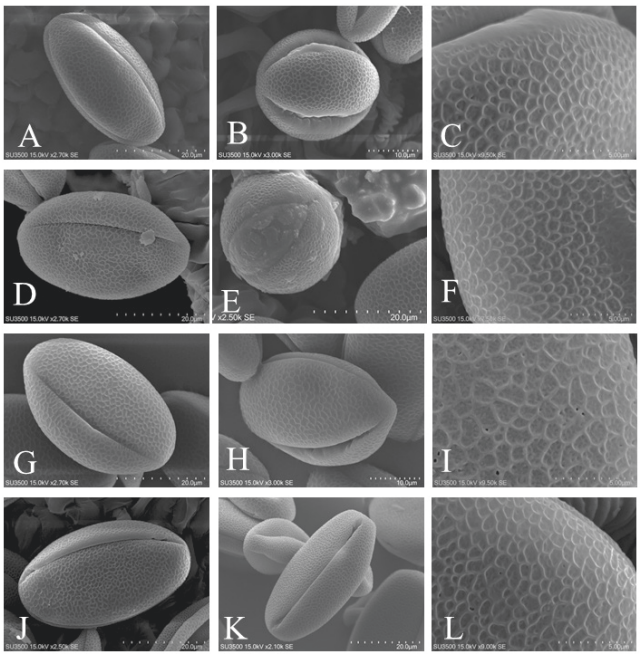

Figure 4. SEM micrographs of pollen grains in the *Lagochilus* taxa examined. A-C: *L. alutaceus*. D-F: *L. cabulicus*. G-I: *L. aucheri* ssp. *aucheri* var. *elegans*. J-L: *L. aucheri* ssp. *aucheri* var. *aucheri* 3.

basal cell, a short stalk cell and a multicellular head (4-8 cells). Its highest number was recorded on the leaves of *L. aucheri* ssp. *aucheri* var. *aucheri* 3, *L. cabulicus* and *L. alutaceus,* and also on the calyx of *L. aucheri* ssp. *aucheri* var. *kotschyanus* (Table 2; Fig. 3H).

General pollen features

Pollen size and shape

The pollen grains were monads and mostly small to medium in size. The polar axis length varied from 29.35 μm in *L. aucheri* ssp. *aucheri* var. *aucheri* 2 to 43.91 μm in *L. aucheri* ssp. *aucheri* var. *aucheri* 1, while the equatorial diameter length varied from 17.6 μm in *L. aucheri* ssp. *aucheri* var. *kotschyanus* to 24.59 μm in *L. aucheri* ssp. *aucheri* var. *aucheri* 3 (Table 3). The shape of all pollen grains was prolate (P/E = 1.57-1.9) in equatorial view, except for *L. aucheri* ssp. *aucheri* var. *aucheri* 2, which was prolate-subprolate (P/E = 1.34) (Table 3). In polar view, the shape of all pollen grains was circular.

Apertures

Pollen grains were isopolar and tricolpate in all examined taxa. Simple colpi were elongated and narrowing at the poles. Colpus length ranges from 25.84 μm in *L. aucheri* ssp. *aucheri* var. *aucheri* 2 to 41.46 μm in *L. aucheri* ssp. *aucheri* var. *aucheri* 3 (Table 3). Mesocolpium value varied from 12.5 μm in *L. aucheri* ssp. *aucheri* var. *kotschyanus* to 19.55

Table 3. Summary of pollen morphological data for the *Lagochilus* taxa examined. All sizes are in µm. Numbers refer to mean ± standard deviation (minimum-maximum). Clg: colpus length. P: polar axis. E: equatorial axis. Sc: sculpturing type 1a, 1b, 1c = bireticulate; 2: reticulate; 3: microreticulate; 4: incomplete reticulate. All measurements are in µm.

Taxon	P	E	P/E	Clg	Mesocolpium	Apocolpium	Sc	Shape
L. aucheri ssp. *aucheri* var. *aucheri 1*	43.91 ± 1.7 (40.9-46.83)	23 ± 2.2 (20.17-26.26)	1.90	41 ± 1.9 (37.65-43.19)	15.68 ± 1.41 (14.36–17.95)	4.2 ± 1.04 (3.69–5.41)	1c	Prolate
L. aucheri ssp. *aucheri* var. *elegans*	41.31 ± 1.24 (35.68-42.94)	22.8 ± 1.42 (20.93-25.18)	1.81	38.51 ± 1.06 (37.05-40.04)	16.53 ± 1.8 (15.21-17.85)	4.35 ± 1.7 (5.7-6.2)	1a	Prolate
L. aucheri ssp. *aucheri* var. *kotschyanus*	33.08 ± 1.41 (31.22-34.29)	17.6 ± 0.62 (16.97-18.16)	1.87	30.56 ± 1.64 (29.50-32.44)	12.5 ± 1.36 (10.75-15.3)	3 ± 0.72 (2.4–4.03)	1c	Prolate
L. aucheri ssp. *aucheri* var. *tomentosus*	39.82 ± 0.91 (38.57-40.98)	22.95 ± 0.97 (21.21-24.35)	1.73	37.81 ± 1.15 (35.5-39.49)	15.61 ± 2.29 (13.69–18.72)	4.7 ± 0.45 (4.04–5.13)	4	Prolate
L. aucheri ssp. *aucheri* var. *aucheri 2*	29.35 ± 0.92 (27.62-30.34)	21.78 ± 0.84 (20.73-22.67)	1.34	25.84 ± 0.74 (25.20-26.59)	14 ± 0.78 (12.8-15.21)	4.6 ± 1.1 (3.91-5.22)	2	Prolate-subprolate
L. aucheri ssp. *aucheri* var. *aucheri 3*	43.71 ± 0.96 (42.66-44.78)	24.59 ± 0.99 (24.36-25.65)	1.77	41.46 ± 0.45 (41.05-41.92)	19.55 ± 1 (19.1-20.2)	4.8 ± 1.03 (3.30–6.02)	1a	Prolate
L. alutaceus	35.59 ± 2.27 (33.12-39.93)	19.21 ± 1.81 (15.46-21.70)	1.85	31.56 ± 2.09 (30.16-35.07)	14.72 ± 1.35 (13.15-15.47)	2.45 ± 0.21 (2.34–2.78)	1a	Prolate
L. cabulicus	38.96 ± 1.38 (36.30-40.77)	21.74 ± 1.71 (19.36-23.03)	1.79	36.57 ± 0.23 (36.52-36.85)	16.26 ± 0.96 (15.53-17)	4.15 ± 0.98 (3.5-4.8)	1a	Prolate
L. lasiocalyx	33.73 ± 1.54 (30.03-36.14)	21.43 ± 1.5 (19.08-23.64)	1.57	31.2 ± 1.62 (29.38-34.57)	16.13 ± 1.17 (15-18.11)	3.2 ± 0.83 (2.5-3.92)	3	Prolate
L. macracanthus	39.83 ± 0.74 (39.08-40.69)	23.66 ± 1.5 (22.42-24.51)	1.68	37.78 ± 0.95 (36.05-39.98)	16.03 ± 1.73 (13.75-18.06)	4.85 ± 0.63 (4.11-5.63)	1b	Prolate

µm in *L. aucheri* ssp. *aucheri* var. *aucheri* 3. Apocolpium diameter ranges from 2.45 µm in *L. alutaceus* to 4.85 µm in *L. macracanthus* (Table 3).

Exine ornamentation

Exine sculpture displayed four distinct types of surface ornamentation: bireticulate or suprareticulate (Fig. 4A-L, Fig. 5A-F, and Table 3), reticulate (Fig. 5G-L, Table 3), microreticulate (Fig. 6A-C, Table 3) and incomplete reticulate (Fig. 6D-F, Table 3). Bireticulate patterns can be subdivided into three subtypes, based on the detailed configuration of the exine ornamentation patterns.

Bireticulate sculpture pattern. The most common (seven taxa) sculpture pattern among the studied taxa was the bireticulate sculpture pattern (special type of reticulate ornamentation, where a two-layered reticulum consisting of a suprareticulum supported by a microreticulate layer). According to the number of perforations per 25 µm^2, it can be divided into three subtypes (a-c). In subtype 1a, the number of perforations was <5 (*L. alutaceus, L. cabulicus, L. aucheri* ssp. *aucheri* var. *elegans* and *L. aucheri* ssp. *aucheri* var. *aucheri* 3, Fig. 4A-L). In subtype 1b, the number of perforations was >5 (Fig. 5A-C, *L. macracanthus*). Bireticulate subtype 1c was determined with prolonged primary lumina without perforations, which was reported from *L. aucheri* ssp. *aucheri* var. *kotschyanus* (Fig. 5D-F) and *L. aucheri* ssp. *aucheri* var. *aucheri* 1 (Fig. 5G-I).

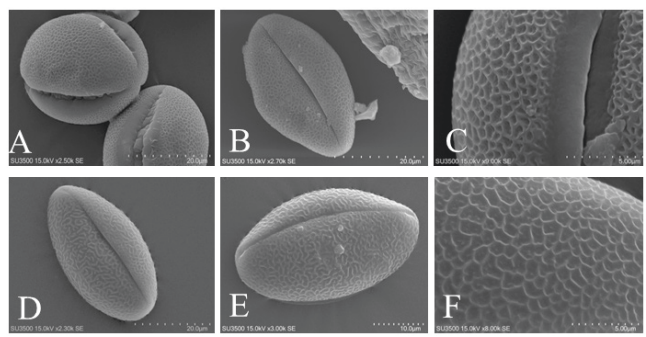

Figure 6. SEM micrographs of pollen grains in the *Lagochilus* taxa examined. A-C: *L. lasiocalyx*. D-F: *L. aucheri* ssp. *aucheri* var. *tomentosus*.

Reticulate sculpture pattern. Among the examined taxa, *L. aucheri* ssp. *aucheri* var. *aucheri* 2 had reticulate sculpture pattern (Fig. 5J-L).

Microreticulate sculpture pattern. The microreticulate sculpture pattern is observed only in *L. lasiocalyx* (Fig. 6A-C). In this pattern diameter of lumina is smaller than 1 µm.

Incomplete reticulate sculpture pattern. Incomplete reticulate sculpture pattern (network like pattern formed by exine elements, is incomplete), occurs for *L. aucheri* ssp. *aucheri* var. *tomentosus* (Fig. 6D-F).

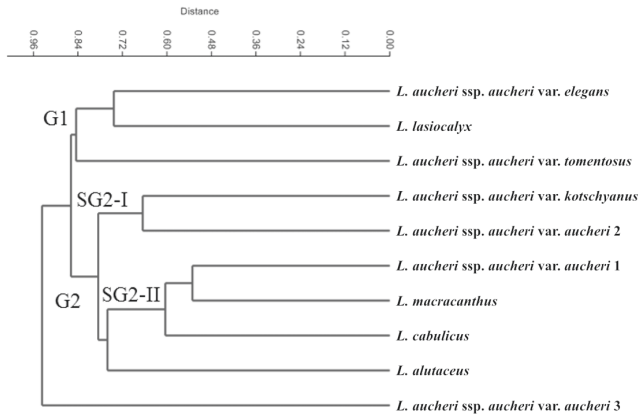

Figure 7. UPGMA dendrogram of the studied *Lagochilus* taxa based on micromorphological and palynological characteristics. G: group. SG: subgroup.

Statistical analysis

The UPGMA dendrogram based on the micromorphological and palynological features showed the existence of two main clusters (Fig. 7). Group1 (G1) contained specimens with three- or four- celled trichomes on the stems or calyces (*L. lasiocalyx*, *L. aucheri* ssp. *aucheri* var. *elegans* and *L. aucheri* ssp. *aucheri* var. *tomentosus*), while Group 2 (G2) was subdivided into two subgroups: subgroup I (SG2-I) contained specimens with two-celled trichomes of type B1 (*L. aucheri* ssp. *aucheri* var. *aucheri* 2 and *L. aucheri* ssp. *aucheri* var. *kotschyanus*). Subgroup II (SG2-II) contained specimens with short unicellular thin-walled trichomes on the stems and calyces (*L. aucheri* ssp. *aucheri* var. *aucheri* 1, *L. macracanthus*, *L. cabulicus* and *L. alutaceus*). *L. aucheri* ssp. *aucheri* var. *aucheri* 3 was sister to all *Lagochilus* species (Fig. 7). As seen in Figure 7, known varieties of *L. aucheri* were distributed through the tree.

The ANOVA result did not show significant differences ($p \leq 0.05$) in the number between all observed types of trichomes, however, PCA-biplot showed that some of species had distinct type of trichomes that were useful in identification of them (Fig. 8). For example, the number of trichomes type A1 on the calyces is a distinguishing trait for identification of *L. aucheri* ssp. *aucheri* var. *kotschyanus*, however, *L. aucheri* ssp. *aucheri* var. *tomentosus* were identified by highest number of trichomes of type A1on the leaves. In addition, trichomes of type B2 and C on the stems was significant trait for *L. alutaceus*.

Discussion

Micromorphological characters

Both glandular and non-glandular trichomes were existed on the stems, leaves and calyces of all investigated taxa. The trichomes types presented on the studied species were mostly similar to those of family Lamiaceae reported by Navarro and El Qualidi (2000), Cantino (1990) and Atalay et al. (2016a). Generally, number of non-glandular trichomes was higher than glandular ones, which is a common feature in Lamiaceae family (Metcalfe and Chalk 1950).

Our study showed that the size and cell number of trichomes were valuable and could be applied to classify the non-glandular trichomes into four types including 10 forms; therefore, they can be used as taxonomic tools in species and intraspecific identification.

Two main types of glandular trichomes were capitate and peltate. The studied taxa had two types of capitate trichomes which differed from each other in their stalk length. Talebi and Rezakhanlou (2012) reported the capitate trichomes with a basic and two apical cells in *L. macracanthus*. The peltate trichomes of Lamiaceae have mostly a secretory head of four central and 6-14 peripheral cells (Werker 1993). Peltate glandular hairs with eight-celled head were previously reported in *L. macracanthus* (Talebi and Rezakhanlou 2012). The distribution of glandular trichomes is obviously correlated with their role in pollination (Navarro and El Qualidi, 2000). In *Lagochilus* genus, this type totally appears on the outer side of the calyces and sparse on the stems.

Pollen grain morphology

Erdtman (1945) classified the Lamiaceae family into two subfamilies based on the number of apertures and nuclei in the mature pollen grains. The first group comprises the subfamily Lamioideae with tricolpate pollen grains and the second group contains the subfamily Nepetoideae characterized by hexacolpate pollen grains. According to the latest molecular phylogenetic studies by Bendiksby et al. (2011) the genus *Lagochilus*, included in the subfamily Lamioideae and tribe Leonureae. The present study showed that the all the examined taxa have tricolpate pollen grains similar with the other genera of subfamily Lamioideae (Abu-Asab and Cantino 1994; Atalay et al. 2016b).

The shapes of the pollen grains in equatorial view is prolate except for *L. aucheri* ssp. *aucheri* var. *aucheri* 2, with prolate-subprolate shape (P/E = 1.34). The state of hydration and/or fixation could be affecting the pollen shape (Demissew and Harley 1992; León-Arencibia and La-Serna Ramos 1992; Moon et al. 2008a). Thus, differences in shape among the pollen grains may not be significant or even applicable in their taxonomy (Xiang et al. 2013). Moon et al. (2008a) suggested, in order preserving a more natural form, careful processing such as critical point drying of the fresh material is required.

The observed exine sculpture patterns in *Lagochilus* were determined as bireticulate, reticulate, microreticulate and also incomplete reticulate. Reticulate and microreticulate exins are common in several species of subfamily Lamioideae and in other genera of Lamiaceae (Wagstaff 1992; Abu-Asab and Cantino 1992, 1994; Çelenk et al. 2008 a,b; Moon et al. 2008 a,b,c; Özler et al. 2011, 2013; Atalay et al. 2016b). Bireticulate exin are a plesiomorphic in subfamily Lamioidae, while it is apomorphic in Lamiaceae (Cantino 1992 a,b). Derived states as psilate, granulate, rugulate and suprareticulate-rugulate forms of sculpturing pattern and branched columellae occur in some members of Lamioids. Similar pollen features suggest relationships within and between certain genera in Lamioidae (Abu-Asab and Cantino 1994; Atalay et al. 2016b). Incomplete reticulate sculpture pattern occured for *L.aucheri* ssp. *aucheri* var. *tomentosus* (Fig. 6D-F). This pattern not been reported previously in Lamiaceae.

Among the investigated taxa, palynological properties of *L. aucheri* have been provided by Abu-Asab and Cantino (1994). Characteristics investigated by them correlate with our current results, except for the P/E ratios, which are possibly due to differences in procedure of preparation.

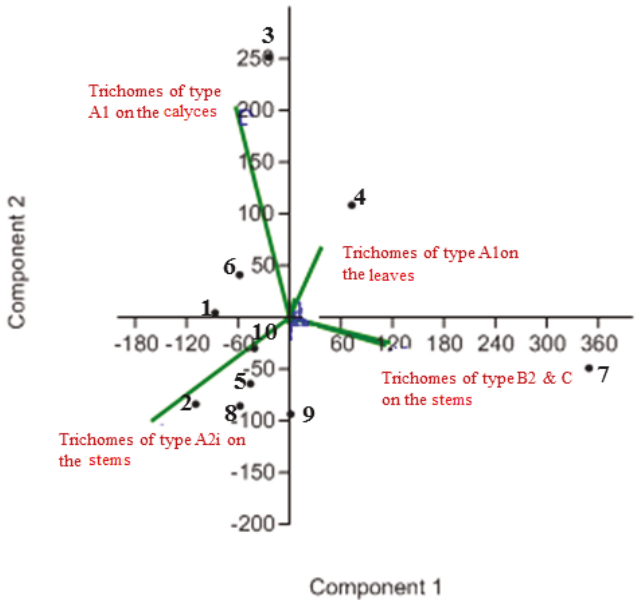

Figure 8. PCA-biplot of the studied taxa and their trichome features. 1: *L. aucheri* ssp. *aucheri* var. *aucheri* 1. 2: *L. aucheri* ssp. *aucheri* var. *elegans*. 3: *L. aucheri* ssp. *aucheri* var. *kotschyanus*. 4: *L. aucheri* ssp. *aucheri* var. *tomentosus*. 5: *L. aucheri* ssp. *aucheri* var. *aucheri* 2. 6: *L. aucheri* ssp. *aucheri* var. *aucheri* 3. 7: *L. alutaceus*. 8: *L. cabulicus*. 9: *L. lasiocalyx*. 10: *L. macracanthus*.

Systematic significance of trichome and pollen grains micromorphology

L. aucheri complex

Jamzad (1988), in her taxonomic revision of the genus *Lagochilus* in Iran, recognized two subspecies for *L. aucheri*: ssp. *heterophyllus* and ssp. *aucheri*. Moreover, she identified four varieties for ssp. *aucheri*. She stated that the indumentum is one of the characteristics that can be used in distinguishing varieties. Results of our investigation showed that the trichomes micromorphology can be used in distinguishing varieties that presented by Jamzad (1988). She has reported that *L. aucheri* ssp. *aucheri* var. *aucheri* was characterized by glabrous stem and calyx, while we observed short unicellular trichomes on the stem and calyx of this taxon. Moreover, leaves of this variety had lowest number of prenominated trichomes.

L. kotschyanus Boiss. was originally described as a species but was reduced to a variety of *L. aucheri* by Bornmüller (1907). *L. aucheri* ssp. *aucheri* var. *kotschyanus* has long unicellular trichomes on the stems and tricelled trichomes on the calyces, which were not observed in any other varieties of the species.

L. aucheri ssp. *aucheri* var. *elegans* and *L. aucheri* ssp. *aucheri* var. *tomentosus*, are two new infraspecific taxa that were described by Jamzad (1988). In our study, *L. aucheri* ssp. *aucheri* var. *elegans* was characterized by four-celled trichomes on the calyces, and *L. aucheri* ssp. *aucheri* var. *tomentosus* was identified by short unicellular trichomes on the stems and bicelled trichomes on the calyces. In addition, *L. aucheri* ssp. *aucheri* var. *tomentosus* identified by highest number of trichomes of type A1on the leaves.

In carrying out of determination of specimens, we identified plants which have basic traits of *L. aucheri* but differed from known species in some morphological characteristics such as ratio of teeth length /calyx tube or calyx teeth numbers. This holds true for plants of Zanjan (*L. aucheri* ssp. *aucheri* var. *aucheri* 2) and Dizin (*L. aucheri* ssp. *aucheri* var. *aucheri* 3) populations. Detailed micromorphological analysis revealed that trichomes of type A1 were observed on the leaves and calyces of all specimens, except *L. aucheri* ssp. *aucheri* var. *aucheri* 3, while, unicellular thin-walled trichomes with 200-300 µm in size (A2 i type), present only on the leaves, stems and calyces of *L. aucheri* ssp. *aucheri* var. *aucheri* 3. Similarly, bicelled trichomes of type B1 were observed on the stems of *L. aucheri* ssp. *aucheri* var. *aucheri* 2 and *L. aucheri* ssp. *aucheri* var. *kotschyanus* , however, latter vary from *L. aucheri* ssp. *aucheri* var. *aucheri* 2 in having trichomes of type A2ii on the stems and trichomes of type C on the calyces. The basic shape of the pollen grains in most taxa was prolate, however prolate-subprolate pollen grains was recorded for *L. aucheri* ssp. *aucheri* var. *aucheri* 2. Moreover, reticulate sculpturing pattern of pollen grains were observed only in *L. aucheri* ssp. *aucheri* var. *aucheri*

2. *L. aucheri* ssp. *aucheri* var. *aucheri* 3 had highest value of colpus length and mesocolpium area among all taxa examined. Therefore, it seems to be new intraspecific ranks in *L. aucheri* complex that need to additional and detailed morphological and molecular studies.

In our UPGMA tree of micromorphological and palynological characteristics, the examined taxa are separated from each other, but varieties of *L. aucheri* do not grouped together and not nested in the same clade as the members of *L. aucheri*. Therefore, *L. aucheri* seems to be a polyphyletic and this genus needs to revise of morphological characteristics for identifying of species.

Other Lagochilus species

Jamzad (1988) described *L. lasiocalyx* as the new combination, based on *L. aucheri* var. *lasiocalyx* Stapf., and treated *L. aucheri* var. *perhispidus* Bornm. as a synonym of *L. lasiocalyx*. In flora of Iran (Jamzad 2012), *L. lasiocalyx* has placed toward known varieties of *L. aucheri*. Result of UPGMA tree of micromorphological characteristics corroborates her morphology-based conclusion; *L. lasiocalyx* showed a close relationship with *L. aucheri* ssp. *aucheri* var. *elegans* and *L. aucheri* ssp. *aucheri* var. *tomentosus*.

According to Jamzad (1988), there was close affinity and the high degree of morphological similarities between *L. cabulicus* and *L. aucheri*, in so far as it is difficult to distinguish them. We could differentiate them by trichomes and pollen grains characteristics. The trichomes size on the leaves of *L. cabulicus* was very short (< 50μm) while it varied from 100-200 μm in *L. aucheri* 1, also we could differentiate them by the shorter size of the pollen grains in *L. cabulicus*. The polar and equatorial axis ranged from 36.30-40.77 μm and 19.36-23.03 μm, respectively in *L. cabulicus*, while they varied from 40.9-46.83 μm and 20.17-26.26 μm in *L. aucheri* 1. Despite bireticulate sculpture pattern observed in both species, they varied from each other according to the number of perforations per 25 μm^2.

In the UPGMA tree, a close relationship could be identified among *L. cabulicus*, *L. macracanthus* and *L. alutaceus*, which these results, generally were corroborate with Rechinger classification (1982).

The result of statistical analysis showed that trichomes characteristics such as density and cell numbers of non-glandular trichomes could be used as a relevant features for identification of the investigated taxa concerning they stable position between studied populations of each species.

Key to studied taxa according to non-glandular trichomes

Based on our results of trichomes morphology and density of *Lagochilus* species, we proposed that the type of indumentum can be used as a significant trait for identification of the examined taxa. Among non-glandular trichomes, size, cell number and density are considered as valuable, therefore, a key to the studied taxa of *Lagochilus* according to the result of the non-glandular trichomes are given below.

1 a. Leaves only with unicellular trichomes shorter than 50 μm..... ***L. cabulicus***
b. Leaves with unicellular trichomes both shorter and longer than 50 μm 2

2 a. Leaves with unicellular trichomes range 50-200 μm..... 3
b. Leaves with unicellular trichomes range 200-300 μm..... ***L. aucheri* ssp. *aucheri* var. *aucheri* 3**

3 a. Stems only with unicellular trichomes..... 4
b. Stems both with uni- and multi-cellular trichomes..... 5

4 a. Stems with unicellular trichomes shorter than 50 μm..... ***L. macracanthus***
b. Stems with unicellular trichomes longer than 50 μm..... 6

5 a. Stems both with uni- and bicelled trichomes..... 7
b. Stems both with uni- and tricelled trichomes..... 8

6 a. Calyces with short unicellular trichomes up to 100 μm..... ***L. aucheri* ssp. *aucheri* var. *aucheri* 1**
b. Calyces with bicelled trichomes range 100-200 μm..... ***L. aucheri* ssp. *aucheri* var. *tomentosus***

7 a. Stems with short unicellular trichomes (50-200 μm), calyces only with unicellular trichomes..... ***L. aucheri* ssp. *aucheri* var. *aucheri* 2**
b. Stems with long unicellular trichomes (1000-2000 μm), calyces with uni- and tricelled trichomes..... ***L. aucheri* ssp. *aucheri* var. *kotschyanus***

8 a. Calyces with uni- and bicelled trichomes..... 9
b. Calyces with uni- and tricelled trichomes..... ***L. lasiocalyx***

9 a. Calyces with bicelled trichomes range 500-1000 μm, without four-celled trichomes..... ***L. alutaceus***
b. Calyces with bicelled trichomes ranges 100-200 μm, with four-celled trichomes..... ***L. aucheri* ssp. *aucheri* var. *elegans***

Conclusion

According to the Plant List (Govaerts et al. 2013), some of species and infraspecific taxa currently recognized as synonyms (e.g., *L. lasiocalyx*, , *L. aucheri* ssp. *aucheri* var. *elegans* and *L. aucheri* ssp. *aucheri* var. *tomentosus*), while, based on micromorphological results were presented here, all known species and infraspecific taxa were delimited.

In conclusion, the present study provides micromorphological and palynological characteristics of the genus *Lagochilus* that would be applicable in identification,

delimitation and classification of the genus; however, Phylogenetic and morphological studies of *Lagochilus*, based on complete sampling will be necessary to confirm existence of new taxa and to illuminate the intraspecific relationships of the genus.

Acknowledgements

We would like to thank Mr. A. Javadi Anaghizi (Central Laboratory of the Shahid Beheshti University) for his help in SEM.

References

Abu-Asab MS, Cantino PD (1989) Pollen morphology of *Trichostema* (Labiatae) and its sytematic implications. Syst Bot 14:359-369.

Abu-Asab MS, Cantino PD (1992) Pollen morphology in subfamily Lamioideae (Labiatae) and its phylogenetic implications. In Harley RM, Reynolds T, Eds., Advances in Labiatae Science. Royal Botanic Gardens, Kew, pp. 97-112.

Abu-Asab MS, Cantino PD (1993a) Phylogenetic implications of pollen morphology in tribe Ajugeae (Labiatae). Syst Bot 18:100-122.

Abu-Asab MS, Cantino PD (1993b) Systematic implications of pollen morphology in tribe Prostanthereae (Labiatae). Syst Bot 18:563-574.

Abu-Asab MS, Cantino PD (1994) Systematic implications of pollen morphology in subfamilies Lamioideae and Pogostemonoiedae (Labiatae). Ann Missouri Bot Gard 81:635-686.

Atalay Z, Celep F, Bara F, Doğan M (2016a) Systematic significance of anatomy and trichome morphology in *Lamium* (Lamioideae; Lamiaceae). Flora 22:60-75.

Atalay Z, Celep F, Bara F, Doğan M (2016b) Pollen morphology of the genus *Lamium* L. (Lamiaceae) and its systematic implications. Flora 21:68-84.

Badamtsetseg B, Myoung LS, Yuon LH (2012) Pollen morphology of the family Lamiaceae in Mongolia. J Korean Nat 5:169-179.

Bendiksby M, Thorbek LB, Scheen AC, Lindqvist C, Ryding O (2011) An updated phylogeny and classification of Lamiaceae subfamily Lamioideae. Taxon 60:471-484.

Boissier E (1879) Flora Orientalis. Vol. 4, 768-77 L. Basiliae & Genevae.

Boissier E (1848) In De Candolle AP, Ed, Prodromus Systematis Naturalis Regni Vegetabilis, Vol. 12. Victor Masson, Paris, 515.

Bornmüller JFN (1907) Plantae Straussianae – sive enumeratio plantarum a Th. Strauss annis 1889–1899 in Persia occidentali collectarum. Pars III. Beih Bot Centralbl, Abt. 22:134.

Cantino PD (1990) The phylogenetic significance of stomata and trichomes in the Labiatae and Verbenaceae. J Arnold Arbor 71:323-370.

Cantino PD (1992a) Evidence for a polyphyletic origin of the Labiatae. Ann Missouri Bot Gard 79:361-379.

Cantino PD (1992b) Toward a phylogenetic classification of the Labiatae. In Harley RM, Reynolds T, Eds, Advances in Labiatae Science. Royal Botanic Gardens, Kew, pp 27-37.

Çelenk S, Tarimcilar G, Biçakçi A, Kaynak G, Malyer H (2008a) A palynological study of *Mentha* L. Bot J Linn Soc 157:141-154.

Çelenk S, Dirmenci T, Malyer H, Biçakçi A (2008b) A palynological study of the genus *Nepeta* L. (Lamiaceae). Plant Syst Evol 276:105-123.

Chizhov OS, Kessenikh AV, Yakovlev IP, Zolotarev BM, Petukhov VA (1970) Bull Acad Sci USSR, Div Chem Sci 19:1866.

Demissew SD, Harley MM (1992) Trichome, seed surface and pollen characters in *Stachys* (Lamioideae: Labiatae) in tropical Africa. In Harley RM, Reynolds T, Eds., Advances in Labiatae Science. Royal Botanical Gardens, London, Kew, pp 149-166.

Doaigey AR (1991) Trichome types in the genus *Otostegia* Benth. (Lamiaceae). J King Saud Univ Sci 3:23-30.

Erdtman G (1945) Pollen morphology and plant taxonomy. IV. Labiatae,Verbenaceae, and Avicenniaceae. Svensk Bot Tidskr 39:279-285.

Faegri K, Iversen J (1975) Textbook of Pollen Analysis, 3rd ed. Munksgaard, Copenhagen.

Firdous S, Habib A, Manzoor H, Muqarrab S (2015) Pollen morphology of *Ajuga* L., *Lamium* L. and *Phlomis* L. (Lamiaceae) from district Abbottabad Pakistan. Pak J Bot 47:269-274.

Gairola S, Naidoo Y, Bhatt A, Nicholas A (2009) An investigation of the foliar trichomes of *Tetradenia riparia* (Hochst.) Codd [Lamiaceae]: an important medicinal plant of Southern Africa. Flora 204:325-330.

Gonzales WL, Negrittoa MA, Suarez LH, Gianoli E (2008) Induction of glandular and non-glandular trichomes by damage in leaves of *Madia sativa* under contrasting water regimes. Acta Oecol 33:128-132.

Govaerts R, Paton A, Harvey Y, Navarro T (2013) World checklist of Lamiaceae and Verbenaceae. Kew, Richmond: The Board of Trustees of the Royal Botanic Gardens. http://www.kew.org/wcsp/lamiaceae/.

Harley MM, Paton A, Harley RM, Cade PG (1992) Pollen morphological studies in tribe Ocimeae (Nepetoideae: Labiatae): I. *Ocimum* L. Grana 31:161-176.

Harley RM, Atkinson S, Budantsev AL, Cantino PD, Conn BJ, Grayer R, Harley MM, Dekok R, Krestovskaja T,

Morales R, Paton AJ, Ryding O, Upson T (2004) Labiatae. In Kadereit JW, Ed., The Families and Genera of Vascular Plants. Vol. 7. Springer, Berlin, pp. 167-275.

Hassan N, Osman AK, El Garf IA (2009) Pollen types of the Egyptian species of the genus *Salvia* (Lamiaceae). Feddes Repert 120:394-404.

Hesse M, Halbritter H, Zetter R, Weber M, Buchner R, Frosch-Radivo A, Ulrich S (2009) Pollen Terminology - An Illustrated Handbook. Springer, Wien, New York.

Ikramov MI (1976) Rod Lagochilus Srednej Azii. Izdat Taskent, Izdat Fan Uzbekskoj SSR.

Jalili A, Jamzd Z (1999) Red Data Book of Iran. Research Institute of Forests and Rangelands, Tehran, Iran.

Jamzad Z (1988) The genus *Lagochilus* (Labiatae) in Iran. Iranian J Bot 4:91-103.

Jamzad Z (2012) Lamiaceae. In Assadi M, Maassoumi A, Mozaffarian V, Eds., Flora of Iran. Vol. 76. Research Institute of Forests and Rangelands, Tehran (*in Persian*), pp 337-349.

Jiao Y, Zhang CG, Zhang T, Chou GX, Xu H LQ (2014) Anti-inflammatory effects of aqueous extracts of whole herbs from five *Lagochilus* species in vitro. Chinese Journal of New Drugs and Clinical Remedies 33:204-211.

León-Arencibia MC, La-Serna Ramos IE (1992) Palynological study of *Lavandula* (sect. *Pterostoechas*, Labiatae): Canario-maderiense endemics. Grana 31:187-195.

Bini Maleci L, Servettaz O (1991) Morphology and distribution of trichomes in Italian species of *Teucrium* Sect. *Chamaedrys* (*Labiatae*) - a taxonomical evaluation. Plant Syst Evol 174:83-91.

Metcalfe CR, Chalk L (1950) Anatomy of the Dicotyledons. Vol. 2. Oxford Press, London.

Moon HK, Hong SP (2003) Pollen morphology of the genus *Lycopus* (Lamiaceae). Ann Bot Fenn 40:191-198.

Moon HK, Vinckier S, Smets E, Huysmans S (2008a) Comparative pollen morphology and ultrastructure of Mentheae subtribe Nepetinae (Lamiaceae). Rev Paleobot Palynol 149:174-186.

Moon HK, Vinckier S, Walker JB, Smets E, Huysmans S (2008b) A search for phylogenetically informative pollen characters in the subtribe Salviinae/Mentheae: Lamiaceae. Int J Plant Sci 169:455-471.

Moon HK, Vinckier S, Smets E, Huysmans S (2008c) Palynological evolutionary trends within the tribe Mentheae with special emphasis on subtribe Menthinae (Nepetoideae: Lamiaceae). Plant Syst Evol 275:93-108.

Navarro T, El Qualidi J (2000) Trichome morphology in *Teucrium* L. (Labiatae): a taxonomic review. Ann Bot Garden Madrid 57:277-297.

Özler H, Pehlivan S, Kahraman A, Doğan M, Celep F, Başer B, Yavru A, Bagherpour S (2011) Pollen morphology of the genus *Salvia* L. (Lamiaceae) in Turkey. Flora 206:316-327.

Özler H, Pehlivan S, Celep F, Doğan M, Kahraman A, Fisne AY, Başer B, Bagherpour S (2013) Pollen morphology of *Hymenosphace* and *Aethiopis* sections of the genus *Salvia* (Lamiaceae) in Turkey. Turk J Bot 37:1070-1084.

Parsa A (1949) Flora de I'Iran. Vol. 4:821-826.

Peter J, Shanower T (1998) Plant glandular trichomes chemical factories with many potential uses. Resonance 3:41-45.

Podani J (2000) Introduction to the Exploration of Multivariate Biological Data. Backhuys Publisher, Leiden, p. 407.

Rechinger KH (1982) Flora Iranica. No. 150. Akademische Druck- u. Verlagsanstalt, Graz, pp. 337-344.

Salmaki Y, Jamzad Z, Zarre S, Brauchler C (2008) Pollen morphology of *Stachys* (Lamiaceae) in Iran and its systematic implication. Flora 203:627-639.

Salmaki Y, Zarre S, Jamzad Z, Bräuchler C (2009) Trichome micromorphology of Iranian *Stachys* (Lamiaceae) with emphasis on its systematic implication. Flora 20:371-381.

Taban S, Masoudi Sh, Chalabian F, Delnavaz B, Rustaiyan A (2009) Chemical composition and antimicrobial activities of the essential oils from flower and leaves of *Lagochilus kotschyanus* Boiss. A new species from Iran. J Med Plant 8:58-63.

Talebi SM, Rezakhanlou A (2012) Biological study of *Lagochilus maracanthus* Fish. et Mey. endemic species of Iran. J Chem Pharm Res 4:633-639.

Talebi SM, Mahdiyeh M, Ghorbani Nohooji M, Akhani M (2018a) Analysis of trichome morphology and density in *Salvia nemorosa* L. (Lamiaceae) of Iran. Botanica 24:49-58.

Talebi SM, Ghorbani Nohooji M**,** Yarmohammadi M, Azizi N, Matsyura A (2018b) Trichomes morphology and density analysis in some *Nepeta* species of Iran. Med Bot 39:51-62.

Wagner GJ (1991) Secreting glandular trichomes: more than just hairs. Plant Physiol 96:675-679.

Wagstaff SJ (1992) A phylogenetic interpretation of pollen morphology in tribe Mentheae (Labiatae). In Harley RM, Reynolds T, Eds., Advances in Labiatae Science. Royal Botanic Gardens, Kew, pp. 113-124.

Werker E (1993) Fuction of essential oil secreting glandular hairs in aromatic plants of the Lamiaceae. A review. Flavour Fragr J 8:249-255.

Wunderlich R (1967) Ein Vorschlag zu einer natürlichen Gliederung der Labiaten auf Grund der Pollenkörner, der Samenentwicklung und des reifen Samens. Österr Bot Z 114:383-483.

Xiang CL, Funamoto T, Evangelista EV, Zhangd Q, Penga H (2013) Pollen morphology of the East Asiatic genus *Chelonopsis* (Lamioideae: Lamiaceae) and allied genera, with reference to taxonomic implications and potential pollination ecology. Plant Biosys 147:620-628.

Xiao K, Mao X, Lin Y, Xu H, Zhu Y, Cai Q, Xie H, Zhang J (2017) Trichome, a functional diversity phenotype in plant. Mol Biol 6:1. DOI: 10.4172/2168-9547.1000183

Zhang LM, Zeng XQ, Sanderson SC, Byalt VV, Sukhorukov AP (2017) Insight into Central Asian flora from the Cenozoic Tianshan montane origin and radiation of *Lagochilus* (Lamiaceae). PloS ONE 12(9):e0178389.

Acta Biologica Szegediensis

Volume 63(2):157-168, 2019
Acta Biologica Szegediensis
http://abs.bibl.u-szeged.hu/index.php/abs
DOI:10.14232/abs.2019.2.157-168

ARTICLE

Biosystematic study of the genus *Lallemantia* (Lamiaceae): species delimitation and relationship

Fahimeh Koohdar*, Masoud Sheidai

Faculty of Biological Sciences and Biotechnology, Shahid Beheshti University, Tehran, Iran.

ABSTRACT *Lallemantia* (Lamiaceae) is a small genus with 5 species. In general, little biosystematics and molecular study has been performed on the genus *Lallemantia*. Moreover, the studies used only some of the species; none of them has considered all 5 species as a whole in one specific approach. Therefore, the species inter-relationship or nexus in the genus is not thoroughly probed. The present study investigated the molecular phylogeny and species relationship of all five species in the genus *Lallemantia*, using ribosomal protein L16 and the multilocus ISSR markers. It also compared their morphometric, anatomical and seed results. The species were efficaciously delimited by the morphological, anatomical and seed characters, as well as by ISSR and cpDNA markers. The PCA (Principal components analysis) plot of the species based upon the morphological characters, the MDS (Multidimensional Scaling) plot of the species based on the nutlet and anatomical characters, the NJ (neighbor joining) tree plot of ISSR data and the ML tree of cpDNA revealed closer affinity between *L. iberica* and *L. canescens* and *L. peltata* was placed at some distance from these species. The phylogenetic trees displayed monophyly of the genus *Lallemantia*. The Bayesian Evolutionary Analysis by Sampling Trees (BEAST) analysis unveiled that the studied *Lallemantia* species started to diverge about 25 million years ago. **Acta Biol Szeged 63(2):157-168 (2019)**

KEY WORDS
anatomy
biogeography
cpDNA
ISSR
molecular phylogeny
morphology
nutlet

ARTICLE INFORMATION
Submitted
10 November 2019.
Accepted
31 January 2020.
***Corresponding author**
E-mail: f_koohdar@yahoo.com

Introduction

The genus *Lallemantia* (Lamiaceae) comprises of 5 species which are widely distributed in Afghanistan, China, India, Kazakhstan, Kyrgyzstan, Pakistan, Iran, Russia, Tajikistan, Turkmenistan, Uzbekistan, SW Asia and Europe, with the Caucasian region as the center of origin. All 5 *Lallemantia* species are found in Iran (Rechinger 1982). The species of *Lallemantia* are herbaceous plants, characterized by simple leaves; a thyrsoid, spike-like or oblong, often interrupted inflorescence; ovate to rotund or sometimes linear, aristate-toothed bracteoles; and oblong, trigonous, smooth and mucilaginous nutlets (Harley et al. 2004). The genus *Lallemantia* is closely related to *Dracocephalum* L., but it differs from *Dracocephalum* in having the upper lip of corolla with two internal longitudinal folds and distinctively 15-veins bracteoles which are aristate-dentate (Edmondson 1982). The *Lallemantia* species have been adopted as a source of food and medicine. For example, *L. iberica* (M.Bieb.) Fisch. & C.A. Mey. is consumed as an oil-seed plant in Iran and the USSR (Rivera-Nunez and Obonde-Gastro 1992; Dinç et al. 2009), furthermore, *L. royleana* (Benth.) Benth. seeds have significant antibacterial properties and are a good remedy for skin diseases and the gastro-intestinal maladies (Mahmood et al. 2013).

Research on the nutlet in Lamiaceae has demonstrated that it is efficacious at various echelons of the taxonomic hierarchy to varying degrees. Specifically, pertained to myxocarpy (i.e. the phenomenon of mucilage production when the nutlets get wet), the anatomy of the pericarp in the family Lamiaceae has also been deemed an extremely useful taxonomic feature (Harley et al. 2004; Moon and Hong 2006; Dinç et al. 2009). The anatomical data as well as the nutlet surface sculpturing patterns have been proven to have a wide range of variation and diagnostic value for species recognition and taxonomy of Lamiaceae (e.g., Kaya et al. 2007; Alan et al. 2010; Kahraman et al. 2010a,b; Celep et al. 2014).

The molecular systematic investigations in the plants are carried out for different purposes: species delimitation, population divergence, species relationships, date of divergence determination, etc. (Broadhurst et al. 2004; Millar et al. 2011). Different molecular markers have been utilized to accomplish the tasks, e.g., AFLP (Amplified Fragments Length Polymorphism), SSRs (Simple Sequence Repeats), ISSRs (Inter-Simple Sequence Repeats). (Sheidai et al. 2012, 2013, 2014; Minaeifar et al. 2015). Both within and between the plant species, the technique of ISSR has been employed extensively for assessing the genetic as-

sociations. Apart from being easy and proffering a quick screen for the DNA polymorphism, ISSR only requires just infinitesimal amounts of DNA. Moreover, it does not need the information on the DNA template sequence. The molecular markers used in the phylogenetic investigations in plant groups are based on the investigation of nuclear ribosomal DNA and chloroplast genes and spacers (e.g., Olmstead and Palmer 1994; Zhang et al. 2015; Minaeifar et al. 2016). There is a consensus on the combination and simultaneous analysis of all the available data sets (Byrne 2003; Bakker et al. 2004). The ISSR and cpDNA information were used in the present study because these molecular markers are efficient for the species delimitation and the determination of the species relationships (Sheidai et al. 2013; Minaeifar et al. 2016).

Limited literature exists on the biosystematics studies on the genus *Lallemantia*. Dinç et al. (2009) reported the micro-morphological features of pollen, nutlet and trichome in three species of *L. iberica*, *L. canescens* (L.) Fisch. & C.A.Mey. and *L. peltata* (L.) Fisch. & C.A.Mey. occurring in Turkey. Alan et al. (2010) studied the anatomical facets in stem, leaf and root of the same species and Özcan et al. (2015) reported the chromosome number (2n = 14) for them.

Similarly, only a few biosystematic and molecular studies have been reported on the genus *Lallemantia* in Iran. Talebi and Rezakhanlou (2010) carried out the morphological analysis of all 5 species, while Dolatyari and Kamrani (2015) reported the karyotype features of four species. Jamzad et al. (2000) displayed a close kinship between *Nepeta* L. to *Lallemantia*, and their distinction from *Dracocephalum*. Additionally, according to Kamrani and Riyahi (2017) *Lallemantia* is a monophyletic genus.

In the present study, biosystematics investigation of the genus *Lallemantia* was performed using the morphological, anatomical and seed characters. Furthermore, the molecular analyses of all 5 species were carried out by the nuclear ISSR and the chloroplast DNA sequences to reveal the species delimitation and species relationships (Sheidai et al. 2013; Minaeifar et al. 2016).

Material and methods

Plant materials

Field investigations and collections were carried out in 2013-2015. For this study, 42 specimens of 5 species (*Lallemantia royleana*, *L. canescens*, *L. baldschuanica* Gontsch., *L. iberica* and *L. peltate*) were randomly collected from different geographic populations. Voucher specimens are deposited in Herbarium of Shahid Beheshti University (HSBU) (Table 1).

Table 1. *Lallemantia* species, their locality and voucher specimens.

Species	Locality	Voucher specimens	Accession number for cp-DNA study
L. peltata	Tehran	2014370	-
L. peltata	Alborz	2014371	MH453501
L. canescens	Qazvin	2014372	MH453498
L. canescens	West Azerbaijan	2014373	-
L. canescens	Zanjan	2014374	-
L. baldshuanica	Khorasan, Kalat	2014375	MH453499
L. iberica	Qazvin	2014376	-
L. iberica	West Azerbaijan	2014377	-
L. iberica	Zanjan	2014378	MH453500
L. iberica	Markazi	2014379	-
L. iberica	Kermanshah	2014380	-
L. royleana	Qazvin	2014381	-
L. royleana	Markazi	2014382	-
L. royleana	Mazandaran	2014383	-
L. royleana	Qom	2014384	-
L. royleana	Khorasan	2014385	MH453497
L. royleana	Tehran	2014386	-
L. royleana	Kerman	2014387	-
L. royleana	Shiraz	2014388	-

Morphometry and anatomy

Morphological characters studied displayed in Table 2.

For anatomical studies embedded materials were prepared as follows: three adult plants samples were excised and immediately fixed in formalin-acetic acid-alcohol (FAA) (formalin 5%, acetic acid 5% and 50% ethanol 90%) (Jensen 1962) for 48 to 72 h, and stored at 4 °C until sectioning. Samples then dehydrated in a graded ethanol series and embedded. After preparation of free transverse hand sections of the lamina and stem samples were washed

Table 2. Morphological characters studied in *Lallemantia* species.

Characters	The state of character
Plant habitat	1) annual; 2) biannual
Shape of bracteole	1) oval; 2) wedge; 3) circular
Plant height	
Length of basal leaf	
Width of basal leaf	
Length of petiole	
Length of stem leaf	
Width of stem leaf	
Length of bracteole	
Width of bracteole	
Length of calyx	
Length of corolla	
Length of nutlet	

Table 3. Anatomical characters studied in *Lallemantia* species.

No	Character
1	Thickness of epidermis in stem
2	Thickness of collenchymas in stem
3	Thickness of parenchyma in stem
4	Thickness of sclerenchyma in stem
5	Thickness of upper phloem in stem
6	Thickness of lower phloem in stem
7	Thickness of xylem in stem
8	Thickness of pith in stem
9	Thickness of epidermis in cross section of stem
10	Thickness of simple trichomes in stem
11	Thickness of glandular trichomes in stem
12	Thickness of upper epidermis in leaf
13	Thickness of lower epidermis in leaf
14	Thickness of collenchymas in leaf
15	Thickness of parenchyma in leaf
16	Thickness of mesophyll in leaf
17	Thickness of upper phloem in leaf
18	Thickness of lower phloem in leaf
19	Thickness of xylem in leaf
20	Thickness of simple trichomes in leaf

with distilled water and placed in 5% sodium hypochlorite solution for 20 min for clearing and rinsed with distilled water. The sections were stained with methylene blue and carmine and mounted on the slides using Canada balsam. Thin cut sections were observed under a microscope fitted with digital camera. Anatomical characters of stem and leaf were recorded in Table 3.

Nutlet

For scanning electron microscopy (SEM), nutlet samples were mounted on stubs using double-sided adhesive tape and coated with gold. The specimens were examined with a Phillips × L20 SEM. UTHSCSA Image Tool Version 3.0 was used to carry out required measurements. Nutlet characters were randomly measured and were used in phenetic analyses (Table 4).

Molecular studies

According to Sheidai et al. (2018) and Koohdar and Sheidai (2019), ISSR and cpDNA data were used for the purpose of studying the spices delimitation and relationships in *Lallemantia* genus. *Nepeta* L. (accession number: KT178247) and *Paeonia* L. (accession number: KJ946020.1) were used as outgroups.

Data analyses

Species differences for morphological characters were investigated by ANOVA (Analysis of Variance) (Podani 2000). For multivariate morphological analyses, quantitative characters were divided into discrete groups and along with qualitative characters were coded as multistate characters. Grouping of the species was done by different ordination methods such MDS (Multidimensional scaling), and PCA (Principal components analysis) (Podani 2000). PCA was performed to identify the most variable morphological characters among the species studied (Podani 2000). PAST version 2.17 (Hammer et al. 2012) was used for multivariate analysis.

ANOVA was also performed to show anatomical difference among the species**.** Anatomical characters were first standardized (mean = 0, variance = 1) and used to establish Euclidean distance among pairs of taxa (Podani 2000). For grouping of the plant specimens, MDS was used (Podani 2000). PAST version 2.17 (Hammer et al. 2012) was used for multivariate analysis.

The ANOVA test was performed to show significant nutlet difference between the studied species. For grouping of the plant specimens, MDS was used. Nutlet data was standardized (mean = 0, variance = 1) for these analyses (Podani 2000). PCA was performed to identify the most variable nutlet characters among the populations studied.

Table 4. Nutlet characters studied in *Lallemantia* species.

Nutlets characters	The state of character
Nutlet shape	1) oblong; 2) oblong-triangular; 3) triangular
The apex shape of nutlet	1) obtuse; 2) acute
Nutlet surface	1) rounded cell arrangement; 2) verrucate; 3) verrucate- rugulate
Nutlet color	1) brown; 2) black
Length of nutlet	
Width of nutlet	
Length of wall sculpturing	
Width of wall sculpturing	
Length of cord	
Width of cord	

Table 5. Morphological data of *Lallemantia* species

Characters	*L. iberica*	*L. royleana*	*L. peltata*	*L. canescens*	*L. baldshuanica*
Plant habitat	Annual	Perennial	Annual	Annual	Annual
Shape of bracteole	Wedge	Elliptic	Rounded	Wedge	Elliptic
Plant height (cm)	20.5	26.3	24.9	9	20.62
Length of basal leaf (mm)	21.5	19.5	29.1	15.4	7.6
Width of basal leaf (mm)	13.5	8.2	15.9	11.8	4.5
Length of petiole of basal leaf (mm)	14	23.2	17	14.2	14
Length of stem leaf (mm)	16.5	28.4	31.1	7.6	26.8
Width of stem leaf (mm)	4	6.3	17.9	3.6	6.35
The length of bracteole (mm)	4.5	5	12.3	5.6	4.65
Width of bracteole (mm)	1	3.2	12.2	2.3	2.4
Length of calyx (mm)	7.5	18.7	16.2	6	10.3
Length of corolla (mm)	10.5	28.7	16.95	9.43	12.15
Length of nutlet (mm)	3.25	3.34	2.97	3	3.35

For ISSR analyses binary characters (presence = 1, absence = 0) were used to encode ISSR bands. NJ (neighbor joining) (Saitou and Nei 1987; Podani 2000) was used for grouping. Paleontological statistics (PAST) ver. 2.17 was used for analysis (Hammer et al. 2012).

In case of cp-DNA sequences analyses, several phylogenetic methods were applied. The intron in the gene for ribosomal protein L16 (rpL16) was aligned with MUSCLE (Robert, 2004) implemented in MEGA 5. The molecular clock test was performed as implemented in MEGA 5 (Tamura et al. 2011). The test was done by comparing the ML value for the given topology with and without the molecular clock constraints under the Tamura and Nei (1993). Before estimating time of divergence, we used MEGA 5 to test the molecular clock and to find the best substitution model for the given sequences. The equal evolutionary rate of the studied sequences was rejected at a 5% significance level and, therefore, we used the relaxed molecular clock model in further analyses (Minaeifar et al. 2016). Moreover, Hasegawa, Kishino and Yano model (HKY)

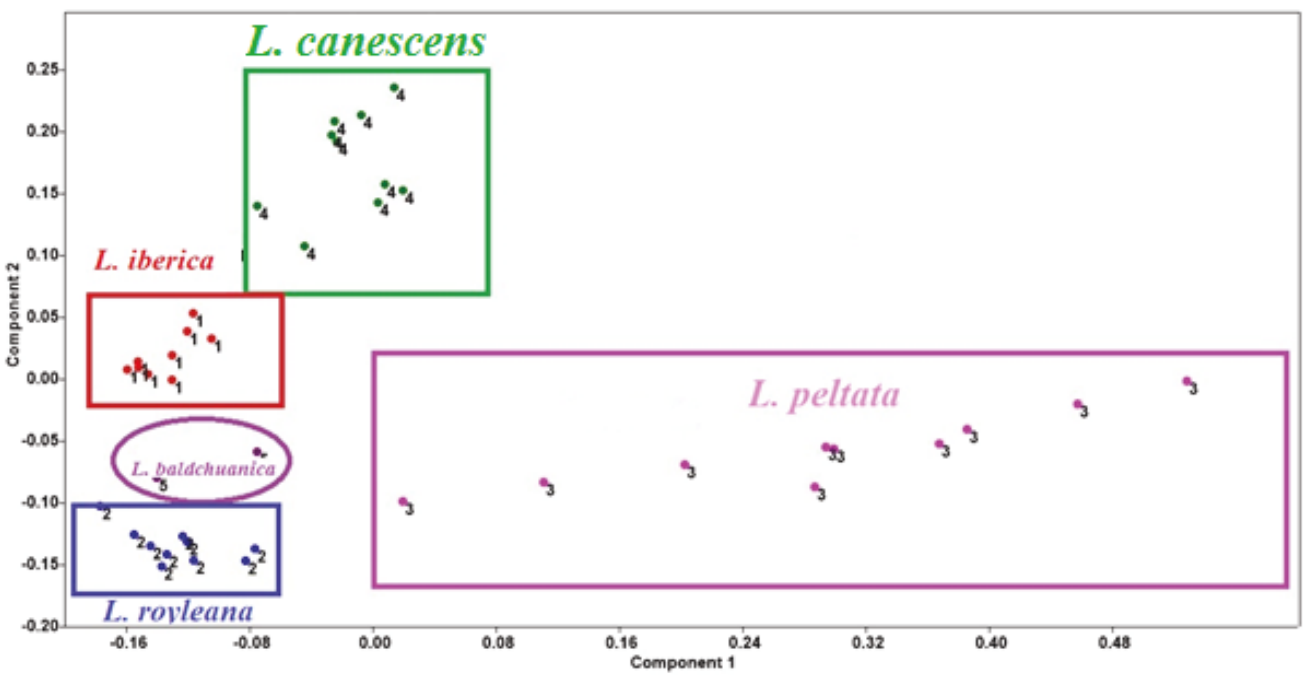

Figure 1. PCA plot of morphological characters in *Lallemantia* species.

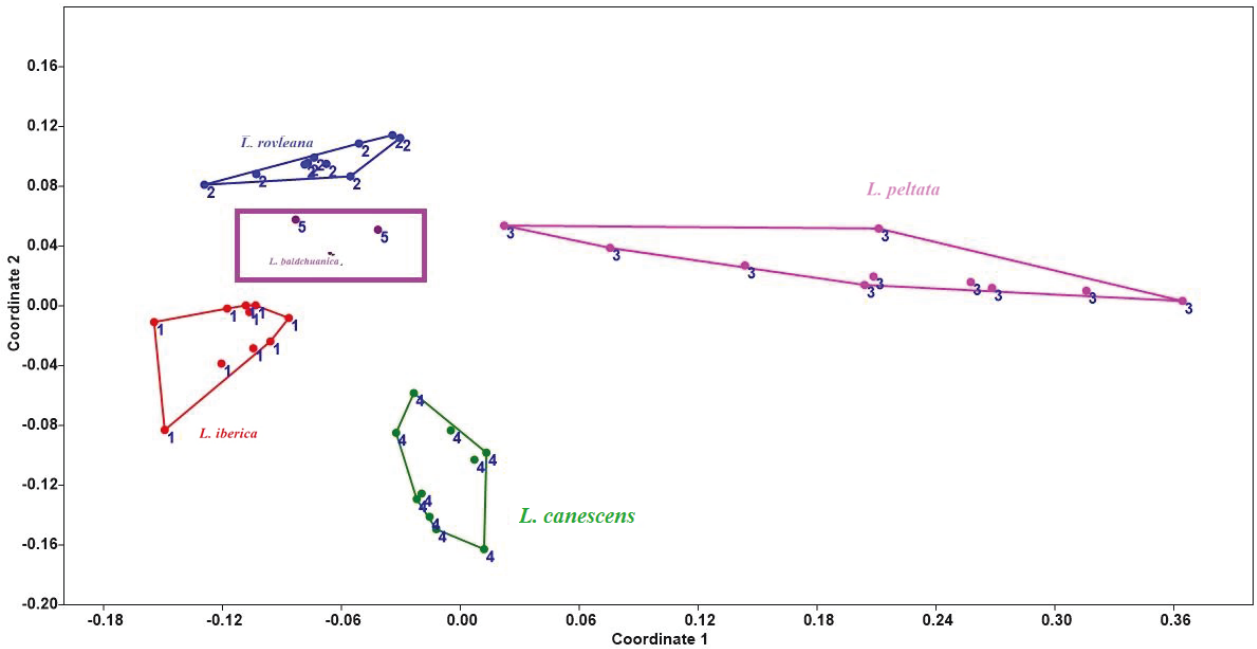

Figure 2. MDS plot of morphological characters in *Lallemantia* species.

was the best substitution model identified by model test as implemented in MEGA 5 (Tamura et al. 2011).

BEAST v1.6.1 (Drummond et al. 2010a; Drummond et al. 2010b) was used for the Bayesian Markov chain Monte Carlo (MCMC) inferred analyses of the nucleotide sequence data (Rambaut and Drummond 2007). *Nepeta* L. (accession number: KT178247) and *Paeonia* L. (accession number: KJ946020.1) were used as out groups.

BEAUti (Bayesian Evolutionary Analysis Utility version) v1.6.1 (Drummond et al. 2010a,b) was utilized to generate initial xml files for BEAST. A Yule process of speciation (a 'pure birth' process) was used as a tree prior for all the tree model analyses. The Yule tree prior is widely recognized as giving the best-fit model for trees describing the relationships between different species (Drummond et al. 2010a,b) and can be regarded as explaining the net speciation rate (Nee 2006). For the MCMC analysis, the chain length was 10000000. After discarding 100 trees representing the burn-in, 10000 trees were used for the analysis. The BEAUti xml file was run in BEAST v1.6.1 (Drummond et al. 2010a, 2010b). Because no fossils were available for the studied species, we assumed a rate of evolution of the plastid sequence ($u = 1.0 \times 10^{-9}$ s s^{-1} $year^{-1}$; Zurawski et al. 1984; Minaeifar et al. 2016). This was included in the option of molecular clock model in BEAUti v1.6.1. The normal distribution (mean = 0; standard deviation = 1) was used for priors.

Tracer v1.5 (Drummond and Rambaut 2007) was used to examine sampling and convergence. Tree Annotator v1.6.1 (Drummond and Rambaut 2007) was used to annotate the phylogenetic results generated by BEAST to form a single 'target' tree (Maximum Clade Credibility tree, MCC) including summary statistics. FigTree v1.3.1 (Rambaut 2009) was used to produce the annotated BEAST MCC tree.

Results

Morphometry

Details of mean of morphological characteristics in five studied species are provided in Table 5.

The ANOVA test showed significant difference ($p < 0.05$) for quantitative morphological characters among *Lallemantia* species. Different ordination methods like PCA and MDS produced similar results. PCA and MDS plots of morphological characters (Figs. 1 and 2) separated the studied species from each other. In this plot, *L. iberica* and *L. canescens* were placed close to each other, while *L. peltata* was placed far from the others due to diference in characters width of stem leaf , the length of bracteole and width of bracteole.

PCA analysis revealed that the first 3 components comprised about 88% of total morphological variability. In the first PCA components with about 57% of total variation, characters like length of basal leaf, width of stem leaf, length of bracteole, width of bracteole, shape of bracteole showed the highest positive correlation (> 0.80).

Table 6. Anatomical data of *Lallemantia* species.

Characters	*L. canescens*	*L. peltata*	*L. iberica*	*L. royleana*
Thickness of epidermis in stem	28	32.2	25.8	28.6
Thickness of collenchyma in stem	181.6	238.1	224.2	126.9
Thickness of parenchyma in stem	67.9	91.5	67.8	48.6
Thickness of sclerenchyma in stem	27.3	37.7	33	30
Thickness of upper phloem in stem	38.2	50.8	56.6	39.1
Thickness of lower phloem in stem	168.7	180.07	179.5	156.9
Thickness of xylem in stem	67.4	87.02	63.4	57.8
Thickness of pith in stem	1596.3	993.42	1196.9	937.4
Thickness of epidermis in cross section of stem	2041.6	1511.9	1939.8	1362.4
Thickness of simple trichomes in stem	107.8	108.6	104.8	118.6
Thickness of glandular trichomes in stem	29.1	27.5	40.08	35.8
Thickness of upper epidermis in leaf	20.0	20.8	22.3	17.1
Thickness of lower epidermis in leaf	26.6	17.75	21.00	27.3
Thickness of collenchyma in leaf	42.7	37.4	41.2	60.1
Thickness of parenchyma in leaf	92.6	60.8	86.0	94.7
Thickness of mesophyll in leaf	195.5	171.6	188.8	272.5
Thickness of upper phloem in leaf	29.7	36.9	34.9	37.5
Thickness of lower phloem in leaf	31.67	29.50	26.40	34.00
Thickness of xylem in leaf	85.0	47.7	38.9	60.1
Thickness of simple trichomes in leaf	75.00	64.50	53.40	79.67

The length of corolla, shape of inflorescence, life-history strategy, showed the highest positive correlation (> 0.80) with the second PCA component. These characters may be used in taxonomy of the genus and delimiting *Lallemantia* species.

Anatomy

The detailed descriptions of the anatomical features in the studied species are displayed in Table 6. The representative anatomy of each species is displayed in Figures 3 and 4.

The stems in the cross section have a square form with pronounced angles and are covered with a one-layered epidermis. Collenchyma is single layered among the angles, but 5-10 layers of collenchyma are observed below the epidermis at the angles. Phloem and xylem were regular cylinders. The highest epidermis (32.2 µm), collenchyma (238.1 µm), parenchyma (91.5 µm), sclerenchyma (37.7 µm),

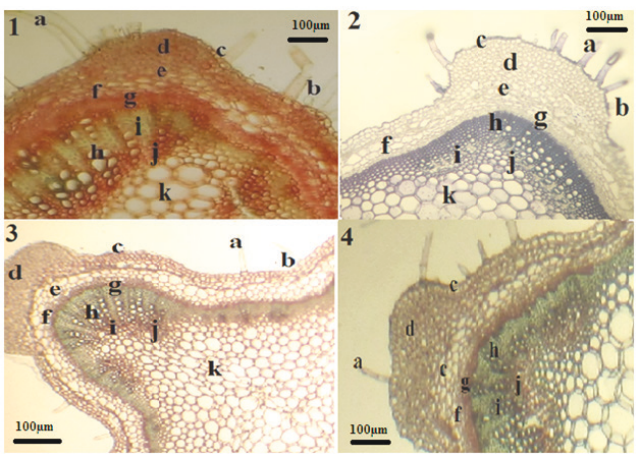

Figure 3. Appearance of stem in *Lallemantia* species.

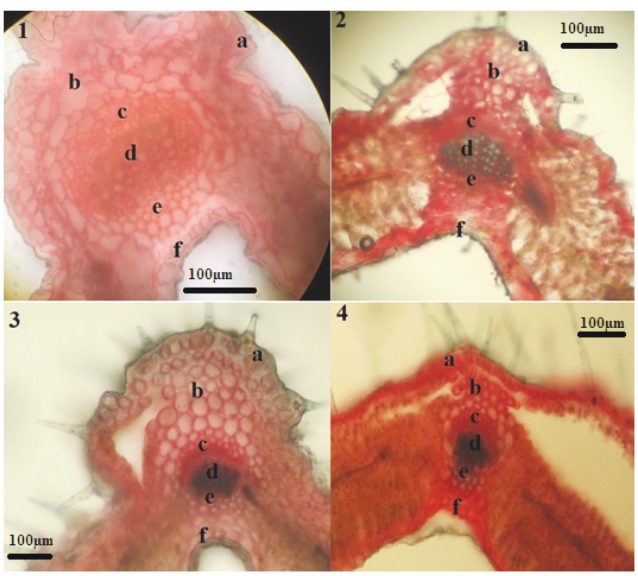

Figure 4. Appearance of leaf in *Lallemantia* species.

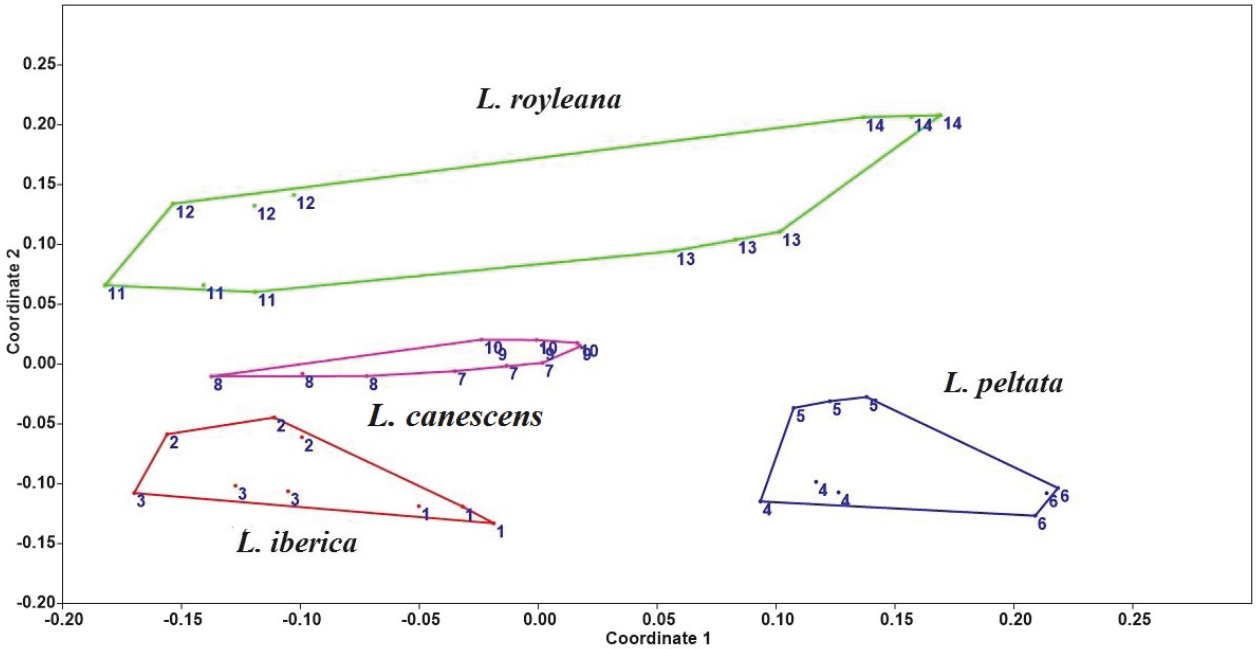

Figure 5. MDS plot of anatomical characters in *Lallemantia* species.

xylem (180.07 µm) and lower phloem (87.02 µm) length in stem was observed in *L. peltata* while *L. canescens* had the highest value length of pith in stem (1596.3 µm), length of stem in transverse transects (2041.6 µm) and width of stem in transverse transects (1881.3 µm).

All of the leaves in the sections were bifacial (dorsiventral and amphistomatic mesophyll) type and were composed of one layered epidermis. The highest length of the lower epidermis (27.3 µm), collenchyma (60.1 µm), parenchyma (94.7 µm), mesophyll (272.5 µm), upper phloem (37.5 µm) and lower phloem (34.00 µm) in leaf was observed in *L. royleana*. The ANOVA test exhibited significant difference ($p < 0.05$) for the quantitative anatomical characters among *Lallemantia* species.

The MDS plot of the anatomical characters (Fig. 5) separated the scrutinized species from one another. In this plot, *L. iberica* and *L. canescens* were placed close to each other because of the traits such as the number of layers in collenchyma and parenchyma in stem; *L. peltata*, however due to its shape of collenchyma and *L. royleana* were placed far from the others.

Nutlet

The details for mean of the nutlet characteristics in 5 studied species are depicted in Table 7. The SEM micrographs of nutlets are presented in Figure 6. The shapes of nutlets are oblong in *L. royleana* and *L. baldshuanica*, triangular in *L. peltata* and oblong-triangular in *L. canescens* and *L.*

Table 7. Nutlet data of *Lallemantia* species.

Characters	*L. iberica*	*L. royleana*	*L. peltata*	*L. canescens*	*L. baldshuanica*
Nutlet shape	Oblong	Oblong-triangular	Triangular	Oblong	Oblong triangular
The apex shape of nutlet	Obtuse	Acute	Acute	Obtuse	Acute
Nutlet surface	Rounded cell arrangement	Verrucate	Verrucate- rugulate	Rounded cell arrangement	Verrucate
Color	Black	Black	Black	Black	Black
Length of nutlet (µm)	3554	2664	2538	3448	3021
Width of nutlet (µm)	1115.2	1400	959.48	978	1650
Length of cord nutlet (µm)	202.69	865	645.76	219	951.29
Width of cord nutlet (µm)	269.91	721	351.81	338	897.2
Length of wall sculpturing (µm)	47.74	52.32	40.86	72.59	56.75
Width of wall sculpturing (µm)	41.42	41.48	27.97	28.4	26.28

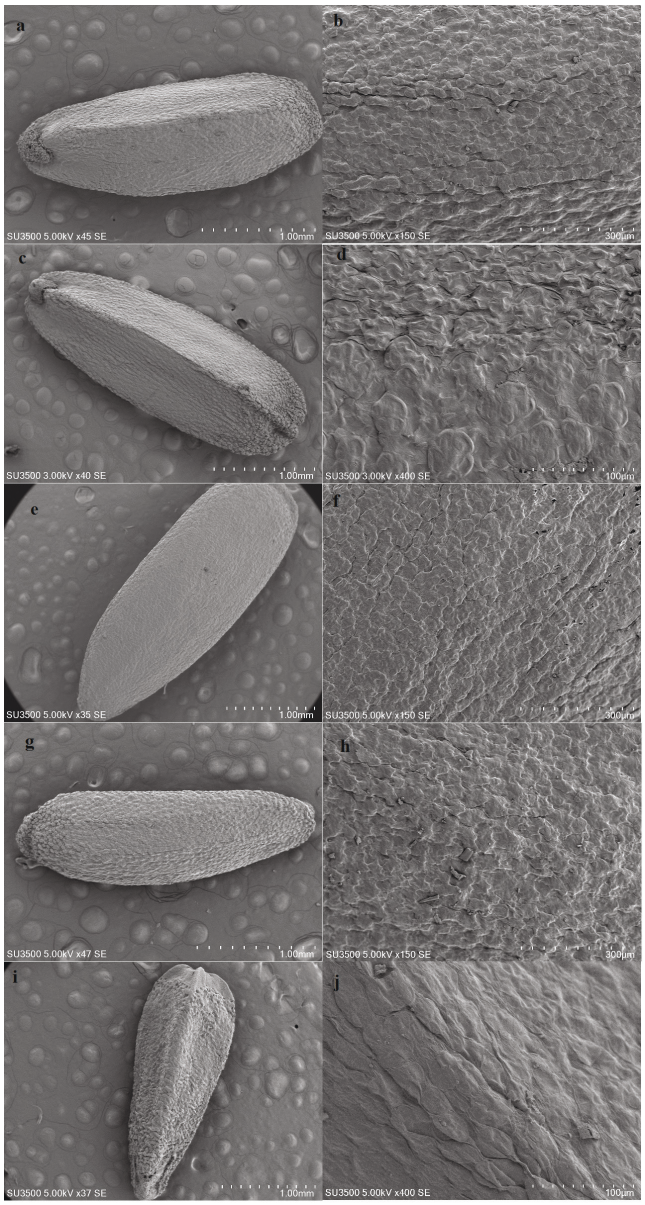

Figure 6. General appearance and surface details of nutlets of *Lallemantia* species. a, b: *L. royleana*; c, d: *L. baldshuanica*; e, f: *L. canescens*; g, h: *L. peltata*; i, j: *L. iberica*.

iberica. The colors of nutlet in all the examined species alter from brown to black. The apex of nutlet is obtuse or acute. The nutlet surface is verrucate-rugulate in *L. peltata*, verrucate in *L. iberica* and *L. canescens* and rounded cell arrangement in *L. royleana* and *L. baldshuanica.* The highest length of nutlet (3.55 µm), width of nutlet (1.64 µm), length of cord nutlet (951.29 µm), width of cord nutlet (897.2) were observed in *L. iberica* while *L. peltata* had the highest value length of wall sculpturing (1596.3 µm). The highest length of wall sculpturing was observed in *L. royleana* (72.59 µm).

ANOVA revealed significant difference in the nutlet quantitative characters. The MDS plot (Fig.7) of nutlet showed that while *L. iberica, L. canescens, L. baldshuanica* and *L. royleana* were placed close to one another, *L. peltata* was placed far from the others.

ISSR analyses

Almost all the ISSR primers produced bands were used and finally a data matrix of 42 × 104 was formed for further analysis. The highest number of the bands was observed in *L. royleana* (53) and *L. peltata* (45), while *L. baldshuanica* had the lowest value (21). *L. baldshuanica*, *L. iberica* and *L. canescens* had 3, 1 and 1 unique bands, respectively, the other bands were common in the studied samples.

The NJ tree of ISSR data (Fig. 8) grouped the specimens of each species together in a single cluster, separated from the other species. This means that ISSR molecular markers are of taxonomic value and can delimit the *Lallemantia* species. The NJ tree showed closer genetic affinity between *L. iberica* and *L. canescens* while *L. peltata* differes from the others.

Species relationship based on cpDNA sequences

After Cp-DNA multiple sequence alignment by MUltiple Sequence Comparison by Log-Expectation (MUSCLE) and curing the sequences, 385 sequences remained for phylogenetic tree construction. Out of these 91 sequences was parsimony informative. Different phylogenetic analyses produced similar results. Therefore, only maximum likelihood (ML) and Bayesian phylogenetic tree are presented (Figs. 9a and b). In both phylogenetic trees, *L. canescens*, and *L. iberica* were placed close to each other in a single clade. In both analyses, the out-group was separated from the other species studied.

Species divergence time

In order to choose the type of the nucleotide evolution in BEAST, the molecular clock test was performed by comparing the ML value for the given topology with and without the molecular clock constraints under the Kimura 2-parameter model (+G). The null hypothesis of the equal evolutionary rate throughout the tree was rejected at a 5% significance level (P = 0.016). Hence, the relaxed molecular clock was utilized in further analysis. The Bayesian tree (phylogram) of BEAST is provided in Fig. 9c.

The oldest node of *Lallemantia* appeared in Iran about 25 Mya, followed by the node that led to the formation of *L. royleana* and *L. peltata* in about 23 Mya. The elicited tree dates back the *L. baldshuanica* appearance to about 15 Mya. However, active radiation occurred from 12-13 Mya.

Discussion

The morphometric, anatomical data, nutlet features and molecular data which were obtained after this study could differentiate the *Lallemantia* species efficaciously. Dinç et al. (2009) gives confidence to the above statement by their previous study. The present study revealed that the gleaned species relationship based on the molecular data almost agrees with the morphological, anatomical and nutlet micro-morphological data. The only difference between these two types of data is found in *L. baldshuanica*. The species relationship presented here is supported also by the morphological studies of Talebi and Rezakhanlou (2010).

The nutlet surface sculpturing patterns as seen by SEM demonstrate a vast array of variation and have diagnostic value for species recognition in the tribe Mentheae (Jamzad et al. 2000; Moon and Hong 2006; Kaya and Baser 2007). Nevertheless, in *Lallemantia*, external nutlet characters and nutlet surface sculpturing patterns are clearly a good indicator for the interspecific classification.

From the findings obtained from the previous studies, it can be concluded that the anatomical characteristics are as useful as taxonomic characters at the species level in Lamiaceae (Pădure 2003).The stems of it in cross section have a square form with pronounced angles and are covered with a one-layered epidermis. Collenchyma is single layered among the angles, but 5-10 layers of collenchyma are observed below the epidermis at the angles. Phloem and xylem were regular cylinders. The highest epidermis, collenchyma, parenchyma, sclerenchyma, xylem, and lower phloem length in stem was observed in *L. peltata* while *L. canescens* had the highest value length of pith in stem, length of stem in transverse transects and width of stem in transverse (1881.3 μm). All of the leaves in the sections were bifacial (dorsiventral and amphistomatic mesophyll) type and were composed of one layered epidermis. The highest length of lower epidermis, collenchyma, parenchyma, mesophyll, upper phloem and lower phloem in leaf were observed in *L. royleana*.

According to our BEAST results, the node leading to the formation of *royleana* appeared in Iran about 23 Mya; therefore, it can be stated that *L. royleana* appeared first in Khorasan province and then due to population genetic divergence, *L. baldshuanica* was formed about 15 Mya in Khorasan province.

L. baldshuanica showed close genetic affinity with *L. iberica* and *L. canescens*. These two latter species occur in Zanjan and Qazvin provinces that are in the vicinity of Tehran in the North-West part of Iran. It may also be safe to conclude that the process of speciation and migration had occurred from East towards West of Iran; the formation of *L. iberica* and *L. canescens* seems to have taken placed in these regions, too.

High physiographical heterogeneity is considered to be a major influence on the high floral diversity (Grimm and Denk 2014). One component of this heterogeneity is a series of mountains extending from West to the

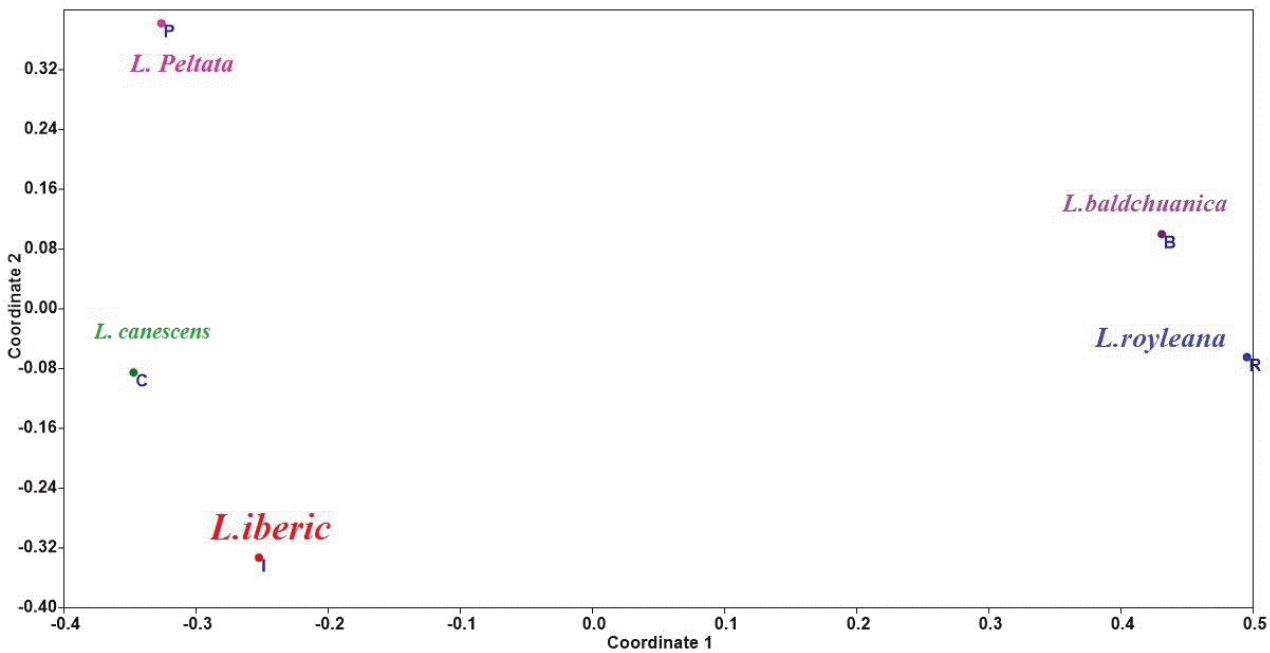

Figure 7. MDS plot of seed characters in *Lallemantia* species.

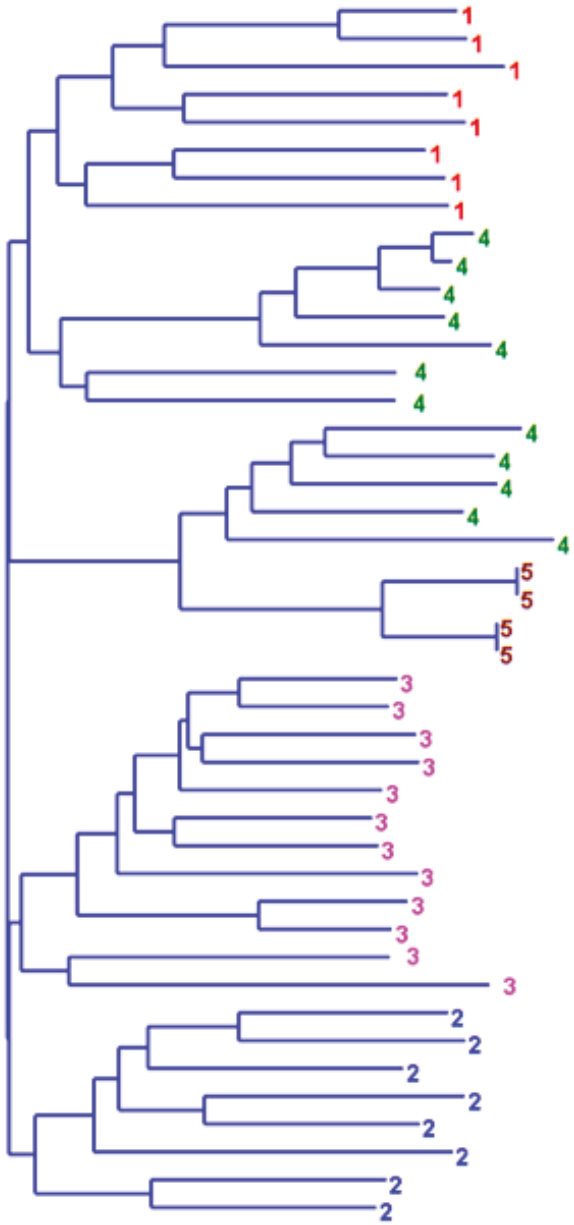

Figure 8. Neighbor joining tree of ISSR data in the studied *Lallemantia* species. 1: *L. canescens*; 2: *L. royleana*; 3: *L. peltata*; 4: *L. iberica*; 5: *L. baldshuanica*.

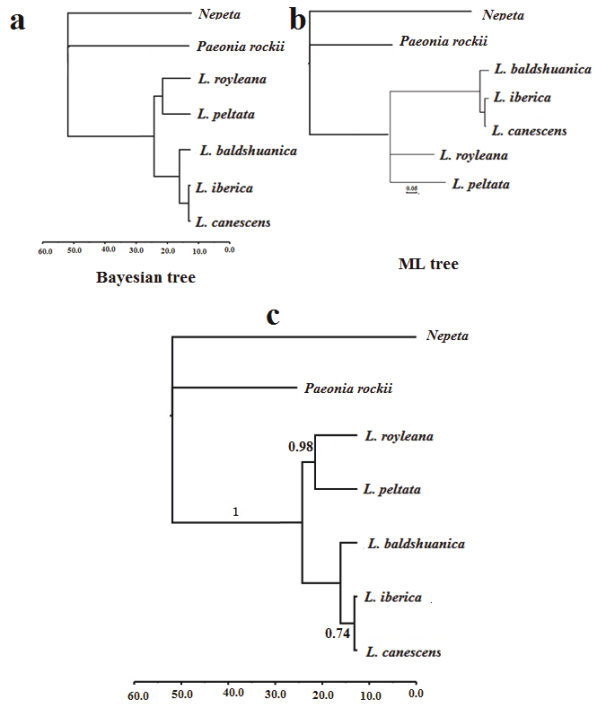

Figure 9. a: Bayesian phylogenetic tree; b: Maximum likelihood phylogenetic tree of Lallemantia species based on the cp-DNA dataset (rpL16). Values of all branches are above 90% bootstrap values. Scale: million years ago. c: Phylogenetic tree and chronogram using BEAST Bayesian inference based on the cp-DNA dataset (rpL16). Values at left of nodes on the tree are bootstrap support above, and posterior probability below. At the right of nodes are the estimated dating values and their 95% HPD from BEAST..

Northeast of Iran where *Lallemantia* species are growing. The *Lallemantia* species are distributed in different ecological regions with altitude of -20 to 1500 meters high from sea level in Iran. This extensive heterogeneity may bring about some degree of genetic differentiation and accelerate the speciation process witnessed in Western Iran. The active speciation during 12-13 Mya in these mountainous regions may be due to their reactions to the Pleistocene glaciations.

The palaeogeographic reconstructions signal that the area corresponding to the Southern part of the present Alborz Mountains was not depositional/ erosional and most likely formed a mountain range since the Late Cretaceous time at ca. 65 Ma. Unlike the southern section of Alborz, however, the northern section is a geologically younger area which was subsiding under the Paratethys Ocean until the middle Miocene about 10-15 Mya (Berberian and King 1981).This is in agreement with the earlier appearance of *L. peltata* in Alborz mountain than the other studied species appeared in the Western region of Zagros mountain, like *L. iberica* and *L. canescens* appearing most recently in Zanjan and Qazvin. Kuhle (2008) in his glacio-geomorphological study of Iran estimated the snowline descent to be approximately 1400 to1600 m with temperature decline of 11 to 15 °C, and the occurrence of Pleistocene glaciation in Zagros.

Drew and Systma (2012) studied the biogeography of the tribe Mentheae by using ITS molecular data and *L. canescens* as the representative of *Lallemantia*. They took the Miocene period (about 11 Mya) to be the probable divergence time for *L. canescens*; this finding was in ac-

cordance with the present paper.

In conclusion, the present study revealed the taxonomic implication of the multiple data sets in *Lallemantia* species delimitation and also uncovered the species relationship. The monophyly of the genus *Lallemantia* was shown through the phylogenetic trees.

References

Alan S, Özkan Y, Tunçer Ö (2010) Taxonomical morphological and anatomical studies on *Lallemantia* Fisch & Mey. Ankara Ecz Fak Derg 39:17-34.

Bakker AB, Demerouti E, Verbeke W (2004) Using the job demands-resources model to predict burnout and performance. Hum Resour Manag 43:83-104.

Berberian M, King GCP (1981) Towards a paleogeography and tectonic evolution of Iran. Can J Forest Res 18:210-265.

Broadhurst L, Byrne M, Craven L, Lepschi B (2004) Genetic congruence with new species boundaries in the *Melaleuca uncinata* complex (Myrtaceae). Aust J Bot 52(6):729-737.

Byrne CH (2004) A unified treatment of some iterative algorithms in signal processing and image reconstruction. Inverse Probl 20:103-120.

Celep F, Kahraman A, Atalay Z, Doğan M (2014) Morphology anatomy palynology mericarp and trichome micromorphology of the rediscovered Turkish endemic *Salvia quezelii* (Lamiaceae) and their taxonomic implications. Plant Syst Evol 300:1945-1958.

Dinç M, Pinar NM, Dogu SL, Yildirimli SI (2009) Micromorphological studies of *Lallemantia* L (Lamiaceae) species growing in Turkey. Acta Biol Cracov Ser Bot 51:45-54.

Dolatyari A, Kamrani A (2015) Chromosome number of some accessions and morphology of four species of *Lallemantia* Fisch. & C.A. Mey (Lamiaceae) from Iran. Wulfenia 22:127-135.

Drew BT, Systma KJ (2012) Phylogenetics biogeography and staminal evolution in the tribe Mentheae (Lamiaceae). Am J Bot 99(5):933-953.

Edmondson JK (1982) *Dracocephallum*. In Davis PH, ed., Flora of Turkey and the East Aegean Islands. Edinburgh University Press, Edinburgh, 289-291.

Hammer Ø, Harper DAT, Ryan PD (2012) PAST: Paleontological Statistics software package for education and data analysis. Palaeontol Electron 4(1):9.

Harley RM, Atkins S, Budantsev AL, Cantino PD, Conn BJ, Grayer R, Harley MM, De Kok R, Krestovskaja T, Morales R, Paton AJ, Ryding O, Upson T (2004) The families and genera of vascular plants. In Kadereit JW, ed., Lamiaceae (Lamiales) Springer, Berlin, 167-282.

Jamzad Z, Harley MM, Ingrouille M, Simmonds MSJ, Jalili A (2000) Pollen exine and nutlet surface morphology of the annual species of *Nepeta* L (Lamiaceae) in Iran. In Harley MM, Morton GM, Blackmore S, ed., Pollen and Spores: Morphology and Biology. Royal Botanic Gardens, Kew, London, 385-397.

Kahraman A, Celep F, Dogan M (2010b) Morphology anatomy palynology and nutlet micromorphology of *Salvia macrochlamys* (Labiatae) in Turkey. Biologia 65(2):219-227.

Kahraman A, Dogan M, Celep F, Akaydin A, Koyuncu M (2010a) Morphology anatomy palynology and nutlet micromorphology of the rediscovered Turkish endemic *Salvia ballsiana* (Lamiaceae) and their taxonomic implications. Nord J Bot 28:91-99.

Kamrani A, Riahi M (2017) Using molecular data to test the monophyly of *Lallemantia* in the subtribe Nepetinae (Mentheae, Lamiaceae). Plant Biosys 152:857-862.

Kaya A, Goger F, Baser HC (2007) Morphological anatomical and palynological characteristics of *Salvia halophila* endemic to Turkey. Nord J Bot 25:351-358.

Koohdar F, Sheidai M (2019) Molecular investigation in few spices of *Dacocephalum* in Iran: Species relationship, reticulation and divergence time. Ind Crops Prod 141:111758.

Kuhle M (2007) The Pleistocene glaciation (LGP and pre-LGP, pre-LGM) of SE Iranian mountains exemplified by the Kuh-i-Jupar, Kuh-i-Lalezar and Kuh-i-Hezar massifs in the Zagros. Polar Res 77:71-88.

Mahmood S, Hayat MQ, Sadiq A, Ishtiaq SH, Malik S, Ashra M (2013) Antibacterial activity of *Lallemantia royleana* Benth indigenous to Pakistan. Afr J Microbiol Res 7:4006-4009.

Millar MA, Byrne M, O'Sullivan WO (2011) Defining entities in the *Acacia saligna* (Fabaceae) species complex using a population genetics approach. Aust J Bot 59:137-148.

Minaeifar AA, Sheidai M, Attar F, Noormohammadi Z, Ghasemzadeh-Baraki B (2015) Genetic and morphological diversity in *Cousinia tabrisiana* (Asteraceae) populations. Biologia 70:328-338.

Minaeifar AA, Sheidai M, Attar F, Noormohammadi Z, Ghasemzadeh-Baraki S (2016) Biosystematic study in the genus *Cousinia* Cass (Asteraceae) section *Cousinia*. Biochem Syst Ecol 69:252-260.

Moon HK, Hong SP (2006) Nutlet morphology and anatomy of the genus *Lycopus* (Lamiaceae: Mentheae). J Plant Res 119:633-644.

Nee S (2006) Birth-death models in macroevolution Annu Rev Ecol Evol Syst 37:1-17.

Olmstead RG, Palmer JD (1994) Chloroplast DNA systematics: a review of methods and data analysis. Am J Bot 81:1205-1224.

Özcan T, Gezer E, Martin E, Dirmenci T, Altınordu F (2015) Karyotype analyses on the genus *Lallemantia* Fisch & CA Mey (Lamiaceae) from Turkey. Cytologia 79:553-559.

Pădure IM (2003) Fruit morphology anatomy and mixocarpy in *Nepeta cataria* L 'Citriodora' and *Nepeta grandiflora* Bieb (Lamiaceae). Rev Roum Biol 48(1-2):23-30.

Podani J (2000) Introduction to the Exploration of Multivariate Data. Backhuyes, Leiden.

Rambaut A (2009) FigTree v.1.3. 1. Available: http://tree.bio.ed.ac.uk.

Rambaut A, Drummond A (2007) Tracer v.1.5. Available: http://beast.bio.ed.ac.uk/Tracer.

Rechinger KH (1982) Labiatae. In Browicz KH, Persson K, Wendelbo P, eds., Flora Iranica. Austria, Graz, Wien, Academische Druck-und, Verlasantalt, 25-44.

Rivera Nunez D, Obon DE, Gastro C (1992) The ethnobotany of Lamiaceae of old world. In Harley RM, Reynolds T, eds., Advances in *Lamiaceae* Science. Royal Botanical Gardens, Kew, 455-473.

Robert CE (2004) MUSCLE: multiple sequence alignment with high accuracy and high throughput. Nucleic Acids Res 32:1792-1797.

Saitou N, Nei M (1987) The neighbor joining method: a new method for constructing phylogenetic trees. Mol Biol Evol 4:406-425.

Shaw J, Small RL (2005) Chloroplast DNA phylogeny and phylogeography of the North American plums (*Prunus* subgenus *Prunus* section *Prunocerasus* Rosaceae). Am J Bot 92:2011-2030.

Sheidai M, Koohdar F, Poode ZM (2018) Molecular phylogeny of *Lallemantia* L. (Lamiaceae): Incongruence between phylogenetic trees and the occurrence of HGT. Genetika 50(3):907-918.

Sheidai M, Seif E, Nouroozi M, Noormohammadi Z (2012) Cytogenetic and molecular diversity of *Cirsium arvense* (Asteraceae) populations in Iran. J Jap Bot 87:193-205.

Sheidai M, Zanganeh S, Haji-Ramezanali R, Nouroozi M, Noormohammadi Z, Ghsemzadeh-Baraki S (2013) Genetic diversity and population structure in four *Cirsium* (Asteraceae) species. Biologia 68:384-397.

Sheidai M, Ziaee S, Farahani F, Talebi SM, Noormohammadi Z, Hasheminejad Ahangarani Farahani Y (2014) Infra-specific genetic and morphological diversity in *Linum album* (Linaceae). Biologia 69:32e39.

Talebi SM, Rezakhanlou A (2010) The morphological study of the genus *Lallemantia* Fisch et Mey. (Lamiaceae) in Iran. Plant Ecosyst 5(21):3-20.

Tamura K, Nei M (1993) Estimation of the number of nucleotide substitutions in the control region of mitochondrial DNA in humans and chimpanzees. Mol Biol Evol 10:512-526.

Tamura K, Peterson D, Peterson N, Stecher G, Nei M, Kumar S (2011) MEGA5: Molecular evolutionary genetics analysis using maximum likelihood evolutionary distance and maximum parsimony methods. Mol Biol Evol 28:2731-2739.

Zhang Q, Field TS, Antonelli A (2015) Assessing the impact of phylogenetic incongruence on taxonomy floral evolution biogeographical history and phylogenetic diversity. Am J Bot 102:566-580.

Zurawski G, Clegg MT, Brown AHD (1984) The nature of nucleotide sequence divergence between barley and maize chloroplast DNA. Genetics 106:735-749.

Acta Biologica Szegediensis

Volume 63(2):169-179, 2019
Acta Biologica Szegediensis
http://abs.bibl.u-szeged.hu/index.php/abs
DOI:10.14232/abs.2019.2.169-179

ARTICLE

Can metal-tolerant endophytic biocontrol agents promote plant-growth under metal stress?

Carrie Siew Fang Sim[1,2], Yuen Lin Cheow[1], Si Ling Ng[3], Adeline Su Yien Ting[1,2]*

[1] School of Science, Monash University Malaysia, Jalan Lagoon Selatan, 47500 Bandar Sunway, Selangor, Malaysia.
[2] Tropical Medicine and Biology Multidisciplinary Platform, Monash University Malaysia, Jalan Lagoon Selatan, 47500 Bandar Sunway, Selangor, Malaysia.
[3] School of Chemical Sciences, Universiti Sains Malaysia, 11800 USM, Penang, Malaysia.

ABSTRACT Five metal-tolerant endophytic isolates (*Bipolaris sp*. LF7, *Diaporthe miriciae* LF9, *Trichoderma asperellum* LF11, *Phomopsis asparagi* LF15, *Saccharicola bicolor* LF22), with known metal-tolerance attributes and biocontrol activities against *Ganoderma boninense*, were tested for growth-promoting activities independent of (*in vitro)* and associated with plants (height, weight, root mass and stem circumference) (*in vivo*). Results revealed that metal-tolerant endophytes did not significantly render benefit to host plants as plant growth was compromised by the presence of metals. Lower production of indole-acetic acid (0.74-21.77 μg mL^{-1}), siderophores (8.82-90.26%), and deaminase activities of 1-aminocyclopropane carboxylic acid (3.00-69.2 μmol mg $protein^{-1}$ hr^{-1}) were observed.
Acta Biol Szeged 63(2):169-179 (2019)

KEY WORDS
1-aminocyclopropane carboxylic acid deaminase
growth parameterr
indole-acetic acid
phosphate solubilisation
plant hormone
siderophore

ARTICLE INFORMATION
Submitted
10 February 2020.
Accepted
6 March 2020.
***Corresponding author**
E-mail: adelsuyien@yahoo.com
adeline.ting@monash.edu

Introduction

Endophytes are a group of microorganisms known to colonize plant tissues asymptomatically. They render numerous benefits to the host plants, which include protecting host plants against pathogens, herbivores and insect pests (Rúa et al. 2013); enhancing tolerance towards unfavourable environmental conditions (Naveed et al. 2014; Zhang et al. 2011); and stimulating plant growth (Nascimento et al. 2016). Endophytes that are biocontrol agents (BCAs), typically have multiple mechanisms to suppress pathogen; via inhibitory compounds, induced host resistance, and by improving growth and vigour of host plants.

Several endophytic species have been reported to stimulate plant growth successfully. They include *Penicillium chrysogenum*, *P. crustosum*, *Piriformospora indica, Serratia quinivorans*, *Bacillus cereus*, *B. subtilis*, *Pseudomonas aeruginosa* and *Pantoea amanatis* (Sirrenberg et al. 2007; Nascimento et al. 2016; Hassan 2017; Wu et al. 2018). These endophytes stimulate plant growth by solubilising phosphate (*P. chrysogenum*, *P. crustosum, B. cereus*, *B. subtilis*), producing iron-chelating siderophores (*Ps. aeruginosa*), producing indole-acetic acid to stimulate root growth (*Pi. indica*), and by modulation of the hormone ethylene via the deaminase activity of 1-aminocyclopropane carboxylic acid (*Pa. amanatis*). Improved plant growth is important as it contributes to plant vigour and delays disease progression and the onset of disease symptoms (Ting 2014).

In this study, the growth-promoting activities of metal-tolerant endophytes were investigated under metal stress. Metal-tolerant endophytes are a new group of biocontrol agents that are hypothesized to render benefits to host plants in metal-laden soils. In earlier studies, these metal-tolerant endophytes were discovered to demonstrate biocontrol activities towards *Ganoderma boninense,* a causal agent of Basal Stem Rot disease of oil palm (Sim et al. 2019a, 2019b, 2019c). In those studies, the mechanisms of action were attributed to antifungal compounds produced. For this study, the ability of metal-tolerant endophytes in promoting plant-growth is determined. This observation is important as it suggests the potential role of metal-tolerant endophytic biocontrol agents in enhancing plant growth in the presence of metals and pathogen. Furthermore, various landscapes are now being used for oil palm planting; from desirable inland top-soils, to undesirable peat swamp and acid sulphate

soils. While inland terrain soils are suitable soils, peat and acid sulphate soils are acidic and has bioavailable forms of metal cations such as copper (Cu^{2+}), lead (Pb^{2+}), zinc (Zn^{2+}) and cadmium (Cd^{2+}), prompting the exploration of metal-tolerant endophytes. According to Zarcinas et al. (2004), Cu^{2+} levels in soils were between 10.1-47.2 mg kg^{-1}, for Zn^{2+} between 27.6-40.0 mg kg^{-1}, for Pb^{2+} between 23.9-29.0 mg kg^{-1}, and between 0.1-0.4 mg kg^{-1} for Cd^{2+}. With the presence of metals in soils, plant growth is generally affected due to metal toxicity. Therefore, to mitigate this, metal-tolerant endophytes with plant growth promoting properties (in addition to biocontrol potential) are investigated for potential as biocontrol agents. This is to enable the management of disease via plant growth promotion, albeit under metal stress conditions.

This study aims to establish the role of these endophytes in promoting plant growth, and this was evaluated under the influence of metal-stress, as the endophytes used are metal-tolerant endophytes. The endophytes were first tested via *in vitro* assays to determine their expression of plant growth-promoting attributes. The endophytes were exposed to conditions with and without metal stress, and the productions of the following compounds (or their activities) were quantified: indole-acetic acid (IAA), siderophore, phosphate solubilisation, and deaminase activity of 1-aminocyclopropane carboxylic acid (ACC). Two isolates with the most promising activities were subsequently selected for inoculation to oil palm ramets to validate their impact on growth (height, weight, root mass and stem circumference). This study is one of the few publications documenting the influence of metals on the growth-promoting activities of metal-tolerant biocontrol endophytes. This provides an overview of the possible use of these endophytes to improve plant growth and vigour, and in suppressing disease in metal-laden soils.

Materials and methods

Both *in vitro* and *in vivo* tests were performed to evaluate the growth promoting activities of the metal-tolerant biocontrol endophytes. The *in vitro* tests involved quantification of indole-acetic acid (IAA), siderophore production, phosphate solubilisation, and deaminase activity of 1-aminocyclopropane carboxylic acid (ACC) produced by the endophytes. In the *in vivo* assessment, growth parameters such as height, weight, root mass and stem circumference were measured to determine plant-growth promoting activities of two selected endophytes. Both *in vitro* and *in vivo* tests were carried out in conditions under metal-stress and in the absence of metal stress.

Culture establishment of endophytes and preparation of metal solutions

Five metal-tolerant endophytes previously identified by Sim et al. (2018) as *Bipolaris* sp. LF7 (GenBank accession no. KX510121), *Diaporthe miriciae* LF9 (GenBank accession no. KX398059), *Trichoderma asperellum* LF11 (GenBank accession no. KX510127), *Phomopsis asparagi* LF15 (GenBank accession no. KX510125) and *Saccharicola bicolor* LF22 (GenBank accession no. KX510132), were selected for this study. These endophytes were isolated from the phytoremediator plant *Phragmites* sp. and demonstrated strong antifungal activities towards the pathogen *Ganoderma boninense*: they were able to suppress disease development when applied to oil palm seedlings (Sim et al. 2019a, 2019b). The isolates were cultured, incubated and maintained on Potato Dextrose Agar (PDA, Merck) (7 days, 25 ± 2 °C) for subsequent tests.

Stock solutions of various metal solutions were prepared to 1000 mg L^{-1}. This includes for $Cd(NO_3)_2{\cdot}4H_2O$ (Aldrich Chemical), $Cu(NO_3)_2{\cdot}3H_2O$ (Riendemann Schmidt Chemical), $Pb(NO_3)_2$ (Emsure) and $Zn(NO_3)_2{\cdot}6H_2O$ (R&M Chemicals). Prepared stock solutions were diluted to concentrations of 10 and 25 mg L^{-1} (additional 50 mg L^{-1} for Cu^{2+}). The working solutions was adjusted to pH 5 using 0.1 M HCl and 0.1 M NaOH.

Production of indole-acetic acid (IAA)

Three mycelial plugs of each endophyte (5 mm diameter) were inoculated into 100 mL of Potato Dextrose Broth (PDB, Merck) supplemented with 100 mg L^{-1} tryptophan and incubated at 25 ± 2 °C for 28 days. After every 7-day interval, 5 mL of the culture was pipetted into a falcon tube and centrifuged (25 ± 2 °C, 12 000 rpm, 10 min). The supernatant (1 mL) was collected, mixed with 2 mL of Salkowski reagent, and incubated in the dark for 20 min prior to absorbance measurement at 535 nm (Babu et al. 2014). Standard curves were constructed from concentrations of 0-100 μg mL^{-1} and the IAA produced by the endophytes was determined. The influence of metals on the production of IAA was assayed by preparing a similar experimental set-up. The difference in this set-up is that that isolates were cultured in PDB supplemented with Cu^{2+}, Pb^{2+}, Zn^{2+}, Cd^{2+} (at concentrations of 10 and 25 mg L^{-1} for each metal, an additional 50 mg L^{-1} for Cu^{2+}). The supernatant obtained were subjected to similar assay conditions.

Production of siderophore

Production of siderophore by the endophytes was determined via qualitative and quantitative assays. For qualitative analysis, Chrome azurol S (CAS) was used as an indirect method to indicate the production of siderophore. This dye competes with siderophores for iron. The endophytes were first qualitatively assessed

for siderophore production using the modified half CAS blue agar method (Machuca and Milagres 2003). The CAS blue agar was prepared according to Louden et al. (2011). Half of the agar (PDA) was cut and replaced with the CAS blue agar. The mycelial plug of the endophyte (5 mm diameter) was subsequently inoculated onto the PDA and incubated (28 days, 25 ± 2 °C). At every 7-day interval for the next 28 days, colour changes of the CAS agar were observed and measured. Deep colourisation of the CAS dye indicated that more iron bonded to the dye due to lesser siderophore production/competition. In contrast, lighter dye intensity indicated higher siderophore production/competition as less iron is available to bind to the dye (lighter intensity). This reflected that more iron is uptake by siderophores. The influence of metals on the production of siderophore was determined by preparing a similar CAS blue agar set-up, with the CAS agar supplemented with Cu^{2+}, Pb^{2+}, Zn^{2+}, Cd^{2+} at 10 and 25 mg L^{-1} (and an additional 50 mg L^{-1} for Cu^{2+}).

The siderophore production by endophytes was also quantified. This quantitative assay is a less common approach used compared to the qualitative CAS blue agar technique. Nevertheless, it allows for the quantification of siderophores for comparative purpose. Three mycelial plugs of each endophyte were firstly inoculated into 100 mL PDB (28 days, 25 ± 2 °C). At every 7-day interval for the following 28 days, 1 mL of the supernatant was mixed with 1 mL of CAS solution and incubated for 60 min. Absorbance was read at 630 nm and siderophore production (%) was determined (Eq. 1) (Machuca and Milagres 2003). The influence of metals on the production of siderophore in broth was evaluated by preparing a similar set-up, using supernatant recovered from cultures established in PDB supplemented with Cu^{2+}, Pb^{2+}, Zn^{2+}, Cd^{2+} at 10 and 25 mg L^{-1} (and an additional 50 mg L^{-1} for Cu^{2+}).

$$\text{Production of siderophore (\%)} = \frac{(\text{Initial absorbance} - \text{Absorbance of sample})}{\text{Initial absorbance} \times 100}$$

Production of siderophore (%) = (Initial absorbance-Absorbance of sample) / Initial absorbance × 100%

Phosphate solubilisation

The endophytes (mycelial plug, 5 mm diameter) were inoculated onto Pikovskya's agar (HiMedia Laboratories) and incubated (28 days, 25 ± 2 °C). Phosphate solubilisation is indicated by the formation of a clear halo zone on the agar. The phosphate solubilisation capacity of the endophytes is quantified as phosphate solubilizing efficiency (SE, %) (Eq. 2). The SE (%) were observed for day 7th, 14th, 21st and 28th (Srivastav et al., 2004). To determine phosphate solubilisation activities of endophytes under metal stress, the procedure was repeated using Pikovskya's agar supplemented with Cu^{2+}, Pb^{2+}, Zn^{2+}, Cd^{2+} (at 10 and 25 mg L^{-1}, and an additional 50 mg L^{-1} for Cu^{2+}.

$$\text{Solubilising efficiency (SE)(\%)} = \frac{(\text{Diameter of solubilization zone} - \text{Diameter of colony})}{\text{Diameter of colony} \times 100}$$

Solubilising efficiency (SE)(%) = (Diameter of solubilization zone-Diameter of colony) / Diameter of colony × 100

Deaminase activity of 1-aminocyclopropane carboxylic acid (ACC) of endophytes

Three mycelial plugs (5 mm diameter) of each endophyte were inoculated into flasks containing 100 mL PDB (28 days, 25 ± 2 °C). The culture was allowed to grow and the mycelium was then filtered. The filtrate was collected and 200 µL was pipetted and reacted with 25 µL toluene and vortexed for 30 sec (Saleh and Glick 2001). Then, 20 µL of 0.45 M ACC of the enzyme ACC was added and incubated at 30 °C. After 10 min, the reaction was stopped with 1 mL of 0.56 N HCl. The lysates were centrifuged (10 000 *g*, 10 min), and 1 mL of the supernatant was pipetted and mixed with 800 µL of 0.56 N HCl and 300 µL of 2,4-dinitrophenylhydrazine. The mixture was incubated (30 min, 30 °C) and added with 2 mL of 2 N NaOH. The absorbance was measured at 540 nm and the ACC deaminase activity was calculated based on standard curves constructed. The ACC deaminase activities by endophytes under the influence of metals was assayed by preparing a similar set-up, using endophyte suspension recovered from cultures established in PDB supplemented with Cu^{2+}, Pb^{2+}, Zn^{2+}, Cd^{2+} at 10 and 25 mg L^{-1} (and an additional 50 mg L^{-1} for Cu^{2+}). The assay was carried out in a similar manner.

In vivo *plant growth promoting activities of selected endophytes*

Two endophytic isolates (*D. miriciae* LF9 and *T. asperellum* LF11) with the most promising results observed from the *in vitro* assays were selected. The isolates were first cultured in 250 mL PDB (14 days, 25 ± 2 °C). The mycelium was then homogenized using LabGen 125 homogenizer (Cole-Parmer, USA) and the homogenized mycelium was adjusted to a concentration of 10^6 of colony forming unit (cfu mL^{-1}) each. The adjusted inoculums were prepared in 100 mL and were used to inoculate the

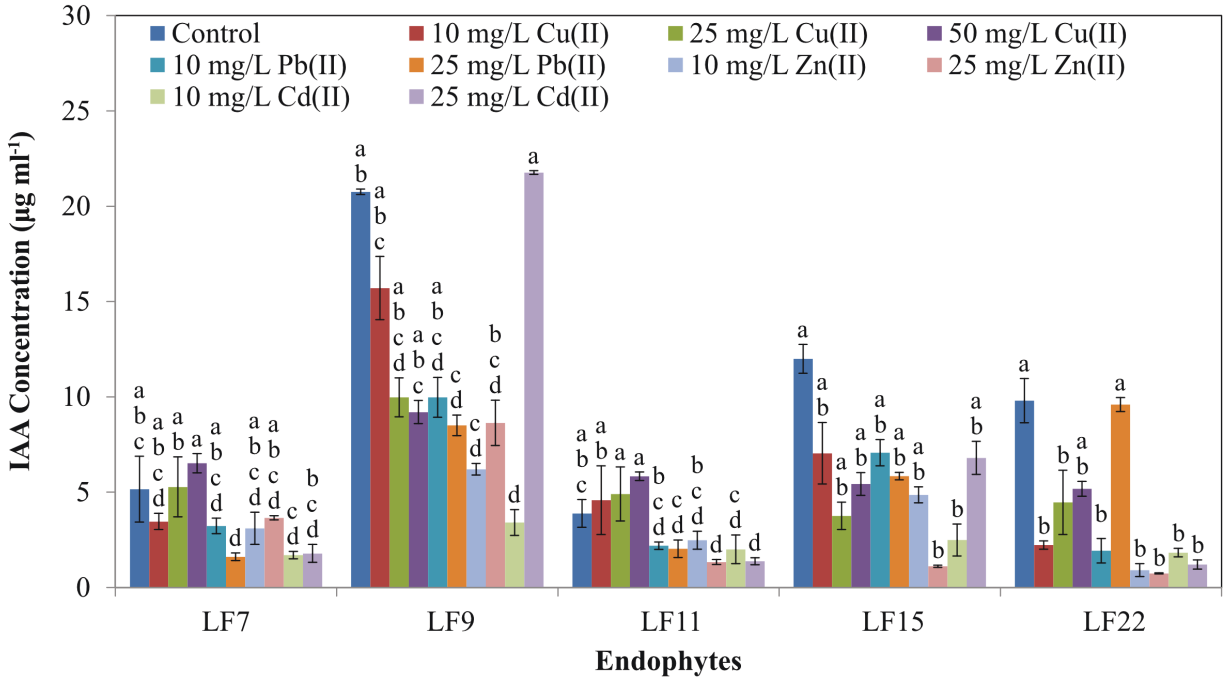

Figure 1. Indole-acetic acid (IAA) (µg mL^{-1}) produced by metal-tolerant endophytes (*Bipolaris sp*. LF7, *D. miriciae* LF9, *T. asperellum* LF11, *P. asparagi* LF15, *S. bicolor* LF22) after 28 days incubation with exposure to Cu^{2+}, Pb^{2+}, Zn^{2+} and Cd^{2+}. Controls were incubations without metal supplementation. Bars indicate standard deviations of means (±SD). Means with the same letters for each isolate are not significantly different ($HSD_{(0.05)}$).

soils via soil-drenching. The tissue-cultured ramets, at 3-4 leaf stage and 14-16 cm in height, were then planted into the drenched soils and allowed to grow in shade (28 ± 2 °C, 12 h photoperiod). For control, soil drenching was performed using sterile distilled water. Solutions for each metal (Cu^{2+}, Pb^{2+}, Zn^{2+}, Cd^{2+} at 10 and 25 mg L^{-1}; additional 50 mg L^{-1} for Cu^{2+}) were used to water the soil to create metal-laden soils. Controls were established with endophyte-free ramets watered using sterile distilled water. Growth parameters such as height, weight, root mass and stem circumference were measured at 7th, 14th, 21st and 28th day.

Statistical analysis

All the experiments/assays were carried out in triplicates, with data analysed using ANOVA (Analysis of Variance). The means and standard deviations were compared with Tukey comparisons ($HSD_{(0.05)}$) using the Statistical Packaging for the Social Science (SPSS) (software version 20.0).

Results and Discussion

Production of indole-acetic acid (IAA)

Lower levels of IAA were produced by endophytes subjected to metal stress (0.74-21.77 µg mL^{-1}) compared to non-metal conditions (control) (3.88-20.76 µg mL^{-1}). Among the isolates tested, *D. miriciae* LF9 was the least affected (3.41-21.77 µg mL^{-1} IAA production) whilst *T. asperellum* LF11 was the most susceptible to presence of metals as minimal IAA levels were detected (1.33-5.83 µg mL^{-1}) (Fig. 1). In the absence of metals, higher IAA production by *D. miriciae* LF9 (20.76 µg mL^{-1}), *P. asparagi* LF15 (11.99 µg mL^{-1}), *S. bicolor* LF22 (9.80 µg mL^{-1}), *Bipolaris* sp. LF7 (5.16 µg mL^{-1}) and *T. asperellum* LF11 (3.88 µg mL^{-1}) (Fig. 1) were detected. This suggested that the production of IAA and subsequently their growth promoting effect was influenced by the presence/absence of metals. Nevertheless, the production of IAA by all isolates under metal stress were somewhat maintained throughout the 28 days (Supplementary Fig. 1), although the IAA levels were lower than observations from endophytes in non-metal conditions.

It was evident that metals affected the production of IAA by the isolates. This was also observed by Acuna et al. (2011) in which the presence of metals such as Fe and Al reduced IAA production by *Bacillus* sp. and *Paenibacillus* sp.. The reduction in IAA production under metal stress was presumably attributed to the complexation of metal cations with IAA (Du et al. 2011). This suggested that metals lowered the production of IAA, hampering root elongation (Hilbert et al. 2012; Sukumar et al. 2012) and

Table 1 Chrome Azurol S (CAS) reaction rates of the isolates (mm/day) under the influence of metals after 28 days.

Endophytes	Metal concentrations (mg L^{-1})									
	Cu			Pb		Zn		Cd		Control
	10	25	50	10	25	10	25	10	25	0
Bipolaris sp. LF7	±	±	±	±	±	±	±	±	±	±
D. *miriciae* LF9	±	±	±	±	+	+	+	+	+	+
T. asperellum LF11	±	±	±	+	+	±	+	+	+	+
P. asparagi LF15	±	±	±	±	±	+	±	+	+	±
S. bicolor LF22	±	±	±	±	±	±	±	±	±	±

Note: ± for rates < 0.5 mm/day (mild) and + for rates between 0.5-1.0 mm/day (moderate)

consequently implicating water and nutrient uptake. It was also interesting to note that the metal tolerance attributes of the endophytes, did not render "immunity" to the isolates from the influence of metals on IAA production.

The production of IAA as a growth-promoting factor has been reported in various species of *Trichoderma* and *Phomopsis*. The low levels of IAA produced by *T. asperellum* LF11 (highest at 5.83 μg mL^{-1} IAA) was similar to observations by Gravel et al. (2007) that showed *T. atroviride* (another species of *Trichoderma*) producing only 6.20 μg mL^{-1} IAA. The production of IAA by *P. asparagi* LF15 in this study further strengthen the IAA-producing capacity of *Phomopsis* sp. This was also observed by Chen et al. (2011) and Chithra et al. (2017) in *Phomopsis* sp. isolated from *Piper nigrum,* and *P. liquidambari* from *Bischofa polycarp*, respectively. On the contrary, IAA production by *S. bicolor* LF22, *D. miriciae* LF9 as well as *Bipolaris* sp. LF7, were detected and reported for the first time. To summarize, results here highlighted that presence of metals generally reduced the production of IAA in endophytes, subsequently leading to absence or weak stimulation of root growth in the presence of metals. And the metal-tolerant endophytes were also not exempted from this metal-IAA production interaction.

Production of siderophore

The plate assay revealed that in the presence of metals, the reaction rates by *D. miriciae* LF9 and *T. asperellum* LF11 were generally moderate (0.5-1.0 mm/day) whilst *Bipolaris* sp. LF7, *P. asparagi* LF15 as well as *S. bicolor* LF22 showed mild CAS reaction rates (<0.5 mm/day) (Table 1). The reaction rates remained throughout the 28 days (Supplementary Table 1). The reaction rates for endophytes in CAS plates without metals remained similar as well (Table 1). Since the observation using CAS blue agar was deemed to be preliminary, presumptive and inconclusive, the quantitative test was performed.

The quantification of siderophore production revealed that under the influence of various metals, siderophore production was generally lower (8.82-90.26%) in most endophytes (except *T. asperellum* LF11) compared to non-metal solutions (66.75-84.44%). Isolates *S. bicolor* LF22, *P. asparagi* LF15, *D. miriciae* LF9 and *Bipolaris* sp. LF7, were susceptible to the presence of some of the metals, resulting in lower siderophore production; ranging from 8.82-80.51%, 0.08-78.20%, 32.81-76.05% and 21.94-78.24%, respectively (Fig. 2). In the absence of metals, siderophore production was generally higher for all isolates; *T. asperellum* LF11 (84.44%), *P. asparagi* LF15 (75.92%), *D. miriciae* LF9 (74.32%), *Bipolaris* sp. LF7 (73.70%) and *S. bicolor* LF22 (66.75%) (Fig. 2). Among the isolates, only isolate *T. asperellum* LF11 appeared to be less susceptible to metals with levels of siderophore production (19.21-90.26%) comparable to control. Nevertheless, siderophore production was maintained throughout the 28 days for the isolates, even in the presence of metal stress (Supplementary Fig. 2). The discovery of siderophore production by *P. asparagi* LF15, *D. miriciae* LF9, *Bipolaris* sp. LF7 and *S. bicolor* LF22 are relatively novel as limited reports are available on this. By contrast, the siderophore-producing attribute in *T. asperellum* LF11, is well known as it has been reported for other *Trichoderma* sp. such as *Trichoderma virens* (Babu et al. 2014). *Trichoderma* spp. are one of the most common filamentous fungi with siderophore-producing capacity, alongside *Aspergillus* spp. and *Penicillum menonorum* (Babu et al. 2015; Machuca and Milagres 2003).

The CAS assays also revealed that in some instances, the colour intensity does not reflect the CAS production of the endophytes. The lower concentrations of siderophore (from liquid medium) recorded, were attributed to the nature of this compound to form complexes with other metal cations other than the desired iron (Fe^{2+}) (Dimkpa et al. 2008; Aguado-Santacruz et al. 2012). Since metal cations are abundant in this study, the siderophores could have bind easily to any cations supplemented (Cu^{2+}, Pb^{2+}, Zn^{2+}, Cd^{2+}). The ability of siderophores to bind to metal cations not only aids in enhancing tolerance to metal-stress conditions, it is also a means of bioremediation. This mechanism has been exploited to bind toxic metals and consequently removing the toxic metals from the

environment. Thus, siderophore production is a highly valuable trait for biocontrol agents applied to metal-laden soils. With the production of siderophores, the biocontrol agents is expected to ameliorate the soil environment as toxic metals are removed, thus improving survivability of plants in metal-contaminated sites. Siderophores produced by biocontrol agents also deprives iron from pathogens, thus suppressing the growth of pathogens (Verma et al. 2011; Yu et al. 2011; Beneduzi et al. 2012).

Phosphate solubilisation

Four of the five endophytic isolates solubilised phosphate, in both the presence or absence of metals. Formation of clear halo zones was detected on Pikovskya's agar with and without metal supplementation. Results further suggested that phosphate solubilisation by the endophytes were higher in the presence of metals (3.94-79.82%) than in non-metal (17.64-20.83%) conditions. Higher phosphate solubilisation efficiency under metal stress was demonstrated by *P. asparagi* LF15 (18.81-79.82%) (Fig. 3). Solubilisation of phosphate was also regulated by *D. miriciae* LF9 (12.43-56.24%), *Bipolaris* sp. LF7 (3.94-34.00%) and *T. asperellum* LF11 (12.44-22.07%) (Fig. 3). The gradual increase in phosphate solubilisation by the isolates was observed throughout the 28 days (Supplementary Fig. 3). By contrast, the absence of metals resulted in inferior phosphate solubilisation activities by *D. miriciae* LF9 (20.83%), followed by *P. asparagi* LF15 (18.4%) and *Bipolaris* sp. LF7 (17.64%) (after 28 days). Interestingly, phosphate solubilisation was, however, not observed in *T. asperellum* LF11 (Fig. 3) in the absence of metal stress (control). This is presumably due to the rapid growth rate of LF11 (to the extent of overgrowing) on the metal-free agar. Phosphate solubilisation was also absent in *S. bicolor* LF22, when cultured in the absence and presence of metals, as no formation of halo zones were detected. This suggested that the isolate *S. bicolor* LF22 is not a phosphate solubilizer.

The findings in this study, which showed endophytes (except *S. bicolor* LF22) having generally higher phosphate solubilisation under metal stress, agreed with Zúñiga-Silva et al. (2015). Endophytes are proven to have similar capacity as other phosphate-solubilising fungi to solubilize

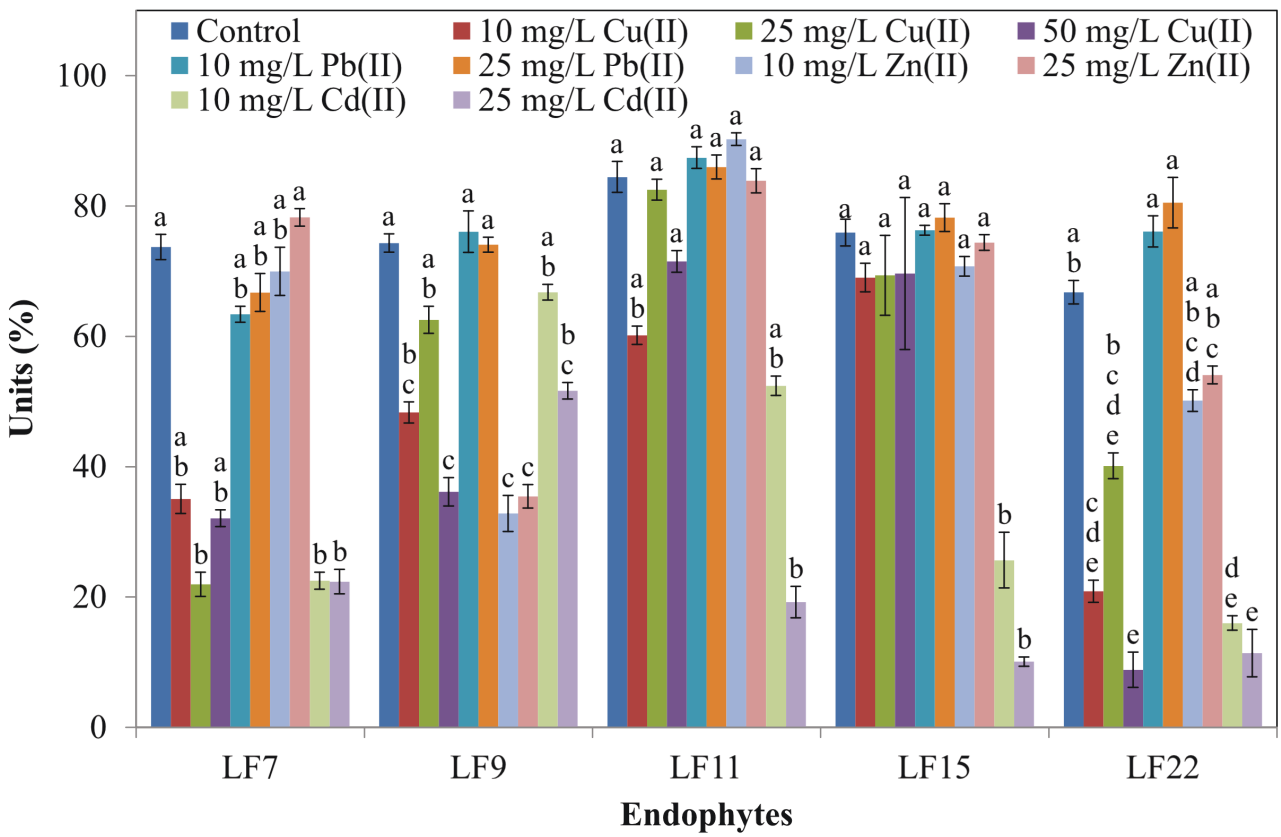

Figure 2. Siderophore production (%) by metal-tolerant endophytes (*Bipolaris sp*. LF7, *D. miriciae* LF9, *T. asperellum* LF11, *P. asparagi* LF15, *S. bicolor* LF22) after 28 days incubation with exposure to Cu^{2+}, Pb^{2+}, Zn^{2+} and Cd^{2+}. Controls were incubations without metal supplementation. Bars indicate standard deviations of means (±SD). Means with the same letters for each isolate are not significantly different ($HSD_{(0.05)}$).

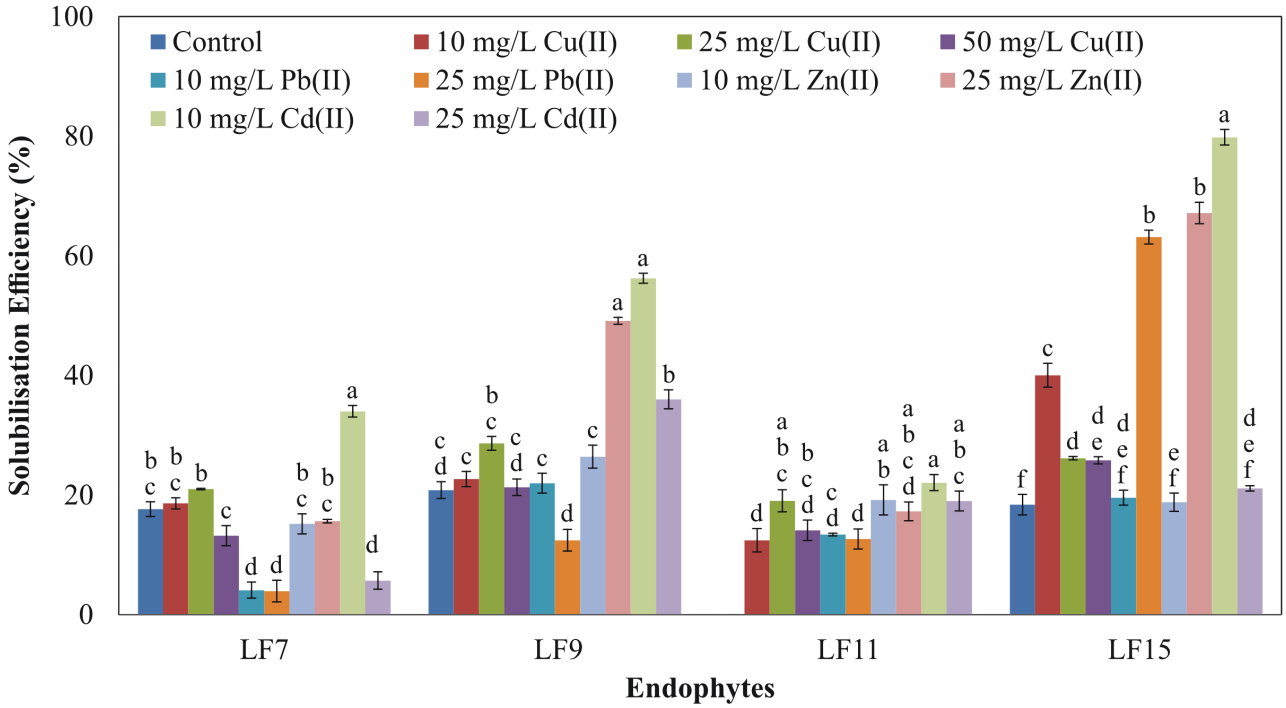

Figure 3. Phosphate solubilisation efficiency (%) by metal-tolerant endophytes (*Bipolaris sp*. LF7, *D. miriciae* LF9, *T. asperellum* LF11, *P. asparagi* LF15, *S. bicolor* LF22) after 28 days incubation with exposure to Cu^{2+}, Pb^{2+}, Zn^{2+} and Cd^{2+}. Controls were incubations without metal supplementation. Bars indicate standard deviations of means (±SD). Means with the same letters for each isolate are not significantly different ($HSD_{(0.05)}$).

phosphate for uptake and use. Phosphate-solubilising fungi acidify and secrete siderophores to solubilize the naturally-limited phosphate into available forms, particularly in response to metal stress, and this ultimately results in the dissolution of bound phosphate (Walpola and Yoon 2013). This study has revealed for the first time, the phosphate-solubilising potential in endophytic *Bipolaris* sp. LF7, *D. miriciae* LF9 and *P. asparagi* LF15, as well as the non-phosphate solubilising activity of *S. bicolor* LF22. Existing literature on this is limited, although studies on phosphate-solubilizing by *Trichoderma* sp. has been reported. This study, which revealed phosphate solubilisation by *T. asperellum* LF11 in both the presence and absence of metals agreed with Zúñiga-Silva et al. (2015) (using *T. atroviride*), suggesting that phosphate solubilisation could be a common trait for *Trichoderma* sp.. In short, the endophytes tested in this study were able to solubilise phosphate in both conditions (in the absence and presence of metal stress), except for *S. bicolor* LF22. The increased phosphate-solubilising activities under metal stress conditions suggested higher phosphate acquisition by endophytes when applied in metal-laden soils.

Deaminase activity of 1-aminocyclopropane carboxylic acid (ACC)

This assay measures the α-ketobutyrate, one of the products of the 1-aminocyclopropane carboxylic acid (ACC) deaminase activity. It was revealed that ACC deaminase activity in endophytes were generally lower when exposed to metals (3.00-69.2 µmol mg protein^{-1} hr^{-1}) as compared to the absence of metals (control) (19.17-54.30 µmol mg protein^{-1} hr^{-1}). Among the five isolates tested, *T. asperellum* LF11 was the least susceptible to metal stress, exhibiting the highest ACC deaminase activity (8.69-69.2 µmol mg protein^{-1} hr^{-1}) especially in the presence of Pb and Cd (Fig. 4). The ACC deaminase activity by *T. asperellum* LF11 is comparable to other *Trichoderma* species, such as *T. atroviride* and *T. virens* (Babu et al. 2014; Gravel et al. 2007). On the contrary, presence of metals severely impacted ACC deaminase activity in the other endophytic isolates, particularly *Bipolaris* sp. LF7. This isolate produced the lowest ACC deaminase activities in the presence of metals (3.00-17.54 µmol mg protein^{-1} hr^{-1}) (Fig. 4). Presence of metals was less detrimental on the ACC deaminase activities of the other three isolates. Isolates *P. asparagi* LF15 (6.23-38.26 µmol mg protein^{-1} hr^{-1}), *D. miriciae* LF9 (6.15-32.83 µmol mg protein^{-1} hr^{-1}) and *S. bicolor* LF22 (7.5-15.41 µmol mg protein^{-1} hr^{-1}) (Fig. 4) retained their ACC deaminase activities under metal stress, but the activities were significantly lower compared to ACC deaminase activities in the absence of metal. In the absence of metals, the highest activity was observed for *D.*

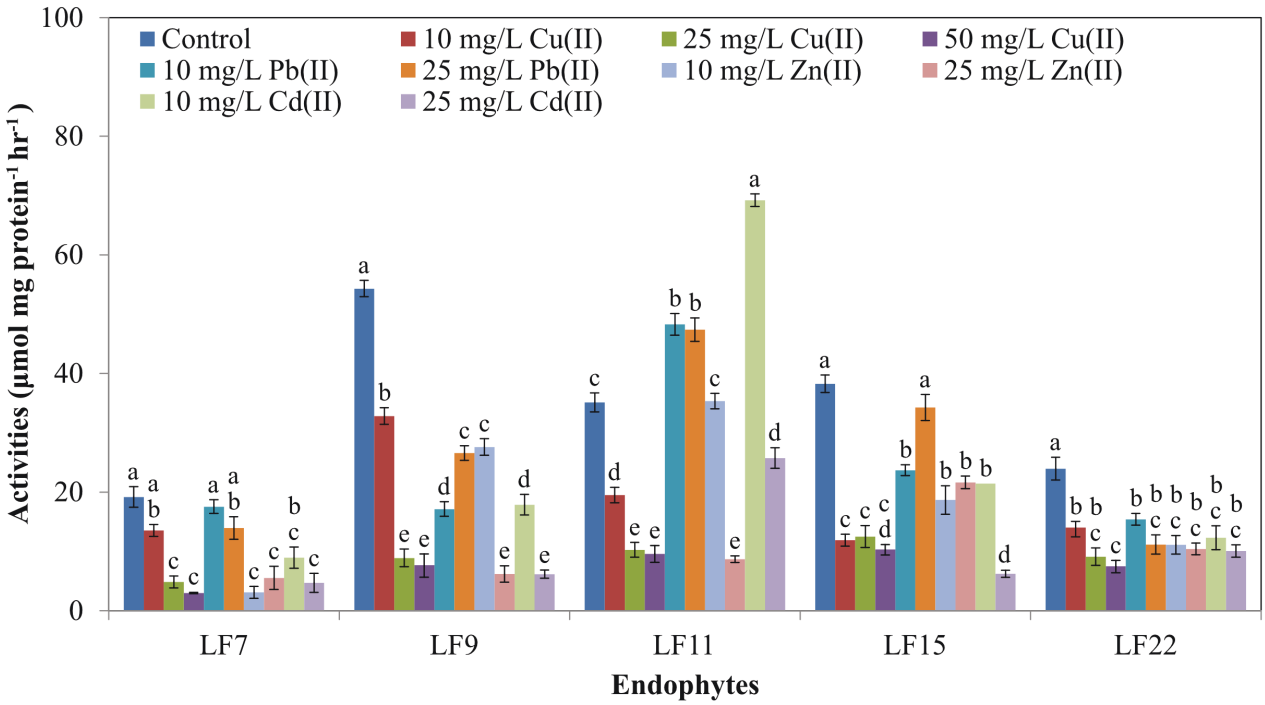

Figure 4. Activities of ACC deaminase (µmol protein mg^{-1} hr^{-1}) by metal-tolerant endophytes (*Bipolaris sp*. LF7, *D. miriciae* LF9, *T. asperellum* LF11, *P. asparagi* LF15, *S. bicolor* LF22) after 28 days incubation with exposure to Cu^{2+}, Pb^{2+}, Zn^{2+} and Cd^{2+}. Controls were incubations without metal supplementation. Bars indicate standard deviations of means (±SD). Means with the same letters for each isolate are not significantly different ($HSD_{(0.05)}$).

miriciae LF9 (54.30 µmol mg protein^{-1} hr^{-1}), followed by *P. asparagi* LF15 (38.26 µmol mg protein^{-1} hr^{-1}), *T. asperellum* LF11 (35.11 µmol mg protein^{-1} hr^{-1}), *S. bicolor* LF22 (23.95 µmol mg protein^{-1} hr^{-1}) and *Bipolaris* sp. LF7 (19.17 µmol mg protein^{-1} hr^{-1}) (Fig. 4). Observations based on time intervals indicated that the ACC deaminase activities were lower in the initial stages, gradually increasing in the next 28 days (Supplementary Fig. 4).

The present study showed that ACC deaminase activities by the endophytes decreased when metals were present as a stress factor. The inhibition of ACC deaminase activities by metals was not specific to just fungal endophytes, as similar observations have been reported on bacteria. Carlos et al. (2016) discovered *Serratia* sp. strain Mc107, having lesser ACC deaminase activities when cultured in the presence of Pb^{2+}, Cu^{2+} and Cd^{2+}. Only *Trichoderma* species appeared to have ACC deaminase activities that were not implicated by presence of metals. Additionally, the initial decreasing trend of ACC deaminase activities followed by a gradual increase in activities follows the model described by Glick et al. (2007). According to the model, the initial decreasing trend was possibly associated with the reaction of ACC deaminase upon ACC to prevent the precursor from converting to ethylene. The activities gradually diminished throughout 21 days in this study, as lesser ACC was available. Following that, environmental stress (metals, in this study) may have triggered follow-up production of ACC (Yang and Hoffman 1984), consequently resulting in a rise in the activities of ACC deaminase. The increase in ACC deaminase activities was to prevent the build-up of the precursor ACC and their further conversion to ethylene. As such, ACC deaminase activities aid in reducing ethylene levels in plants, which enhances plant growth. In general, the decreased ACC deaminase activities of the endophytes under metal stress suggested lower phytohormone modulation in metal-contaminated soils, which could implicate plant growth.

In vivo plant growth promoting activities of selected endophytes

In non-metal soils, improved growth was observed in ramets treated with both selected endophytes (*D. miriciae* LF9 and *T. asperellum* LF11). Of the two isolates, inoculation with *D. miriciae* LF9 showed better growth of ramets with increased height (4.68 cm), weight (1.14 g), root growth (0.39 g) as well as stem circumference (0.30 cm) (Fig. 5). Ramets inoculated with *T. asperellum* LF11 also exhibited similar positive influence; improved height (3.90 cm), weight (0.94 g), root mass (0.32 g) and stem circumference (0.18 cm) (Fig. 5). This further verified the

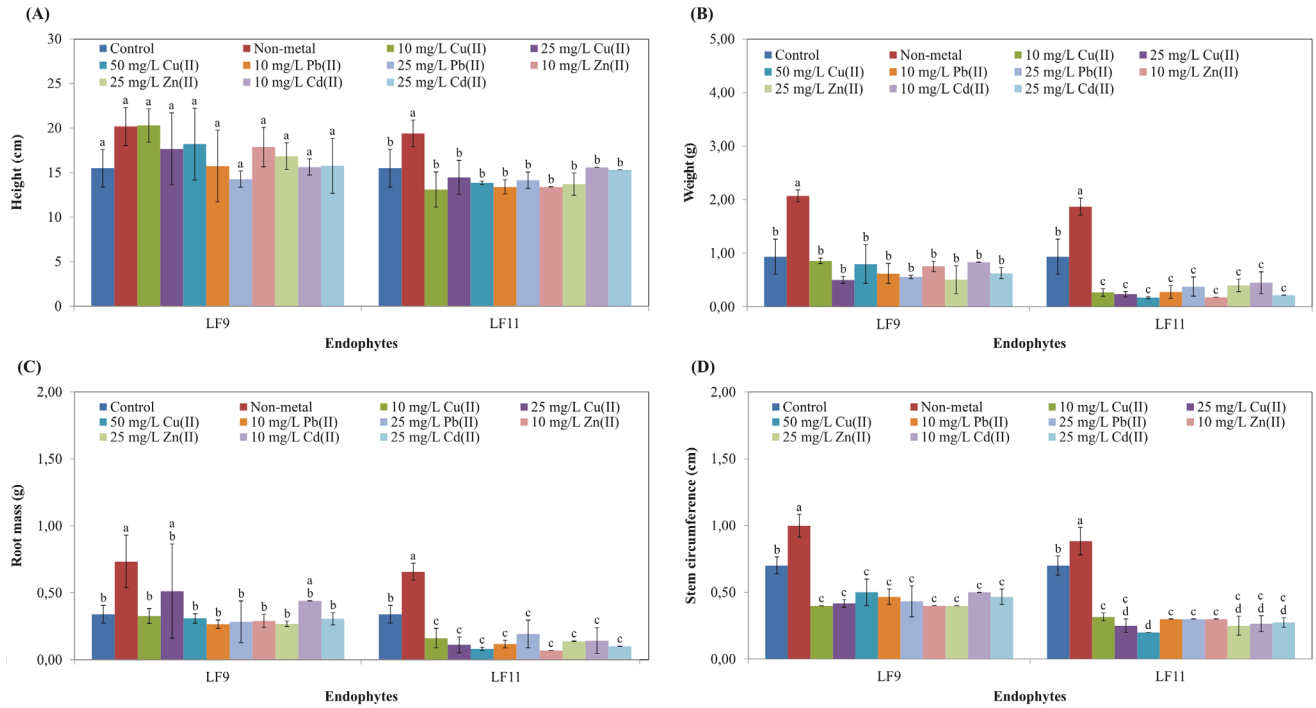

Figure 5. Growth parameters of (A) height (B) weight (C) root mass and (D) stem circumferences of ramets inoculated with metal-tolerant endophytes *D. miriciae* LF9 and *T. asperellum* LF11 in metal-laden soils consisting of Cu^{2+}, Pb^{2+}, Zn^{2+} and Cd^{2+}. Controls were endophyte-free ramets watered with sterile distilled water. Bars indicate standard deviations of means (±SD). Means with the same letters for each isolate are not significantly different ($HSD_{(0.05)}$).

growth-promoting ability of *Trichoderma* species, alongside *T. atroviride*, *T. harzianum* and *T. psedokoningii*, which were reported to effectively promote growth of tomato and maize (Babu et al. 2014; Gravel et al. 2007). However, in metal-laden soils, only *D. miriciae* LF9 appeared to have benefitted the ramets. Ramets inoculated with *D. miriciae* LF9 showed similar growth to ramets in non-metal soils with comparable height (0.13-4.80 cm), weight (0.08-0.43 g), and root mass (0.01-0.17 g) achieved. The stem circumference of the ramets was however affected (0.20-0.30 cm) (Figure 5). For ramets inoculated with *T. asperellum* LF11 and cultivated in soils with metals, poorer growth was observed compared to ramets in non-metal soils. In these ramets, inferior growth was evident with low growth measurements (height 0.10-2.4 cm, weight 0.49-0.76 g, root mass 0.15-0.27 g and stem circumference 0.38-0.50 cm) recorded (Fig. 5).

The *in vivo* findings were aligned to the *in vitro* results, which revealed lesser growth promoting activities when endophytes were exposed to metals compared to non-metal conditions. Ramets inoculated with *D. miriciae* LF9 were less susceptible to metal stress, but ramets treated with *T. asperellum* LF11 were not able to tolerate metal stress and this affected the growth of the ramets (low weight, root mass and stem circumference). This also revealed that the association of *Trichoderma* species with host plant may not necessarily be beneficial in metal-laden soils. The poor growths observed in ramets grown in soils supplemented with metals, is attributed to the effect of metals in inhibiting the production of IAA, siderophore, and ACC deaminase activities by the endophytic biocontrol agents (albeit at varying degrees). In the instance where the growth-promoting attribute is not inhibited, ramets continued to grow well. This explains the continued growth of ramets inoculated with *D. miriciae* LF9, as the phosphate solubilisation activity of LF9 in metal soils was detectable. This study also revealed that despite of the metal-tolerant attributes of the endophytes (Sim et al. 2018, 2019a, 2019b), the presence of metals did have an impact on the expression of plant growth-promoting activities. It also highlights that careful selection and investigation has to be performed, as not all metal-tolerant endophytes are ideal for application as biocontrol agents in metal-laden soil conditions.

Conclusions

The five endophytic isolates (*Bipolaris* sp. LF7, *D. miriciae* LF9, *T. asperellum* LF11, *P. asparagi* LF15, *S. bicolor* LF22)

demonstrated the potential to stimulate plant growth *in vitro* assays. This is a desirable attribute for biocontrol agents, as application of these bioagents would not only suppress disease development, but also to promote growth and strengthen the plant to delay disease progression. However, their beneficial role was generally affected by metal stress, with decreased IAA and siderophore production, and ACC deaminase activities. Hence, the metal-tolerant attributes of endophytes did not necessarily render significant benefits to the host-plants. Nevertheless, of the two isolates tested, *D. miriciae* LF9 showed better potential and prospect for further development as a biocontrol agent.

Acknowledgements

The authors are grateful to Monash University Malaysia and the Tropical Medicine and Biology Multidisciplinary Platform for the funding and research facilities. The authors also thank Applied Agricultural Resources (AAR, Selangor, Malaysia) for supplying the ramets. The first author was a recipient of the PhD scholarship by Monash University Malaysia.

References

Acuna JJ, Jorquera MA, Martinez OA, Menezes-Blackburn D, Fernandez MT, Marschner P, Greiner R, Mora ML (2011) Indole acetic acid and phytase activity produced by rhizosphere bacilli as affected by pH and metals. J Soil Sci Plant Nutr 11:1-12.

Aguado-Santacruz GA, Moreno-Gomez B, Jimenez-Francisco B, Garcia-Moya E, Preciado-Ortiz RE (2012) Impact of the microbial siderophores and phytosiderophores on the iron assimilation by plants: a synthesis. Rev Fitotec Mex 35:9-21.

Babu AG, Kim SW, Yadav DR, Hyum U, Adhikari M, Lee YS (2015) *Penicillium menonorum*: a novel fungus to promote growth and nutrient management in cucumber plants. Mycobiol 43:49-56.

Babu AG, Shim J, Bang KS, Shea PJ, Oh BT (2014) *Trichoderma virens* PDR-28: A heavy metal-tolerant and plant growth-promoting fungus for remediation and bioenergy crop production on mine tailing soil. J Environ Manage 132:129-134.

Beneduzi A, Ambrosini A, Passaglia LMP (2012) Plant growth-promoting rhizobacteria (PGPR): Their potential as antagonists and biocontrol agents. Genet Mol Biol 35:1044-1051.

Carlos MHJ, Stefani PVY, Janette AM, Melani MSS, Gabriela PO (2016) Assessing the effects of heavy metals in ACC deaminase and IAA production on plant growth-promoting bacteria. Microbiol Res 188:53-61.

Chen Y, Peng Y, Dai CC, Ju Q (2011) Biodegradation of 4-hydroxybenzoic acid by *Phomopsis liquidambari*. Appl Soil Ecol 51:102-110.

Chithra S, Jasim B, Mathew J, Radhakrishnan EK (2017) Endophytic *Phomopsis* sp colonization in *Oryza sativa* was found to result in plant growth promotion and piperine production. Physiol Plant 160:437-446.

Dimkpa CO, Svatos A, Dabrowska P, Schmidt A, Boland W, Kothe E (2008) Involvement of siderophores in the reduction of metal-induced inhibition of auxin synthesis in *Streptomyces* spp. Chemosphere 74:19-25.

Du RJ, He EK, Tang YT, Hu PJ, Ying RR, Morel JL, Qiu RL (2011) How phytohormone IAA and chelator EDTA affect lead uptake by Zn/Cd hyperaccumulator *Picris divaricata*. Int J Phytoremed 13:1024-1036.

Glick BR, Cheng Z, Czarny J, Duan J (2007) Promotion of plant growth by ACC deaminase-producing soil bacteria. Eur J Plant Pathol 119:329-339.

Gravel V, Antoun H, Tweddell RJ (2007) Growth stimulation and fruit yield improvement of greenhouse tomato plants by inoculation with *Pseudomonas putida* or *Trichoderma atroviride*: possible role of indole acetic acid (IAA). Soil Biol Biochem 39:1968-1977.

Hassan SE (2017) Plant growth-promoting activities for bacterial and fungal endophytes isolated from medicinal plant of *Teucrium polium* L. J Advanced Res 8:687-695.

Hilbert M, Voll Lars M, Ding Y, Hofmann J, Sharma M, Zuccaro A (2012) Indole derivative production by the root endophyte *Piriformospora indica* is not required for growth promotion but for biotrophic colonization of barley roots. New Phytol 196:520-534.

Louden BC, Haarmann D, Lynne AM (2011) Use of blue agar CAS assay for siderophore detection. J Microbiol Biol Educ 12:51-53.

Machuca A, Milagres AMF (2003) Use of CAS-agar plate modified to study the effect of different variables on the siderophore production by *Aspergillus*. Lett Appl Microbiol 36:177-181.

Nascimento FX, Espada M, Barbosa P, Rossi MJ, Vicente CSL, Mota M (2016) Non-specific transient mutualism between the plant parasitic nematode, *Bursaphelenchus xylophilus*, and the opportunistic bacterium *Serratia quinivorans* BXF1, a plant-growth promoting pine endophyte with antagonistic effects. Environ Microbiol 18:5265-5276.

Naveed M, Hussain MB. Zahir ZA, Mitter B, Sessitsch A (2014) Drought stress amelioration in wheat through inoculation with *Burkholderia phytofirmans* strain PsJN. Plant Growth Regul 73:121-131.

Nieto-Jacobo MF, Steyaert JM, Salazar-Badillo FB, Nguyen DV, Rostas M, Braithwaite M, De Souza JT, Jimenez-

Bremont JF, Ohkura M, Stewart A, Mendoza-Mendoza A (2017) Environmental growth conditions of *Trichoderma* spp. affects indole acetic acid derivatives, volatile organic compounds, and plant growth promotion. Front Plant Sci 8:102.

Patten CL, Glick BR (1996) Bacterial biosynthesis of indole-3-acetic acid. Can J Microbiol 42: 207-220.

Rúa MA, McCulley RL, Mitchell CE (2013) Fungal endophyte infection and host genetic background jointly modulate host response to an aphid-transmitted viral pathogen. J Ecol 101:1007-1018.

Saleh SS, Glick BR (2001) Involvement of gacS and rpoS in enhancement of the plant growth-promoting capabilities of *Enterobacter cloacae* CAL2 and UW4. Can J Microbiol 47:698-705.

Sim CSF, Cheow YL, Ng SL, Ting ASY (2018) Discovering metal-tolerant endophytic fungi from the phytoremediator plant *Phragmites*. Water Air Soil Poll 229:68.

Sim CSF, Yue CS, Cheow YL, Ting ASY (2019a) Influence of metal stress on production of volatile inhibitory compounds by endophytes against *Ganoderma boninense,* Biocontrol Sci Technol 29(9):860-876.

Sim CSF, Cheow YL, Ng SL, Ting ASY (2019b) Antifungal activities of metal-tolerant endophytes against *Ganoderma boninense* under the influence of metal stress. Biol Control 130:9-17.

Sim CSF, Cheow YL, Ng SL, Ting ASY (2019c) Biocontrol activities of metal-tolerant endophytes against *Ganoderma boninense* in oil palm seedlings cultivated under metal stress. Biol Control 132:66-71.

Sirrenberg A, Goebel C, Grond S, Czempinski N, Ratzinger A, Karlovsky P, Santos P, Feussner I, Pawlowski K (2007) *Piriformospora indica* affects plant growth by auxin production. Physiol Plant 131:581-589.

Srivastav S, Yadav KS, Kundu BS (2004) Prospects of using phosphate solubilizing *Pseudomonas* as biofungicide. Indian J Microbiol 44:91-94.

Sukumar P, Legué V, Vayssiéres A, Martin F, Tuskan GA, Kalluri UC (2012) Involvement of auxin pathways in modulating root architecture during beneficial plant–microorganism interactions. Plant Cell Environ 36:909-919.

Ting ASY (2014) Biosourcing endophytes as biocontrol agents of wilt diseases. In Verma VC, Gange AC, Eds., Advances in Endophytic Research. Springer India. Pp. 283-300.

Verma VC, Singh SK, Prakash S (2011) Bio-control and plant growth promotion potential of siderophore producing endophytic *Streptomyces* from *Azadirachta indica* A. Juss. J Basic Microbiol 51:550-556.

Walpola B, Yoon MH (2013) In vitro solubilization of inorganic phosphates by phosphate solubilizing microorganisms. Afr J Microbiol Res 7:3534-3541.

Wu T, Xu J, Xie WJ, Yao ZG, Yang HJ, Sun CL, Li XB (2018) *Pseudomonas aeruginosa* L10: A hydrocarbon-degrading, biosurfactant-producing, and plant-growth-promoting endophytic bacterium isolated from a reed (*Phragmites australis*). Front Microbiol 9:1-12.

Yang SF, Hoffman NE (1984) Ethylene biosynthesis and its regulation in higher plants. Ann Rev Plant Physiol 35:155-189.

Yu XM, Ai CX, Xin L, Zhou GF (2011) The siderophore-producing bacterium, *Bacillus subtilis* CAS15, has a biocontrol effect on *Fusarium* wilt and promotes the growth of pepper. Eur J Soil Biol 47:138-145.

Zarcinas BA, Ishak CF, McLaughlin MJ, Cozens G (2004) Heavy metals in soils and crops in southeast Asia. 1. Peninsular Malaysia. Environ Geochem Health 26:343-357.

Zhang YF, He LY, Chen ZJ, Wang QY, Qian M, Sheng XF (2011) Characterization of ACC deaminase-producing endophytic bacteria isolated from copper-tolerant plants and their potential in promoting the growth and copper accumulation of *Brassica napus*. Chemosphere 83:57-62.

Zúñiga-Silva JR, Chan-Cupul W, Loera O, Aguilar-López R, Xoconostle-Cázares B, Rodríguez Vázquez R (2015) *In vitro* toxic effects of heavy metals on fungal growth and phosphate-solubilising abilities of isolates obtained from *Phragmites australis* rhizosphere. Chem Ecol 32:49-67.

Acta Biologica Szegediensis

Volume 63(2):181-184, 2019
Acta Biologica Szegediensis
http://abs.bibl.u-szeged.hu/index.php/abs
DOI:10.14232/abs.2019.2.181-184

ARTICLE

In vitro interactions of amphotericin B and non-antifungal compounds against opportunistic human pathogen *Cryptococcus neoformans*

Bettina Szerencsés, Anna Mülbacher, Csaba Vágvölgyi, Ilona Pfeiffer*

Department of Microbiology, Faculty of Science and Informatics, University of Szeged, Szeged, Hungary

ABSTRACT The incidence of opportunistic human pathogen *Cryptococcus neoformans* caused infections have been higher during the last few decades along with the increasing number of susceptible individuals around the world. Recommended treatment of cryptococcal meningoencephalitis is a combined therapy with amphotericin B deoxycholate and flucytosine. Despite of the efficiency of this drug combination, the mortality rate of the disease is high due to the limited accessibility and the high cost of these antifungals in the most severely affected areas. The broad-spectrum activity of non-antifungal drugs and their potential to enhance the efficiency of conventional antifungal agents have been recognised previously. In this study, the *in vitro* activity of amantadine, valproic acid, trifluoperazine and chlorpromazine was tested against five *C. neoformans* strains individually and in combination with amphotericin B. All the four compounds exerted slight antifungal activity against the studied *C. neoformans* strains. Their combination with amphotericin B revealed additive and synergistic interactions.
Acta Biol Szeged 63(2):181-184 (2019)

KEY WORDS
amphotericin B
Cryptococcus neoformans
cryptococcosis
non-antifungal compounds

ARTICLE INFORMATION
Submitted
15 October 2019.
Accepted
22 November 2019.
***Corresponding author**
E-mail: pfeiffer@bio.u-szeged.hu

Introduction

The encapsulated basidiomycetous yeast, *Cryptococcus neoformans* is distributed world-wide mainly in association with bird excrement (Srikanta et al. 2014). The species is an opportunistic human pathogen and can cause serious disease primarily in immunocompromised individuals, i.e. HIV-positive patients, patients with organ transplants undergoing immunosuppressive therapy and cancer patients going through chemotherapy; making them vulnerable to fungal infection. The infection of immunocompetent hosts is rare. The disease caused by *C. neoformans* is called cryptococcosis. The infection starts with the inhalation of the airborne basidiospores or dried cells (Köhler et al. 2015). The spores germinate in the lungs, thereafter the cells disseminated by the blood stream can reach and colonize the central nervous system establishing meningoencephalitis. Cryptococcosis affects about 1 million people in the world - most of them are HIV-infected - and causes the death of more than 600 000 patients per year (Warkentien and Crum-Cianfloan 2010). The majority of the cases are registered in certain parts of Africa and Asia where the incidence of HIV-infection is higher (Sloan and Parris 2014).

A combined antifungal therapy involving amphotericin B deoxycholate and flucytosine is recommended for the treatment of cryptococcal meningoencephalitis (Day et al. 2013). However, flucytosine is an unregistered drug in most parts of Asia and Africa and its cost is high because of the limited number of manufacturers and these factors make the administration of this drug near impossible (Loyse et al. 2013).

Many non-antifungal pharmaceuticals have an antifungal side effect. Some of them can act alone while others can enhance the activity of antifungal agents when used together (Afeltra and Verwe 2003; Judd and Martin 2010; Nyilasi et al. 2010). Among the non-antifungals, the activity of phenothiazines like trifluoperazine and chlorpromazine, have been studied in detail. However, the antifungal activity of amantadine and valproic acid were only recognised recently against opportunistic human pathogenic fungal species (Wood and Nugent 1985; Eilam et al. 1987; Homa et al. 2015; Chaillat et al. 2017). Amantadine is an ion channel blocker used to treat Parkinson's disease (Blanpied et al. 2005). The anti-epileptic drug, valproic acid inhibits the action of histone deacetylases (HDACs) and induces the degradation of HDAC2 (Göttlicher 2004). The antipsychotic drugs chlorpromazine and trifluoperazine exert their antifungal activity via arresting the cell cycle and destroying the cell membrane integrity in the susceptible species (Eilam et al. 1987). All

Table 1. List of the tested strains

Species	Strain number
Cryptococcus neoformans	IFM 5844
Cryptococcus neoformans	IFO 410
Cryptococcus neoformans	SZMC 26851
Cryptococcus neoformans	SZMC 26852
Cryptococcus neoformans	IFM 48637

IFM: Culture Collection of the Research Centre for Pathogenic Fungi and Microbial Toxicoses, Chiba University, Chiba, Japan
IFO: Institute for Fermentation, Osaka, Japan
SZMC: Szeged Microbiological Collection

these drugs can penetrate across the blood brain barrier and can act in the central nervous system.

The aim of this study was to test the *in vitro* anti-*Cryptococcus* activity of amantadine, chlorpromazine, trifluoperazine and valproic acid against five *C. neoformans* strains, and to evaluate their interaction with amphotericin B.

Materials and methods

Yeast strains and growth conditions

The *C. neoformans* strains used in the present study are listed in Table 1. The strains were cultivated on Yeast Peptone Dextrose medium (YPD, 0.5% yeast extract, 1% peptone, 1% dextrose, 2% agar) at 30 °C for 48 hours and were kept at 4 °C until use.

The experiments were carried out with actively growing cells; therefore, a single colony was transferred to 2 mL sterile YPD medium and incubated at 30 °C for overnight. Cells were then harvested by centrifugation at 10000 rpm for 5 minutes in Heraeus Pico 17 centrifuge (Thermo Scientific, Waltham, MA, US) and washed twice with sterile distilled water, finally they were suspended in RPMI 1640 medium (Sigma-Aldrich, Germany).

Non-antifungal compounds

Amantadine hydrochloride, chlorpromazine hydrochloride, trifluoperazine hydrochloride, valproic acid sodium salt (Sigma-Aldrich, Germany) and amphotericin B (AppliChem, Darmstadt, Germany) were provided by the manufacturers as standard powder. The non-antifungal compounds were dissolved in 96% ethanol while amphotericin B in dimethyl sulfoxide (DMSO) to prepare stock solutions (10 mg/mL and 1 mg/mL, respectively) which was stored at -20 °C until used. Further dilutions were performed in RPMI 1640 medium.

Antifungal activity assays

Determination of Minimal Inhibitory Concentration (MIC)

The antifungal effect of the drugs was determined by broth micro-dilution assay in 96-well flat bottom microplate. Fifty µl serially twofold diluted compounds were added to 50 µl of standardized cell suspension (8 x 10^4 cell/mL in RPMI 1640 medium). The final concentration of the amphotericin B was ranged from 0.156 to 5.0 µg/mL, and those of amantadine, chlorpromazine, trifluoperazine and valproic acid from 7.81 to 500 µg/mL. The control samples contained 50 µl cell suspension and 50 µl RPMI 1640 medium. Solvent control was used to check the effect of the ethanol and DMSO on the growth rate of the strains.

The plates were incubated at 30 °C for 48 h. At the end of the incubation, the optical density of the samples was detected at 620 nm in SPECTROstar Nano plate reader (BMG LabTech, Offenburg, Germany). The experiments were carried out at least three times always in triplicates. The MIC was defined as the concentration of the compound caused total inhibition of cell growth.

Interaction between amphotericin B and the non-antifungal compounds

The *in vitro* interaction of the compounds and amphotericin B was determined by standard checkerboard titration method. The amphotericin B was tested in a concentration range from 0.156 to 2.5 µg/mL while the concentration ranges of all the other compounds varied from 7.81 to 125 µg/mL. The cell concentration in each well was 4 x 10^4 cell/mL. After the incubation for 48 h at 30 °C, the optical density of the cultures was detected at 620 nm

Table 2. Antifungal activity of the compounds

Species	Minimal inhibitory concentrations (µg/mL)				
	amphotericin B	amantadine	chlorpromazine	trifluoperazine	valproic acid
Cr. neoformans IFM 5844	0.625	>500	125	62.5	>500
Cr. neoformans IFO 410	0.625	>500	62.5	62.5	>500
Cr. neoformans SZMC 26851	0.625	>500	125	62.5	>500
Cr. neoformans SZMC 26852	0.625	>500	125	62.5	>500
Cr. neoformans IFM 48637	0.625	>500	125	62.5	>500

Table 3. Interaction ratios between amphotericin B and amantadine, chlorpromazine, trifluoperazine and valproic acid after 48-h incubation at 30 °C

	Drugs	Strains				
		IFM 5844	IFO 410	SZMC 26851	SZMC 26852	IFM 48637
AMB +	amantadine	0.93 ADD	1.04 ADD	0.82 ADD	0.70 ADD	0.92 ADD
	chlorpromazine	0.94 ADD	1.04 ADD	0.85 ADD	0.88 ADD	0.97 ADD
	trifluoperazine	1.29 ADD	1.02 ADD	1.51 SYN	1.29 ADD	1.09 ADD
	valproic acid	1.07 ADD	0.86 ADD	1.88 SYN	1.12 ADD	1.55 SYN

AMB: amphotericin B; ADD: additive interaction; SYN: synergistic interaction

in SPECTROstar Nano plate reader (BMG LabTech, Offenburg, Germany). The MIC was determined for each compound alone and in combinations. The experiments were carried out at least three times always in triplicates.

Data analysis

For calculation of the inhibition rates, the absorbencies of the untreated control cultures were assumed to be 100% growth in each case. Expected efficacy of each combination was determined by the Abbott formula: $I_e = X + Y - (XY/100)$, where I_e is the expected percent inhibition for a given interaction, and X and Y are the percent growth inhibited by the compounds when used alone. The nature of interaction of these antifungal compounds was determined by the interaction ratios (IRs), which were computed as $IR = I_o/I_e$ (I_o, observed percent inhibition). IRs between 0.5 and 1.5 represent additive interactions, ratios of >1.5 represent synergistic interaction, and ratios of <0.5 represent antagonistic interactions.

Results

Antifungal activity of the tested drugs

The antifungal activities are summarised in Table 2. All the examined strains were slightly susceptible to the drugs. Among the non-antifungal compounds, the MIC of trifluoperazine proved the lowest: 62.5 μg/mL. Chlorpromazine showed the same MIC (62.5 μg/mL) for *C. neoformans* IFO 410 strain, all the other strains were less susceptible, as the MIC was 125 μg/mL in that case. The MIC of amantadine and valproic acid could not be established as it was out of the applied concentration range. The MIC of amphotericin B was 0.625 μg/mL for each strain.

Interaction between amphotericin B and the non-antifungal compounds

Positive interactions were detected between the amphotericin B and each compound. All the tested drugs augment the effectiveness of the amphotericin B against *C. neoformans* strains as additive and synergistic interactions occurred between them (Table 3). Using *C. neoformans* SZMC 26851 as susceptible strain synergism was detected combining amphotericin B either with valproic acid or trifluoperazine. Valproic acid and amphotericin B combination showed synergistic interaction against IFM 48637 strain too. All the other combinations demonstrated additive interactions between amphotericin B and the drugs against the tested strains.

Discussion

Cryptococcosis is a world-wide infectious disease associated mainly with immunodeficient hosts. The disease most commonly manifests as cryptococcal meningitis. However, pulmonary and primary cutaneous cryptococcosis also exist (Sloan and Parris 2014). As other invasive fungal infections, cryptococcosis is associated with high morbidity and mortality rate. Particularly the treatment of cryptococcal meningoencephalities affecting the central nervous system is difficult because amphotericin B having significant role in the treatment penetrates poorly across the blood brain barrier due to its relatively high molecular weight (Nau et al. 2010). Additional problem is the low accessibility of the other recommended drug, flucytosine (Loyse et al. 2013).

The in vitro broad-spectrum activity of non-antifungal compounds against human pathogenic fungi was published earlier (Judd and Martin 2009). Testing the activity of phenothiazines such as chlorpromazine and trifluoperazine against medically important yeasts such as *C. neoformans* proved that it is one of the most susceptible species (Eilam et al. 1987). Although, the anti-*Cryptococcus* activity of these compounds has been established earlier, their interaction with amphotericin B was not investigated. In this present study, the in vitro action of chlorpromazine, trifluoperazine, valproic acid and amantadine individually and in combination with amphotericin B were studied. The results showed that all the examined compounds possess antifungal activ-

ity as they slightly reduced the growth of *C. neoformans* strains when applied alone. Trifluoperazine was the most efficient drug as it had the lowest MIC against all the five strains involved in this study. The drugs and amphotericin B established additive or synergistic interactions as in combination with amphotericin B they achieved more effective growth inhibition than being used alone. Amphotericin B in combination with the studied drugs attained more efficient growth reduction in lower concentrations than used alone.

The positive interaction between the drugs and amphotericin B can be explained by the ability of amphotericin B to bind to the ergosterol and forming pores in the fungal cell membrane (Gallis et al. 1990). Non-antifungal agents could enter the cells via these pores and could exert their activity within the fungal cell. Amantadine, chlorpromazine, trifluoperazine and valproic acid accumulates in the central nervous system and there is potential to apply them in combination with amphotericin B in the treatment of *Cryptococcus*-caused meningoencephalitis.

Acknowledgements

This work was supported by the Hungarian Government and European Union through grant GINOP-2.3.2-15-2016-00012. It is also connected to the project GINOP-2.3.3-15-2016-00006 (Széchenyi 2020 Programme) providing infrastructural development.

References

Afeltra J, Verwe PE (2003) Antifungal activity of nonantifungal drugs. Eur J Clin Microbiol Infect Dis 22:397-407.

Blanpied TA, Clarke RJ, Johnson JW (2005) Amantadine inhibits NMDA receptors by accelerating channel closure during channel block. J Neurosci 25(13):3312-3322.

Chaillot J, Tebbji F, García C, Wurtele H, Pelletier R, Sellam A (2017) pH-dependant antifungal activity of valproic acid against the human fungal pathogen *Candida albicans*. Front Microbiol 8:1956. doi: 10.3389/fmicb.2017.01956.

Day JN, Chau TTH, Wolbers M, Mai PP, Dung NT, Mai NH, Phu NH, Nghia HD, Phong ND, Thai CQ, Thai LH, Chuong LV, Sinh DX, Duong VA, Hoang TN, Diep PT, Campbell JI, Sieu TPM, Baker SG, Chau NVV, Hien TT, Lalloo DG, Farrar JJ (2013) Combination antifungal therapy for cryptococcal meningitis. N Engl J Med 368(14):1291-1302.

Eilam Y, Polacheck I, Ben Gigi G, Chernichovsky D (1987) Activity of phenothiazines against medically important yeasts. Antimicrob Agents Chemother 31(5):834-836.

Gallis HA, Drew RH, Pickard WW (1990) Amphotericin B: 30 years of clinical experience. Rev Infect Dis 2(2):308-329.

Göttlicher M (2004) Valproic acid: an old drug newly discovered as inhibitor of histone deacetylases. Ann Hematol 83(Suppl 1):S91-92.

Homa M, Galgóczy L, Tóth E, Tóth L, Papp T, Chandrasekaran M, Kadaikunnan S, Alharbi NS, Vágvölgyi Cs (2015) In vitro antifungal activity of antipsychotic drugs and their combinations with conventional antifungals against *Scedosporium* and *Pseudallescheria* isolates. Med Mycol 53:890-895.

Judd WR, Martin CA (2009) Antifungal activity of nontraditional antifungal agents. Curr Fungal Infect Rep 3(2):86-95.

Kohler JR, Casadevall A, Perfect J (2015) The spectrum of fungi that infects humans. Cold Spring Harb Perspect Med 5:a019273.

Loyse A, Bicanic T, Jarvis JN (2013) Combination antifungal therapy for cryptococcal meningitis. N Engl J Med 368(26):2522.

Nau R, Sörgel F, Eiffert H (2010) Penetration of drugs through the blood-cerebrospinal fluid/blood-brain barrier for treatment of central nervous system infections. Clin Microbiol Rev 23(4):858-883.

Nyilasi I, Kocsubé S, Galgóczy L, Papp T, Pesti M, Vágvölgyi Cs (2010) Effect of different statins on the antifungal activity of polyene antimycotics. Acta Biol Szeged 54(1):33-36.

Sloan D, Parris V (2014) Cryptococcal meningitis: epidemiology and therapeutic options. Clin Epidemiol 6:169-182.

Srikanta D, Santiago-Tirado FH, Doering TL (2014) *Cryptococcus neoformans*: Historical curiosity to modern pathogen. Yeast 31(2):47-60.

Warkentien T, Crum-Cianflone NF (2010) An update on cryptococcosis among HIV-infected persons. Int J STD AIDS 21(10):679-684.

Wood NC, Nugent KM (1985) Inhibitory effects of chlorpromazine on *Candida* species. Antimicrob Agents Chemother 27(5):692-694.

Acta Biologica Szegediensis

Volume 63(2):185-193, 2019
Acta Biologica Szegediensis
http://abs.bibl.u-szeged.hu/index.php/abs

DOI:10.14232/abs.2019.2.185-193

ARTICLE

Vegetative anatomy of *Tabernaemontana alternifolia* L. (Apocynaceae) endemic to southern Western Ghats, India

Yuvarani Seenu, Koshila Ravi Ravichandran, Anaswara Sivadas, Balachandar Mayakrishnan*, Muthukumar Thangavelu

Root and Soil Biology Laboratory, Department of Botany, Bharathiar University, Coimbatore 641 046, Tamil Nadu, India

ABSTRACT The anatomical description of vegetative parts of *Taberenaemontana alternifolia* L. belonging to the family Apocynaceae was investigated in the present study. The leaves of *T. alternifolia* is hypostomatic with paracytic stomata, uniseriate epidermis made up of thin-walled parenchymatous cells covered by thin cuticle on both adaxial and abaxial surfaces. The hypodermis comprises of angular collenchyma cells. Mesophyll is dorsiventral containing silica bodies and vascular bundles are bicollateral. The petiole is flattened adaxially and arch-shaped abaxially with a uniseriate epidermis covered by a thin cuticle. The hypodermis is 7-8 layered angular collenchyma cells consisting of laticifers and parenchymatic, cortical layers consisting of silica bodies and thick-walled fibers and U-shaped bicollateral vascular bundles. Secondary growth in stems is characterized by the formation of periderm and thick-walled fibers in the vascular tissues. Bicollateral vascular bundles are covered by sclerenchymatous patches, parenchymatous cortex and pith consist of fibers, laticifers and silica bodies. The root possess unicellular root hairs, compactly arranged thin-walled uniseriate epidermis, 16-18 layered cortex containing silica bodies and fibers, indistinct endodermis, radially arranged vascular bundles and 14-16 arched xylem. Pitted water-storage cells are present in the conjunctive tissue. Lignin deposition was observed in the root stelar region and pith is absent.
Acta Biol Szeged 63(2):185-193 (2019)

KEY WORDS
anatomical features
collenchymas
fibers
laticifers
secondary growth

ARTICLE INFORMATION
Submitted
23 August 2019.
Accepted
13 November 2019.
***Corresponding author**
E-mail: mbalachandar241055@gmail.com

Introduction

The genus *Tabernaemontana* belonging to the family Apocynaceae comprises of around 102 species occurring throughout the tropical and also in some subtropical regions of the world (Van Beek et al. 1984). *Tabernaemontana* includes shrubs or small deciduous trees bearing white latex, dichotomously branched stem and opposite leaves. *Tabernaemontana alternifolia* L. (= *Tabernaemontana heyneana* Wall) is a small tree growing up to 8 m tall and produce milky white latex (Ignacimuthu et al. 2006). It is commonly found in open forests of Western Ghats from Maharashtra to Kerala at an elevation of 900 m (Sathishkumar et al. 2012) and it is endemic to southern Western Ghats (Manasa and Chandrashekar 2015). Typically, this species is considered to be a potential medicinal plant as it possesses antimicrobial activity, antioxidant and is used in the treatment of the nervous disorder, diabetics, chronic bronchitis, lymphocytic leukaemia, snake bite; respiratory and skin problems (Sukumaran and Raj 2008; Sathishkumar and Baskar 2012). Besides these medicinal uses, *T. alternifolia* also consists of several secondary metabolites including alkaloids, flavonoids, steroids, tannins, glycosides and resins (Srivastava et al. 2001; Roy et al. 2002; Sathishkumar et al. 2008).

Anatomical investigations help in understanding the phylogenetic interactions as well as the physiological progression (Yeung 1998; Liu and Zhu 2011) and support in the identification of plants when floral characteristics are unavailable (Dengler 2002). The anatomy of vegetative parts of certain species of Apocynaceae has been examined. However, most of these studies have examined only the foliar anatomy and the stem and root anatomy of Apocynaceae is not well studied. Duarte and Larrosa (2011) examined the anatomical features of leaf and stem in *Mandevilla coccinea* (Hook & Arn.) Woodson and reported uniseriate epidermis with thick and striate cuticle, paracytic stomata on both the leaf surfaces, dorsiventral mesophyll and collateral vascular bundles in leaves; and cambium formation, sclerenchymatous sheath with non-lignified fibers, bicollateral vascular bundles, large parenchymatous pith with amyloplasts in the stem; and occurrence of laticifers and phenolic compounds in both stem and leaf. A comparative study on the anatomical characters of *Nerium oleander* L. and *Catharanthus roseus*

(L.) G. Don leaf by Abdalla et al. (2016) revealed that the dorsiventral leaf consisted of a single-layered epidermis with sparse epidermal hairs in *C. roseus* and isobilateral leaves, four-layered epidermis bearing numerous epidermal hairs, presence of sunken stomata and calcium oxalate crystals in *N. oleander*.

Although literature is available on the morpho-anatomical features of leaf and stems of various genus of Apocynaceae (Rio et al. 2005; Larrosa and Duarta 2006; Maciel et al. 2010; Abdalla et al. 2016), anatomical description of the genus *Tabernaemontana* is very limited. Omino (1996) investigated the leaf anatomy 37 species in 26 genera of Apocynaceae including four species of *Tabernaemontana* (*Tabernaemontana pachysiphon* Stapf, *Tabernaemontana elegans* Stapf, *Tabernaemontana stapfiana* Britten, *Tabernaemontana ventricosa* Hochst. ex A.DC) occurring in Africa and observed paracytic stomata in all the examined species, single-layered epidermal cells on both the foliar surfaces except in *T. pachysiphon* (1-2 layered), bifacial mesophyll with numerous intercellular spaces, collenchymatous cells in the ground tissue of midrib, clustered crystals in both the epidermal layer, mesophyll and in the ground tissue of midrib region in *T. ventricosa*; numerous solitary crystals in lower epidermis and star-shaped crystals in palisade layer of *T. pachysiphon* whereas small star-like crystals were reported in phloem parenchyma of *T. stapfiana*. The vascular bundles were deep V-shaped in all four species of *Tabernaemontana* (Omino 1996). The wood anatomy of *Tabernaemontana eglandulosa* Stapf, and *Tabernaemontana siphilitica* (L.f) Leeuwenb., revealed distinct growth rings, vessel grouping in radial multiples, vessels with sporadically double simple perforations, septate fibers with simple to minutely bordered pits and axial parenchyma were either scarce or absent (Lens et al. 2008).

Guidoti et al. (2015) studied the morpho-anatomical characters of *Tabernaemontana catharinesis* A.DC leaves and observed uniseriate epidermis devoid of trichomes, six to seven layers of angular collenchyma, thin-walled parenchymatous cortex, and bicollateral vascular bundle. *Tabernaemontana catharinesis* stem possessed uni-stratified epidermis, angular collenchyma cells and fibers in the cortical region and the secondary growth revealed the presence of periderm and fibers in external phloem patches. The petiole in *T. catharinesis* had uni-stratified epidermis, thick cuticle, and angular collenchyma adjacent to the epidermis and bicollateral vascular arrangement (Guidoti et al. 2015). As *T. alternifolia* is an endemic plant with high medicinal value, it is important to conserve this species through various means including vegetative propagation. Therefore, anatomical investigation of vegetative parts like leaf, stem and root could be helpful in understanding the regeneration of the plant during vegetative propagation. In addition, information on vegetative anatomy of *Tabernaemontana* species is scanty. Therefore, the present study was carried out to investigate the vegetative characters including the leaf, petiole, stem and root in *T. alternifolia*.

Material and methods

Samples of leaf, stem, and roots were collected from mature plants of *T. alternifolia* during the month of February 2019 from Nadugani, Gudalur taluk of Nilgiri district, Tamilnadu, India. The latitude and longitude of the study site are 11.4718° N to 76.4107° E at an elevation of ~ 1000 m a.s.l., and the average rainfall is 2020 mm. The plant specimens were authenticated by Botanical Survey of India, Southern circle and a voucher was deposited in the Bharati Herbarium, Department of Botany, Bharathiar University, Coimbatore, India (accession number: 007744). The collected plant samples were transferred to the laboratory by placing the samples in an ice-box. The plant materials were washed with distilled water and preserved in formalin-acetic acid-alcohol (FAA) solution until processing. The leaf and petiole sections were taken from the fully developed 5th leaf from the top. Stem sections were taken at the 5th internode from the shoot tip and root sections were taken from 5cm from the root tip. The preserved material (leaf, stem, petiole and root) of *T. alternifolia* were freehand sectioned using a sharp razor blade for the histological observations using different types of stains like safranin, phloroglucinol-HCl, and toluidine blue O to identify the cell inclusions such as cutin, suberin and lignin (Gurav et al. 2014). Around 1 cm square leaf pieces were placed in Jeffrey's maceration solution for 72 hours at 35 °C for the observation of the epidermal layer (Kigkr 1971). The specimens in Jeffrey's fluid were later washed, stained with safranin and examined under an Olympus BX51 light microscope attached with a fluorescence setup (Olympus, U- RFL-T, U-25 ND 25 neutral density filter).

A calibrated ocular scale was used to measure the dimensions of the cells and the size of the different regions in the sections. The variables measured include the thickness of cuticle, the pore size of stomata, the length and width of the epidermis, collenchyma cells, palisade and spongy parenchyma cells, cortex, sclerenchymatous fibers and vascular bundles and pith cells. Images and autofluorescence of the observed specimens were captured with a ProgRes3 camera fitted to the Olympus BX 51 light microscope. The stomatal index (SI %) was calculated according to Salisbury (1927) using the formula (S/S+E) × 100 where S and E denotes the number of stomata and epidermal cells respectively. All the observations are

presented either as an average value or range (minimum value and maximum values) or average ± standard error. Two dimensional values are presented as length × breadth.

Results

Leaf

Leaves are hypostomatic containing stomata only on abaxial surface and the adaxial surface is devoid of stomata (Fig. 1a,b). The stomata are of the paracytic type with two subsidiary cells parallel to the guard cells (Fig.1c). The cell dimensions of subsidiary cells and guard cells are respectively 26.75 ± 0.91 × 10.5 ± 0.89 µm and 22.75 ± 1.17 × 7.5 ± 0.64 µm. The stomatal pore measures 13.5 ± 0.55 × 2.75 ± 0.25 µm. The leaf consists of both adaxial and abaxial epidermis covered by a thin cuticle. The cuticle on the adaxial surface (5 µm) is 25.85% thicker than the cuticle on the abaxial surface (3 µm). The average stomatal index is 8.76%. The upper and lower epidermis is uniseriate, consisting of a compactly arranged square to rectangular thin-walled parenchymatous cells (Fig. 1g). The length and width of epidermal cells of the upper and lower surface of the leaves are respectively 16.20 ± 0.43 × 25.62 ± 0.74 µm and 18.08 ± 0.45 × 24 ± 0.62 µm. Hypodermis on the abaxial surface is 5-6 layered and is composed of angular collenchyma cells whereas on the adaxial side, hypodermal cells are 7-8 layered (Fig. 1e). The adaxial and abaxial collenchyma cells measures 16.20 ± 0.43 × 25.62 ± 0.73 µm and 20.6 ± 1.17 × 15.66 ± 0.82 µm, respectively. The mesophyll is dorsiventral differentiated into palisade and spongy parenchyma cells. The palisade parenchyma is 2-3 layered and composed of thin-walled parenchymatous cells measuring 16.5 ± 1.18 × 11.75 ± 0.65 µm. The palisade parenchyma is followed by 8-10 layered spongy parenchyma cells bearing large intercellular spaces. The length and width of spongy parenchyma cells are 23.5 ± 1.79 × 20.75 ± 1.13 µm. Silica bodies are present in both palisade and spongy parenchyma cells. In cross-section, the leaf midrib is biconvex. A sub-epidermal layer comprising of 14-18 layered thin-walled parenchyma cells are observed on both adaxial and abaxial sides (Fig. 1d). This region is characterized by the presence of thick-walled fibers (Fig. 1h), lactiferous cells and silica bodies. A V-shaped bicollateral vascular bundle is present in the midrib region. Xylem consists of metaxylem and protoxylem vessels. The metaxylem and protoxylem cells measures 30.5 ± 0.78 × 25.25 ± 0.53 µm and 14.12 ± 0.32 × 14.37 ± 0.39 µm, respectively. The protoxylem is oriented towards the upper epidermis and metaxylem is located towards the lower epidermis. Xylem is surrounded by internal and external phloem (Fig. 1f). The internal phloem forms a continuous strand (Fig. 1i) whereas, the external phloem appears as patches or small groups (Fig. 1j). The xylem arches range between 40 and 43.

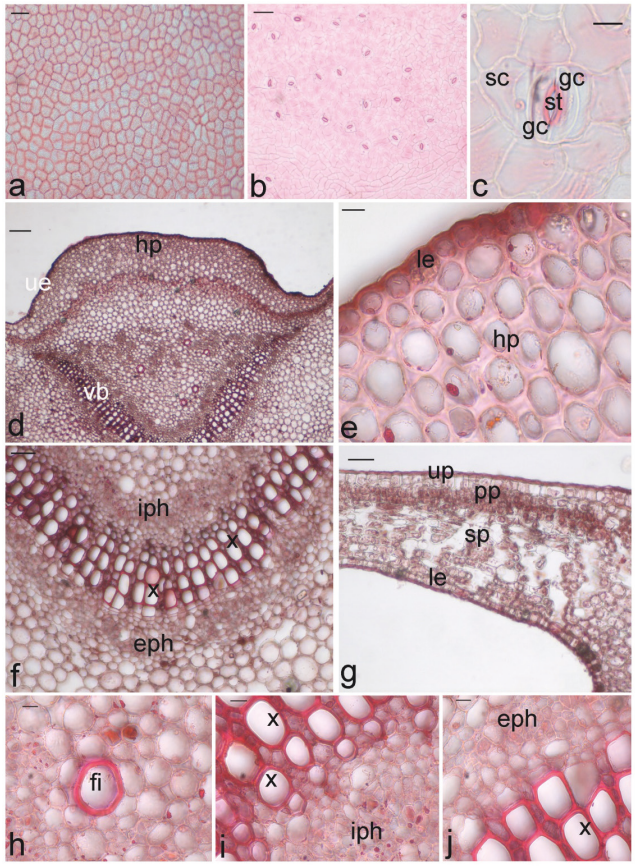

Figure 1. Vegetative anatomy of *Tabernaemontana alternifolia* leaf (a-j). **a**. Epidermal peeling of the adaxial surface of the leaf; **b**. Abaxial surface showing the distribution of stomata; **c**. Stomata with guard cells arranged parallel to the subsidiary cells; **d**. Transverse section (T.S.) of leaf along the midrib region showing upper epidermis, hypodermis and vascular bundle; **e**. Lower epidermis covered by a thin cuticle, and collenchymatous hypodermis; **f**. Bicollateral vascular bundles, xylem surrounded by internal phloem and external phloem; **g**. Leaf lamina uniseriate upper epidermis, lower epidermis, palisade parenchyma and spongy parenchyma; **h**. Thick-walled fibers; **i**. Internal phloem adjacent to xylem cells; **j**. External phloem and xylem.

st = stomata, gc = guard cell, ue = upper epidermis, hp = hypodermis, vb = vascular bundle, le = lower epidermis, x = xylem, iph = internal phloem, eph = external phloem, pp = palisade parenchyma, sp = spongy parenchyma, fi = sclerenchymatous fiber. Scale bars = 50 µm.

Petiole

The petiole is a flattened arch and lightly winged at the edges on the adaxial side in transverse section. The epidermis is single-layered with a compactly arranged round to oval thin-walled parenchymatous cells measuring 15.3 ± 0.56 × 11.2 ± 0.25 µm and covered by 2-3 µm thick smooth cuticle (Fig. 2a). The hypodermis is a continuous band of 7-8 layered angular collenchyma cells measuring

35.75 ± 2.29 × 28 ± 2.49 µm (Fig. 2c). Laticifers occur in the hypodermis. Around 12-16 cell layers of thin-walled parenchyma cells enclosing triangular or rectangular intercellular spaces subtends the hypodermis (Fig. 2b). Silica bodies and thick-walled fibers are present in the parenchymatic layer (Fig. 2d). The length and width of the parenchyma cells are 42.25 ± 3.90 × 43.5 ± 2.83 µm. Vascular bundles are bicollateral and U-shaped. Xylem consists of protoxylem and metaxylem that measures 24.5 ± 1.29 × 22.5 ± 0.55 µm and 11.25 ± 0.55 × 11.5 ± 0.85 µm, respectively. The protoxylem is oriented towards the epidermis. Xylem is surrounded by small patches of external and internal phloem (Fig. 2e,f). The external phloem patches measures 44.25 ± 2.07 × 47.25 ± 4.17 µm and the internal phloem patches measure 37.75 ± 2.09 × 39 ± 2.77 µm.

Stem

The stem is circular in outline (Fig. 3a). The cuticle is smooth and 4-5 µm thick. The periderm is three-layered forming an outer layer and consists of loosely arranged thin-walled parenchymatous cells. The hypodermis is composed of 5-6 layers of angular collenchyma cells measuring16.3 ± 0.50 × 14.15 ± 0.37 µm. Idioblasts comprising of phenolic compounds are observed in the collenchymatic hypodermis (Fig. 3b). The parenchymatous cortex is 11-13 layered with cells measuring 30.25 ± 0.72 × 30.2 ± 0.84 µm. Non-articulated laticifers, silica bodies and thick-walled fibers occur in the parenchymatic cortical cells which enclose triangular or rectangular or squarish intercellular spaces (Fig. 3c-e). The sclerenchymatous fibrous patches surrounding the vascular bundles are irregular and measures 67.7 ± 2.30 × 64.1 ± 2.33 µm and cells with lignin thickened walls (Fig. 3f).

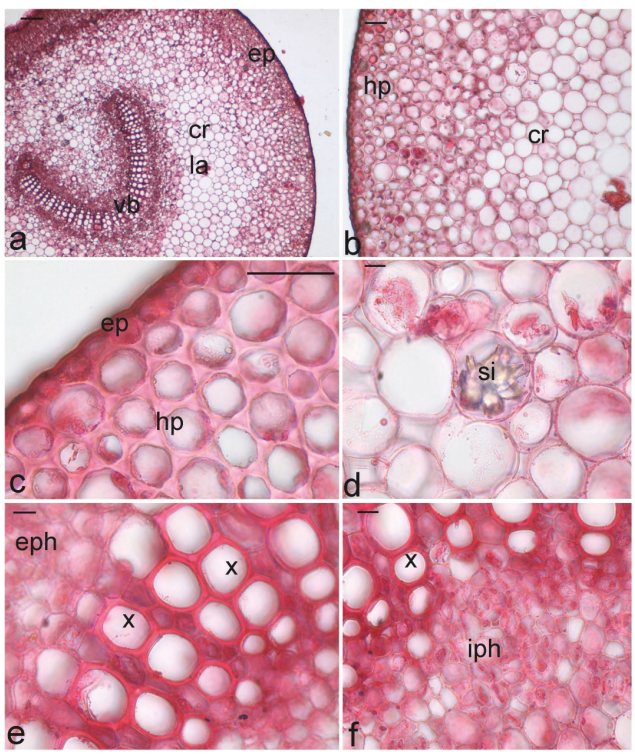

Figure 2. Vegetative anatomy of *Tabernaemontana alternifolia* petiole (a-f). **a**. Transverse section (T.S.) of petiole showing epidermis, cortex, laticifers and U-shaped vascular bundle; **b**. hypodermis and cortex; **c**. Uniseriate epidermis and hypodermis; **d**. Silica bodies in the cortical region, **e**,**f**. Vascular bundle showing xylem bordered by external phloem and internal phloem.

ep = epidermis, cr = cortex, la = laticifers, vb = vascular bundles , hp = hypodermis, si = silica bodies, eph = external phloem, iph = internal phloem, x = xylem. Scale bars = 50 µm.

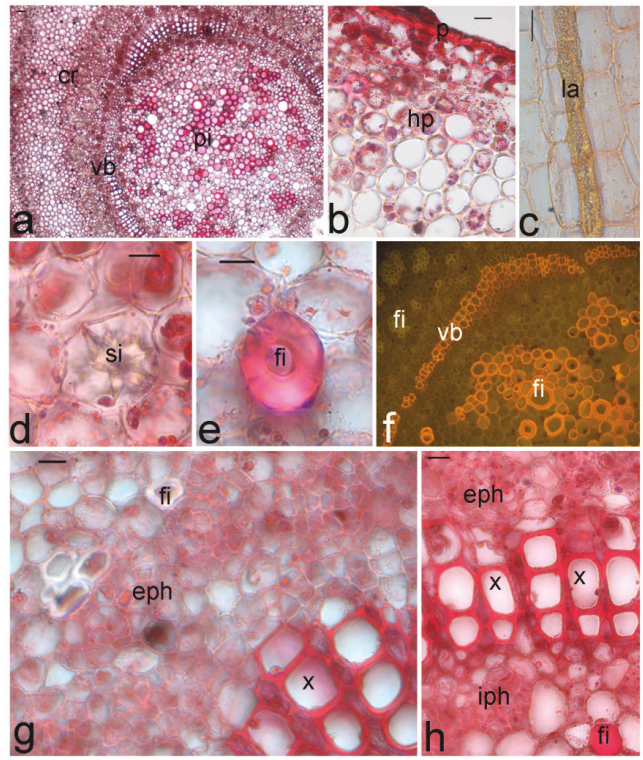

Figure 3. Vegetative anatomy of *Tabernaemontana alternifolia* stem (a-h). **a**. Transverse section (T.S.) of the stem showing periderm, bicollateral vascular bundle and pith; **b**. Periderm and hypodermis made up of angular collenchyma cells; **c**. Longitudinal section (L.S) of the stem showing non- articulated laticifers; **d**. Silica bodies in cortex; **e**. Thick-walled sclerenchymatous patches and fibers; **f**. Fluorescent image showing deposition of lignin in vascular bundles, sclerenchymatous fibers and sclerenchymatous fibers patches; **g**. Vascular bundles with xylem enclosed by external phloem and sclerenchymatous fibers; **h**. Xylem covered by external phloem and internal phloem and fibers in the pith region.

p = periderm, vb = vascular bundle, hp = hypodermis, la = laticifers, si = silica bodies, fi = sclerenchymatous patches and fibers, x = xylem, eph = external phloem, iph = internal phloem, pi = pith. Scale bars = 50µm.

The vascular bundles are bicollateral and oval-shaped. The cambial zone consists of 2-3 rows of thin-walled small rectangular and meristematic cells arranged radially. The external and internal phloem are arranged in small groups or patches adjoining the xylem (Fig. 3g,h). The internal and external phloem patches measures 34.5 ± 1.95 × 38.5 ± 1.95 µm and 38.33 ± 1.51 × 48.33 × 2.01 µm, respectively. The vessels of the metaxylem measure 41.95 ± 0.86 × 32.2 ± 0.65 µm and the protoxylem cells measure 20.1 ± 0.68 × 14.9 ± 0.47 µm. Pith is composed of thin-walled parenchyma cells with intercellular spaces. Fibers, laticifers and silica bodies occur in the pith region (Fig. 3a). The pith cells measure 50.5 ± 5.51 × 53.83 ± 6.11 µm. The anatomical features of the mature stem are almost similar to that of the young stem except with few differences. The epidermal layer forms the outer layer in young stems and sclerenchymatous sheath consisting of fibers around the stellar region in mature stems is absent in the young stems. Moreover, the epidermis in young stem is replaced by the periderm in the older stems.

Root

The root appears circular in transverse section (Fig. 4a). Unicellular root hairs are present. The root hair measures 45.5 ± 3.6 × 12.6 ± 0.45 µm. The epidermis is uniseriate, compactly arranged, and composed of oval to round shaped thin-walled parenchymatous cells (Fig. 4b). The cell dimensions of epidermal cells are 33.66 ± 2.24 × 39.23 ± 2.38 µm. Cortex is 16-18 layered, made up of thin-walled larger to smaller circular to oval-shaped parenchymatic cells enclosing triangular or squarish intercellular space. The cells in the cortical region measure 36.45 ± 1.26 × 44.83 ± 2.03 µm. Silica bodies and thick-walled fibers occur in the cortex (Fig. 4a). The length and width of fibers are 36.66 ± 2.24 × 39.23 ± 2.38 µm. Endodermis and pericycle are indistinct. Vascular bundles are arranged radially. Xylem is exarch. Xylem and phloem cells are differentiated by conjunctive tissue made up of parenchymatous cells (Fig. 4e). Xylem arches are 14-16 and the stele bears pitted water storage cells, and cells with lignin thickened walls (Fig. 4d,f). The water-storage cells measure 17.00 ± 1.27 × 11.05 ± 0.87 µm. Pith is absent.

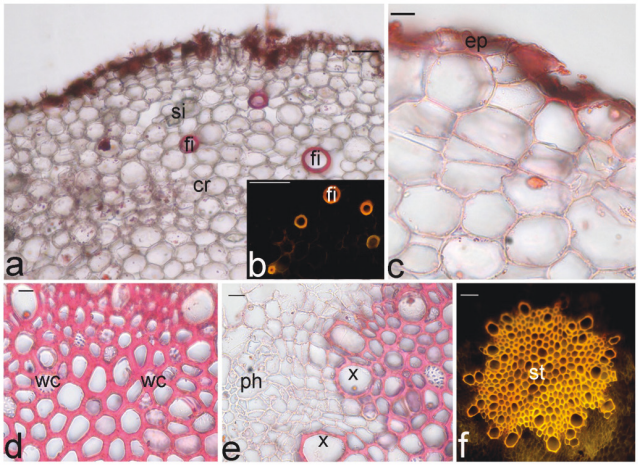

Figure 4. Vegetative anatomy of *Tabernaemontana alternifolia* root (a-f) **a**. Transverse section (T.S.) of root showing epidermis, sclerenchymatous fibers, silica bodies in the cortex **b**. Fluorescent image (insert) showing deposition of lignin in sclerenchymatous fibers, **c**. Epidermis, **d**. Pitted water-storage cells in the stelar region, **e**. vascular bundles with xylem and phloem, **f**. Fluorescent image of stele indicating the presence of lignin deposition. Scale bars = 50 µm.

ep = epidermis, fi = sclerenchymatous fiber, si = silica bodies, cr = cortex, wc = water-storage cells, x = xylem, ph = phloem, st = stele. Scale bars = 50 µm.

Discussion

The vegetative anatomy of *T. alternifolia* revealed certain variations in their anatomical traits when compared to other members of the Apocynaceae family. Trichomes are absent in leaves of *T. alternifolia* as reported in other species of *Tabernaemontana* (Omino 1996; Guidoti et al. 2015). However, trichomes have been reported in members of the Apocynanceae like *Mandevilla velutina* (A.DC.) Woodson and *N. oleander* (Santos et al. 2009; Maciel et al. 2010). The hypostomatic leaves and paracytic stomata in *T. alternifolia* are similar to those reported by Omino (1996) in *T. stapfiana, T. pachysiphon, T. ventricosa* and *T. elagans*. However, in contrast to the observation of the present study, amphistomatic leaves were reported in *T. catharinensis* (Guidoti et al. 2015) and *M. coccinea* (Durate and Larrosa 2011). The presence of stomata on the abaxial surface of the leaf in *T. alternifolia* helps to minimize the water loss (Mbagwu et al. 2008). Moreover, paracytic type of stomata is the characteristic feature of the genus *Tabernaemontana* (Metcalfe and Chalk 1950, 1988; Omino 1996). The stomatal index of 73.42% in *T. alternifolia* is less than that of the stomatal index reported in *Tabernaemontana divaricata* (L.) R.Br. ex Roem. & Schult. However special type of stomata called giant stomata is reported in *T. divaricata* (Gowramma and Sultan 2018) is absent in leaves of *T. alternifolia*. The differences in the stomatal index could be due to the physiological responses to various environmental factors (Adegbite 2008; Aworinde et al. 2012). Cuticle acts as an apoplastic barrier against water loss and also prevents the entry of other solutes from external sources into the plant tissue (Yeats and Rose 2013). Leaves of *T. alternifolia* possessed thin-cuticle over the leaf that contradicts studies where a thick cuticle has been reported to cover the leaves in *Tabernaemontana* species (Omino 1996; Guidoti et al. 2015). However, Mayberry (1937) observed thin cuticle covering the leaves of *Amsonia tabernaemontana* Walter. In contrast to the observations

of the present study, a bilayered epidermis covering both the leaf surfaces has been reported in *T. pachysiphon* and *T. stapfiana* (Omino 1996).

The mesophyll is dorsiventral in *T. alternifolia* which is similar to the other members of the Apocynaceae family (Metcalfe and Chalk 1950). The ecological anatomy of the tree species suggested that the degree of mesophyll differentiation mostly depends on the degree of exposure to the sun (Hanson 1917; Ryder 1954). The mesophyll in *T. alternifolia* resembles that of *T. catharinensis* consisting of 2-3 layers of palisade parenchyma cells (Guidoti et al. 2015). On the contrary, palisade parenchyma was 3-4 layered in *T. stapfiana* (Omino 1996). The spongy parenchyma cells in *T. alternifolia* are similar to those of other *Tabernaemontana* species (Omino 1996; Guidoti et al. 2015). Laticifers and crystals present in mesophyll, multilayered hypodermis and bicollateral vascular bundles in *T. alternifolia* are the common characteristic features of Apocynaceae (Matclafe and Chalk 1950; Omino 1996).

The petiole is flattened arch-shaped with small projections in *T. alternifolia* is similar to those observed in *T. catharinensis*. Nevertheless, concave-convex structured petiole was reported in *Forsteronia glabrescens* Müll.Arg. and *M. coccinea* of Apocynancea family (Larrosa and Duarte 2006; Durate and Larrosa 2011). The presence of non-lignified fibers in *F. glabrescens* adjacent to the internal phloem is in accordance with the observations of the present study (Larrosa and Duarte 2006). Angular collenchyma cells present in the hypodermal region of *T. alternifolia* is similar to those in *T. catharinensis* (Guidoti et al. 2015) and contrastingly, annular collenchyma was noted in *M. coccinea* (Duarte and Larrosa, 2011). Silica bodies and laticifers observed in *T. alternifolia* are similar to those of *T. catharinensis*. The presence of silica bodies in *T. alternifolia* could prevent from collapsing of the plant during drought (Matcalfe and Chalk 1979). In the present study, vascular bundles are U-shaped and bicollateral. Similar observations were reported in *T. elegans, T. stapfiana* and *T. catharinensis* (Omino 1996; Guidoti et al. 2015). In contrast to the results of the present study, V-shaped, shallow and curved arc-shaped bicollateral vascular bundles were reported in *Himatanthus sucuuba* (Spruce ex Müll.Arg.) Woodson, *Voacanga thouarsii* Roem. & Schult., *Rauvolfia mombasiana* Stapf and *Strophanthus barteri* Franch (Larrosa and Duarte 2005; Omino 1996).

The secondary growth in *T. alternifolia* stem reveals the formation of the periderm in the outermost layer that is in line with the observations of Larrosa and Duarte (2006) and Guidoti et al. (2015) in *H. sucuuba* and *T. catharinensis.* Nevertheless, an incipient secondary growth in *M. coccinea* stem possessed single-layered epidermis covered with thick striated cuticle (Duarte and Larrosa, 2011). Periderm forms a protective tissue during the secondary growth replacing the epidermis (Evert 2006). The angular collenchyma cells, sclerenchymatous sheath consisting of lignified thick-walled fibers enclosing the vascular bundles in *T. alternifolia* is as same as *T. catharinensis* (Guidoti et al. 2015). The thick-walled fibers commonly found in patches, provides rigidity and flexibility to the plants (Esau 1974; Costa et al. 2006; Scatena and Scremin-Dias 2006). Similar to *T. alternifolia*, the stem of *T. catharinensis* in transverse section showed the presence of fibers and laticifers in the cortical region (Guidoti et al. 2015). Moreover, the distribution of laticifers differs among the species, for example, laticifers occur only in the cortex in *Himatanthus lancifolius* (Müll.Arg.) Woodson (Baratto et al. 2010a) whereas, in *Rauvolfia sellowii* Stapf, it was reported in the phloem cells and marrow (Baratto et al. 2010b). The laticifers produce latex due to physical damage and consist of varied latex compounds that protect the plants against herbivores or pathogens (Ramos et al. 2019). Occurrence of laticifers is very common in Apocynaceae family (Metcalf and Chalk 1950) and may be branched or unbranched or non-articulated (Esau 1977; Mahlberg 1993). Laticifers in the *T. alternifolia* are non-articulated as observed in *Tabernaemontana coronaria* Willd (Rao and Malaviya 1966). However, articulated laticifers have been reported in the other member of Apocynaceae like *T. catharinensis* (Canaveze and Machado 2016), *Mandevilla atroviolacea* (Stadelm.) Woodson (Lopes et al. 2009) and *Allamanda blanchetii* A. DC. (Gama et al. 2017)

Silica bodies were present in cortex and pith regions of *T. alternifolia*. However, the idioblasts containing silica bodies were not observed in *T. catharinensis* (Guidoti et al. 2015). Contrastingly to the observations of *T. alternifolia* in the present study, starch grains were reported in some species of Apocynaceae (El-Kashef et al. 2015; Duarte and Larrosa 2011). The intraxylary or internal phloem in *T. alternifolia* is a common feature of Apocynaceae family. In the present study, internal phloem existed as an isolated strand forming a group of patches similar in other species of the family, like *A. tabernaemontana* (Mayberry 1937) and *M. coccinea* (Larrosa and Duarte 2011). In contrast to the results of the present study, internal phloem formed a continuous ring in *N. oleander* (Maciel et al. 2010). According to Metcalfe and Chalk (1950), internal phloem commonly occurs in a continuous ring or isolated groups in the Apocynaceae. The function of internal phloem in stems of climbers includes prevention of breakage when stems are coiled or twisted and enhance the mechanical flexibility of stems (Sckench 1893). However, in trees Premakumari et al. (1985) reported that internal phloem help in the translocation of photosynthates. Therefore, the presence of internal phloem in *T. alternifolia* stem may also perform certain functions like translocation of growth substances.

The anatomy of the root in Apocynaceae is relatively less explored when compared leaves and petiole. *Tabernaemontana alternifolia* had uniseriate epidermis. The cortex in *T. alternifolia* is 16-18 layered in contrast to *Carissa macrocarpa* (Eckl.) A.DC. where the cortex is only 12-15 layered (Allam et al. 2016). However, the indistinct endodermis of *T. alternifolia* resembles with endodermis reported in *C. macrocarpa*. Starch grains were absent in the roots of *T. alternifolia* as reported in other species of Apocynaceae (Appezzato-da-Glória and Estelita 1997; Boutebtoub et al. 2009; Allam et al. 2016). Laticifers are one of the important characteristic features of Apocynaceae. Nevertheless, in the present study, although, laticifers were observed in leaves, petiole and stem of *T. alternifolia*, it was absent in the roots. Pitted water-storage cells could help *T. alternifolia* during the xerophytic or drought conditions. Vascular bundles are arranged radially in *T. alternifolia*. The pith was absent in *T. alternifolia* root similar to that reported in *C. macrocarpa* (Allam et al. 2016). The lignin deposition in stelar region as supported by the auto fluorescence could also provide additional structural support to the plant (Willemse 1989).

Conclusion

The present study revealed that the presence of paracytic stomata restricted to abaxial surface of the leaf, thin cuticle on adaxial and abaxial side in leaves, thick-walled sclerenchymatous patches, isolated internal phloem strands in stems; water storage cells, and deposition of lignin in root stelar region could contribute to the identification of this endemic plant.

Acknowledgement

We thank Dr. C. Murugan, Director, Botanical Survey of India, Southern Circle, Coimbatore, Tamil Nadu, India for authenticating the specimens and Dr. C. Udhayavani for assistance during plant collection. We thank the University Grants Commission (UGC)–Special Assistance Programme [Ref No:F.5-16/2016/DRS1 (SAP-II)] for providing financial assistance during the course of this work. Yuvarani Seenu thanks DST-PURSE scheme (Phase-II) for the award of Project fellowing (BU/ DST-Purse (II) / APPOINTMENT / 233).

References

Abdalla MM, Eltahir AS, El-Kamali HH (2016) Comparative morph-anatomical leaf characters of *Nerium oleander* and *Catharanthus roseus* family (Apocynaceae). EJBAS 3:68-73.

Adegbite AE (2008) Leaf anatomical studies in some species of the tribe Cichorieae (Asteraceae) in Nigeria. Comp Newsl 46:49-58.

Allam KM, El-Kader AMA, Mostafa MAH, Fouad MA (2016) Botanical studies of the leaf, stem and root of *Carissa macrocarpa*, (Apocynaceae), cultivated in Egypt. J Pharmacogn Phytochem 5:106-113.

Appezzato-da-Glória B, Estelita ME (1997) Laticifer systems in *Mandevilla illustris* and *Mandevilla velutina* Apocynaceae. Acta Soc Bot Pol 66:301-306.

Aworinde DO, Ogundairo BO, Osuntoyinbo KF, Olanloye OA (2012) Foliar epidermal characters of some Sterculiaceae species in Nigeria. Bayero J Pure Appl Sci 5 48-56.

Baratto LC, Hohlemwerger SVA, Guedes MLS, Duarte MR, Santos CAM (2010a) *Himatanthus lancifolius* (Müll. Arg.) Woodson, Apocynaceae: estudo farmacobotânico de uma planta medicinal da Farmacopeia Brasileira 1ª edição. Rev Bras Farmacogn 20:651-658.

Baratto LC, Duarte MDR, Santos CADM (2010b) Pharmacobotanic characterization of young stems and stem barks of *Rauvolfia sellowii* Müll. Arg., Apocynaceae. Braz J Pharm Sci 46:555-561.

Boutebtoub W, Chevalier M, Mauget JC, Sigogne M, Morel P, Galopin G (2009) Localizing starch reserves in *Mandevilla sanderi* (Hemsl.) Woodson using a combined histochemical and biochemical approach. J Am Soc Hortic Sci 44:1879-1883.

Canaveze Y, Machado SR (2016) The occurrence of intrusive growth associated with articulated laticifers in *Tabernaemontana catharinensis* A. DC., a new record for Apocynaceae. Int J Plant Sci 177:458-467.

Costa CG, Callado CH, Coradin VTR, Carmello-Guerreiro SM (2006) Xilema. In Appezzato-da-Glória B, Carmello-Guerreiro SM, Orgs., Anatomia Vegetal. Viçosa, Editora da UFV. 129-154.

Dengler NG (2002) An integral part of botany. Am J Bot 89:369-374.

Duarte MR, Larrosa CRR (2011) Morpho-anatomical characters of the leaf and stem of *Mandevilla coccinea* (Hook. et Arn.) Woodson, Apocynaceae. Braz J Pharm Sci 47:137-144.

El-Kashef DF, Hamed ANE, Khalil HE, Kamel MS (2015) Triterpenes and sterols of family Apocynaceae). A review. J Pharmacogn Phytochem 4:21-39.

Esau K (1977) Anatomy of Seed Plants. Wiley, New York.

Esau K (1974) Anatomia das Plantas com Sementes. Editora Blucher, São Paulo.

Evert RF (2006) Esau's Plant Anatomy, Meristems, Cells, and Tissues of the Plant Body: their Structure, Function, and Development. John Wiley & Sons, New Jersey.

Gama TDSS, Rubiano VS, Demarco D (2017) Laticifer development and its growth mode in *Allamanda blanchetii*

A. DC. (Apocynaceae). J Torrey Bot Soc 144:303-313.
Gowramma B, Sultan B (2018) Comparative study of stomatal index at family level. J Bas App Res 8:1114-1129.
Guidoti DGG, Guidoti DT, Rocha CLMSC, Mourão KSM (2015) Morphoanatomic characterization of the stem and the leaf of *Tabernaemontana catharinensis* (Apocynaceae) and antimutagenic activity of its leaves. Bras Pl Med Campinas 17:667-679.
Gurav S, Tilloo S, Burade K (2014) Histological and histochemical staining techniques. In Gurav SS, Gurav NS, Eds., Indian Herbal Drug Microscopy. Springer, New York, 9-14.
Hanson HC (1917) Leaf structure as related to the environment. Am J Bot 4:533-559.
Ignacimuthu S, Ayyanar M, Sivaraman K (2006) Ethnobotanical investigations among tribes in madurai district of Tamil Nadu, India. J Ethnobiol Ethnomed 2:1-7.
Kigkr RW (1971) Epidermal and cuticular mounts of plant material obtained by maceration. Stain Technol 46:71-75.
Larrosa CRR, Duarte MDR (2005) Contribution to the anatomical study of the stem of *Himatanthus sucuuba* (Spruce ex Müll. Arg.) Woodson, Apocynaceae. Rev Bras Farmacogn 15:110-114.
Larrosa CRR, Duarte MR (2006) Anatomia foliar e caulinar de *Forsteronia glabrescens,* Apocynaceae. Acta Farm Bonaer 25:28-34.
Lens F, Endress ME, Baas P, Jansen S, Smets E (2008) Wood anatomy of Rauvolfioideae (Apocynaceae): a search for meaningful non-DNA characters at the tribal level. Am J Bot 95:1199-1215.
Liu W, Zhu XY (2011) Leaf epidermal characters and taxonomic revision of *Schizophragma* and *Pileostegia* (Hydrangeaceae). Bot J Linn Soc 165:285-314.
Lopes KLB, Thadeo M, Azevedo AA, Soares AA, Meira RMSA (2009) Articulated laticifers in the vegetative organs of Mandevilla atroviolacea (Apocynaceae, Apocynoideae). Botany 87:202-209.
Maciel VEO, Corrêa PG, Silva MD, Chagas MGS, Pimentel RMM (2010) Anatomia e histoquímica do caule e folha de *Nerium oleander* L. In X Jornada de Ensino Pesquisa e Extensão - JEPEX, 2010, Recife. Apresentação de trabalho. Resumo Expandid 42:585-598.
Mahlberg PG (1993) Laticifers: an historical perspective. Bot Rev 59:1-23.
Manasa DJ, Chandrashekar KR (2015) Antioxidant and antimicrobial activities of *Tabernaemontana heyneana* WALL. An endemic plant of Western Ghats. Int J Pharm Sci 7:311-315.
Mayberry MW (1937) Some anatomical features of *Amsonia tabernaemontana*. Trans Kans Acad Sci 40:75-81.
Mbagwu FN, Nwachukwu CU, Okoro OO (2008) Comparative leaf epidermal studies on *Solanum marcocarpon* and *Solanum nigrum*. Res J Bot 3:45-48.
Metcalfe CR, Chalk L (1950) Anatomy of the Dicotyledons. Clarendon Press, Oxford.
Metcalfe CR, Chalk L (1988) Anatomy of the Dicotyledons. Volume 1: Systematic Anatomy of the Leaf and Stem. Clarendon Press, Oxford.
Metcalfe CR, Chalk L (1979) Anatomy of the Dicotyledons Volume II: Wood Structure and Conclusion of the General Introduction. Clarendon Press, Oxford.
Omino EA (1996) Contribution to the leaf anatomy and taxonomy of Apocynaceae in Africa: the leaf anatomy of Apocynaceae in East Africa; a monograph of Pleiocarpinae (Series of revisions of Apocynaceae XLI). Backhuys Publisher, Leiden.
Premakumari D, Panikkar AON, Sobhana S (1985) Occurrence of intraxylary phloem in *Hevea brasiliensis* (Willd. ex A. Juss.) Muell. Arg. Ann Bot 55:275-277.
Ramos MV, Demarco D, da Costa Souza IC, de Freitas CDT (2019) Laticifers, latex, and their role in plant defense. Trends Plant Sci 24:553-567.
Rao AR, Malaviya M (1966) The non-articulated laticifers and latex of *Tabernaemontana coronaria* Willd. Proc Natl Acad Sci India B 32:233-242.
Rio MCS, Kinoshita LS, Castro MM (2005) Anatomia foliar como subsídio para a taxonomia de espécies de Forsteronia G. Mey. (Apocynaceae) dos cerrados paulistas. Braz J Bot 28:713-726.
Roy R, Grover RK, Srivastva S, Kulshreshtha DK (2002) A new stereoisomer of stem made nine alkaloid from *Tabernaemontana heyneana* Wall. Magn Reson Chem 40:474-476.
Ryder VL (1954) On the morphology of leaves. Bot Riv 20:263-267.
Salisbury EJ (1927) On the causes and ecological significance of stomatal frequency, with special reference to the woodland flora. Philos 216:1-65.
Santos MCA, Freitas SDP, Aroucha EMM, Santos ALA (2009) Anatomia e histoquímica de folhas e raízes de vinca (*Catharanthus roseus* (L.) G. Don). Rev Boil Ciên 9:24-30.
Sathishkumar T, Baskar R, Rajeshkumar M (2012) *In vitro* antibacterial and antifungal activities of *Tabernaemontana heyneana* Wall. leaves. J Appl Pharm Sci 2:107-111.
Sathishkumar T, Baskar R (2012) Evaluation of antioxidant properties of *Tabernaemontana heyneana* Wall. leaves. Indian J Nat Prod Resour 3:197-207.
Sathishkumar T, Baskar R, Shanmugam S, Rajasekaran P, Sadasivam S, Manikandan V (2008) Optimization of flavonoids extraction from the leaves of *Tabernaemontana heyneana* Wall. using L16 orthogonal design. Natr Sci 6:10-21.
Scatena VL, Scremin-Dias E (2006) Parênquima, colênquima e esclerênquima. In Appezzato-da-Glória B, Carmello-Guerreiro SM, Orgs., Anatomia Vegetal. Viçosa, Editora da UFV. 109-128.

Schenck H (1893) Beiträge zur Biologie und Anatomie der Lianen, im Besonderen der in Brasilien einheimischen Arten. II. Beiträge zur Biologie der Lianen. Bot. Mitt. Tropen 5:1-271.

Srivastava S, Singh MM, Kulshreshtha DK (2001) A new alkaloid and other anti-implantation principles from *Tabernaemontana heyneana*. Planta Med 67:577-579.

Sukumaran S, Raj ADS (2008) Rare, endemic, threatened (RET) trees and lianas in the sacred groves of Kanyakumari district. Indian For 133:1254-1267.

Van Beek TA, Verpoorte R, Svendsen AB, Leewenberg AJM, Bisset NG (1984) *Tabernaemontana* L. (Apocynaceae): A review of its taxonomy, phytochemistry, ethnobotany and pharmacology. J Ethnopharmacol Lausanne 10:1-156.

Yeats TH, Rose JK (2013) The formation and function of plant cuticles. Plant Physiol 163:5-20.

Yeung E (1998) A beginner's guide to the study plant structure. Purdue University, Lafayatte, In Karcher SJ, Ed.,Tested Studies for Laboratory Teaching, Proceedings of the 19th Workshop /Conference of the Association for Biology Laboratory Education(ABLE). 19:125-142.

Willemse MTM (1989) Cell wall autofluorescence. In Chesson A, Ørskov ER, eds., Physico-Chemical Characterisation of Plant Residues for Industrial and Feed Use. Springer, Dordrecht. 50-57.

Acta Biologica Szegediensis

Volume 63(2):195-205, 2019
Acta Biologica Szegediensis
http://abs.bibl.u-szeged.hu/index.php/abs
DOI:10.14232/abs.2019.2.195-205

ARTICLE

Influence of biologically active raw materials on rheological properties of flour confectionery products

Alfiya Chernenkova[1]*, Svetlana Leonova[1], Valery Chernykh[2], Evgeniy Chernenkov[1]

[1]Department of Technology of the Catering and Processing of Vegetable Raw Materials, Federal State Budgetary Educational Institution of Higher Education, Bashkir State Agrarian University, 450001, Ufa, Russia
[2]Center Rheology Food Environments, State Scientific Research Institute Baking Industry, 450001, Moscow, Russia

ABSTRACT New achievements in science, food technologies and medicine call for sounder, scientifically proven nutrition. Food must be functional being aimed at preventing numerous diseases, improving performance capacity and health. Cereals, in particular bakery and confectionery, have the highest potential to be modified to get functional properties. Currently the assortment of this daily food has been actively enlarged. Therefore, the purpose of this work is to improve the production technology of the national flour confectionery "Chak-chak" using biologically active raw materials of the Republic of Bashkortostan. As the result of the conducted studies the ratio of the main ingredients and biologically active raw materials (bee pollen, honey and oat talkan) in flour confectionery as well as production parameters are improved. Therefore, the developed product (chak-chak with bee products and oat talkan), having no analogues, can find its place among other flour confectionery goods.
Acta Biol Szeged 63(2):195-205 (2019)

KEY WORDS
oat talkan
bee products
chak-chak
structural and mechanical properties
optimization of formula ingredients

ARTICLE INFORMATION
Submitted
27 January 2020.
Accepted
26 March 2020.
***Corresponding author**
E-mail: ala_chernenkov@rambler.ru

Introduction

Many manufacturers, guided by current trends in the development of the healthy food market, are focused on the production of functional products (Siro et al. 2008). Domestic production of functional food products is mainly based on enriched vitamins, minerals, dietary fibers and lower energy value (Kinyuru et al. 2015). One of the most promising goods to be modified in this way is cereals, including flour confectionery (Šebečić et al. 2007; Okpala and Ofoedu 2018; Tugush et al. 2018; Saleh et al. 2019). Biologically active raw materials added to their formulas will provide higher number of important nutrients required to the daily intake.

The fundamental point is to find the optimal proportions of non-traditional ingredients. Besides solving the main task of increasing the nutritional and biological value of products, it is possible to improve their production technology, make organoleptic, physico-chemical and structural-mechanical properties of finished products better, and extend their shelf life (Šebečić et al. 2007; Rumiantseva et al. 2012; Leonova et al. 2018).

Currently, it has become relevant to study the possible use of non-traditional raw materials being able to increase nutritional value of products in manufacturing flour confectionery goods. There is a developed formula of cereal bars with a high content of protein and vitamins based on soy protein, wheat germ and oat, enriched with ascorbic acid and α-tocopherol (Amjid et al. 2013). Some works are devoted to the development of flour confectionery goods with a high content of dietary fibers. It is done by adding oat flour, amaranth, soy flour and carob flour (Arghire et al. 2016). Gluten-free snacks with amaranth, orach and quinoa seed flour were also studied (Codină et al. 2019).

When developing new types of flour confectionery goods with specified properties and composition to optimize the production process, it is necessary to monitor the technological parameters as well as rheological characteristics of raw materials and semi-finished products (Codină et al. 2019). Flour confectionery goods production is associated with processing of bound-dispersion systems and the formation of coagulate, mixed and condense-crystallized structures. Rheology allows to control structural and mechanical properties as well as the quality of products by adding additives, changing modes and methods of mechanical and technological processing (Novotni et al. 2009; Munteanu et al. 2016; Gabitov et al. 2018).

There is a study on the effect of the plantain seed powder on the structural and mechanical properties of flour confectionery goods, in particular hard-dough biscuits. The main physical and chemical indicators, organoleptic characteristics, spreading coefficient, volume and texture

were determined. The additive used helped to increase the spreading behavior of cookies and reduce their volume and density (Krystyjan et al. 2018).

There are studies on the influence of various dietary fibers on the rheology of semi-finished products for bread and bakery products. The dough rheological properties are examined with a farinograph (Brabender, Germany) and a texture analyzer (Stable Micro Systems, UK). It was found that inulin added to the formula affects the dough consistency, elasticity and adhesion. When dextrin is included, the viscosity increases, but it does not have a significant impact on other dough properties (Novotni et al. 2007).

The influence of bee pollen on the quality of flour confectionery goods is also studied. The increased dosage of bee pollen is found to improve structural and mechanical properties of bakery, such as volume, structure, consistency and crust color (Conte et al. 2018).

In the light of the foregoing, the research goal is to assess the impact of oat talkan and bee products on structural, mechanical and technological properties of finished and semi-finished products as well as to improve the chak-chak formula with biologically active raw materials as oat talkan, honey and bee pollen.

Materials and methods

The research is carried out in the scientific research laboratories of the Bashkir State Agrarian University, the Bashkir Agricultural Research Institute and the Research Institute of the Baking Industry.

The investigation is based on traditional and special chemical, physico-chemical, structural and mechanical methods to study properties of raw materials, semi-finished and finished products. Physico-chemical and organoleptic quality indicators of products are recognized according to the Russian Sate Standard GOST 5897-90. Organoleptic evaluation is conducted using a 30-point scale. The quality of the product is estimated by the total assessment. 30-25 points correspond to the excellent product quality, 24-20 points as good and 19-10 points as satisfactory.

Flour humidity was determined in accordance with State All-Union Standard (GOST) 9404-88 using an electric SESH-3M drying cabinet, in which the drying chamber temperature is up to 150 °C. The cabinet has a temperature controller that creates drying temperature and keeps the heat in the working zone at 130-140 °C (accurate within ±2 °C). Humidity is determined in two parallel hangers. Two clean dried metal weighing bottles are removed from the desiccator and weighed with an error of no more than 0.01 g. The product isolated from the average sample according to GOST 27668 for determining humidity is thoroughly shaked in the container and selected from different places. Then, it is put in each weighing bottle of a product batch weight with the mass of (5.00 ± 0.01) g. After that the weighing bottles are covered with lids and placed in the desiccator. When the temperature in the drying cabinet reaches 130 °C, the thermometer is turned off and the oven is heated to 140 °C. Then the thermometer is turned on, and open weighing bottles with batch weight of the product are quickly placed into the cabinet upon the removed lids. Empty cabinet slots are filled with empty weighing bottles. The product is dried for 40 min from the moment the temperature of 130 °C was re-created. It is allowed not to heat the drying cabinet to 140 °C, if after its full loading the temperature of 130 °C is re-created within 5-10 min. After drying, the weighing bottles with the product are removed from the cabinet with crucible tongs, closed with lids and transferred to the desiccator for complete cooling for about 20 min (but no more than 2 hours). Cooled weighing bottles are weighed with an error of no more than 0.01 g and placed in the desiccator until the analysis results are processed.

Product humidity (X) as a percentage is calculated using the Formula 1:

$$X = 100\ \frac{m_1 - m_2}{m_2}$$

where m_1 is the mass of flour and bran weight batch before drying (g); m_2 is the mass of flour and bran weight batch after drying (g).

The effect of bee pollen, honey and oat talkan on the structural and mechanical properties of semi-finished products as dough is studied on fried semi-finished chak-chak and syrup. The structural and mechanical properties were analyzed with «ST-2 structure meter». Chak-chak wheat dough kneading parameters are determined with an information measuring complex, including Farinograph-E (Brabender, Germany), a kneading trough, a programmable thermostat and a personal computer.

Strength test determination is based on finding the extreme load on the "Knife" indenter. The product placed on the table is loaded at 10g/s after being touched in the middle with a force of 10 g.

Syrup viscosity test method is based on finding the loading force on the "Disk" indenter when it is introduced into the prepared syrup sample to a depth of 4 mm at 0.5 mm/s after the contact force of 5 g. The maximum value of the loading force F_c expressed in grams is interpreted as the compressive strength of the paste. Then the position of the indenter is fixed for 5 s and the indenter is extracted from the product at a distance of 45 mm at 0.5 mm/s with the maximum tension force of the paste Ft.

Table 1. Significance test results for the syrup model coefficients.

Standard (RMS) beta coefficient deviation	Coefficients	Standard error	t-statistics	P-value	Lower endpoint (95% confidence interval)	Upper endpoint (95% confidence interval)
a_0	50.51746	0.613	82.447	0.000	49.303	51.731
a_1	-0.52421	0.028	-18.558	0.000	-0.580	-0.468
a_2	-0.29575	0.023	-12.725	0.000	-0.342	-0.250
a_3	0.004341	0.000	14.373	0.000	0.004	0.005
a_4	-0.00032	0.000	-1.082	0.282	-0.001	0.000
a_5	0.002566	0.000	9.638	0.000	0.002	0.003
a_6	-0.00019	0.000	-15.398	0.000	0.000	0.000
a_7	1.71 E-05	0,000	1.723	0.088	0.000	0.000

Chak-chak wheat dough kneading parameters are found with the help of an information measuring complex, including Farinograph-E (Brabender, Germany), a kneading trough, a programmable thermostat and a personal computer. Dough properties are tested with farinograph by kneading wheat flour with oat talkan. Dough consistency of 500 ± 20 f.u. is received by estimating the required amount of water. The farinograph operation procedure and principle: a flour sample of 300 g on a 14% moisture basis is placed in a mixing bowl and stirred for 1 min. Then water is added from the right front corner of the buret for 25 s. (Rumiantseva et al. 2012). The dynamics of rheological behavior of the chak-chak dough with a rational dosage of 6% of oat talkan and the control sample without oat talkan during kneading is tested on the Brabender Farinograph-E. During the analysis, the dough development time and strength are recorded.

Determination of dough formation time

Dough formation time (min) is the difference between the time of adding water and the time when the first signs of a decrease in consistency appear. In cases where farinogram shows two maxima, the value of the higher maximum is used to measure the time of dough formation. The arithmetic mean value of the dough formation time is accepted as a result and is calculated according to two farinograms with a rounding to 0.5 min, provided that the difference between the two results does not exceed 1 min for values of the dough formation time up to 4 min or 25% of their average value for values of the dough formation time more than 4 min.

Determination of dough resistance

Dough resistance (min) is calculated within the accuracy up to 0.5 min as the time difference between the points, at which the upper limit of the farinogram crosses for the first time and re-crosses the line 500 UF. This value characterizes dough resistance to mixing. If the actual maximum consistency deviates from the 500 UF line, but not more than ± 20 UF (9.1), then the line corresponding to the actual consistency must be used for the reading.

Experimental samples of chak-chak are made according to the traditional formula modified by replacing wheat with 2-12% of oat talkan. The control samples are without oat talkan. The syrup to dress chak-chak is made of bee pollen used instead of sugar in the amount of 25 to 100%. Results are compared with the control sample of the syrup without bee pollen.

Results

Nonlinear multi-dimensional statistical models are used to optimize the ratio of the chak-chak ingredients and the syrup.

Chak-chak and syrup formula improvement based on mathematical models

Nonlinear multi-dimensional statistical models are developed to evaluate the effect of bee products and oat talkan on the organoleptic and physico-chemical properties of chak-chak (Gabitov et al. 2018, 2018b). A similar method of optimizing flour confectionery recipes is used to improve the formulation of bakery products. The mathematical model is applied to the baking process. A mathematical model completely related to the change in the volume output is developed (Zhang and Datta 2006).

At the first stage, the syrup formulation is optimized with the addition of bee pollen (see Table 1). The response function for the syrup viscosity is represented by the dependence:

$$z(x,y)_1 = a_0 + a_1(x - 50) + a_2(y - 57{,}5) + a_3(x - 50)^2 + a_4(y - 57{,}5)^2 + a_5(x - 50)(y - 57{,}5) + a_6(x - 50)^3 + a_7(y - 57{,}5)^3$$

where x is the mass fraction of bee pollen, y is the time that 1 quart (946 cm^3) of the substance comes out of the

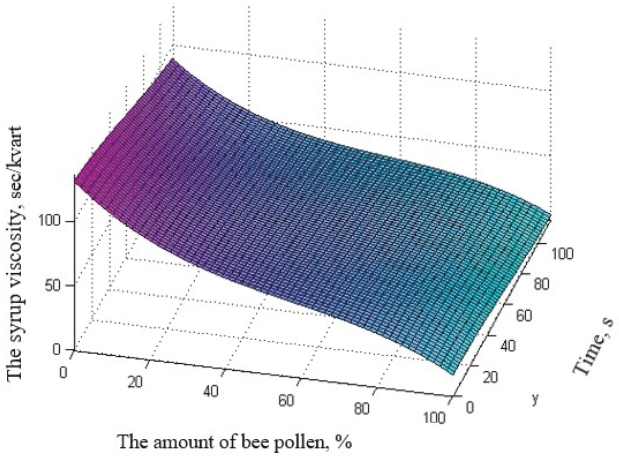

Figure 1. Effect of the bee polen dosage on the syrup viscosity.

filled funnel. The coefficient of multiple correlation= 0,99534175. The observed value of Fisher's F-criterion is 1705,.392471.

The multi-criteria optimization with one explanatory parameter is described by the generalized desirability function D (Kirillova and Kanevskaia 2017; Tugush et al. 2018). The optimal dosage of oat talkan is determined according to physical and chemical properties. The generalized desirability function D is the proportional average of individual indicators.

$$D = \sqrt[n]{d_1 d_2 ... d_n}$$

where is the individual desirability *i* indicator, n is the number of indicators. "Desirability" d refers to a desired level of the indicator. The d value of can vary from 0 to 1.

Since there are unilateral restrictions on the indicators, the desirability function has the form:

$$d_i = exp\,(-e^{-y_i})$$

where is some dimensionless quantity associated with the natural exponent (*x*).

The values of dimensional (natural) exponents (*x*) indicating the quality of semi-finished and finished products can be changed in dimensionless (*y*) at the nonlinear relationship according to the formula:

$$y_i = a_0 + a_1 x_i + a_2 x_i^2 + a_3 x_i^3 \qquad \text{(eq. a)}$$

Having twice logged the equation, we obtain an expression for y_i

$$y_i = ln\ \frac{1}{ln\frac{1}{d_i}}$$

Substituting the values into the equation (eq. a), we get:

$$a_0 + a_1 x_i + a_2 x_i^2 + a_3 x_i^3 = ln\frac{1}{ln\frac{1}{d_i}} \qquad \text{(eq. b)}$$

Let's make a system of equations for the known values of *x* and *d*. Solving the system together, we find the values of the coefficients a_0, a_1, a_2 and a_3. As the result, there is an equation of the nonlinear dependence between the studied parameter and dimensionless values. According to this equation, one can find *y* for any *x*, and then the desirability index according to the Formula 2 (Kirillova and Kanevskaia 2017; Tugush et al. 2018). Assessment scales for dimensional indicators of chak-chak and biscuit semi-finished product are given in Tables 2 and 3.

"Excellent", "good", "satisfactory" and "poor" rates for organoleptic indicators of quality correspond to 25, 20, 10 and 5 score values. Substituting these values in the formula (eq. b), we get:

$$\begin{cases} a_0 + 25a_1 + 25^2 a_2 + 25^3 a_3 = ln\frac{1}{ln\frac{1}{d_i}} \\ a_0 + 20a_1 + 20^2 a_2 + 20^3 a_3 = ln\frac{1}{ln\frac{1}{d_i}} \\ a_0 + 10a_1 + 10^2 a_2 + 10^3 a_3 = ln\frac{1}{ln\frac{1}{d_i}} \\ a_0 + 5a_1 + 5^2 a_2 + 5^3 a_3 = ln\frac{1}{ln\frac{1}{d_i}} \end{cases}$$

Table 2. Chak-chak dimensional indicators and standard assessment criteria based on the desirability scale.

Quality gradations	Desirability scale	Density (kg/m3)	Moisture weight (%)	Water absorption (%)	Total sugar weight (%)	Fat weight (%)	Organoleptic indicators
1	2	3	4	5	6	7	8
Excellent	0.80 ≤ *d* < 1.00	< 48	< 12	> 180	< 28	< 14	> 25
Good	0.63 ≤ *d* < 0.80	> 48	> 12	< 180	>28	> 14	< 25
Satisfactory	0.37 ≤ *d* < 0.63	> 50	> 15	< 170	> 30	> 16	< 20
Poor	0.20 ≤ *d* < 0.37	> 52	> 17	< 150	> 32	> 18	< 10
Very poor	0.00 ≤ *d* < 0.20	> 54	> 18	< 140	> 34	> 20	< 5

Table 3. Equation coefficients of the nonlinear dependence between product properties and the dimensionless indicators of the standard evaluation based on the desirability scale.

Indicator name	Equation coefficients			
	a_0	a_1	a_2	a_3
Chak-chak				
Density (kg/m3)	-832.969	50.58465	-1.01489	0.006733813
Moisture weight (%)	1.753842	0.014651	0.006439	-0.000785284
Water absorption (%)	-145.942	2.739339	-0.01731	3.69272E-05
Total sugar weight (%)	-173.36	18.06974	-0.61086	0.006733813
Fat weight (%)	-21.6347	4.925181	-0.32804	0.006733813
Organoleptic quality indicators	-1.3186	0.219421	-0.01165	0.000295418

The equation of the nonlinear dependence between the texture indicator and the dimensionless value of the standard evaluation based on the desirability scale will be as follows:
The calculation results are shown in Table 3. Natural

$$y_1 = -1.31 + 0.21x_1 + -0.01x_1^2 + 0.002x_1^3$$

and generalized quality indicators of chak-chakby the desirability function as well as the corresponding values are presented in Figure 2 and Table 4.

It is established that the generalized desirability function has the greatest value for samples 1-4.

Hence, the best amount of oat talkan for chak-chak is no more than 6%. Therefore, further studies were carried out on products with 6% of oat talkan.

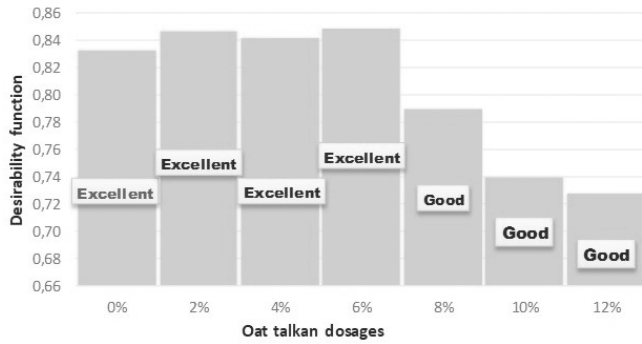

Figure 2. Chak-chak values by the desirability function at different oat talkan dosages.

Table 4. Natural and generalized chak-chak indicators by the desirability function.

Samples	Natural values responses						Individual desirability responses						Generalized desirability function D	Evaluation according to the desirability scale
	Density (kg/m3)	Moisture weight (%)	Water absorption (%)	Total sugar weight (%)	Fat weight (%)	Organoleptic quality indicators	Density (kg/m3)	Moisture weight (%)	Water absorption, (%)	Total sugar weight (%)	Fat weight (%)	Organoleptic quality indicators		
	x_1	x_2	x_3	x_4	x_5	x_6	d_1	d_2	d_3	d_4	d_5	d_6		
No. 1.	46.33	10.23	204.8	28.0	14.0	23,00	0.85	0.84	1.00	0.80	0.80	0.73	0.83	excellent
No. 2.	47.67	7.28	202.7	28.4	13.8	26,00	0.82	0.86	1.00	0.78	0.81	0.83	0.85	excellent
No. 3.	48.07	10.34	201.5	28.7	12.7	26,00	0.80	0.84	0.99	0.76	0.85	0.83	0.84	excellent
No. 4.	48.57	10.40	199.1	29.0	12.0	26,00	0.76	0.84	0.99	0.73	0.86	0.83	0.85	excellent
No. 5.	49.17	10.44	196.2	29.1	12.2	21,00	0.72	0.84	0.98	0.72	0.86	0.66	0.79	good
No. 6.	49.93	10.51	195.1	29.3	11.9	16,00	0.64	0.83	0.98	0.70	0.86	0.52	0.74	good
No. 7.	50.10	10.54	193.2	29.6	11.8	16,00	0.62	0.83	0.96	0.67	0.86	0.52	0.73	good

Sample No. 1.: control. Samples No. 2., No. 3., No. 4., No. 5., No. 6., and No. 7. are chak-chak with 2%, 4%, 6%, 8%, 10% and 12% of oat talkan, respectively.

Influence of oat talkan and bee products on structural and mechanical properties of chak-chak

Structural and mechanical properties of chak-chak dough are extremely important for the formation and subsequent roasting of semi-finished products (Muratova and Smolikhina 2013). The research results of the oat talkan effect on the dough properties are shown in Figures 3, 4. Similar methods to determine the rheological characteristics of flour and dough using a farinograph and a mixograph are widely used in researches to optimize the formula of bakery products (Munteanu et al. 2016). Particular parameters of the dough for confectionery products were studied using the farinograph. The data obtained are presented in the Table 5.

It is found that the dough development time of the control sample is 5.3 min, its resistance to mixing is 17.6 min. The score (an indicator of the flour "strength") is 200. The dough development time with oat talkan is shorter and amounts to 4.6 min. The dough resistance to mixing is longer by 18.1 min. At the same time, the dough with oat talkan has more homogeneous structure compared to the control sample. Therefore, it can be concluded that oat talkan accelerates the gluten development and the technological process of chak-chak production.

Table 5. Dough for confectionery products parameters

No.	Parameters	Control	Chak-chak with oat talkan
1	Wheat flour moisture content (%)	14.0	14.0
2	Dough formation time (min)	5.3	4.6
3	Resistance (min)	17.6	18.1
4	Consistency (FU)	580	550
5	Water absorption (%)	59	62

Influence of Oat Talkan on the Technological Process of Making Chak-Chak

To determine the effect of oat talkan on the production process, the time to fry dough pieces of chak-chak duration in deep fat is analyzed. During the studies, goods with 6% of oat talkan have been manufactured. The control samples of chak-chak are made according to the traditional recipe. The readiness of the chak-chak dough pieces is identified by humidity and appearance. The moisture content after frying was 8.9-9%. The results are shown in Figure 3.

It is found that the color of the dough pieces with oat talkan becomes golden brown in 2-3 min, while the control sample is still corn-colored. Moreover, the moisture content of the dough pieces with oat talkan decreases to 9% at the 3rd minute of roasting that indicates the readiness of the product.

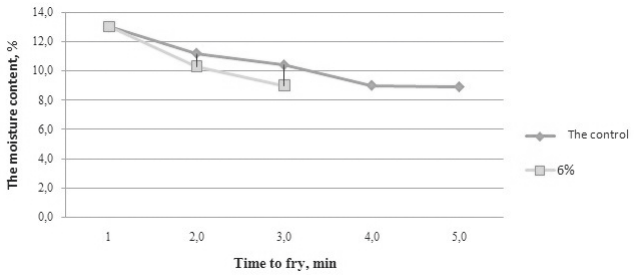

Figure 3. The effect of oat talkan on the time to fry chak-chak dough pieces.

Thus, the addition of oat talkan reduces the duration of frying by 2 min compared to the control sample. It can result from higher content of dietary fibers in oat talkan that provide acceleration of heat and moisture exchange processes.

Influence of oat talkan on structural and mechanical properties of fried semi-finished products of chak-chak

In the course of studies, the influence of different dosages of oat talkan on the density of fried dough pieces of chak-chak is identified. To conduct the study, fried semi-finished products of chak-chak with a dosage of oat talkan from 0 to 12% (in 2% increments) are used. The results are shown in Figure 4.

The dough height-diameter ratio increases in proportion to the amount of oat talkan. This demonstrates lower dough firmness.

The next stage of the research is the study of the structural and mechanical properties of deep-fried semi-finished chak-chak. The studies are carried out using the «ST-2 structure meter». During the study, 6 goods with

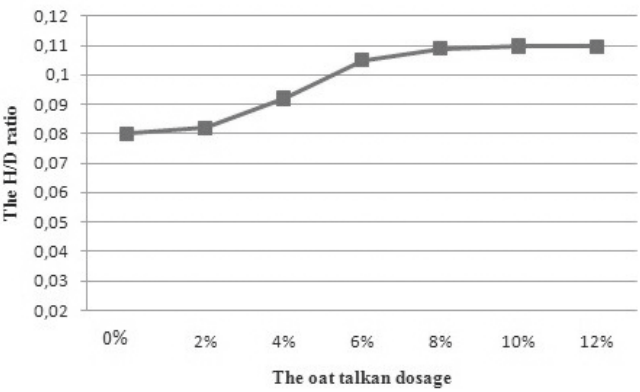

Figure 4. The height-diameter ratio of fried semi-finished products of chak-chak.

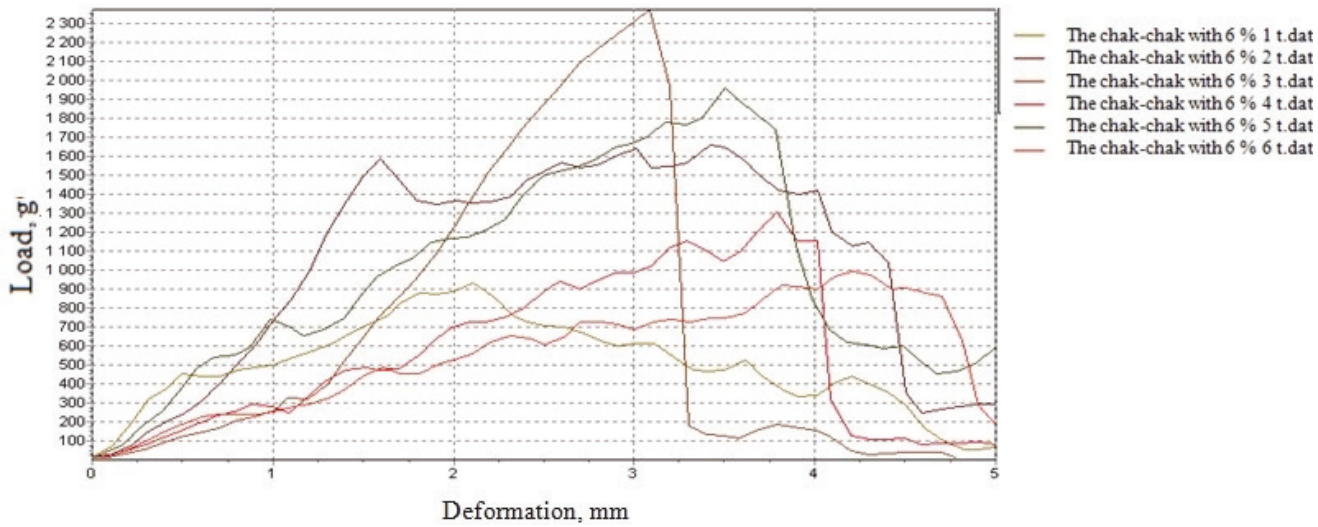

Figure 5. Assessing the strength of fried semi-finished chak-chak (the control sample).

6% of oat talkan from each batch and the control sample are selected. The strength and fragility of semi-finished products are examined with the help of the "Knife" indenter. The results are presented in Figures 5, 6.

The resulting data makes it possible to evaluate the structure and consistency of fried semi-finished products. The control samples are found to have a denser structure and less developed texture than the products with talkan. There is an increase in the volume of fried semi-finished chak-chak with talkan. Also, according to the data received, the fragility of products when adding oat talkan to the formula, is higher that is a positive property for this type of flour confectionery products.

Based on the conducted research, it can be concluded that oat talkan improves the consistency and structure of fried semi-finished chak-chak, which is why its addition to the chak-chak formula is reasonable. Chakkaravarthi et al. (2009) studied the rheological parameters of dough and fried semi-finished confectionery jalebi using a rheometer with a controlled voltage. Similar studies of the influence of various non-traditional raw materials on the structural and mechanical properties of flour confectionery and bakery were conducted by researchers (Thakur and Nanda 2018, 2019; Saleh et al. 2019).

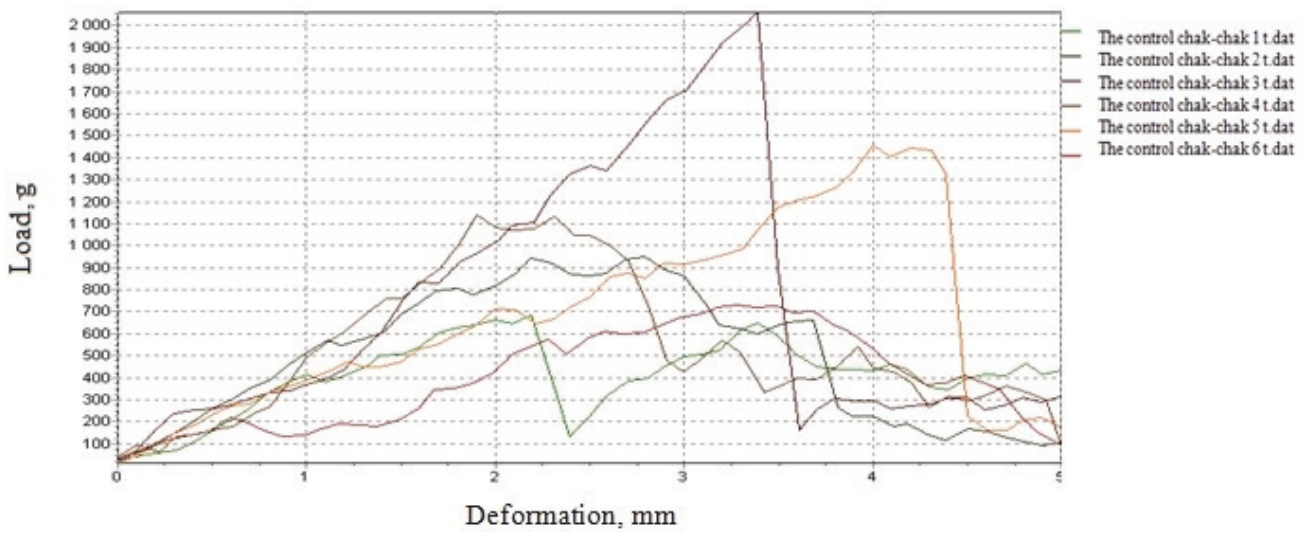

Figure 6. Evaluating the strength of fried semi-finished chak-chak with 6% of oat talkan

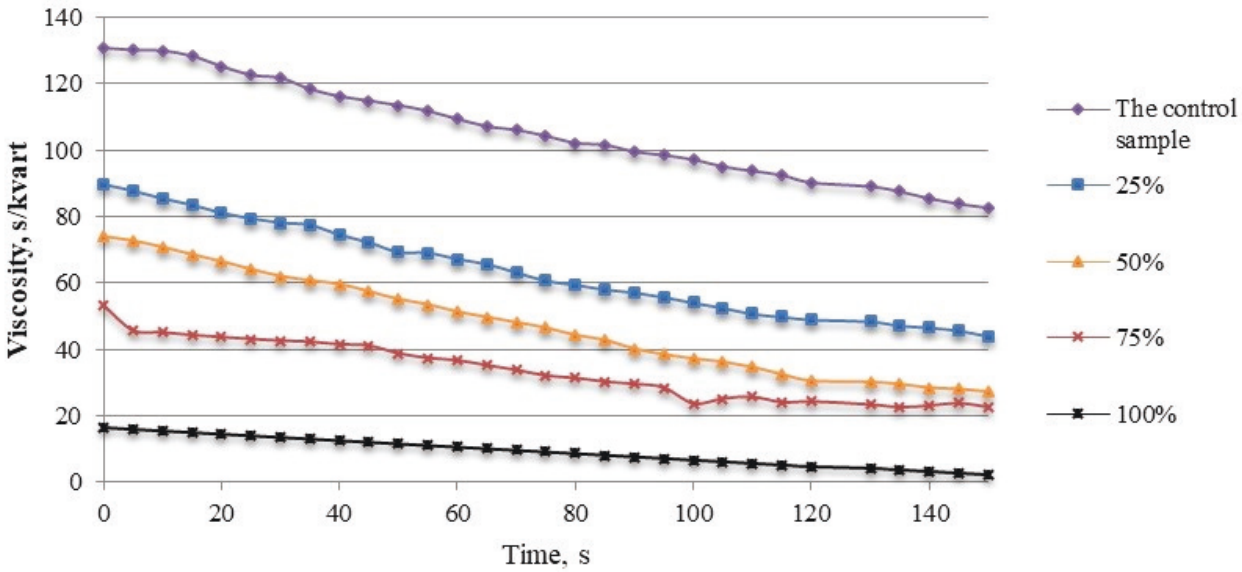

Figure 7. Dependence of the syrup viscosity on bee pollen content.

Development of a syrup formula for Chak-Chak with bee pollen

Since chak-chak is a high-calorie product, one of the goals of this work is to reduce the amount of sugar in the chak-chak syrup formula. Therefore, sugar in the syrup formula is replaced with bee pollen in the amount of 25%, 50%, 75%, and 100% of the sugar mass.

We identified the effect of the bee pollen dosage on the organoleptic characteristics of the syrup. With added bee pollen the color of the syrup becomes deep golden. There is also a pleasant taste and flavor pertinent to honey and bee pollen. There is also an organoleptic evaluation of the syrup with different dosages of bee pollen (results not shown).

It is found that the syrup with 25% of bee pollen has the highest organoleptic score being 30 points. It corresponds to the "excellent" assessment. With higher dosage of bee pollen there is a further change in the syrup color to brown and bitter taste. It is unacceptable for this type of finishing product.

To test the effect of bee pollen on the structural and mechanical properties of the syrup, its viscosity is examined. The results presented in Figure 7 clearly demonstrate the dependence of the syrup flow time in the March funnel on the dosage of bee pollen.

Bee pollen added to the syrup is found to reduce its viscosity. It can complicate the process of finishing the end product. To confirm the received results the strength characteristics and the syrup viscosity are analyzed on the «ST-2 structure meter» using the "Disk" indenter. It is conducted at 33 °C. The results are shown in Figure 8.

It is established that introducing the indenter in the control sample of the syrup requires more force than the indentation in the syrup with bee pollen. The results indicate a decrease in the syrup viscosity when bee pollen is added. Obviously, this is due to vitamins, minerals and amino acids in bee pollen that prevent the sucrose crystallization.

Discussion

The chak-chak product is authentic and has no analogues in the world. At the same time in many countries attempts have been made to improve the quality and properties of traditional flour confectionery goods by including bee products and different cereals.

There are a number of researches devoted to the change of rheological properties of flour confectionery under the influence of introduced ingredients. Thus, the influence of different flour from different varieties of flax seeds on rheological properties of wheat flour is studied. The rheological properties are evaluated by the Mixolab device. The dough microstructure is evaluated by epifluorescence light microscopy. Higher dosage of flaxseed flour brings in an increase in water absorption capacity and stability of the dough (Codină and Mironeasa 2016).

There are papers that study factors influencing the rheological characteristics of the dough, the effect of different additives as well as the interaction of ingredients. The most frequently used methods of rheological tests and their relation to the product functionality are also

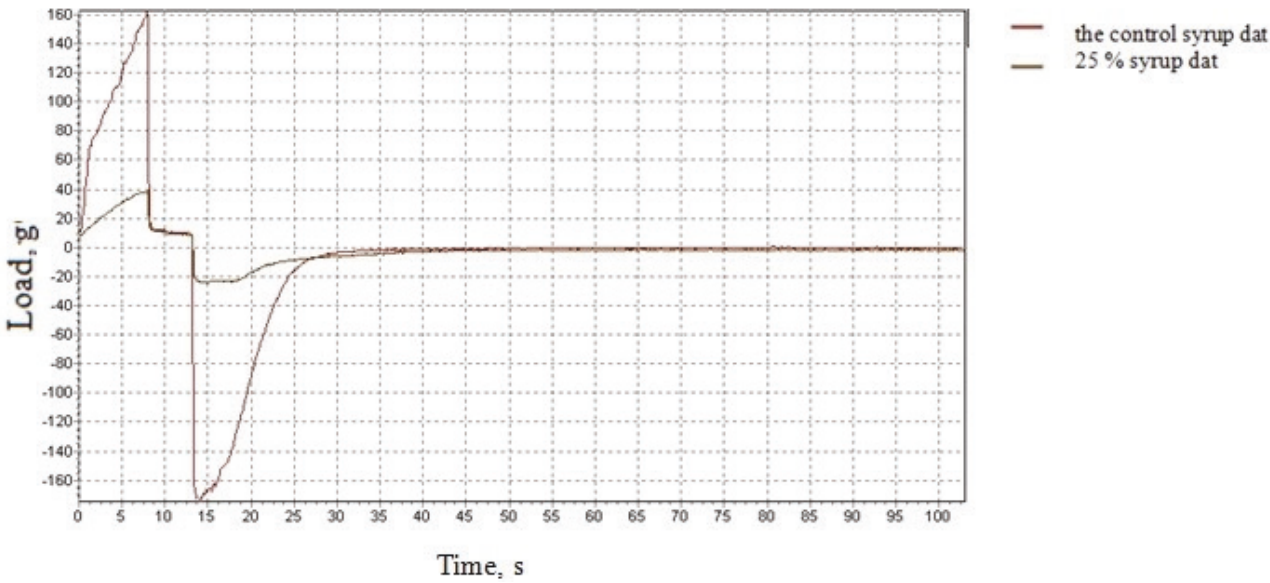

Figure 8. Effect of the bee pollen on the syrup viscosity.

analyzed (Amjid et al. 2013).

Studies on optimizing the content of iron (FE) and oligofructose (OF) in order to get wheat flour dough with the best rheological properties using the methodology of the response surface (RSM) are conducted. The rheological properties of the dough are tested with farinograph, alveograph, amylograph, falling number and rheofermentometer. Added iron and oligofructose are found to improve the structure of the product. With higher levels of oligofructose, water absorption, dough strength, its extensibility, the falling number, the temperature at high viscosity are significantly lower (Codină et al. 2019).

There are also a number of research works aimed at optimizing bakery and flour confectionery goods using the methodology of the response surface (Zhang and Datta 2006; Arghire et al. 2016; Munteanu et al. 2016; Tugush et al. 2018) and the desirability function (Zhang and Datta 2006; Myers et al. 2016; Tugush et al. 2018; Kilic et al. 2019). At the same time, the formula component optimization by creating mathematical models for the developed product has not been carried out. Therefore, we have developed nonlinear, multiple regression models based on the received data, natural and generalized desirability values. These provided the evidence base to justify practicability of ingredient introduction.

There is a work (Krystyjan et al. 2015), devoted to the study of the bee pollen influence on the qualitative properties of flour confectionery goods. Studies prove that bee pollen does not affect the fat content of cookies. However, there was a small but significant increase in the protein and mineral content of the product. Basically, the data obtained by other researchers indicate that the addition of processed cereal products, bee pollen and other bee products increases the biological and nutritional value of the end good that is also confirmed by our results.

Conclusions

As the result of the conducted studies nonlinear multidimensional statistical models are developed. The formula of chak-chak with oat talkan and the syrup with sugar replaced by bee pollen is optimized. The rational dosages are found to be as follows: wheat flour replaced with oat talkan in the amount of 6% (in the chak-chak formula) and sugar replaced with bee pollen in the amount of no more than 25% (in the syrup recipe).

The influence of oat talkan and bee products on the structural and mechanical properties of semi-finished products and finished products, as well as on the parameters of the manufacturing process is identified. When adding oat talkan to the chak-chak formula, the dough development time is reduced by 4.5 min, while the dough stability during kneading is increased by 1.5 min. Compared to the control sample, the products with oat talkan have a more aerated structure and developed porosity. There is an increase in the volume of fried semi-finished chak-chak with talkan. The addition of bee pollen is found to reduce the syrup viscosity.

It is found to be reasonable to use bee products and oat talkan in the chak-chak formula to improve the structural and mechanical properties of the product and reduce

the production process by accelerated time for dough development and dough pieces frying.

References

Amjid MR, Shehzad A, Hussain S, Shabbir MA, Khan MR, Shoaib M (2013) A comprehensive review on wheat flour dough rheology. Ak J Agr Sci 23:105-123.

Arghire C, Mironeasa S, Codină GG (2016) Optimization of bread quality of 650 wheat flour type with native inulin by response surface methodology. Annal Unive Dunae Jos Gal Fasce VI: Food Technol 40.

Codină GG, Dabija A, Stroe SG, Ropciuc S (2019) Optimization of iron-oligofructose formulation on wheat flour dough rheological properties. J. Food Process 43:e13857.

Codină GG, Mironeasa S (2016) Use of response surface methodology to investigate the effects of brown and golden flaxseed on wheat flour dough microstructure and rheological properties. J. Food Sci Technol 53:4149-4158.

Conte P, Del Caro A, Balestra F, Piga A, Fadda C (2018) Bee pollen as a functional ingredient in gluten-free bread: A physical-chemical, technological and sensory approach. Lwt-Food Sci Technol 90:1-7.

Gabitov I, Mudarisov S, Gafurov I, Ableeva A, Negovora A, Davletshin M, Rakhimov Z, Khamaletdinov R, Martynov V, Yukhin G (2018) Evaluation of the efficiency of mechanized technological processes of agricultural production. J Eng Appl Sci 13:8338-8345.

Gabitov II, Badretdinov ID, Mudarisov SG, Khasanov E, Lukmanov R, Nasyrov RR, Tuktarov MF, Atnagulov DT, Nazli A, Timeriashev D, Pavlenko VA (2018) Modeling the process of heap separation in the grain harvester cleaning system. J Eng Appl Sci 13:6517-6526.

Gbenga-Fabusiwa FJ, Oladele EP, Oboh G, Adefegha SA, Oshodi A (2018) Nutritional properties, sensory qualities and glycemic response of biscuits produced from pigeon pea-wheat composite flour. J Food Biochem 42:e12505.

Kilic D, Ebegil M, Bayrak H, Ozkaya B, Avsar BA (2019) Optimization of multi responses using data envelopment analysis: The application in food industry. Gazi Univ J Sci 32:1083-1090.

Kinyuru JN, Konyole SO, Onyango-Omolo SA, Kenji G, Onyango CA, Owino VO, Owuor BO, Estambale BB, Roos N (2015) Nutrients, functional properties, storage stability and costing of complementary foods enriched with either termites and fish or commercial micronutrients. J Insec Food Feed 1:149-158.

Kirillova TV, Kanevskaia IYu (2017) Statistical Dependence. 2nd Ed, Saratov.

Krystyjan M, Gumul D, Korus A, Korus J, Sikora M (2018) Physicochemical properties and sensory acceptance of biscuits fortified with *Plantago psyllium* flour. Emir J Food Agric 30:758-763.

Krystyjan M, Gumul D, Ziobro R, Korus A (2015) The fortification of biscuits with bee pollen and its effect on physicochemical properties and antioxidant in biscuits. Lwt-Food Sci Technol 63:640-646.

Leonova SA, Badamshina EV, Meleshkina P, Weber AL, Kaluzhina OY, Vitol IS, Chernenkova AA, Gaifullina DT (2018) Spelt as raw material for food industry and peculiarities of its processing. J Eng Appl Sci 13:8300-8309.

Munteanu M-G, Voicu G, Ungureanu N, Zăbavă B-M, Ionescu M, Constantin G, Istrate I (2016) Methods for determining the characteristics of flour and dough. 5th Int Conf Therm Equip, Renew Ener Rural Devt (TE-RE-RD), June 2-4, 2016, Golden Sands, Bulgaria.

Muratova EI, Smolikhina PM (2013) Rheology of Confectionery. Tambov, Tambov State Technical University Publications.

Myers RH, Montgomery DC, Anderson-Cook CM (2016) Response Surface Methodology: Process and Product Optimization using Designed Experiments. John Wiley & Sons.

Novotni D, Ćurić D, Čukelj N, Tušak D, Bauman I, Dugum J (2009) Influence of dietary fibres addition on corn dough rheology. Proc 5th Int Cong Flour-bread. 7th Croat Cong Cereal Technol, 232-238.

Okpala LC, Ofoedu PI (2018) Quality characteristics of cookies produced from sweet potato and wheat flour blend fortified with Brewer's spent grain flour. Curr Res Nutr Food Sci 6:113-119.

Rumiantseva VV, Gurova AYu, Efremova I (2012) Efficiency of non-traditional raw materials in the production of confectionery emulsions. Confect Prod 1:20-22.

Saleh ASM, Wang P, Wang N, Yang S, Xiao Z (2019) Technologies for enhancement of bioactive components and potential health benefits of cereal and cereal-based foods: Research advances and application challenges. Crit Rev Food Sci Nutr 59:207-227.

Šebečić B, Vedrina-Dragojević I, Vitali D, Hečimović M, Dragičević I (2007) Raw materials in fibre enriched biscuits production as source of total phenols. Agric Conspec Sci 72:265-270.

Chakkaravarthi A, Punil Kumar HN, Bhattacharya S (2009). ‍Jilebi: 1. effect of moisture content, curd addition and fermentation time on the rheological properties of dispersions. J Food Sci Technol 46:543-548.

Siro I, Kápolna E, Kápolna B, Lugasi A (2008) Functional food. Product development, marketing and consumer acceptance — A review. Appetite 51:456-67.

Thakur M, Nanda V (2018) Exploring the physical, functional, thermal, and textural properties of bee pollen from different botanical origins of India. J Food Process Eng. 43(1):e12935.

Thakur M, Nanda V (2019) Process optimization of poly-

phenol-rich milk powder using bee pollen based on physicochemical and functional properties. J Food Process Eng 42(6):e13148.

Tugush AR, Sadygova MK, Kirillova TV, Kontareva DD (2018) Optimization of enriching additives in the formula of shortbread cookies. Coll Papers Mat Int Sci Pract Conf 75th Anniv Kurgan Region, 87-90.

Zhang J, Datta AK (2006) Mathematical modeling of bread baking process. J. Food Eng 75:78-89.